

University of Trento  
University IUAV of Venezia

Yue Feng

AN OPTIMIZATION INDEX TO  
IDENTIFY THE OPTIMAL DESIGN SOLUTION OF BRIDGES

Advisor:

Prof. Enzo Siviero  
Università IUAV di Venezia, Venice, Italy

Co-Advisors:

Prof. Baochun Chen, Prof. Bruno Briseghella  
Fuzhou University, Fuzhou, China

Prof. Tobia Zordan  
Tongji University, Shanghai, China

Prof. Luigi Fenu  
University of Cagliari, Cagliari, Italy

2014

UNIVERSITY OF TRENTO

Department of Civil, Environmental and Mechanical Engineering

Final Examination 10 / April / 2014

Board of Examiners

Prof. Maurizio Piazza (Università degli Studi di Trento)

Prof. Andrea Prota (Università degli Studi di Napoli Federico II)

Prof. Carmelo Gentile (Politecnico di Milano)

Prof. Helmut Wenzel (Universita' di Vienna)

## SUMMARY

Structural optimization has become an important tool for structural designers, since it allows a better exploitation of material, thus decreasing structure self-weight and saving material costs. Moreover, it helps the designer to find innovative design solutions and structural forms that not only better exploit material but also give the structure higher aesthetic value from an architectural point of view. When applied to real scale structures like bridges, this approach leads to the definition of voids patterns delimiting regions where fluxes of force migrate from force application point to boundary regions and suggests innovative layouts without renouncing to formal and structural aspects. Nevertheless, the criticality of this powerful tool is related to the ease of defining entire families of possible candidate solutions, by modifying input volume reduction ratio to reduce structural weight as much as possible or defining several starting trial solutions based on the judgment of designer. In this case, structural optimization still leads to the best material distribution, but finding the best compromise between material saving and structural performance is a designer choice.

To face this aspect, a global optimization index (*GOI*) has been defined and applied to the structural optimization of a steel-concrete arch bridge built in San Donà in the province of Venice, Italy. On the basis of this work, a generalized version of the optimization index is proposed and its analytical formulation is discussed in detail in this thesis. The application of proposed optimization index is extended from topology optimization to other optimization techniques. Moreover it allows not only to identify best candidate solution originated by a unique reference model, but even comparing structural performances between candidates solution derived by several starting trial solutions. Through structural optimization procedure performed on three different type bridges, namely footbridges supported by concrete shell, Calatrava Bridge (steel arch bridge) and two cable-stayed bridges, the effectiveness of proposed optimization index is validated. The results show that the proposed optimization index provides to the designer a mathematical procedure able to highlight the best choice among several candidate solutions obtained by the optimization procedure. With the proposed optimization index, a suitable score for each design solution of specific starting layout is assigned, therefore the best overall layout solution which is the best compromise between material saving and structural performance can be highlighted among single-family multi-solutions or multi-families or multi-solutions.



## SOMMARIO

L'ottimizzazione strutturale e' oramai ritenuta essere un importante strumento di supporto ai progettisti in quanto consente di riuscire a sfruttare al meglio il materiale, e in questo modo ottenere una riduzione dei pesi propri e un risparmio nelle quantita' utilizzate. Inoltre, come dimostrato da varie recenti realizzazioni, puo' essere di aiuto al progettista nella ricerca di innovative soluzioni progettuali e forme strutturali che coniugano ad un ottimo utilizzo del materiale anche un alto valore estetico. Se applicate nel campo delle grandi strutture e dei ponti, le tecniche di ottimizzazione e in particolare l'ottimizzazione topologica, possono portare alla identificazione di zone con materiale poco sfruttato in funzione del flusso delle forze dal loro punto di applicazione ai vincoli e quindi alla sua successiva rimozione e alla modifica della forma iniziale e/o alla definizione di cavita' al suo interno. Tuttavia la criticita' di questo strumento e' rappresentata dalla scelta della soluzione progettualmente piu' idonea all'interno della famiglia delle possibili soluzioni definite dal processo di ottimizzazione, che risulta fortemente influenzata dalla scelta degli input iniziali e dei parametri da ottimizzare.

Al fine di aiutare il progettista a trovare la soluzione ottima, in questa tesi si propone e si studia un Indice di Ottimizzazione Globale (GOI). Tale indice, prima introdotto nel processo di ottimizzazione di un ponte ad arco in struttura mista realizzato a San Dona' (Venezia), e' stato in questa ricerca generalizzato e reso applicabile non solo a ottimizzazioni di tipo topologico ma anche ad altre tecniche. Inoltre l'indice proposto permette non solo di identificare la soluzione ottimale ma anche di confrontarne varie provenienti da diversi modelli iniziali. Per validare quanto proposto vengono analizzate diverse tipologie di ponti e in particolare: a) soluzioni di ponti ad arco con un guscio realizzato in calcestruzzo; b) ponti ad arco metallici, e in particolare il ponte della Costituzione a Venezia progettato da Santiago Calatrava; c) vari ponti strallati. I risultati ottenuti dimostrano l'efficacia del metodo presentato come indice della validita' di una soluzione fra varie candidate ottenute dal processo di ottimizzazione. Con l'indice di ottimizzazione studiato e' possibile infatti arrivare ad assegnare a ciascuna proposta progettuale un valore e in questo modo definire la soluzione che rappresenta all'interno di una famiglia o di piu' famiglie il miglior compromesso fra il risparmio di materiale e la miglior performance strutturale.



## DEDICATION

*to my parents  
and  
my wife*





## ACKNOWLEDGEMENTS

Foremost, I would like to express my sincere gratitude to my advisor Prof. Enzo Siviero and Prof. Baochun Chen for the continuous support of my Ph.D study and research during my study in Italy. Their knowledge and expertise have been a precious reference during these three years.

I would like to express my special appreciation and thanks to Prof. Bruno Briseghella and Prof. Tobia Zordan for their great kindest helps and advices not only in my studies but also in my livings, to make this research work possible. They have supported me throughout my thesis with their patience and knowledge whilst provided me the office to work and treated me as a member of their company during these three years.

My sincere thanks also go to Dr. Cheng Lan and Dr. Enrico Mazzarolo for the supports they provided at times of critical need. I appreciate their vast knowledge and skill in structural optimization area, and their assistance in using softwares and writing papers. Some parts of this research are developed on the basis of works done by them.

Special thanks to Prof. Luigi Fenu for providing materials on the case study of shell supported bridges. Sincere thanks to all my dear friends, Junqing Xue, Tao Liu, Yufan Huang, for the stimulating discussions, for the days we were working together, and for all the fun we have had in the last three years.



# CONTENTS

## CHAPTER 1

<b>1. INTRODUCTION .....</b>	<b>1</b>
1.1. THE ORIGIN OF OPTIMIZATION INDEX.....	1
1.2. EXTENSION OF OPTIMIZATION INDEX.....	4
1.3. LAYOUT OF THESIS .....	7

## CHAPTER 2

<b>2. STATE-OF-ART: STRUCTURAL OPTIMIZATION .....</b>	<b>9</b>
2.1. PROBLEM FORMULATION .....	11
2.2. DESIGN OPTIMIZATION METHODS.....	13
2.2.1 <i>Mathematical Programming Techniques</i> .....	14
2.2.2 <i>Optimality Criteria Approaches</i> .....	16
2.2.3 <i>Heuristic Algorithms</i> .....	17
2.2.4 <i>Optimization Problems Using MATLAB</i> .....	18
2.3. NUMERICAL METHODS FOR TOPOLOGICAL OPTIMIZATION .....	19
2.3.1 <i>Material Interpolation Method</i> .....	21
2.3.2 <i>Evolutionary Structural Optimization (ESO) Method</i> .....	25
2.3.3 <i>Level Set Method</i> .....	26
2.3.4 <i>Numerical Instabilities</i> .....	27

## CHAPTER 3

<b>3. PROPOSED OPTIMIZATION INDEX .....</b>	<b>29</b>
3.1. OPTIMUM INDEX FORMULATION FOR SINGLE-FAMILY MULTI-SOLUTIONS .....	30
3.2. GENERALIZED VERSION FOR MULTI-FAMILIES MULTI-SOLUTIONS.....	34

## CHAPTER 4

<b>4. FOOTBRIDGES SUPPORTED BY CONCRETE SHELL .....</b>	<b>37</b>
4.1. SHELL-SUPPORTED BRIDGES DESIGN .....	39
4.1.1 <i>Shell Form-Finding</i> .....	39
4.1.2 <i>Finite Element Model</i> .....	40
4.1.3 <i>Choice of Shell Thickness</i> .....	42
4.2. TOPOLOGICAL OPTIMIZATION .....	44

4.2.1 Different Models Considered.....	45
4.2.2 Results of Shell Bridge T_0.15.....	46
4.2.3 Results of Shell Bridge T_0.20.....	55
4.2.4 Results of Shell Bridge T_0.32.....	63
4.3. COMPARISON BETWEEN TENTATIVE MODELS .....	70
<b>CHAPTER 5</b>	
<b>5. CALATRAVA BRIDGE OF VENICE.....</b>	<b>77</b>
5.1. CALATRAVA BRIDGE .....	80
5.1.1 General Situation.....	80
5.1.2 Finite Element Model.....	81
5.1.3 Mechanical Behaviour.....	82
5.2. STRUCTURAL OPTIMIZATION.....	84
5.2.1 Different Models Considered.....	84
5.2.2 Optimization Results of Minimizing Total Volume.....	86
5.2.3 Optimization Results of Minimizing Horizontal Force.....	92
5.3. IDENTIFICATION OF THE BEST DESIGN SOLUTION.....	99
<b>CHAPTER 6</b>	
<b>6. CABLE-STAYED BRIDGES .....</b>	<b>107</b>
6.1. DESIGN OF CABLES .....	108
6.1.1 Cable Force Optimization Methods.....	108
6.1.2 Optimization Problem Description.....	110
6.1.3 Programs Implemented for Optimization.....	111
6.1.4 Optimization Procedure.....	112
6.2. SINGLE CABLE PLANE CABLE-STAYED BRIDGE.....	113
6.2.1 General Situation.....	113
6.2.2 Finite Element Model.....	115
6.2.3 Cable Area and Initial Force Optimization Results .....	116
6.2.4 Thickness Optimization .....	122
6.2.5 Comparison between Different Models.....	125
6.3. DOUBLE CABLE PLANES CABLE-STAYED BRIDGE.....	127
6.3.1 General Situation.....	127
6.3.2 Finite Element Model.....	129
6.3.3 Cable Area and Cable Force Optimization Results .....	132
6.3.4 Thickness Optimization .....	151
6.3.5 Comparison between Different Models.....	156
<b>CONCLUSIONS .....</b>	<b>163</b>

**BIBLIOGRAPHY .....169**



**CHAPTER 1****1. INTRODUCTION**

## 1.1. The Origin of Optimization Index

Structural optimization is the subject of achieving the best performance for a structure with various constraints such as a given amount of material, limitation of peak stress and deflection. Based on strong demand of lightweight, low-cost and high-performance structures due to the limited material resources and technological competition, optimal structure design is becoming increasingly important (Huang and Xie, 2010) and attracting considerable attention (Banichuk and Neittaanmäki, 2010). Benefit from the availability of high-speed computers and the rapid improvements in algorithms, the structural optimization is rapidly becoming an integral part of the structure design process and as an important tool for designers in the last decades (Huang and Xie, 2009).

Structural optimization can be classified into three categories, namely sizing, shape, and topology optimization, each of them address different aspect of the structural design problem (Christensen and Klarbring, 2009). Sizing optimization is to find the optimal design by changing the size variables such as cross-sectional dimensions of trussed and frames, or the thicknesses of plates (Huang and Xie, 2010). Shape optimization is to find the optimum shape of a domain which defined as design variable. Topology optimization of discrete structures is to search for the optimal spatial order and connectivity of the bars in a typical problem, while topology optimization of continuum structures is to find the optimal designs by determining the best number and locations and shape of cavities in the design domain (Bendsoe and Sigmund, 2003, Huang and Xie, 2010).

Among the different optimization techniques, topology optimization has revealed to be particularly interesting for structural engineering and is by far the most challenging technically (Diehl, 2010). It plays an important role in structural design, the very purpose of which is to find the best solutions from which a designer can achieve a maximum benefit from the available resources. With topology optimization technique, engineers determine where to place material within a design domain and find out the most suitable global shape of a structure depending on the specific target function to be maximized or minimized, such as the structural stiffness or

natural frequencies (Achtziger and Kocvara, 2007, Allaire, et al., 2001, Pedersen, 2000).

When applied to a solid or a shell shaped structure, topology optimization leads to the definition of voids patterns delimiting regions where fluxes of force migrate from force application point to boundary regions. If implemented into FE codes and applied to real scale structures like tall buildings, this approach may suggest innovative layouts and provides higher aesthetic value to the investigated structure, without renouncing to formal and structural aspects. Topology optimization results then to be a valid aid for the designer to find the most suitable structural shape not only from an engineering point of view but even an architectural one, leading to a practical connection between the two complementary disciplines.

In addition when topology optimization applied to bridge structures, it allows not only finding a conceptual layout of a design with the lightest and stiffest structure while satisfying certain specified design constraints, but also simplifying the design process and significantly improving efficiency of design. As we know, in the traditional design of bridge structures, bridges are designed based on engineering theories and previous experience, which would involve the preliminary design, structural analysis and check against requirements of mechanical behavior (Guan, et al., 2003). Such a design is followed by design modification, re-analysis and re-checking process and is very expensive and time-consuming. With the topology optimization technique implemented into FE code, the design process can be defined by a set of design variables and constraints as well as objective function and thereby simplified.

Nevertheless, the criticality of this powerful tool is related to the ease of defining entire families of possible candidate solutions, by simply modifying input volume reduction ( $VR$ ) ratio. Designer could be tempted to reduce structural weight as much as possible. In this case, topology procedure still leads to the best material distribution for the specific target volume, but finding the best compromise between material saving and structural performance is a designer choice.

To face this aspect, an global optimization index ( $GOI$ ) has been defined by Bruno Briseghella et al. (Briseghella, et al., 2012), with the goal to provide a formal mathematical procedure able to highlight the best choice among several candidate solutions obtained by optimization procedure, that represents the best compromise between material saving and structural response.



A former formulation for considered *GOI* was applied to the structural optimization of a steel-concrete arch bridge built in San Donà in the province of Venice, Italy. The bridge was already partially built while the Italian Seismic Code was updated together with a new seismic classification of Italian territory. It prescribed higher acceleration values, requiring a much higher increase of resistance (35%) of the already existing foundations. Hence, seismic retrofitting of this bridge required for a considerable lightening of the superstructure and topological optimization was used to this purpose. Starting from a reference identified solution for the steel deck, consisting in two longitudinal box girder connected by a continuous bottom flange, several candidate solutions were generated from optimization analysis, depending on imposed volume reduction. What is more, although the design objective was the reduction of superstructure weight, the increase in *VR* causes an increase of both the stress and deflections of bridge, whose control was a competing requirement with respect to *VR*. Therefore, an issue to identify the best choice among entire candidate solutions is faced and a global optimization index (*GOI*) defined for this purpose.

Such an index should provide an uncomplicated mathematical procedure for ease application to identify the best design solution, but at the same time has to take into account weight reduction and structural response of candidate solutions. Therefore, two response indexes (*RI*s) are defined firstly to summarize the overall behavior of the whole structure, namely response index of stress  $RI(\sigma)$  and response index of deformation  $RI(d)$ . The former is Von Mises stress averaged throughout the whole steel superstructure and was considered as representative of the stress level, whereas the latter is deflection at mid span and was considered as representative of the deformation level.

To take into account the weight reduction, after the introduction of a penalty exponent  $\beta$  to the scaling coefficient  $1/VR$  which able to favor design solutions with higher *VR*, optimization indexes (*OI*s) of stress and deformation were defined through the comparison of the variation of stress and deformation with respect to the variation of *VR*, respectively. Eventually, global optimization index (*GOI*) considering both stress and deformation of structural response was defined by averaging the two *OI*s.

Through proposed *GOI*, an innovative layout for this kind of bridges consisting in a couple of wide elliptic holes in the bottom flange was identified as the best

compromise between material saving and bridge performances, these letters defined in term of stress field and deformations.

## 1.2. Extension of Optimization Index

However, during earlier designing phases of a project, in particular in the case of spatial shell structures, several starting trial solutions as well as reference solutions might being defined based on the judgment of designer, each solution characterized by a particular layout, material property or distribution of boundary conditions. In this case, topology optimization is still a viable tool to optimize structures, but it would lead to the definition of entire families of possible candidate solutions, depending on input VR target. Therefore, the problem is changed from single-family multi-solutions to multi-families multi-solutions.

To face this particular issue, a further  $GOI^*$  formulation which based on a further  $OI^*$  is presented in this thesis. Proposed global optimization index allows not only to identify best candidate solution originated by a unique reference model, but even comparing structural performances between candidates solution derived by several starting trial solutions.

Same as the index proposed originally, two response indexes ( $RIs$ ) are defined firstly to summarize the overall behavior of structure, namely response index of stress  $RI(\sigma)$  and response index of deformation  $RI(d)$ . The former is considered as representative of the stress level, while the latter is considered as representative of the deformation level. However, to extend the applications of  $OI^*$  to other optimization techniques and bridge structures, according to the structure type and optimization techniques, the stress level can be averaged stress or maximum stress throughout the whole structure, and the deformation level can be deflection at mid span or deflection at tower top.

Following the definition of  $RIs$ , to provide  $OI^*$  a general application thus can be used to multi-families multi-solutions problems, a scaling factor vector  $\alpha$  is introduced to the two optimization indexes ( $OIs$ ). This  $\alpha$  is calculated by structural response comparison of all starting models. Eventually, through the introduction of weight vector  $w$ , global optimization index ( $GOI^*$ ) considering both stress and deformation of structural response is defined by assigning weights to the two  $OIs^*$ .

In this thesis, to present to the reader potentially and effectiveness of defined  $GOI^*$ , three different cases with different structure type or different optimization techniques were studied, namely Optimization of Footbridges Supported By Concrete Shell, Optimization of Calatrava Bridge In Venice and Optimization of Two Cable-stayed Bridges.

In the real case of footbridges supported by concrete shell, the problem related to the tensile stresses rising in concrete shell bridges is faced. When designing bridges supported by a shell in reinforced concrete (RC), it is worth choosing shells with minimal area that, being anticlastic and therefore subject to biaxial compression, well exploited compressive strength of concrete and well prevented cracks propagation. Notwithstanding the use of form-finding algorithms in order to obtain a shell of minimal area subject to biaxial compression, unwished bending moments and related tensile stresses unavoidably arise in some regions of the shell. A previous publication written by the authors (Briseghella, et al., 2013) demonstrated as such unavoidable tensile stresses can be further eliminated by removing material from the shell regions where unwished bending moments arise, thus obtaining a shell structure with voids, by means of topology optimization.

Hence, starting from three footbridges supported by concrete shells with different shape and thicknesses, finite element topological optimization procedures were carried out in order to minimize the volume of the shells of a certain percentage. After identifying the shells regions where the pseudo densities obtained from previous topological optimization results are lower, the geometries of the shells are updated by eliminating the material of these regions. With an iterative procedure of form finding and topological optimization, shells with a pattern of holes are obtained and the areas of shells regions with low tensile stresses are minimized. At the end, the optimum design solutions of three bridges were identified among all the solutions with proposed  $GOI^*$ .

Calatrava Bridge, the fourth bridge spanning the Grand Canal of Venice, later has its official name "Ponte della Costituzione", opened to the public on September 11, 2008. Immediately following the completion of the newest bridge, due to the lack of wheelchair access, lack of necessity, bridge modern appearance and an approximately cost of 10 million euros, made heated criticism rain down on this project. Furthermore the bridge presents some structural defectiveness, which makes the project less rational from the structural point of view. Firstly, the 1/16 rise-to-span ratio cause large horizontal thrusts against the abutment, which is a

critical aspect considering the soft soil of Venice. Secondly, the open cross-section with  $\pi$ -shaped steel plates and the open truss arch ribs with straight-like web members with no diagonals need not only to withstand shear forces of the main arch, but even local bending moments, leading the stress of some members close to critical state. Besides, being the stiffness of main arch rib relatively small, large bending deformation occurs under asymmetric loading. Finally, the third vibration mode of the main arch is close to the pedestrian step frequency, which is extremely liable to cause the pedestrian and bridge resonance.

Some structural defectiveness mentioned above particularly the occurrence of huge horizontal thrust could be reduced if the bridge with better design such as more reasonable thickness distribution or considering bridge's abutment deformability. To this aim, three tentative starting models were identified by considering bridge's abutment deformability through spring-damper elements and introducing tensioning cables along two bottom arches of the bridge, the sizing optimization by means of finite elements of these three models were carried out. Several candidate solutions were obtained due to the different value of elastic stiffness  $K$  of spring-damper elements and initial strain  $\varepsilon$  of tensioning cables and their results are used to validate the effectiveness of the proposed  $GOI^*$ .

Cable-stayed bridges are statically indeterminate structures due to its composition. Their structural behavior is the result of a complex interaction between several parameters. The cable arrangement and stiffness distribution in the cables, deck and pylons affected the structural behavior of cable-stayed bridge greatly (Walther, 1999). In the design of cable-stayed bridges, the total number of cables is an important design consideration. It plays an important role not only in the mechanical behavior of bridges but also in aesthetic point of view. Moreover, to get more attractive appearance, sometimes the designer would like to change the angle of the tower.

In this real case, to discuss the interaction between mechanical behavior of cable-stayed bridge and its parameters like total number of cables and tower angle, two cable-stayed bridges including one Single Tower Single Cable Plane cable-stayed bridge and one Twin Towers Double Cable Planes cable-stayed bridge are served as prototypes, several tentative starting models were characterized by the utilization of different total cables and different angles of tower in vertical direction, the cables cross sectional area and corresponding initial cable force were optimized. Following this, the optimum cable areas and initial cable force are

assigned to starting models to carry out thickness optimization of steel plates of bridge deck. Eventually, the results are used to validate the effectiveness of the proposed  $GOI^*$ .

### 1.3. Layout of Thesis

Besides this chapter, in the main body of the thesis, it consists of 5 chapters, from Ch.2 to Ch.6 that introduced as following:

*Chapter 2*, it states a brief development history of optimization techniques and their applications in structural field, including a general statement of structural optimization problems and the numerical methods of design optimization and topology optimization of continuum structures.

*Chapter 3*, it presents the optimization index to identify the optimal design solution. Based on the original index proposed by Bruno Briseghella et al., a generalized formulation was proposed to solve not only the single-family multi-solutions problem but also multi-families multi-solutions problem.

*Chapter 4*, it presents a case study on footbridges supported by concrete shell. Starting from three footbridges supported by concrete shell, finite element topological optimization procedures were carried out. The geometries of the shells are updated by eliminating the material of shell regions with lower pseudo densities. With an iterative procedure of form finding and topological optimization, shells with a pattern of holes are obtained and the areas of shell regions with low tensile stresses are minimized. At the end, the optimum design solution was identified among all the solutions with proposed index.

*Chapter 5*, it presents a case study on Calatrava Bridge. Starting from three tentative models based on the original design, the sizing optimization by means of finite elements of this three models were carried out, the results are used to validate the effectiveness of the proposed optimization index.

*Chapter 6*, it presents a case study on two cable-stayed bridges. Starting from several tentative models characterized by the utilization of different total cables and different angles of tower in vertical direction, the cables cross sectional area and corresponding initial cable force were optimized, the results are assigned to starting

models to carry out thickness optimization of steel plates of bridge deck and used to validate the effectiveness of the proposed optimization index.

At the end, the conclusions drawn from the research and recommendations for future investigation will be presented.

## CHAPTER 2

### 2. STATE-OF-ART: STRUCTURAL OPTIMIZATION

Optimization is a mathematical discipline that concerns with finding minimum and maximum value of some objective functions while subject to so-called constraints (Ding, 1986, Hsu, 1994, Nocedal and Wright, 2006). The beginnings of optimization problems can be traced to the early period of World War II (Elishakoff and Ohsaki, 2010). During that war, the British military faced the problem of allocating very scarce and limited resources to several activities (Rao and Rao, 2009). The methods developed to solve the allocation of limited resources during that period became known as operations research.

The existence of optimization methods can be traced to the days of Newton, Lagrange and Cauchy (Brandt and Wasitynski, 1963, Ravindran, et al., 2006, Schoofs, 1993). In 1840s, Cauchy made the first application of the steepest descent method to solve unconstrained minimization problems. A long time later in 1947, the development of the simplex method by Dantzig for linear programming methods accelerated the development of methods of constrained optimization (Belegundu and Chandrupatla, 2011, Dantzig, 1998). Following this, the techniques have later grown to be applied to various of scientific and engineering domain (Liang, 2004). Structural optimization is just a traditional and popular subject when the optimization theory applied on structural engineering.

The first analytical work in structural optimization perhaps was by Maxwell in 1869, followed by the better known work of Michell in 1904 (Akin and Arjona-Baez, 2001, Cohn and Dinovitzer, 1994, Vanderplaats, 1982). The latter constructed several optimal trusses given some simple cases of load and offer considerable insight into the structural optimization problem and the design process. Despite these early contributions, very little progress was made until the availability of high-speed digital computers and development of linear programming methods mentioned above (Burns, 2002, Vanderplaats, 1982, Venkayya, 1978). The availability of the digital computer led to application of linear programming techniques to plastic design of frames during 1940s and early 1950s, and made significant early numerical work to solve structural design problems.

In 1960, Schmit (Schmit, 1960) proposed a new approach which has served as a conceptual foundation for the development of many modern structural optimization methods. He introduced an idea of using mathematical programming techniques to solve the nonlinear inequality constrained problem of designing elastic structures under a multiplicity of loading conditions. Prior to that time there were no texts on nonlinear programming.

A few years later, an alternative approach was presented in analytical form by Prager, et al. (Prager and Taylor, 1967), which became popularly known as the “Optimality Criteria” approach. The optimality criteria approach is first to establish the criterion to be satisfied while subject to the constraints. It solves the optimality conditions directly rather than minimize the objective function directly. Although the optimality criteria approach was largely intuitive, its advantage of easily programmed for the computer and relatively independent of problem size make it quite attractive and effective as a design tool.

Since then, the field of structural optimization has experienced many new developments in both computational techniques and applications. In the last decades, based on strong demand of lightweight, low-cost and high-performance structures due to the limited material resources and technological competition, structural optimization with the aim of achieving the best performance for a structure with various constraints is becoming increasingly important, and it has become an important tool for engineering designers benefit from the availability of high-speed computers and the rapid improvements in algorithms (Huang and Xie, 2010).

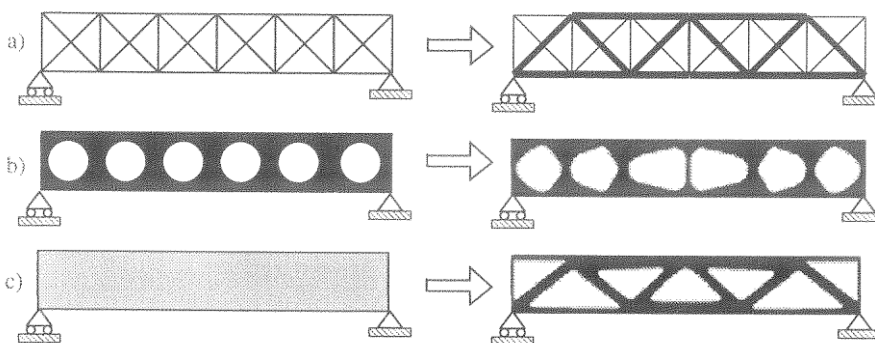


*Fig. 1 Three categories of structural optimization. a) sizing optimization of a truss structure, b) shape optimization and c) topology optimization (Bendsoe and Sigmund, 2003).*

Structural optimization can be classified into three categories, as shown in Fig. 1, namely sizing, shape, and topology optimization, each of them address different



aspect of the structural design problem (Christensen and Klarbring, 2009). Sizing optimization is to find the optimal design by changing the size variables such as cross-sectional dimensions of trussed and frames, or the thicknesses of plates (Huang and Xie, 2010). Shape optimization is to find the optimum shape of a domain which defined as design variable. It is mainly performed on continuum structures by modifying the predetermined boundaries to achieve the optimal designs. Depending on the type of a structure, there are two types of topology optimization, i.e. discrete or continuous. Topology optimization of discrete structures is to search for the optimal spatial order and connectivity of the bars in a typical problem, while topology optimization of continuum structures is to find the optimal designs by determining the number and location and shape of cavities in the design domain (Bendsoe and Sigmund, 2003, Huang and Xie, 2010).

## 2.1. Problem Formulation

Mathematically speaking, optimization is the minimization or maximization of a function subject to constraints on its variables. It can be simply formulate and written as:

$$\text{Minimize } f(\mathbf{x}) \quad (1)$$

Subject to:

$$\begin{cases} l_i(\mathbf{x}) = 0 & i = 1, 2, 3, \dots, n \\ g_j(\mathbf{x}) \leq 0 & j = 1, 2, 3, \dots, m \end{cases} \quad (2)$$

The problem stated above is a constrained optimization problem. The problems are unconstrained optimization problems when there are no any constraints. Here  $\mathbf{x}$  is the Design Variable (DV) vector,  $f(\mathbf{x})$  is termed the Objective Function (OBJ),  $l_i(\mathbf{x})$  and  $g_j(\mathbf{x})$  are known as equality and inequality constraints, respectively. They are also known as State Variables (SVs) in the optimization procedure. The number of design variables and the number of equality and inequality constraints need not be related in any way.

### **Design Variables (DVs)**

Design Variables are independent quantities, which varied to achieve the optimum design (Roy, et al., 2008). Any structural optimization problem is defined by a set of quantities some of which are viewed as variables during the design process. In general, certain quantities are usually fixed at the outset and these are called pre-assigned parameters. All the other quantities are treated as variables in the design process and are called design variables (Rao and Rao, 2009). The design variables describe the design and can be changed during optimization. It may represent geometry or choice of material. When it describes geometry, it may relate to a sophisticated interpolation of shape or it may simply be the area of a bar, or the thickness of a sheet (Spillers and MacBain, 2009).

### **State Variables (SVs)**

State Variables are quantities that constrain the design. They are also known as "dependent variables" due to they are typically response quantities that are functions of the design variables. In many practical problems, the design variables cannot be chosen arbitrarily but have to satisfy certain specified functional and other requirements. The restrictions that must be satisfied to produce an acceptable design are collectively called design constraints (Rao and Rao, 2009). There are two types of constraints, namely functional constraints and geometric constraints. The latter represent physical limitations on the design variables, while the former represent limitations on the behavior or performance of the system and are state variables. For a given mechanical structure, the state variables usually are the response of the structure in terms of displacement, stress, strain or force.

### **Objective Function (OBJ)**

Objective Function is the dependent variable that attempting to minimize. It should be a function of the design variables, means that its value should change when changing the values of the design variables. Objective function returns a number which indicates the goodness of the design (Choi and Kim, 2005). During optimization procedure, usually there will be more than one acceptable design that satisfies the functional and other requirements of the problem, and the purpose of optimization is to choose the best one of the many acceptable designs available. Thus a criterion for selecting the best one by comparing the different alternative acceptable designs has to be defined. When this criterion expressed as a function of the design variables, is known as the objective function (Rao and Rao, 2009). The choice of objective function is governed by the nature of problem. In structural optimization, the objective is usually taken as minimization of weight, displacement in a given direction, effective stress or total cost. In some situations, there may be

more than one criterion to be satisfied simultaneously. An optimization problem involving multiple objective functions is known as a multi-objective optimization.

## 2.2. Design Optimization Methods

The purpose of many structural design problems is to find the optimum design among many possible candidates (Choi and Kim, 2005). An optimum design is the one that is as effective as possible, and is the one that meets all specified requirements yet demands a minimum in terms of expenses such as weight, surface area, volume, stress, cost, and other factors in structural engineering. In practical engineering, any aspect of design would be optimized, just like dimensions (such as thickness), shape (such as fillet radii), placement of supports, cost of fabrication, natural frequency, material property, and so on (Ansys, 2007).

The definition of an optimization problem always contains several steps which begin from identification of design variables and their bounds, then to the identification of constraints and objective function. Immediately following the defining of optimization problem, the algorithm to find the optimum design is the goal of the design optimization problem. There is no single method available for solving all optimization problems efficiently. Hence a number of optimization methods have been developed for solving different types of optimization problems. In the area of structural, there are three main categories of optimization methods, namely Mathematical Programming Techniques, Optimality Criteria Approaches and Heuristic Algorithms.

Mathematical programming techniques are developed on the basis of operations research. They are useful in finding the minimum of a function of several variables under a prescribed set of constraints through linear or nonlinear programming methods. The structural optimization problems are characterized by finding extreme values of objective function under constraints of stress, displacement and frequency or other constraints in multi-dimensional design space. Compared to optimality criteria approaches and heuristic algorithms, mathematical programming has a rigorous theoretical foundation, high reliability, wide application and guaranteed convergence. However, its disadvantage is the need to frequently calculate the value of the objective function and constraint function and its gradient, thus leading to a large amount of computation and slow convergence. It is more obvious especially for multi-variable optimization problems.

Optimality criteria approaches pre-establish criteria to evaluate the structural performance such as stress, strain energy, frequency and etc. based on experience and mechanical engineering concepts, set the Kuhn-Tucker conditions (referred to as KT conditions) as the requirement that optimal solution should satisfy, then the criteria used to optimize the design variables and update the Lagrange multipliers, find the best solution from all the feasible design solutions through an iterative approach at the end. Optimality criteria approaches have an intuitive physical meaning, need not derivative information of function or constraints, less iterations, high speed convergence and high computational efficiency. Furthermore, it is particularly suitable for large scale projects which need a large amount of calculation due to the insensitivity to the increase of the design variables. However, compare to mathematical programming techniques and heuristic algorithms, the optimization always converge to local optima due to the lack of rigorous theoretical foundation. In addition, it is not a general method which can be applied on different optimization problems.

Heuristic algorithms are optimization methods that conceptually different from the traditional mathematical programming techniques. These methods are labeled as modern or nontraditional methods of optimization. Most of these methods are based on certain characteristics and behavior of biological, molecular, swarm of insects, and neurobiological systems. The most rational structures in the world are often created by nature. Bones of animals, plant stems are the formation of a natural evolution and continuous improvement in the long history. Heuristic algorithms are just methods finding the optimal solution in the feasible region when applied to structural optimization according to the laws of nature. In general, although cannot guarantee the final result is global optimal solution, but generally can approach the global optimal solution. Furthermore, the mathematical calculations are not complex, However, a large amount of calculation always needed due to the difficult convergence.

### 2.2.1 Mathematical Programming Techniques

The problems with linear objective function and linear constraints are Linear Programming (LP) problems. Linear programming is the term used for defining a wide range of optimization problems, in which the objective function to be minimized or maximized is linear in the unknown variables and the constraints are a combination of linear equalities and inequalities (Belegundu and Chandrupatla, 2011,

Dantzig, 1998). In the area of structural, most problems are not linear. However, one way of solving nonlinear programming (NLP) problems is to transform them into a sequence of linear programs (Arora, 2004, Kim, et al., 2002). In addition, some NLP methods solve an LP problem during their iterative solution processes. Thus, linear programming methods are useful in many applications. The standard form of an LP problem with  $m$  constraints and  $n$  variables can be represented as follows:

$$\begin{aligned} \text{minimize} \quad & f = \mathbf{c}^T \mathbf{u} \\ \text{subject to} \quad & \mathbf{A}\mathbf{u} = \mathbf{b} \\ & \mathbf{u} \geq \mathbf{0}, \mathbf{b} \geq \mathbf{0} \end{aligned} \tag{3}$$

Where  $\mathbf{c}$  is the coefficient of the cost function,  $\mathbf{u}$  is the vector of design variables to be determined,  $\mathbf{A}$  is  $m \times n$  matrix, and  $\mathbf{b}$  is  $m \times 1$  vector. Inequality constraints can be transformed to equality constraints by introducing slack variables. Linear programming problems are convex problems. Hence, a local minimum is indeed a global minimum.

The simplex method is a very efficient method for solving linear programming problems. The method was developed by George Dantzig (Dantzig, 1998) in 1947 and has been widely used since then. A positive feature of a linear programming problem is that the solution always lies on the boundary of the feasible region. Thus, the simplex method finds a solution by moving each corner point of the convex boundary. Therefore, the basic idea of the simplex method is to proceed from one basic feasible solution to another in a way that continually decreases the cost function until the minimum is reached (Nocedal and Wright, 2006).

The problems with nonlinear objective function or nonlinear constraints are Nonlinear Programming (NLP) problems. There are two categories of nonlinear programming techniques, namely direct and indirect methods as list in Table 1. The direct methods are also known as non-gradient methods and zeroth-order methods since they require only the objective function values but not the partial derivatives of the function in finding the minimum (Bradie, 2006, Hildebrand, 1987, Nocedal and Wright, 2006). On the contrary, the indirect methods are known as gradient methods since they require not only the function values but also the first and in some cases the second derivatives of the objective function. In general, due to more information about the objective function is used through the use of derivatives, the indirect methods are generally more efficient than direct techniques (Rao and Rao, 2009).

Based on the nature of design variables encountered, optimization problems can be classified into unconstrained optimization problems or constrained optimization problems. When there are no constraints on the design problem, it is referred to as an unconstrained optimization problem. On the contrary, constrained optimization problem are with constraints. A very common instance of a constrained optimization problem arises in finding the minimum weight design of a structure subject to constraints on stress and deflection. Even if most engineering problems have constraints, these problems can be transformed into unconstrained ones by using the penalty method, or the Lagrange multiplier method.

Direct Methods	Indirect Methods
<b><i>Unconstrained Optimization Problems</i></b>	
Random search method	Steepest descent method
Gird search method	Fletcher–Reeves method
Univariate method	Newton's method
Pattern search methods	Marquardt method
Powell's method	Quasi-Newton methods
Simplex method	Conjugate gradient method
<b><i>Constrained Optimization Problems</i></b>	
Random search methods	Transformation of variables technique
Heuristic search methods	Sequential unconstrained minimization techniques
Complex method	Interior penalty function method
Objective and constraint approximation methods	Exterior penalty function method
Sequential linear programming method	Augmented Lagrange multiplier method
Sequential quadratic programming method	
Feasible direction Method	
Zoutendijk's method	
Gradient projection method	
Generalized reduced gradient method	

**Table 1**

*Methods of nonlinear mathematical optimization problems (Rao and Rao, 2009)*

### 2.2.2 Optimality Criteria Approaches

The use of the optimality criteria (OC) method has become widespread and has been applied, with a variety of modifications, to various fields of structural optimization, including building and bridge structures. The main reasons for the popularity of this method are its ease of implementation and fast convergence.

In general, optimality criteria methods are algorithms that seek the optimum through finding a solution that satisfies some pre-specified criteria which are postulated to correspond to the optimal result for the problem. Among the OC methods, the fully stressed design (FSD) method has a long history. Due to its ease of implementation and fast convergence, it was considered a viable alternative to formal optimization algorithms and widely used. However, it has a main weak point that without a rigorous mathematical basis.

Compared with classical optimization, in which problems are described in terms of objective functions and constraints and then solved using some mathematical programming algorithm, optimality criteria methods analyzed a structure and redesigned it on the basis of some resizing rule. Therefore, while the methods of mathematical programming are formal in the sense of mathematics, optimality criteria methods are considered to be heuristic. In these methods the optimum is sought without explicit concern for an objective function (Groenwold and Etman, 2009, Spillers and MacBain, 2009).

The most important topic in the optimality criteria approach is the concept of scaling. The next two important topics are the iterative algorithm together with the specialization of the Lagrangian multipliers. All of these concepts will be derived as function of the sensitivity derivatives of the constraints and the objective functions. Then this optimization will no longer be addressed in the context of a single discipline, but instead it will be derived in terms of sensitivity derivatives which can be obtained for all disciplines (Venkayya, 1989).

### *2.2.3 Heuristic Algorithms*

There are 5 main heuristic algorithms developed in recent years, namely Genetic Algorithms, Simulated Annealing, Particle Swarm Optimization, Ant Colony Optimization and Neural-network-based Methods (Kaveh, et al., 2008, Li and Au, 2010, Madeira, et al., 2009, Martí and González-Vidoso, 2010, Perea, et al., 2008). The genetic algorithms are based on the principles of natural genetics and natural selection. Simulated annealing is based on the simulation of thermal annealing of critically heated solids. The particle swarm optimization is based on the behavior of a colony of living things, such as a swarm of insects, a flock of birds, or a school of fish. Ant colony optimization is based on the cooperative behavior of real ant colonies, which are able to find the shortest path from their nest to a food source. In

neural-network-based methods, the problem is modeled as a network consisting of several neurons, and the network is trained suitably to solve the optimization problem efficiently (Rao and Rao, 2009).

Among all the heuristic algorithms, genetic algorithms (GA) have the most in-depth research and widest application. It generates solutions to optimization problems using techniques inspired by natural evolution, such as inheritance, mutation, selection and crossover. In a genetic algorithm, a population of candidate solutions (called individuals, creatures, or phenotypes) to an optimization problem is evolved toward better solutions. The evolution usually starts from a population of randomly generated individuals which is called a generation, and is an iterative process. In each generation, the fitness (usually the value of the objective function in the optimization problem being solved) of every individual in the population is evaluated. The more fit individuals are stochastically selected from the current population, and genome of each individual is modified to form a new generation. The new generation of candidate solutions is then used in the next iteration of the algorithm. Commonly, the algorithm terminates when either a maximum number of generations has been produced, or a satisfactory fitness level has been reached for the population (Madeira, et al., 2009).

Compared with the traditional optimization methods, heuristic algorithms need not the derivative information of the objective function and provide several potential optimal solutions to designers. Moreover, the conversion process of design solutions is random and the operand is a code group contains the design variable information rather than the design variable itself.

#### *2.2.4 Optimization Problems Using MATLAB*

Several commercial software systems are available to solve optimization problems that arise in different engineering areas. MATLAB can be considered a high-level programming language for numerical computation, data analysis, and graphics for applications in many fields. It is a popular software that is used for the solution of a variety of scientific and engineering problems. Optimization toolbox implemented MATLAB is a specific toolbox developed for solving optimization problems (Andreassen, et al., 2010). It contains a library of programs or m-files, which can be used for the solution of minimization, equations, least squares curve fitting, and related problems. The programs or m-files, also called functions, available in the minimization section of the optimization toolbox are given in Table 2. The basic



information for using the various programs can be found in the user's guide for the optimization toolbox.

Type	Formulation	MATLAB function
Scalar minimization	$\min f(x)$ $\text{s. t. } x_1 < x < x_2$	$x = \text{fminbnd}(\text{fun}, x1, x2)$
Unconstrained minimization	$\min f(x)$	$x = \text{fminunc}(\text{fun}, x0)$ $x = \text{fminsearch}(\text{fun}, x0)$
Linear programming	$\min \mathbf{c}^T \mathbf{x}$ $\text{s. t. } \mathbf{Ax} \leq \mathbf{b}, \mathbf{A}_{eq} \mathbf{x} = \mathbf{b}_{eq}, \mathbf{l} \leq \mathbf{x} \leq \mathbf{u}$	$x = \text{linprog}(\mathbf{f}, \mathbf{A}, \mathbf{b})$
Quadratic programming	$\min f(x) = \frac{1}{2} \mathbf{x}^T \mathbf{G} \mathbf{x} + \mathbf{c}^T \mathbf{x}$ $\text{s. t. } \mathbf{Ax} \leq \mathbf{b}, \mathbf{A}_{eq} \mathbf{x} = \mathbf{b}_{eq}, \mathbf{l} \leq \mathbf{x} \leq \mathbf{u}$	$x = \text{quadprog}(\mathbf{H}, \mathbf{f})$
Constrained minimization	$\min f(x)$ $\text{s. t. } \mathbf{c}(x) \leq 0, \mathbf{c}_{eq} = 0, \mathbf{Ax} \leq \mathbf{b},$ $\mathbf{A}_{eq} \mathbf{x} = \mathbf{b}_{eq}, \mathbf{l} \leq \mathbf{x} \leq \mathbf{u}$	$x = \text{fmincon}(\text{fun}, x0, \mathbf{A}, \mathbf{b})$
Semi-infinite minimization	$\min f(x)$ $\text{s. t. } \mathbf{K}(x, \mathbf{w}) \leq 0, \mathbf{c}(x) \leq 0, \mathbf{c}_{eq} = 0,$ $\mathbf{Ax} \leq \mathbf{b}, \mathbf{A}_{eq} \mathbf{x} = \mathbf{b}_{eq}, \mathbf{l} \leq \mathbf{x} \leq \mathbf{u}$	$x = \text{fseminf}(\text{fun}, x0, n\theta, \text{semifcon})$
Binary integer programming	$\min \mathbf{f}^T \mathbf{x}$ $\text{s. t. } \mathbf{Ax} \leq \mathbf{b}, \mathbf{A}_{eq} \mathbf{x} = \mathbf{b}_{eq}, \mathbf{x} \text{ binary}$	$x = \text{bintprog}(\mathbf{f}, \mathbf{A}, \mathbf{b}, \mathbf{A}_{eq}, \mathbf{b}_{eq}, x0)$
Goal attainment	$\min \boldsymbol{\gamma}$ $\text{s. t. } f(x) - \boldsymbol{\gamma} \leq \mathbf{goal}$ $\mathbf{c}(x) \leq 0, \mathbf{c}_{eq} = 0, \mathbf{Ax} \leq \mathbf{b},$ $\mathbf{A}_{eq} \mathbf{x} = \mathbf{b}_{eq}, \mathbf{l} \leq \mathbf{x} \leq \mathbf{u}$	$x = \text{fgoalattain}(\text{fun}, x0, \mathbf{goal}, \mathbf{weight})$
Minimax	$\min \max \{f_i(x)\}$ $\text{s. t. } \mathbf{c}(x) \leq 0, \mathbf{c}_{eq} = 0, \mathbf{Ax} \leq \mathbf{b},$ $\mathbf{A}_{eq} \mathbf{x} = \mathbf{b}_{eq}, \mathbf{l} \leq \mathbf{x} \leq \mathbf{u}$	$x = \text{fminimax}(\text{fun}, x0)$

Table 2

MATLAB programs or functions for solving optimization problems (Guide, 1998)

### 2.3. Numerical Methods for Topological Optimization

Compared with other types of structural optimization, topology optimization of continuum structures is by far the most challenging technically and at the same time the most rewarding economically. Topology optimization is the first structural

optimization stage, it is used for conceptual design, and thus the stage where lightweight can be achieved. In the past three decades, topology optimization has become a powerful and increasingly popular tool for designers and engineers in the early stages of the design process (Bendsoe and Sigmund, 2003, Rahmatalla and Swan, 2003).

Topology optimization is a rapidly expanding research field in structural optimization, its application to bridge structures is being considered as one of the most challenging and committing tasks in structural design. It is a form of "shape" optimization, sometimes referred to as "layout" optimization. The purpose of topology optimization is to find the best use of material for a body such that an objective criterion (such as global stiffness or natural frequency) takes on a maximum/minimum value subject to given constraints (such as volume reduction). The standard formulation of topology optimization defines the problem as minimizing the structural compliance while satisfying a constraint on the volume of the structure (Release, 2007).

Topology optimization is actually the optimization of spatial materials distribution. Its method solves the basic engineering problem of distributing a limited amount of material in a design space. The first paper on topology optimization was published over a century ago by the versatile Australian inventor Michell, who derived optimality criteria for the least weight layout of trusses. In 1976, Prager and Rozvany formulated the first general theory of topology optimization, termed "optimal layout theory". After that, structural topology optimization has been extensively explored, especially for continuum structures (Rozvany, 2008). Many optimization methods such as the Homogenization Technique, Solid Isotropic Material with Penalization (SIMP), Evolutionary Structural Optimization (ESO) and Bi-directional Evolutionary Structural Optimization (BESO) have been developed.

There are analytical methods and numerical methods for structural topology optimization. The Michell theory is an analytical method, developed early and has a great influence on structural topology optimization study, but still has many difficulties in practice. Numerical methods can be classified into two categories according to the structure is discrete or continuum. Ground structure approach (GSA) is earliest numerical method for discrete structures, while there are three main numerical methods for continuum structures, namely Material Interpolation method (include the most famous SIMP method), Evolutionary Structural Optimization (ESO) method and Level Set method.

Following the topology optimization of structures characterized by mathematical problems through the numerical methods, suitable mathematical optimization method needs to be selected and applied on the structures. As mentioned above, three main categories mathematical optimization methods are available, namely mathematical programming techniques, optimality criteria approaches and heuristic algorithms. During the optimization procedure, there will be some numerical instability problems with the use of finite element analysis software, such as porous, checkerboard, mesh dependency and local minimum that will directly affect the convergence and the results.

### *2.3.1 Material Interpolation Method*

The presently most popular numerical FE-based topology optimization method is the material interpolation method, in which the Solid Isotropic Material with Penalization (SIMP) are most famous and widely applied in the topology optimization (Bruns, 2005, Rozvany, 2001). The basic idea of this approach which so-called Homogenization approach was proposed by Bendsøe in the landmark paper (Bendsøe and Kikuchi, 1988, Sigmund, 2001). Following this idea, numerical methods for topology optimization have been investigated extensively since the late 1980s.

Homogenization approach (Bendsøe and Sigmund, 1999, Suzuki and Kikuchi, 1991) introduced a material model that allow the density of material to cover the complete range of values from 0 (void) over intermediate values (composite) to 1 (solid), namely the hole-in-cell microstructure as shown in Fig. 2 that consists of an isotropic material with rectangular holes (Eschenauer and Olhoff, 2001). For the topology optimization, the orientation  $\theta(x)$  of the microscopic cells and their geometry defined by the length of  $a$  and  $b$ , are applied as design variables. Microstructures are classified as the void that contains no material as  $a$  and  $b$  equal to 0, the solid medium which contains isotropic material as  $a$  and  $b$  equal to 1, and the generalized porous medium which contains orthotropic material for intermediate values of  $a$  and  $b$ .

The components of the stiffness matrix for the microstructure can be obtained numerically on the basis of homogenization for different sets of values of  $a$  and  $b$ . For expedience, the components of the effective stiffness matrix are normally represented as functions of  $a$  and  $b$  via approximation formulas. Therefore, through

the introduction of material model, the structural topology optimization problem is envisioned as finding the optimal material distribution within a prescribed admissible design domain  $\Omega$  while the criteria and constraints are satisfied. As a consequence, the homogenization is utilized to analyze the composite structure.

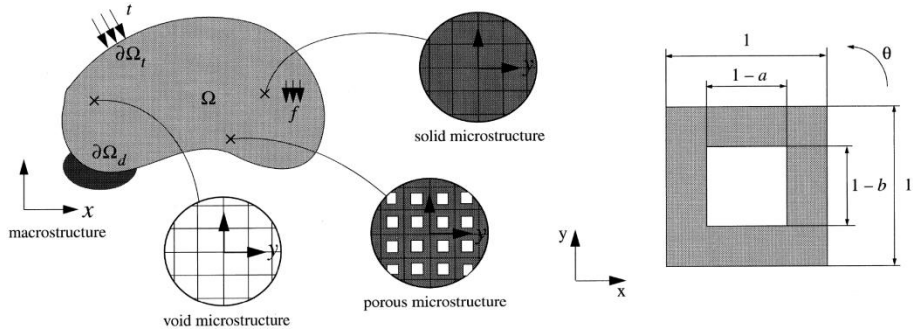


Fig. 2 Microstructure for 2D continuum topology optimization problems (Min, et al., 2000)

Shortly after the homogenization approach to topology optimization was introduced, Bendsøe (Bendsøe, 1989) suggested the so-called SIMP or power-law approach, which first was meant as an easy but artificial way of reducing the complexity of the homogenization approach and improving the convergence to 0-1 solutions. Later a physical justification of SIMP was provided by Bendsøe and Sigmund (Bendsøe and Sigmund, 1999). In the SIMP approach the relation between the density design variable and the material property is given by the power-law, e.g.

$$E_{ef}(\rho_i) = g(\rho_i)E = \rho_i^q E \quad (4)$$

Where  $q$  is the penalization parameter and  $E$  is the Young's modulus of solid material. For  $q$  equal to 1 the optimization problem corresponds to the so-called "variable-thickness-sheet" problem, while  $q$  larger than 1 penalizes intermediate thickness or densities and hence favors 0-1 solutions for the same objective. Choosing  $q$  too low or too high either causes too much grey scale or too fast convergence to local minima (Sigmund and Maute, 2013), its effectiveness can be seen from Fig. 3.

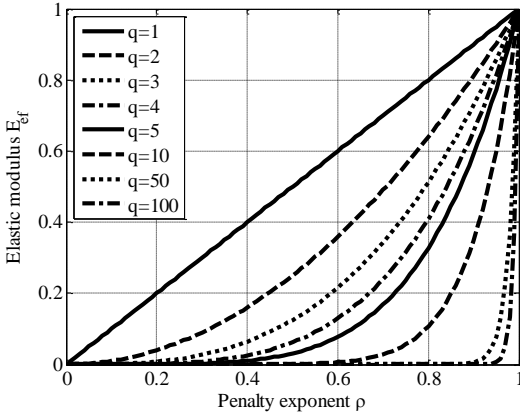


Fig. 3 Actual elastic modulus vs. penalty exponent of SIMP method

When SIMP method implemented into FE code, it is based on the assumption that the stiffness matrix of each element is proportional to its density. If  $E$  is the actual elastic modulus of the material,  $E_{ef} = \eta E$  is defined as the “effective” elastic modulus of each element, lower than  $E$  in design regions with relative pseudo-density  $\eta$  lower than 1. The pseudo-density is defined as  $\eta = \rho^q$ , where  $\rho$  is the relative density referred to the actual density of the material and continuously varying between 0 and 1,  $q$  is a penalty exponent that, for values sufficiently higher than 1 (normally  $q > 3$ ), makes elements with intermediate values of  $E_{ef}$  unfavorable for an economical use of material, thus highly reducing their number in the optimal solution.

Based on these assumptions, the contribution of elements with  $\rho$  nearly 0 to the global stiffness matrix (and therefore to the model compliance), as well as the effect of their removal, is negligible. By referring to the assumed relationship between material properties and density, the design variables were the internal pseudo-densities assigned to each finite element ( $i$ ), whose stiffness matrix was proportional to  $\eta E = \rho^q E$ .

Discretization with finite elements (numbered as  $i=1 \dots N$ ) allows to define  $\mathbf{u}$  and  $\mathbf{f}$  as the displacement and load vectors, respectively, so that compliance  $C = \mathbf{f}^T \mathbf{u}$  could be minimized. The SIMP method was hence performed as a minimum compliance design, where a material distribution problem was to be solved. Since  $\mathbf{K}\mathbf{u} = \mathbf{f}$ , then  $\mathbf{f}$  is related to  $\mathbf{u}$  through the global stiffness matrix  $\mathbf{K}$ , the latter being proportional to the effective elastic modulus  $E_{efi} = \eta_i E$  of each element  $i$ . Hence, if  $V$  is the total volume of the structure after topology optimization, assigned as a percentage of the actual volume  $V_0$  of the structure before the topology optimization process, minimization of compliance  $C$  leads to:

$$\min_{E_{efi}, u_i} \mathbf{f}^T \mathbf{u} \quad (5)$$

and allows to obtain the pseudo-density value  $\eta_i$  in each element for:

$$0 \leq \eta_i \leq 1 \quad \text{and} \quad V = \sum_{i=1}^N \eta_i V_i \leq V_0 \quad (6)$$

After having evaluated the volume  $V_0$  before inserting holes, topology optimization was hence performed by minimizing compliance  $C$  (that is maximizing stiffness) for different given  $VR = (V_0 - V) / V_0$ , thus obtaining a range of solutions.

The SIMP method is a very efficient structural optimization approach that has demonstrated its effectiveness in a large number of examples. It is also the method implemented in many commercial tools (OptiStruct, Genesis, MSC/Nastran, ANSYS, etc.) performing topology optimization. Take the ANSYS for example, the general optimization problem statement of SIMP method implemented in ANSYS is briefly introduced.

The theory of topological optimization seeks to minimize or maximize the objective function ( $f$ ) subject to the constraints ( $g_j$ ) defined. The design variables ( $\eta_i$ ) are internal pseudo-densities that assigned to each finite element ( $i$ ) in the topological problem. The pseudo-density for each element varies from 0 to 1, where  $\eta_i \approx 0$  represents material to be removed, and  $\eta_i \approx 1$  represents material that should be kept. Stated in simple mathematical terms, the optimization problem is as follows:

$$f = \eta_i \quad (\min, \max) \quad (7)$$

Subject to:

$$\begin{cases} 0 < \eta_i \leq 1 & i = 1, 2, 3, \dots, n \\ \underline{g}_j < g_j \leq \bar{g}_j & j = 1, 2, 3, \dots, m \end{cases} \quad (8)$$

Where:  $n$  = number of elements;  $m$  = number of constraints;  $g_j$  = computed  $j$ -th constraint value;  $\underline{g}_j$  = lower bound for  $j$ -th constraint;  $\bar{g}_j$  = upper bound for  $j$ -th constraint.

Common for all the material interpolation approaches is that they represent smooth, differentiable problems that can efficiently be solved by well-proven, gradient-based optimization approaches such as optimality criteria methods, the method of moving asymptotes (MMA) or by other mathematical programming-based optimization algorithms. Apart from OC methods, these optimizers also immediately allow for systematic and straightforward inclusion of additional global constraints. However, while formally it is easy to include local constraints as well, parameterization issues as seen in stress constrained problems may render such problems quite hard to solve in practise (Sigmund and Maute, 2013).

### *2.3.2 Evolutionary Structural Optimization (ESO) Method*

The evolutionary structural optimization (ESO) technique (Huang and Xie, 2008, Xie and Steven, 1993) was originally proposed in 1992 by Professors Mike Xie and Grant Steven. They aimed to develop a very simple but versatile technique for finding optimal structural designs (Xie and Steven, 1993). ESO is based on the concept of slowly removing inefficient materials from a structure so that the residual structure evolves towards the optimum. Practically all aspects of structural behavior can be accommodated within the ESO concept and the optimality constraints can be stress based, stiffness/displacement based, frequency based, buckling load based, with single or multiple environments.

ESO method uses the concept of gradually removing (“hard-kill”) redundant material from a structure based on von Mises stress or strain energy of each element so that the resultant structure evolves toward an optimum (Abolbashari and Keshavarzmanesh, 2006). Compared with other existing methods, the ESO method is much more straightforward and involves no mathematical programming techniques in the optimization process. In fact it can be easily implemented into any general purpose finite element analysis (FEA) program (Chu, et al., 1996, Tanskanen, 2002).

Bidirectional evolutionary structural optimization (BESO) method (Young, et al., 1999) is an extension of ESO, which allows for inefficient materials to be removed from a structure at the same time as the efficient ones to be added. In so doing, the BESO method greatly improves the robustness of the solution process compared to traditional ESO method (Huang and Xie, 2008).

However, the ESO and BESO may result in a non-optimal when these methods are implemented and used. G. I. N. Rozvany (Rozvany, 2008) gave a critical review of ESO method and pointed out some critics. Such as ESO is fully heuristic and exists no rigorous proof that element eliminations or admissions on the above basis do give an optimal solution, ESO procedure cannot be easily extended to other constraints or to multi-load or multi-constraint problems, it is not particularly efficient if designers have to select the best solution by comparison out of a very large number of intuitively generated solutions. Moreover, he pointed out although ESO usually requires a much greater number of iterations than gradient-type methods, it may yield an entirely non-optimal solution even with respect to ESO's objective function, and he verified that through a simple example of cantilever beam in a very brief note (Edwards, et al., 2007, Zhou and Rozvany, 2001).

### 2.3.3 Level Set Method

The level set method (LSM) is a numerical technique proposed by American mathematicians Stanley Osher and James Sethian in the 1980s (Osher and Sethian, 1988) for tracking interfaces and shapes. It has widely application in many disciplines, such as image processing, computer graphics and etc.. In 2000, Sethian and Wiegmann introduced the concept of level set method to structural optimization firstly (Sethian and Wiegmann, 2000, Xia, et al., 2012).

In the level set method, the boundary of the design is defined by the zero level contour of the level set function  $\phi(x)$  and the structure is defined by the domain where the level set function takes positive values, i.e.

$$\rho = \begin{cases} 0: & \forall \mathbf{x} \in \Omega: \phi < 0 \\ 1: & \forall \mathbf{x} \in \Omega: \phi \geq 0 \end{cases} \quad (9)$$

In the past decade numerous level set methods have emerged which can be classified, for example, by the approach for discretizing the level set function, the approach for mapping the level set field onto the mechanical model, and the approach for updating the level set field in the optimization process (Sigmund and Maute, 2013, Wang, et al., 2003).

In contrast to density methods, level set method define the geometry of the structure via the definition of a solid void interface. The principal idea of level set method is to



remove material in regions of low stress and to add material in regions of high stress. A removal rate is established representing a percentage of the maximal initial stress below which material may be eliminated, and above which material should be added. The biggest benefit of this approach is that it is easier to add material at holes' boundaries with high stress than on a triangulated finite element mesh. This approach seeks to improve design by making more efficient use of the material (Allaire, et al., 2002, Osher and Fedkiw, 2001, Wang, et al., 2003).

#### *2.3.4 Numerical Instabilities*

Although the topology optimization method of continuum structures developed speedily from the landmark paper of Bendsoe and Kikuchi and has reached a level of maturity when applied in structural problems, there still exist a number of problems concerning checkerboard, mesh dependency and local minima.

Checkerboard refers to the problem of formation of regions of alternating solid and void elements ordered in a checkerboard like fashion. The appearance of these regions is due to bad numerical modeling of the stiffness of checkerboards and has nothing to do with the approach no matter of homogenization or SIMP method. Diaz and Sigmund (Diaz and Sigmund, 1995) compared the stiffness of checkerboard configurations in a discretized setting to the stiffness of uniformly distributed materials and concluded that the checkerboard structure has artificially high stiffness, which works provide useful guidelines regarding choice of stable elements (Sigmund and Petersson, 1998).

Mesh dependency refers to the problem of not obtaining qualitatively the same solution for different mesh-sizes or discretization. There are two categories of mesh-dependence problems, namely the problem of (necessarily) obtaining finer and finer structure with mesh refinement, which is due to nonexistence of solutions, and problems with many optima, i.e. non-unique solutions. The latter cannot be removed, but by introducing manufacturing constraints such as a minimum area constraint a less oscillating solution can be determined. While the former can be prevented with the utilization of filtering methods such as Restriction Methods, Local Gradient Constraint and Mesh Independent Filtering (Sigmund and Petersson, 1998, Sigmund, 2007).

Local minima refers to the problem of obtaining different solutions to the same discretized problem when choosing different algorithmic parameters or different initial starting point. Therefore, small variations in initial parameters such as move limits, geometry of design domains, number of elements, perimeter constraint value or filter parameter, etc., can result in drastically changes in the "optimal design". Until now, there is no effective method to overcome the problem of local minima, especially for multi-objectives, multi-constraints and complex topology optimization problems. Generally two measures can be used to reduce the impact of local extreme problems, one is considering a suitable optimization algorithm to looking for global optimum, and another is trying to starting from different initial value and select better optimization results.

## CHAPTER 3

**3. PROPOSED OPTIMIZATION INDEX**

Structural optimization has become in the last decades an important mathematical tool for designers. Among the different optimization techniques, sizing and shape optimization allow for identification of structural solutions and layouts characterized by a better exploitation of material, thus decreasing self-weight of structure and saving material costs, topology optimization aids the designers to find the most suitable shape of a structure from a structural and an architectural point of view, which leads to the definition of voids patterns delimiting regions where fluxes of force migrate from force application point to boundary regions.

With the powerful tool of topology optimization, designers can obtain families of candidate solutions by modifying input volume reduction (*VR*) ratio thus reducing structural weight as much as possible. However, find the best compromise between material saving and structural performance among these candidate solutions is a critical issue for designers. To face this issue, an optimization index (*OI*) was originally defined concomitantly with the structural optimization of a steel concrete arch bridge built in San Donà in the province of Venice, Italy (Briseghella, et al., 2012). It provides to the designer a mathematical procedure able to highlight the best choice among several candidate solutions obtained by the optimization procedure.

Moreover, during earlier designing phases of a project, in particular in the case of spatial shell structures, several starting trial solutions as well as tentative solutions might be defined based on the judgment of designer, each solution characterized by a particular layout, material property or distribution of boundary conditions. In this case, structural optimization is still a viable tool to optimize structures, but it would lead to the definition of entire families of possible candidate solutions, depending on input *VR* target and tentative starting models through particular layout, different material property or boundary condition. Therefore, the problem is changed from single-family multi-solutions to multi-families multi-solutions.

In this thesis, a specific scaling factor vector  $\alpha$  is introduced in the *OI* and a generalized version of the original optimization index (*OI\**) is defined. Based on the

$OI^*$ , through the introduction of weight vector  $w$ , a further  $GOI^*$  formulation is presented. The proposed generalized optimization index allows not only to identify best candidate solution originated by a unique reference model, but even comparing structural performances between candidates solution derived by several starting trial solutions.

### 3.1. Optimum Index Formulation for Single-Family Multi-Solutions

The optimization index ( $OI$ ) was originally defined by Briseghella et al. 2012, and has been published in the *Journal of Bridge Engineering*. However, to present to the reader clearly and consecutively, the identified process of  $OI$  was introduced in this section again.

During structural optimization, immediately following the topological optimization procedure on structures, several candidate design solutions with voids for each starting layout are generally defined, as many as input volume reductions. Although the design objective of topology optimization is reduction of structure self-weight, the increase of volume reduction generally causes a variation of both stress distribution and deflection level, whose control is therefore a competing requirement with respect to volume reduction itself. Hence, a way of identifying the most suitable design solution that presents the best compromise between material saving and structural performance among all these different optimized layouts with holes has to be defined.

Since a set of optimum layouts with holes were obtained from topology optimization for different values of volume reduction, a specific optimization index was introduced to give the designer a specific mathematical tool to identify the most suitable design solution. Such an index had to take into account volume reduction (and therefore weight reduction) together with the structural response in terms of both stress and deformation level.

To summarize the overall behaviour of the whole structure, stress index and deformation index were identified as representative of structural response. The former could be the average stress or maximum stress throughout the whole structure that considered as representative of stress level, while the latter could be the maximum deflection at mid-span or at tower top for cable-stayed bridge that was considered as representative of deformation level.

Two Response Indexes ( $RI$ s) were then identified in terms of percentage variation of deformation and stress level with respect to their corresponding values obtained in the starting model (without holes) under same loading condition, that is:

$$RI(\sigma, i) = \frac{\sigma_i - \sigma_0}{\sigma_0}; \quad RI(d, i) = \frac{d_i - d_0}{d_0} \quad (10)$$

In this index  $i$  refers to considered  $i$ -th solution,  $\sigma_0$  and  $d_0$  are the stress and deformation of starting model (without structural optimization),  $\sigma_i$  and  $d_i$  are the stress and deformation of  $i$ -th solution. Response Index ( $RI$ ) is defined in terms of percentage variation of a parameter representative of the behavior of  $i$ -th candidate solution compared to reference one, that is the starting model (without optimization) under the same loading condition.

Although the design is focus on the reduction of objective like as superstructure weight, cable volume, reaction force and etc., the increase of volume reduction causes an increase of both stress level and deflections, whose control is therefore a competing requirement with respect to volume reduction.

Hence, a way of identifying the most suitable design solution among all these different optimised layouts with holes had to be defined. For this purpose, the variation of structural response with respect to the variation of volume reduction can be compared by defining the ratio  $RI/VR$  as optimization index or, conversely, its complement to 1, that is:

$$OI(i) = 1 - \frac{RI(i)}{VR(i)} = [VR(i) - RI(i)] \cdot \frac{1}{VR(i)} \quad (11)$$

$VR$  and  $RI$  are the volume reduction and response index of  $i$ -th solution, respectively. Graphical interpretation of optimization index is shown in Fig. 4, in which both  $VR$  and  $RI$  are expressed in percent, thus varying between 0 and 100.

Considering the cartesian plane where  $VR$  is the  $x$ -axis and  $RI$  the  $y$ -axis, the difference  $VR - RI$  represents the distance between the plane bisetrix and the  $RI$  curve. By scaling the difference  $VR - RI$  through the coefficient  $1/VR$  for each value of volume reduction  $VR$ , the distances between the  $RI$  curve and the plane bisetrix results decreased to  $(VR - RI)/VR$ , so that a curve whose distance from the abscissa

axis is  $VR-(VR-RI)/VR$  is so obtained (Fig. 4 a). Conversely, a curve whose distance from the bisetrix is  $VR-(VR-RI)/VR$  and from the abscissa axis is  $(VR-RI)/VR$  can also be obtained (Fig. 4 b). The latter curve is therefore the *OI* curve defined as above, and therefore expressed in percent as *VR* and *RI*.

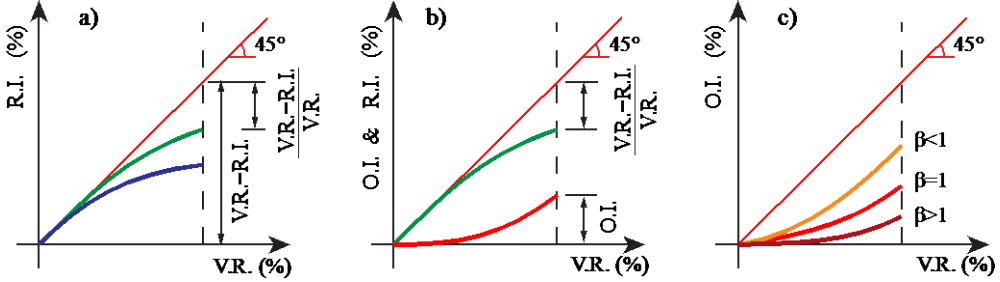


Fig. 4 Graphical interpretation of optimization index

Since the optimization objective was lightening the bridge in most specific engineering case, it was then worth modifying the scaling coefficient  $1/VR$  through a penalty exponent able to favour design solutions with higher volume reduction. For this purpose, after introduction of the penalty exponent, the scaling coefficient became  $(1/VR)^\beta$ , where values of the penalty exponent between 0 and 1 favour design solutions with higher volume reduction, while values higher than 1 favour design solutions with higher performances but higher self-weight, and therefore not convenient to lighten the bridge (Fig. 4 c). Hence, the updated expression of the optimization index *OI* through introduction of the penalty exponent is:

$$OI(i) = [VR(i) - RI(i)] \cdot \frac{1}{(VR(i))^\beta} \quad (12)$$

$\beta$  is a penalty exponent, usually between 0 and 3, able to favor design solutions with lower or higher volume reduction according to  $\beta$  is higher or lower than 1. The application of the penalty exponent  $\beta > 0$  to the scaling factor  $1/VR$  results therefore in lower values of *OI* for  $\beta < 1$  and in higher values for  $\beta > 1$ .

From the left chart of Fig. 5, it can be seen that for  $\beta > 1$  the scaling factor  $(1/VR)^\beta$  as a function of *VR* tends to become a bilinear curve (the more bilinear the curve the higher is  $\beta$ ). In addition, with a vertical branch for *VR* closer to 0, and a horizontal branch whose values are almost 0 in the range of volume reduction values that are significant in the design of the bridge under consideration. On the contrary, for  $\beta < 1$ ,

the scaling factor  $(1/VR)^\beta$  plotted as a function of  $VR$  approaches a hyperbole for  $\beta$  closer to 1, tending to become an horizontal line for  $\beta$  closer to 0.

Hence, while for  $\beta > 1$  design layouts with holes are not favoured and those with low values of volume reduction are conversely favoured already for  $\beta$  slightly higher than 1, for  $\beta < 1$  design solutions with high volume reduction are instead favoured, the higher the volume reduction the lower is  $\beta$ .

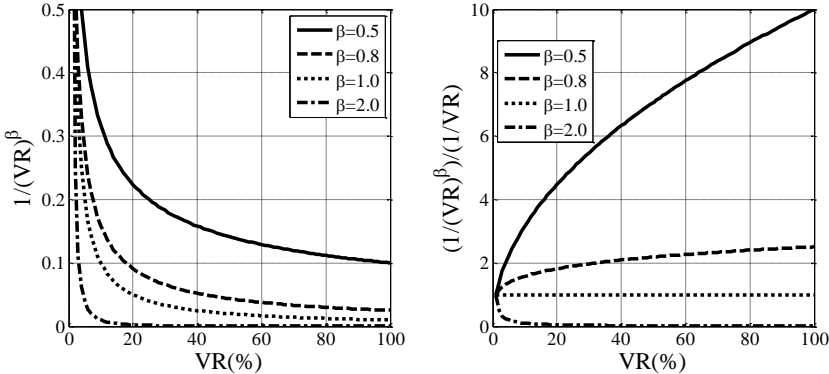


Fig. 5 Scaling factor  $1/VR$  with penalty exponent  $\beta$  vs.  $VR$

In the right chart of Fig. 5, the ratio  $R(\beta)=(1/VR)^\beta/(1/VR)$  is plotted for different values of  $\beta$ . It can be seen that for  $\beta=2$  the ratio  $R(\beta=2)$  is roughly 0 for almost every value of  $VR$ . On the contrary, for  $\beta=0.5$  the ratio  $R(\beta=0.5)$  is a steep function of  $VR$ , meaning that the scaling factor with penalty exponent 0.5 becomes much higher than the one without the penalty exponent even for low values of  $VR$ , becoming 10 times  $1/VR$  for  $VR=100\%$ . An intermediate trend is observed for  $\beta=0.8$ , with  $R$  initially slightly steep, and then even less steep until the value of only 2.5 times  $1/VR$  is reached for  $VR=100\%$ .

Hence, although in general values of  $\beta$  less than 1 favour design solutions with significant volume reduction, values of  $\beta$  less than but suitably close to 1 are able to favour design solutions with intermediate values of volume reduction.

Eventually, since the expression of the above optimization index is referred to a specific structural response in terms of stress or deformation, a global optimization index ( $GOI$ ) considering both these features of structural response can be also defined. By giving the same weight to both deformation and stress level, a global optimization index averaging the two optimization indexes referred to stresses and deformations is then defined as:

$$GOI(i) = (OI(A,i) + OI(d,i)) / 2 \quad (13)$$

With the *GOI*, a suitable score for each design solution is assigned. The one with highest score is the optimum solution that better balances material saving and overall performance of the structure.

### 3.2. Generalized Version for Multi-Families Multi-Solutions

Original formulation for the *OI* reveals itself effective when a unique reference starting layout is clearly identified. However, during earlier designing phases of a project designers could be interested in comparing the behavior of different tentative solutions for the same structure, on the basis of their own engineering judgment. Each trial solution could be characterized like as by different boundary condition, different starting layout or both. If structural optimization procedure applied to each starting solutions, entire families of candidate solutions with voids will be defined depending on input *VR* and trial models. Therefore, the identification of the best overall layout solution becomes a multi-families multi-solutions comparison. To face this issue, and compare performances of different starting models, a specific scaling factor vector  $\alpha$  is introduced in the *OI*. Hence, a generalized version of optimization index *OI\** is proposed:

$$OI(i, j)^* = \alpha_j \cdot [VR(i) - RI(i)] \cdot \frac{1}{(VR(i))^\beta} \quad (i = 1, 2, 3, \dots, m; j = 1, 2, 3, \dots, n) \quad (14)$$

Where *i* refers to considered *i*-th solution as before, *j* refers to *j*-th family that is the different starting model has been defined. *m*, *n* are the number of solutions for each starting model and number of starting models, respectively. Corresponding to response indexes (*RIs*), scaling factors  $\alpha_j$  are formulated both in term of stress and deformation level. They are calculated by comparison of *j*-th starting model response with that of the reference 0-model. The latter can be chosen among all the starting models, without altering the final scoring results given by *OI\**. The value of scaling factors  $\alpha_j$  can be calculated as follows:



$$\left\{ \begin{array}{l} \alpha(A, j) = 1 - \frac{A_{0,j} - A_{0,0}}{A_{0,0}} + \min_{j=1,2,3,\dots,n} \frac{A_{0,j} - A_{0,0}}{A_{0,0}} \\ \alpha(d, j) = 1 - \frac{d_{0,j} - d_{0,0}}{d_{0,0}} + \min_{j=1,2,3,\dots,n} \frac{d_{0,j} - d_{0,0}}{d_{0,0}} \end{array} \right. \quad (15)$$

For a specific  $j$  index,  $A_{0,j}$  and  $d_{0,j}$  are stress and deformation level of the  $j$ -th starting model without volume reduction, respectively.  $A_{0,0}$  and  $d_{0,0}$  are the corresponding value of the reference starting 0-model.

The formulation for  $\alpha$  mainly consists of a percentage variation with reference to starting model of parameter chosen for  $Rl$  (i.e. stress or deformation level). Vector  $\alpha$  is then representative of static behavior of each starting model compared to the 0-model. Additional terms have a scaling effect on the index  $\alpha$ . As model with good static behavior leads to low stress and deformation ratios, the negative of it is considered. Therefore, starting model with better behavior has higher  $\alpha_j$  value. To set the  $\alpha_j$  of starting model with best static performance to 1, the last part which is minimum value of central part is added. Thus  $\alpha_j$  is always less than unity and bigger than 0.

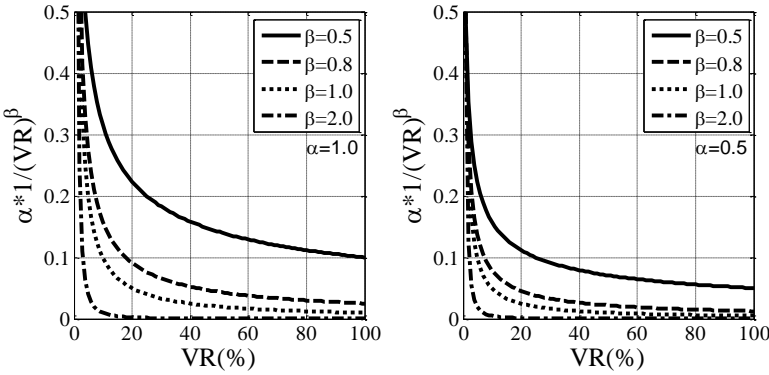


Fig. 6 Scaling component with penalty exponent  $\beta$  and scaling factor  $\alpha$

The contribute of expression  $\alpha^*(1/VR)^\beta$  from optimization index  $OI^*$  formula is plotted in Fig. 6 as a function of  $VR$ , considering different scaling factor  $\alpha$  and penalty exponent  $\beta$ . The  $\beta$  parameter should be set based on the judgment of engineer. On the one hand, it can be seen that the scaling component increases exponentially as  $\beta$  rising, so that penalty exponent  $\beta$  favor design solutions with higher volume reduction. On the other hand, the scaling component increases linearly as  $\alpha$  rising, meaning that scaling factor  $\alpha$  highlight starting models with better static behavior. Hence, the proposed optimization index ( $OI^*$ ) takes into account

performances from different starting models with different volume reduction together and assigns score properly to each design solution of the entire candidate domain.

Finally, since the expression of the above optimization index is referred to a specific structural response in terms of stress or deformation, global optimization index ( $GOI^*$ ) considering both these features of structural response is defined as the original defined optimization index ( $OI^*$ ).

In the originally optimization index,  $GOI$  is defined by averaging the two optimization indexes referred to stresses and deformations. However, in real cases with high stiffness such as the shell structures, the deformation is slightly affected by the insertion of holes while the stress is highly sensitive to the  $VR$ . Sometimes it can be huge difference of the influence due to the rigidity of the structure. Therefore, to consider the effect size of two  $OIs^*$ , through the introduction of weight vector  $\mathbf{w} = (w_1, w_2)$  rather than giving the same weight to deformation and stress level, a  $GOI^*$  is then defined as:

$$GOI(i, j)^* = w_{1j} \cdot OI(A, i, j)^* + w_{2j} \cdot OI(d, i, j)^* \quad (16)$$

The weight vector is calculated according to the  $RIs$ :

$$w_{1j} = \frac{\sum_{i=1}^m |RI(\sigma, i)|}{\left( \sum_{i=1}^m |RI(\sigma, i)| + \sum_{i=1}^m |RI(d, i)| \right)}; \quad w_{2j} = 1 - w_{1j} \quad (17)$$

Through the introduction of scaling factor  $\alpha$ , which calculate from the performances comparison of tentative starting models, the starting model with better mechanical behavior in terms of stress and deformation level has higher  $\alpha$  value and is highlighted from all the starting models. In the same way, higher  $GOI$  value is assigned to the starting model with better static performance. Through the introduction of weight vector  $\mathbf{w}$ , the effect size of two  $OIs^*$  is considered. Hence, the application domain of optimization index to identify the best overall layout solution is extended from 1-D linear to 2-D surface, as well as proposed  $GOI^*$  not only can be used for a single-family multi-solutions comparison but also for a multi-families multi-solutions comparison.

## CHAPTER 4

## 4. FOOTBRIDGES SUPPORTED BY CONCRETE SHELL

Shell supported bridges, which deck is supported by a shell structure, are special spatial shape obtained by means of a form-finding algorithm in order to achieve mainly membrane stresses and avoid bending effects. When designing bridges supported by a shell in reinforced concrete (RC), it is worth choosing shells with minimal area that, being anticlastic and therefore subject to biaxial compression (Fluegge, 1973), well exploit the compressive strength of concrete and prevent crack propagation. Shells of minimal area can fluently and efficiently transfer loads from their points of application to the bridge foundations. The problem was studied in depth by outstanding structural designers, with special reference to Frei Otto (Otto, et al., 1973) and Sergio Musmeci (Musmeci, 1977).

Musmeci was the first to apply this principle to bridges, thereby following in the footsteps of Robert Maillart in removing unexploited material from arch bridges. Robert Maillart, an eminent Swiss designer of RC bridges who developed a well-known typology of RC arch bridges named thereafter as Maillart Bridges, constructed many RC bridges of this type in Swiss Alps. Some of his well-known masterpieces include the Töss Bridge (Fig. 7), Schwandbach Bridge etc. which are recognized as outstanding works by some of the most eminent historians of Modern Architecture. In Maillart bridges, the infill between arch and deck (typical of masonry arch bridges) is removed, while a specific structural duty is assigned to each member. In fact, deck loads are clearly transferred to the shell arch by means of vertical walls, reaching the arch foundations through the abutments.

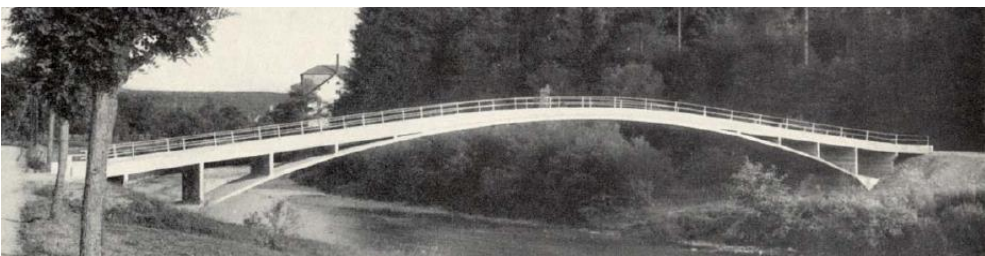


Fig. 7 Töss Bridge - R. Maillart, 1933, Zurich (Switzerland)

Since the vertical walls of Maillart bridges caused stress concentration at their insertion with the shell arch, Musmeci corrected this by replacing both the shell arch and the vertical walls with a shell with double curvature, which supported the deck and fluently transferred deck loads to the bridge foundations. For this purpose, he shaped an anticlastic shell with minimal area, which when subjected to biaxial compression, avoided the occurrence of unwished bending moments (as it happened at the insertion between vertical walls and shell arch of Maillart bridges), thereby allowing better exploitation of concrete compressive strength.

As, for the given boundary conditions, tension structures are shaped as membranes of minimal area that well exploit materials with high tensile strength, Musmeci shaped the concrete shells supporting the deck of his bridges as membranes in tension between deck and foundations. By then inverting the sign of restraint forces and internal stresses, he obtained his fully compressed concrete shells. Through the above procedure, together with integration with finite differences of the membrane equations subjected to the required boundary conditions, he designed his masterpiece, the Basento Bridge in Potenza (Italy), made of RC, whose deck is supported by an amazing anticlastic shell (Fig. 8).



*Fig. 8 Basento Bridge - S. Musmeci, 1969, Potenza (Italy)*

Nowadays, with the widespread use of powerful computers, the design procedure developed by Musmeci through a joint use of physical and analytical models can be pursued by using numerical form-finding algorithms.

In this Chapter, three footbridges supported by concrete shell with different boundary conditions and thicknesses were obtained through a form-finding process. They are named as T\_0.15, T\_0.20 and T\_0.32 according to the shell thickness. It is pointed out that notwithstanding the use of form-finding algorithms in order to obtain a shell of minimal area subjected to biaxial compression, unwished tensile stresses caused by unwished bending moments unavoidably occur in some regions of the shell. Such unavoidable tensile stresses can be further eliminated by removing

material from the shell regions where unwished bending moments arise, thus obtaining a shell structure with cavities.

The method of suitably removing these shell regions by using topology optimization is shown below. Immediately following the form-finding process, a finite element topological optimization by means of Solid Isotropic Material with Penalization (SIMP) is carried out. After identifying the shell regions where the pseudo densities obtained from previous topological optimization results are lower, the geometries of the shells are updated by eliminating the material of these regions. With an iterative procedure of form finding and topological optimization, shells with pattern of holes are obtained and the areas of shell regions with low tensile stresses are minimized.

For each reference shell supported footbridge, three different starting models are defined, each characterized by the same boundary conditions but different edge stiffening. Depending on different input  $VR$  ratio, for each starting model, 4 candidate solutions with voids are defined. Hence, there are 36 candidate solutions in total that is  $3 \times 3 \times 4$  (reference model  $\times$  starting model  $\times$  input  $VR$ ). According to the results of all the candidate solutions, the proposed generalized optimization index, whose analytical formulation defined before is discussed in detail and its effectiveness is validated.

## 4.1. Shell-Supported Bridges Design

### 4.1.1 Shell Form-Finding

To obtain a shell with cavities by means of topology optimization, it was first necessary to design a shell footbridge with deck supported by a concrete shell of minimal area. Three shell footbridges with different boundary conditions were designed to cross a deep canyon (depth 80 m, width 40 m) located in the city of Cagliari (Italy) and named according to the thickness of the shell surface. Although Cagliari is located on the sea, the canyon topography is similar to that of the deep valleys of the Alps where Maillart built his daring and outstanding bridges.

The shell footbridges are shown in Fig. 9, and were shaped using a form-finding method described in (Fenu, 2005, Luigi Fenu, 2006). Each shell of the bridge was shaped as a compressed membrane with the same geometry as a tension structure with same loads, restraint reactions and internal normal forces, but with the opposite

sign. The form-finding algorithm modelled the tension structure as a cable net structure whose form was obtained by minimizing the distance between its nodes and their initial projections on a horizontal plane. Minimization was performed by means of a “simulated annealing” algorithm.



Fig. 9 Shell supported bridges crossing the deep canyon, Cagliari (Italy)

Although shells were shaped in order to avoid tensile stresses, and rise and restraint positions were chosen in order to reduce the occurrence of unwished bending moments, tensile stresses in any case occurred in some localized regions of shells. Because of second-order displacement will occur as shells in compression, contrary to tension structures, the bending stiffness of RC shells is not zero, the occurrence of undesired bending effects is unavoidable. This can be easily checked through modeling the footbridge by finite elements, as shown in the next section.

#### 4.1.2 Finite Element Model

The bridges were modelled with the finite element analysis software ANSYS. The finite element (FE) models of the shell footbridges are shown in Fig. 10. For each model, the deck was simply supported by pinned joints between deck and shell, and the rotations at shell abutments were free.

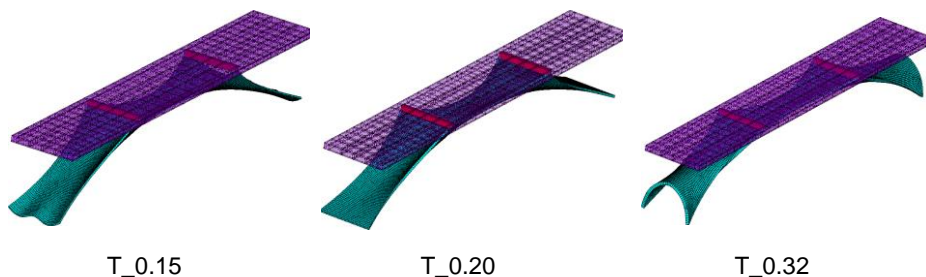


Fig. 10 FE model in ANSYS

The type of elements was chosen taking into account that, after the FE analysis,





topology optimization was to be performed. The shell element SHELL93 was chosen for the concrete shell, being supported by topology optimization implemented in ANSYS (Ansys, 2007). Also, BEAM188 was chosen for the deck girders, while BEAM4 was chosen for the transverse beams and the stiffening beams of the shell free edges. The total number of nodes and elements was shown in Table 3.

Model	Nodes	Shell93	Beam188	Beam4
T_0.15	26987	8800	30	4
T_0.20	25663	8360	30	4
T_0.32	24927	8080	30	4

*Table 3*  
Total number of nodes and elements

For each model, concrete with strength class C30/37 was chosen according to the Eurocode 2. Therefore, its characteristic cylinder strength was 30 MPa. Based on the Eurocode 2 formulation, the average tensile strength of concrete before cracking was 2.9 MPa ( $f_{ctm} = 0.30 f_{ck}^{2/3}$ ). The value of the modulus of elasticity was assumed to be 33 GPa. Poisson's ratio and material density were set, respectively, to 0.3 and 2500 kg/m<sup>3</sup>.

When defining the structural compliance as the objective or constraint of topological optimization, a linear structural static analysis have to be performed during optimization looping. It can be performed for a single load case or collectively for several load cases. In this shell supported bridges case, a uniformly distributed load of pedestrians of 4kN/m<sup>2</sup> was supposed, with 9 different load cases, as presented in Table 4. These load cases are not only defined as multiple compliance function thereafter as topological objective during topological optimization, but also used to calculate the static behavior of updated models with holes.

Load case	Loading condition(s)	Loading area(s)
1	Full length full width	
2	Full length half width	
3		
4	Half length full width	

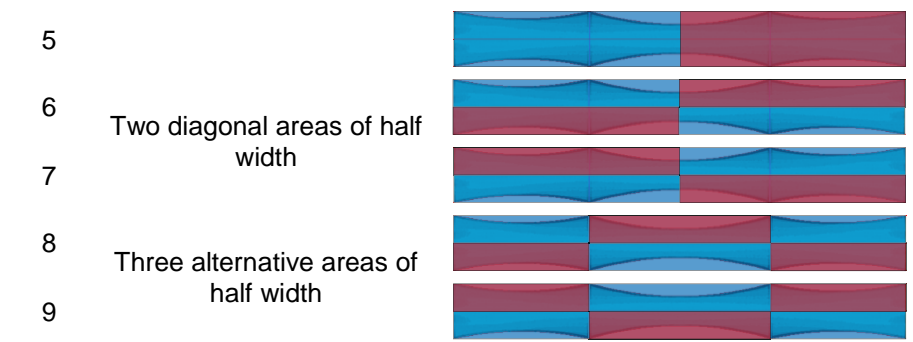


Table 4  
 The uniformly distributed load of pedestrians is 4 kN/m<sup>2</sup>

#### 4.1.3 Choice of Shell Thickness

Tensile stresses in the RC shell were caused by unwished bending moments, the thinner the shell, the higher the unwished tensile. Therefore, it was necessary to choose the most suitable shell thickness.

The shell thicknesses of three models were then optimized by using the design optimization tool implemented in ANSYS. It provides a zero-order method, where the dependent variables are first approximated by means of least squares fitting, and the constrained minimization problem is then converted to an unconstrained one by means of penalty functions, in order to be solved using Powell's modified method.

Shell thickness was assumed as a design variable with values ranging between 0.1m and 0.4m. The optimum thickness was found by minimizing the shell total weight on condition that stress level and deflection were lower than an allowable value. Since the optimum solution was found to depend on the initial values of shell thickness, different initial values were tried in order to avoid local minimum solutions. Where DV is the design variable, SV is the state variable (stress level and deformation level).

#### Shell bridge T\_0.15

The optimization procedure led to an optimum shell thickness of 0.156m. The actual thickness was then chosen to be 0.15m. Table 5 lists the optimization iterative process for an initial value of the shell thickness of 0.2m. The consistent decrease in



the objective function (and therefore the corresponding material saving) is well appreciable.

No.	Shell Thickness (m) (DV)	Max Stress (Pa) (SV)	Max Deformation (m) (SV)	Shell Volume (m <sup>3</sup> ) (OBJ)
SET 1	0.200	2.66E+06	-0.008	33.580
SET 2	0.184	2.79E+06	-0.009	31.014
SET 3	0.151	3.21E+06	-0.011	25.281
SET 4	0.145	3.39E+06	-0.011	24.466
SET 5	0.149	3.24E+06	-0.011	25.142
<b>*SET 6*</b>	<b>0.156</b>	<b>3.06E+06</b>	<b>-0.011</b>	<b>26.334</b>

Table 5

Shell thickness optimization of shell bridge T\_0.15

### Shell bridge T\_0.20

The optimization procedure led to an optimum shell thickness of 0.193m. The actual thickness was then chosen to be 0.20m. Table 6 lists the optimization iterative process for an initial value of the shell thickness of 0.3m.

No.	Shell Thickness (m) (DV)	Max Stress (Pa) (SV)	Max Deformation (m) (SV)	Shell Volume (m <sup>3</sup> ) (OBJ)
SET 1	0.300	2.09E+06	-0.012	51.517
SET 2	0.277	2.08E+06	-0.012	47.581
SET 3	0.218	2.35E+06	-0.015	37.536
SET 4	0.166	3.92E+06	-0.019	28.611
SET 5	0.213	2.43E+06	-0.015	36.61
SET 6	0.197	2.92E+06	-0.016	33.839
<b>*SET 7*</b>	<b>0.193</b>	<b>3.02E+06</b>	<b>-0.017</b>	<b>33.224</b>

Table 6

Shell thickness optimization of shell bridge T\_0.20

### Shell bridge T\_0.32

The optimization procedure led to an optimum shell thickness of 0.328m. The actual thickness was then chosen to be 0.32m. Table 7 lists the optimization iterative process for an initial value of the shell thickness of 0.3m.

No.	Shell Thickness (m) (DV)	Max Stress (Pa) (SV)	Max Deformation (m) (SV)	Shell Volume (m <sup>3</sup> ) (OBJ)
SET 1	0.300	3.19E+06	-0.011	52.488
SET 2	0.369	2.76E+06	-0.009	64.633
SET 3	0.291	3.26E+06	-0.011	50.990
SET 4	0.341	2.92E+06	-0.010	59.592
SET 5	0.331	2.97E+06	-0.010	57.909
<b>*SET 6*</b>	<b>0.328</b>	<b>3.00E+06</b>	<b>-0.010</b>	<b>57.321</b>

Table 7

Shell thickness optimization of shell bridge  $T_{0.32}$

#### 4.2. Topological Optimization

Although minimized by an appropriate choice of rise, shell thickness and boundary conditions, the occurrence of tensile stresses in some shell regions was unavoidable, thus suggesting the need of modifying the shell form by suitably removing material from these shell regions. Cavities were therefore inserted in the shell, whose form was shaped through topology optimization with Solid Isotropic Material with Penalization (SIMP) method, particularly suited when the optimal design solution has internal boundaries due to holes.

The removal through the SIMP method of material not working in compression for the arising of unwished bending effects was carried out by means of the topology optimization routine implemented in ANSYS. The SIMP method was therefore performed after having implemented a finite element model of the shell supported bridge by using ANSYS, and led to the insertion of cavities in the RC shell.

For an assigned value of volume reduction  $VR$ , the insertion of cavities through topology optimization included three main steps:

- (1) Finite element analysis for each load case (Table 4).
- (2) Topological optimization through the SIMP method: the pseudo-densities along the shell were mapped, taking into account all load cases (ANSYS).
- (3) Model updating: the model was updated by removing material (that means elements in FE model) with lower pseudo-densities, and the updated model was then analyzed through FE.

The above procedure was illustrated in Fig. 11. The procedure was then repeated for different values of volume reduction.

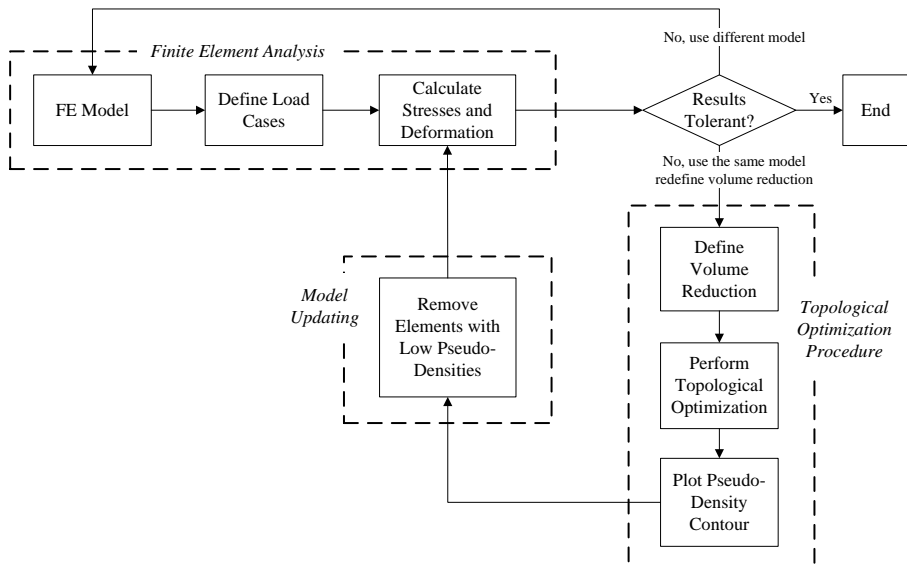


Fig. 11 Flowchart of the optimization procedure

#### 4.2.1 Different Models Considered

Although undesired bending moments can occur in fully compressed shells with minimal area, stiffening their free edges (analogously to tension structures usually stiffened by cables along their free edges) minimizes undesired bending effects not only along the free edges and close to them but also in the inner regions of the shell.

As the paper deals with topology optimization of the shell, in order to minimize the occurrence of unwished tensile stresses in the shell through the insertion of cavities that modify its form, the deck is not involved in the optimization process. Three different starting models were hence considered (Table 8):

- (1) Model I, where topology optimization was performed throughout the whole shell surface.
- (2) Model II, same as Model I, except than for the fact that the shell regions close to the edge (for a distance of 0.20m from the edge) were excluded from topology optimization.

(3) Model III, same as Model II, but stiffening beam elements (width 0.20m, same depth as the shell) were added along the free edges of the shell.

Stiffening the free edges of the shell with beam elements was equivalent to placing stiffening reinforcing bars along the free edges. Similar to stiffening cables, which are absolutely necessary along the free edges of a tension structure, stiffening bars were necessary along the free edges of the concrete shell, especially because the shell was shaped to be fully compressed. For instance, by using a homogenization factor of 15, stiffening the free edges through beam elements 0.20m by 0.15m were equivalent to adding three bars of 20 mm diameter (cover 30 mm) at both extrados and intrados of the shell.

Model	Shell without edge area optimization	Shell with edge stiffening beam
I	No	No
II	Yes	No
III	Yes	Yes

Table 8  
Different models considered

#### 4.2.2 Results of Shell Bridge T\_0.15

Adopting the shell thickness of 15 cm, as suggested in the *Choice of Shell Thickness* Section by thickness optimization, topological optimization of the shell was performed for different values of volume reduction *VR*. Also, topological optimization was applied to all the load cases so that for each value of *VR*, three pseudo-density contours (one per Model, each one obtained as an envelope of all load cases) were plotted (Table 9). All the pseudo-density contours turned out to be symmetric with respect to the symmetry axes of the bridge because even if each non-symmetric load case would have led to a non-symmetric pseudo-density contour. However, their corresponding mirrored load cases led to symmetric pseudo-density contours.

Volume reduction values of 5, 10, 20 and 30% were consequently applied. The plotting of the pseudo-density contours obtained through topology optimization is shown in Table 9. For all models, increasing the values of *VR* resulted in an increase in the area of shell surface with low pseudo-density (blue). This low-density region

(identified through the SIMP method) gradually extended by each part along the bridge from sections near the deck-supports to the abutments, so that from  $VR = 30\%$  onwards, close low-density regions tended to merge one with another, dividing the surface into two parts with higher density.

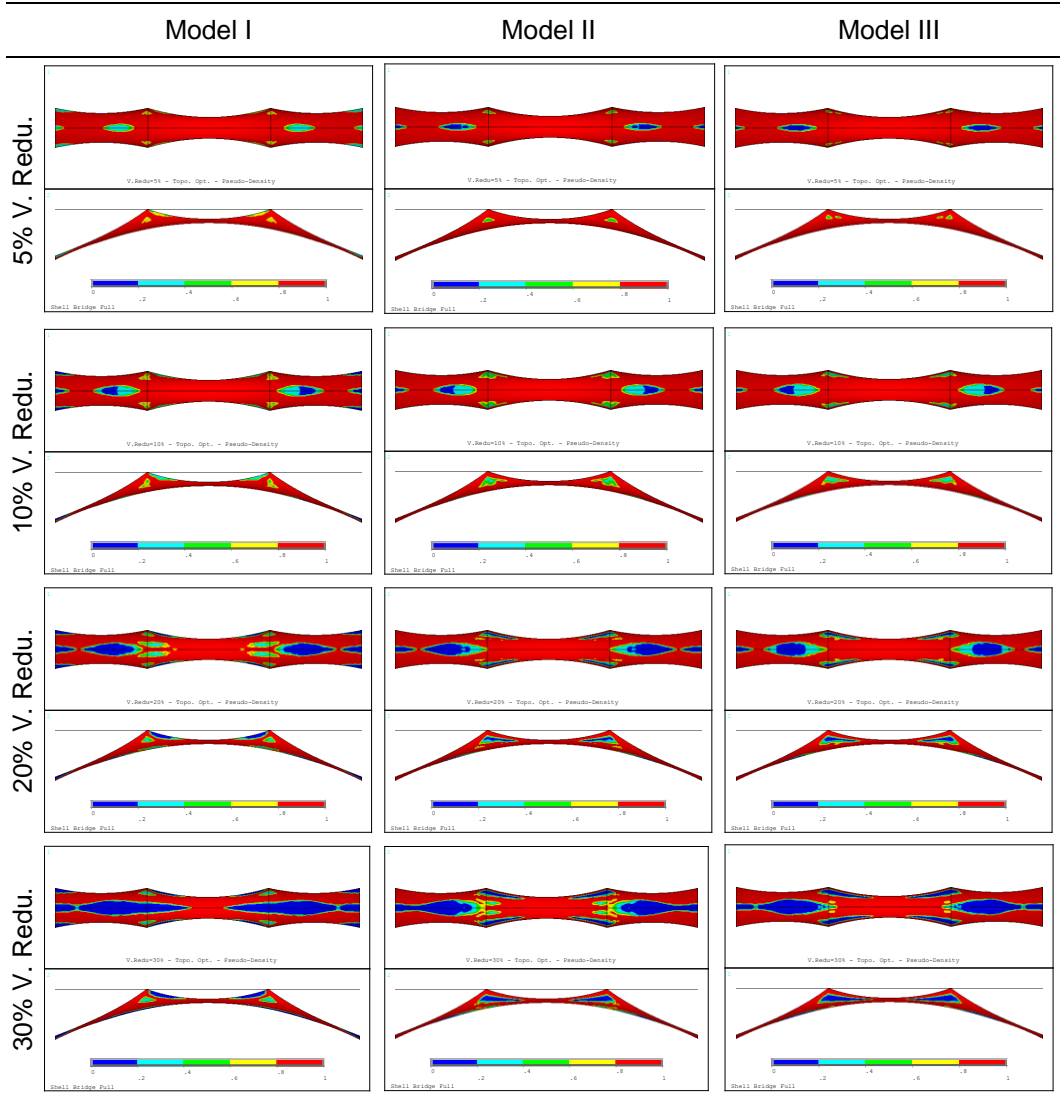


Table 9

Pseudo-density contours from topological optimization with the SIMP method of model  $T\_0.15$

**Stresses and deformations of the updated models with holes**

On the basis of the results of topological optimization, the three models were updated by removing the elements with pseudo-density lower than a specified value. As a consequence, the real volume reduction resulting after removing material was practically the same as that imposed to perform the topology optimization procedure (Table 10).

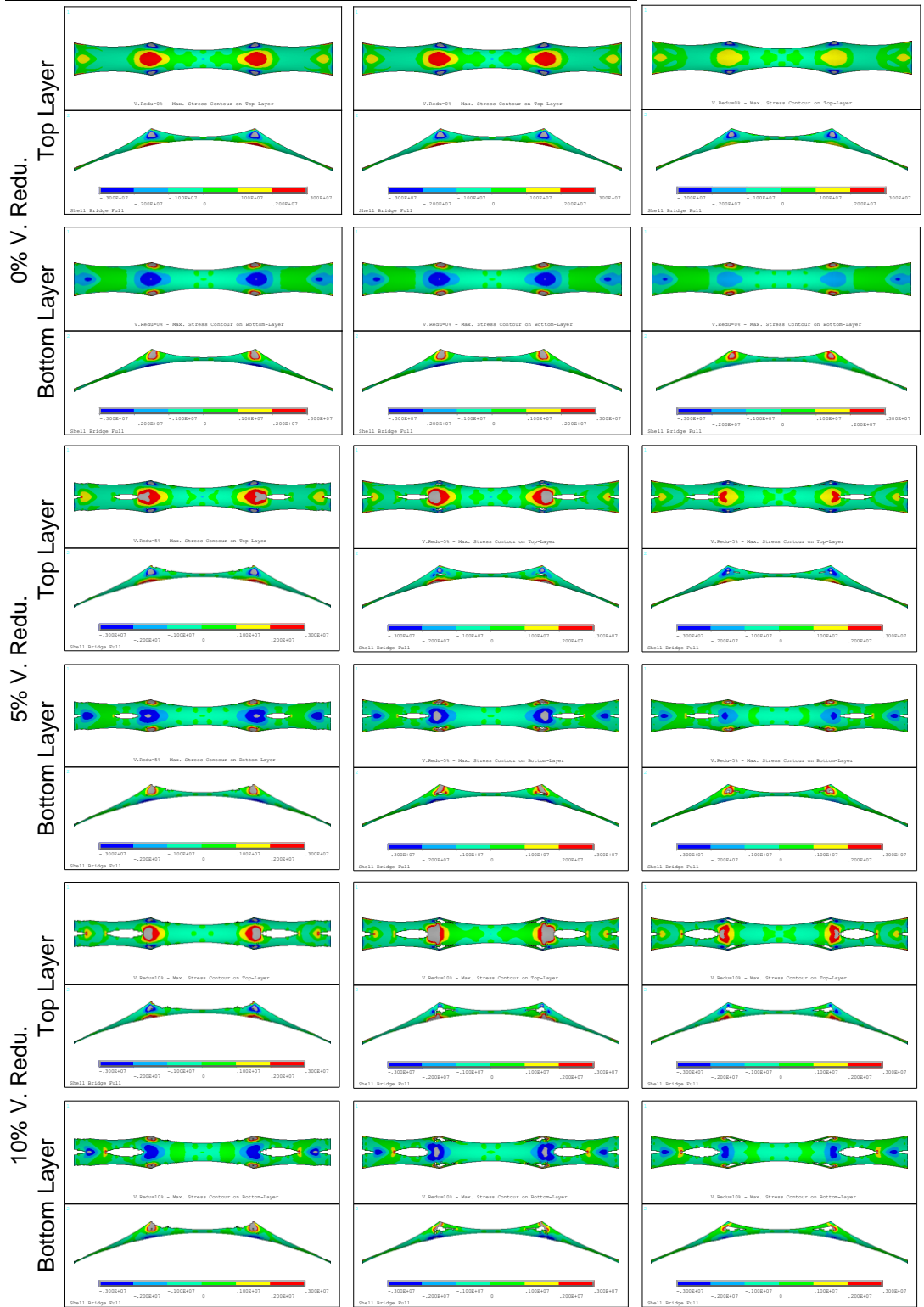
Volume Reduction	Model I		Model II		Model III	
	Pseudo-densities	Real Vol. Red.	Pseudo-densities	Real Vol. Red.	Pseudo-densities	Real Vol. Red.
5%	0.50	5.04%	0.58	5.04%	0.62	4.98%
10%	0.43	10.10%	0.54	10.04%	0.53	10.04%
20%	0.38	20.15%	0.71	19.96%	0.63	19.92%
30%	0.28	30.05%	0.74	29.95%	0.99	29.11%

*Table 10*  
Critical values of pseudo-density and real volume reductions of model T\_0.15

In Table 11, the stress contours obtained after removing these elements for each given value of volume reduction are displayed. The need for increasing stiffness of the shell free edges can be drawn from the contours of Model I. In fact, the absence of edge stiffening caused high tensile stresses especially along the free edges, so that topology optimization was required to remove material along them. This was well evident on the free edges close to the bridge ends for a volume reduction of only 5%, as well as on the free edges between the deck supports for higher values of volume reduction.

Moreover, the stress contours show that the stress distribution in Model III was more uniform than in Model I, with lower peaks of tensile stresses. This clearly showed the need to increase the stiffness of the free edges of the shell in order to limit undesirable peaks of tensile stresses arising not only along the free edges but even in the inner shell regions.

Model I	Model II	Model III
---------	----------	-----------



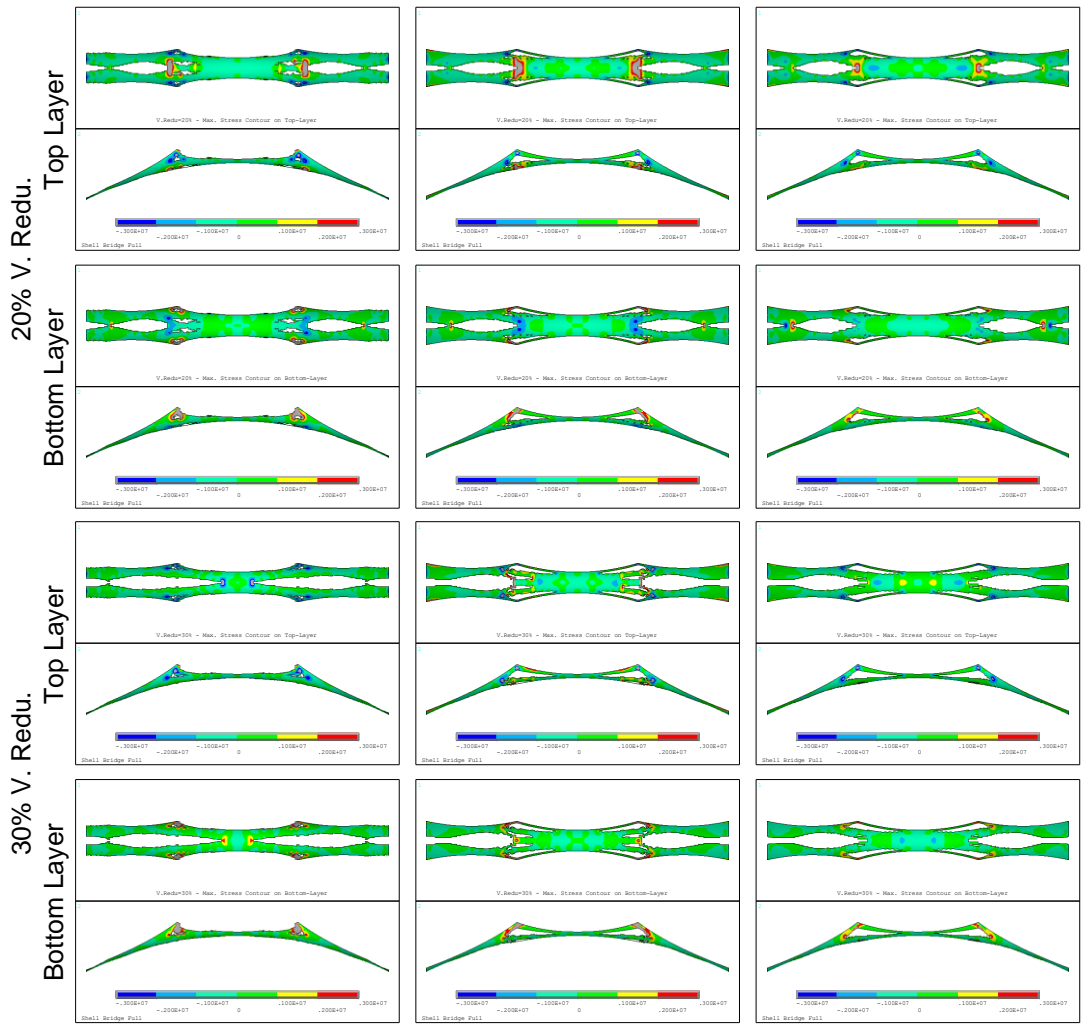


Table 11

Maximum stress contours of updated models with holes of model  $T_{0.15}$

In Table 12, the diagrams obtained from a further analysis of the results emerging from Table 11 are plotted. Considering an allowable tensile stress of concrete of 1.5MPa, the ratio between the area of the elements with tensile stress higher than 1.5MPa and the initial shell area (namely for  $VR = 0$ ) of all models for varying  $VR$  is shown.

From Table 12, the effectiveness of the design method under consideration in reducing tensile stresses throughout the shell is evident, because in all models the shell surface where tensile stresses occurred was minimized by increasing values of volume reduction.



Moreover, the diagrams of Table 12 also show the favourable effect of stiffening the free edges because, notwithstanding the removal of elements along the free edges of Model I (and the consequent reduction of the area of the elements where tensile stresses occurred), the total area of shell elements with tensile stresses higher than 1.5 MPa was always higher in Model I than in Model III.

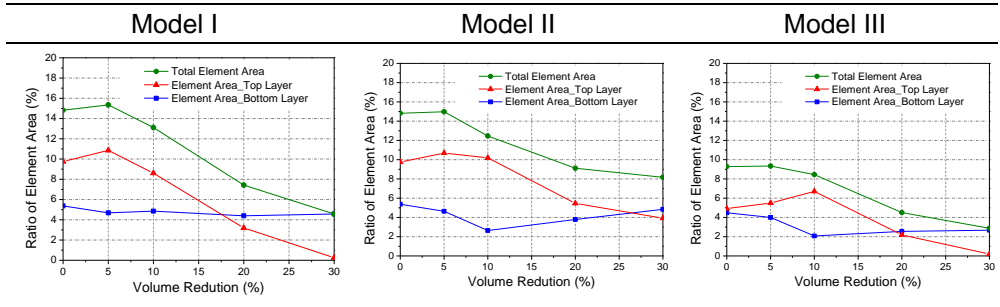


**Table 12**  
Area of finite elements of the updated models with holes with tensile stress higher than 1.5Mpa of model T\_0.15

Finally, Table 13 shows, for all models, the maximum deflections of both deck and shell centerline for different values of the volume reduction *VR*. Dashed lines in shell deflection diagrams indicate that since the related elements along the centreline were already removed, the plotted deflection was chosen to be that of the two closer symmetric elements with same abscissa (thus belonging to the same section). The diagrams of all models show that deflections of the shell footbridge were slightly sensitive to the variation of volume reduction.

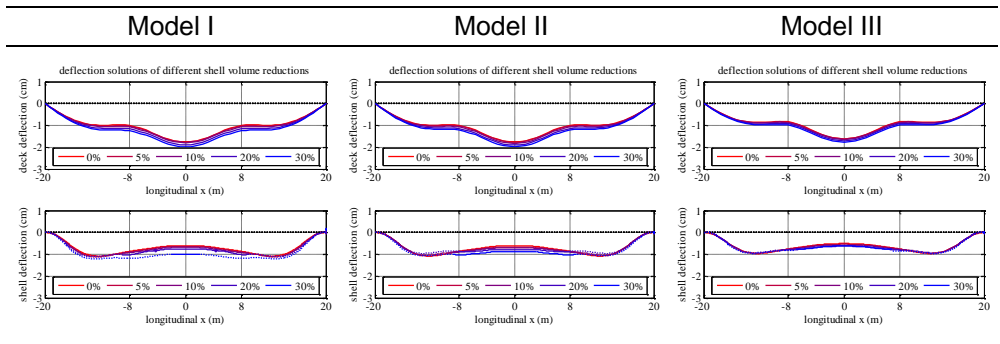


**Table 13**  
Maximum deflections of updated models with holes of model T\_0.15

**Identification of the best design solution**

The technique of eliminating the elements with tensile stresses higher than an allowable value was shown to be effective to decrease the level of tensile stresses throughout the whole shell. As stiffness was also decreased by the insertion of holes, a method to identify the best design solution became necessary, and is therefore described in the following.

The trends of both  $R$ 's for varying  $VR$  of all the three models were illustrated in Fig. 12. It can be noted that all the curves  $RI(A,i)$  decrease for increasing values of volume reduction, meaning that inserting holes through topology optimization was effective in reducing the area of the shell regions where tensile stresses occurred.

Also, Fig. 12a shows that the curve  $RI(A,i)$  of Model III was always significantly lower than the two curves  $RI(A,i)$  of Model I and Model II, thus confirming the effectiveness of stiffening the shell edges. Fig. 12b shows that all the three curves  $RI(d,i)$  were slightly affected by  $VR$ , confirming that shell footbridges were very stiff structures and that the influence of the insertion of holes on their rigidity was not very significant.

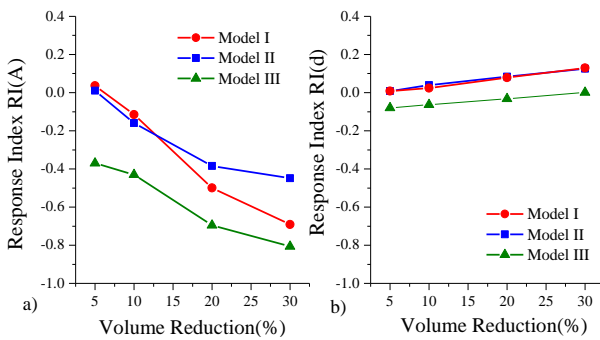


Fig. 12 Response index vs. VR diagrams of model  $T_{0.15}$ : (a)  $RI(A,i)$  and (b)  $RI(d,i)$

On the basis of above reported results, multi-families scaling factors  $\alpha$  reports in Table 14. Model I and II have same value, both concerning stress and deformation level. The corresponding value of parameter  $\alpha$  is 0.627 for stress level and 0.916 for deformation level. Conversely Model III has the highest scaling factor values and attains the maximum value equal to 1 both for stress and deformation levels. The  $\alpha$  factors related to stress confirm the positive effect of holing the shell and stiffening the edge in term of tensile stresses reduction. The  $\alpha$  factors related to deformation

states the limited impact of inserting voids the shell with reference to the deformation level of the shell bridge.

Model	Stress Level	Deformation Level
I	0.627	0.916
II	0.627	0.916
III	1.000	1.000

*Table 14*

*Scaling factor of model T\_0.15*

The global optimization index ( $GOI^*$ ) allows to identify the optimum solution that better balances material saving and overall performance of the structure, both in term of stress distribution and deformation. Its weight  $w$  is calculated first according to the effect size of stress and deformation level and lists in Table 15. Due to the low influence of the insertion of holes on their rigidity but significant influence on the shell stress, the weight of stress level is always higher.

Model	Stress Level	Deformation Level
I	0.848	0.152
II	0.796	0.204
III	0.882	0.118

*Table 15*

*Weight of stress and deformation levels of model T\_0.15*

The  $GOI^*$  as a function of  $VR$  assuming  $\beta=1$  is illustrated in Fig. 13. The left chart refers to the original formulation of the optimization index, namely the scaling factor  $\alpha$  is not considered. In the right chart results refer to the current formulation for  $OI$ , with the effect of the  $\alpha$  scaling factor properly considered.

$GOI^*$  values represent the score assigned to each design solution. In the case  $\beta=1$  solution with 30% volume reduction got the highest score for all three starting models. However, comparing solutions coming from different starting models without introducing the scaling factor  $\alpha$ , make identification of the best overall solution not so clear and easy. On the contrary, using the updated version of the optimization index that considers the  $\alpha$  parameter, Model III is highlighted as the best for almost all the  $VR$  considered in the analysis.

The results show that the structural response of Model III was always better than that of the other two models, for the positive effect that the edge stiffening had on the overall rigidity of the shell footbridge.

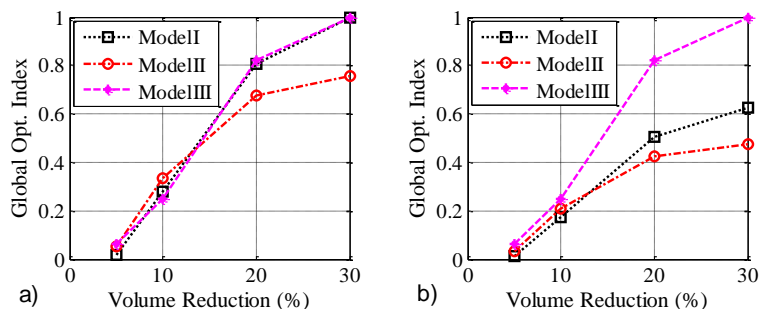


Fig. 13 Global optimization index vs. VR of model T\_0.15: a) without  $\alpha$  b) with  $\alpha$

Evaluating the effect played by  $\beta$  parameter further helps to identify the best overall solution and chose among available ones. In Fig. 14, results are reported for several values of  $\beta$  ranging between 3 and 0. The first limit favors solution with lower VR, while the second limit favors solution with higher VR. Parameter  $\beta$  tends to measure the propensity of the designer about material saving over other aspects and aims to find a solution not only effective from the structures point of view but even appreciable from the architectural one.

Take the  $\beta$  equal to 1 as an example, for varying volume reduction, the global optimization index of Model III is always much higher than that of the other two models. It can be also noted that the variation of  $GOI^*$  with respect to VR was lower for  $20\% \leq VR \leq 30\%$  than for  $10\% \leq VR \leq 20\%$ , meaning that the structural response of the shell footbridge in terms of both unwished tensile stress arising and deformation was highly affected by the insertion of holes for  $10\% \leq VR \leq 20\%$ , and less affected for  $20\% \leq VR \leq 30\%$ . Hence, although the best global response of the shell footbridge with stiffened edges occurred for  $VR= 30\%$ , a good global response was already attained for  $VR= 20\%$ .

For values of  $\beta$  higher than 2 Model III with 20% VR is identified as the best. Further reducing the  $\beta$  parameter until 0, Model III with 30% VR gets highlighted. In this case, the shell layout results separated into two symmetric parts by voids for more than one half of the total shell length. A further increase of VR would have led to a not remarkable improvements of structural response, but the structural scheme would have evolved from a shell to an arched layout, losing its architectural value.

For  $VR=30\%$ , the shell of all models was separated into two symmetric parts for more than one half of the total shell length. A further increase in volume reduction would not have led to an unremarkable improvement in structural response, but the structural scheme would have evolved from a shell to an arched layout. In this latter case, topology optimization would have tended to separate the shell into two symmetric parts so that the shell footbridge, even while maintaining a good structural response, would have lost its architectural value.

Taking into account the above results, the design solution with a volume reduction 20% of Model III appeared then to be the most suitable compromise between structural and architectural issue and even material savings.

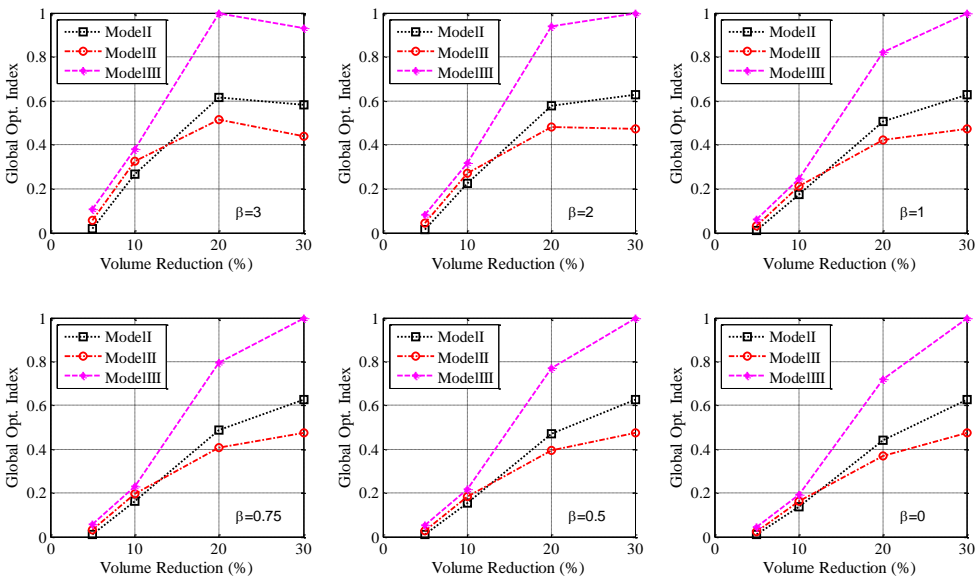


Fig. 14 Global optimization index of model T\_0.15 vs. VR (vs  $\beta$ )

#### 4.2.3 Results of Shell Bridge T\_0.20

Adopting the shell thickness of 20 cm, as suggested in the *Choice of Shell Thickness* Section by thickness optimization, topological optimization of the shell was performed for different values of volume reduction  $VR$ . Also, topological optimization was applied to all the load cases and  $VR$  values of 5, 10, 20 and 30% were

consequently applied so that for each value of  $VR$ , three pseudo-density contours were plotted in Table 16.

All the pseudo-density contours turned out to be symmetric with respect to the symmetry axes of the bridge. For all Models, increasing the values of  $VR$  resulted in an increase in the area of shell surface with low pseudo-density (blue). This low-density region gradually extended by each part along the bridge from sections near the deck-supports to the abutments.

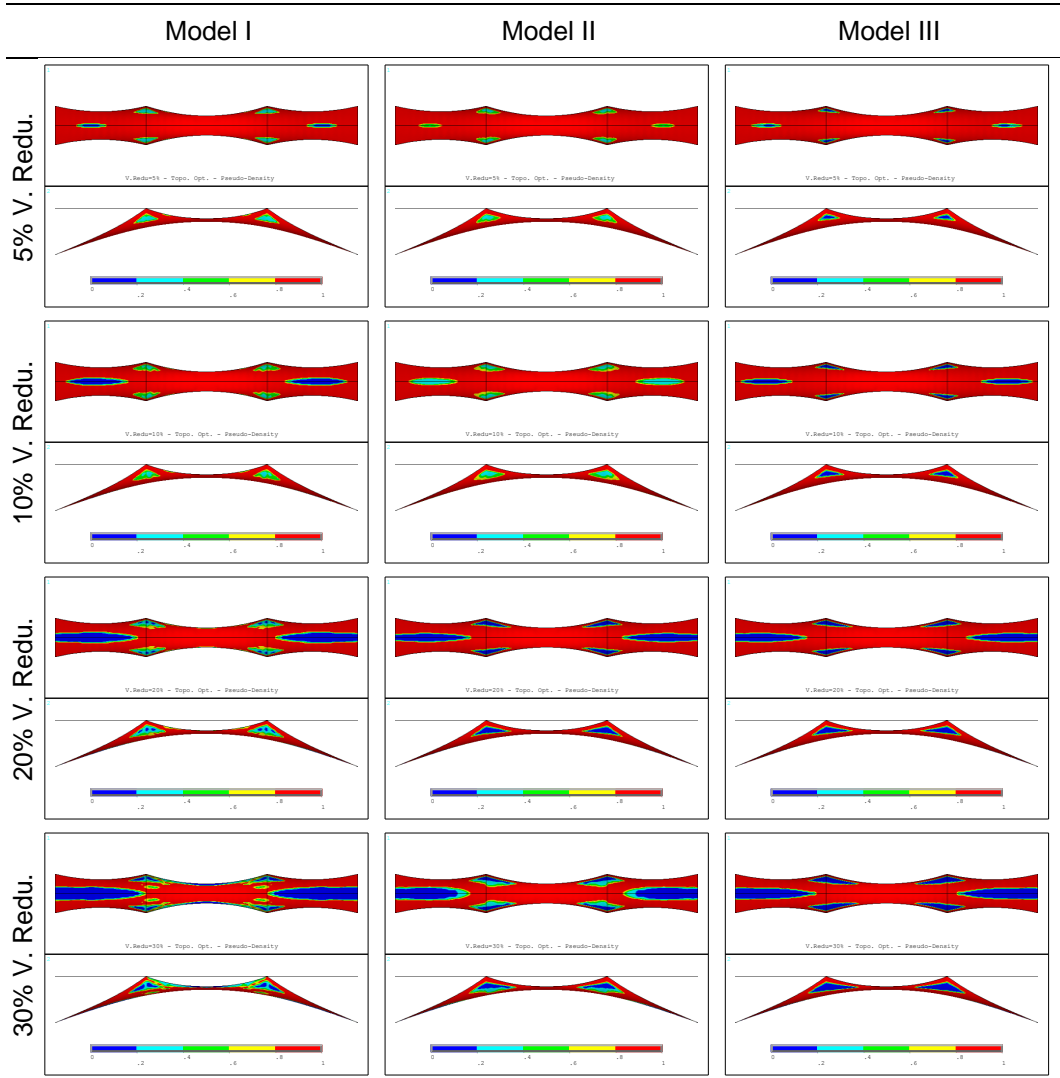


Table 16

Pseudo-density contours from topological optimization with the SIMP method of model  $T_{0.20}$

**Stresses and deformations of the updated models with holes**

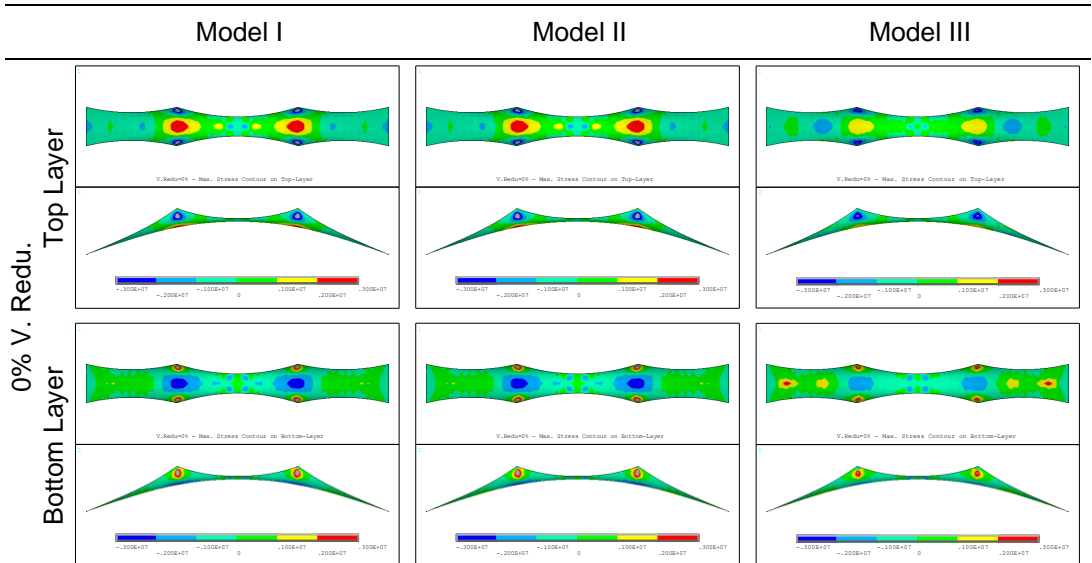
On the basis of the results of topological optimization, the three models were updated by removing the elements with pseudo-density lower than a specified value, as listed in Table 17.

Volume Reduction	Model I		Model II		Model III	
	Pseudo-densities	Real Vol. Red.	Pseudo-densities	Real Vol. Red.	Pseudo-densities	Real Vol. Red.
5%	0.38	5.06%	0.52	5.12%	0.63	5.00%
10%	0.43	10.07%	0.54	10.00%	0.99	9.56%
20%	0.37	20.20%	0.95	19.47%	0.98	19.15%
30%	0.36	30.07%	0.61	30.09%	0.54	30.02%

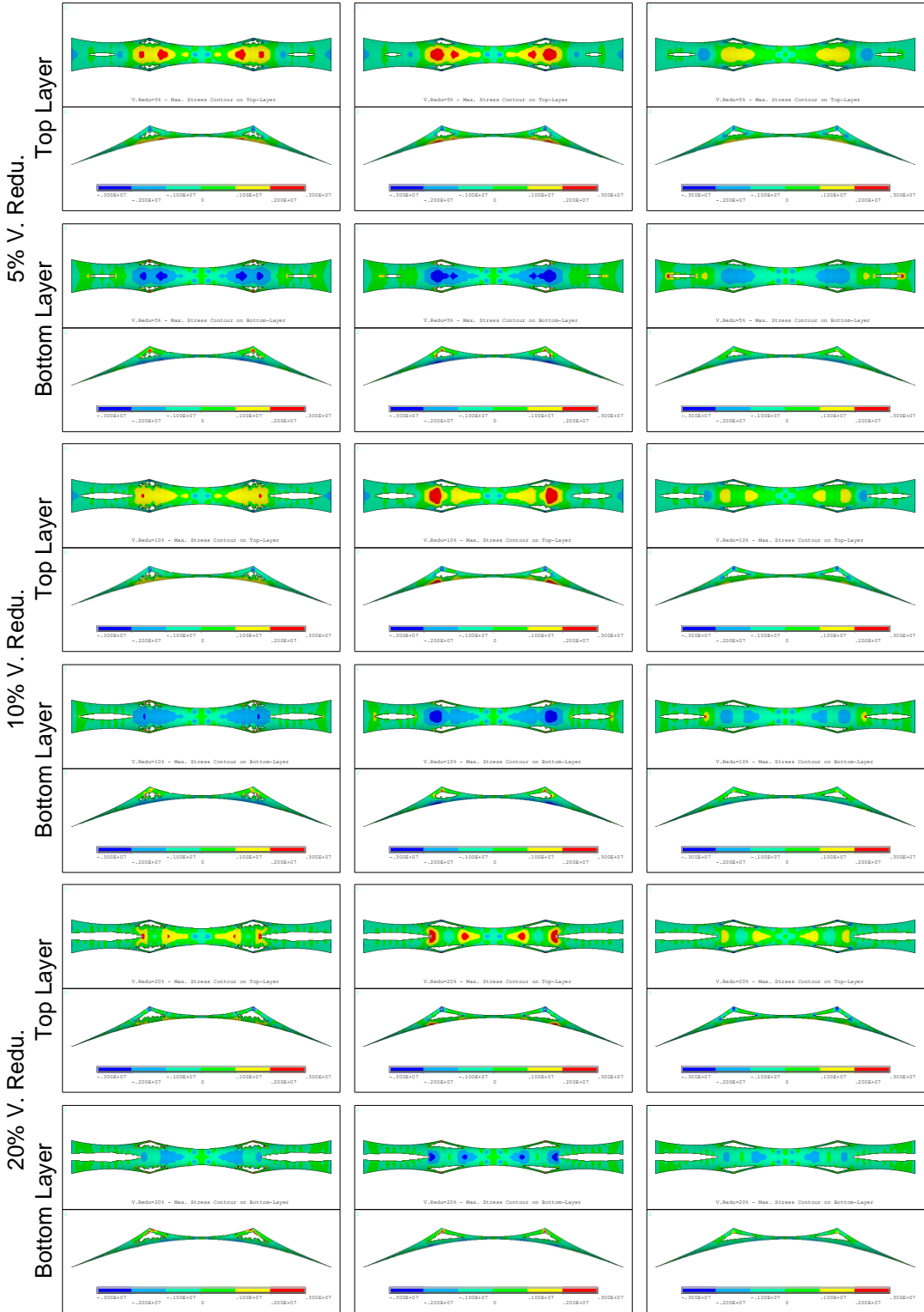
Table 17

Critical values of pseudo-density and real volume reductions of model  $T_{0.20}$

In Table 18, the stress contours obtained after removing these elements for each given value of volume reduction are displayed. The stress contours show that the stress distribution in Model III was more uniform than in Model I, with lower peaks of tensile stresses. This clearly showed the need to increase the stiffness of the free edges of the shell in order to limit undesirable peaks of tensile stresses arising not only along the free edges but even in the inner shell regions.



# AN OPTIMIZATION INDEX TO IDENTIFY THE OPTIMAL DESIGN SOLUTION OF BRIDGES





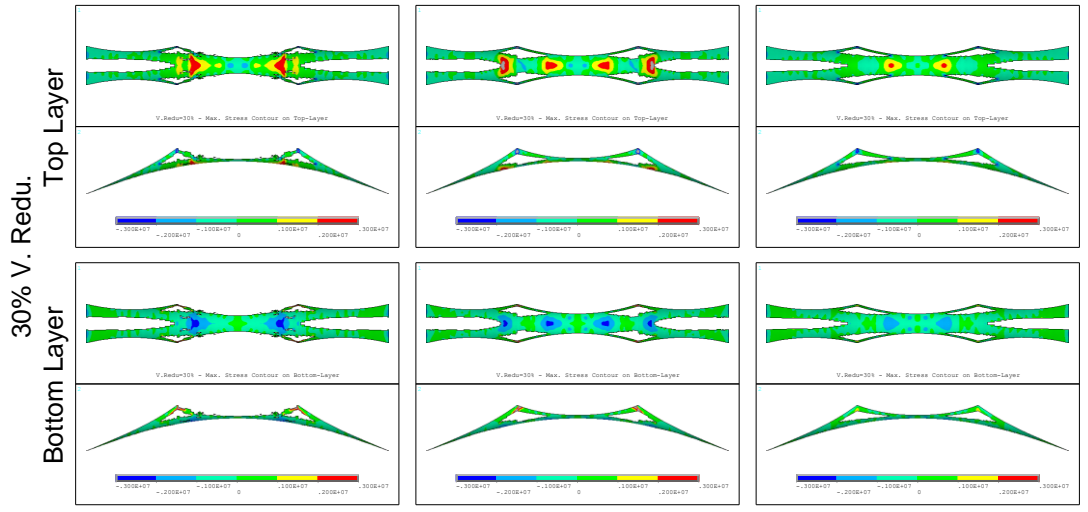


Table 18

Maximum stress contours of updated models with holes of model  $T_{0.20}$

Considering an allowable tensile stress of concrete of 1.5MPa, the ratio between the area of the elements with tensile stress higher than 1.5MPa and the initial shell area (namely for  $VR = 0$ ) of all models for varying  $VR$  is shown in Table 19. The effectiveness of the design method under consideration in reducing tensile stresses throughout the shell is evident, because in all models the shell surface where tensile stresses occurred was minimized by increasing values of volume reduction.

Moreover, the diagrams also show the favourable effect of stiffening the free edges because, notwithstanding the removal of elements along the free edges of Model I, the total area of shell elements with tensile stresses higher than 1.5 MPa was always higher in Model I than in Model III.

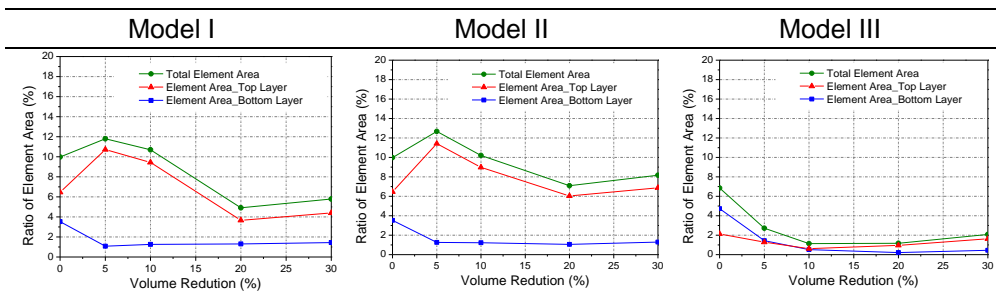
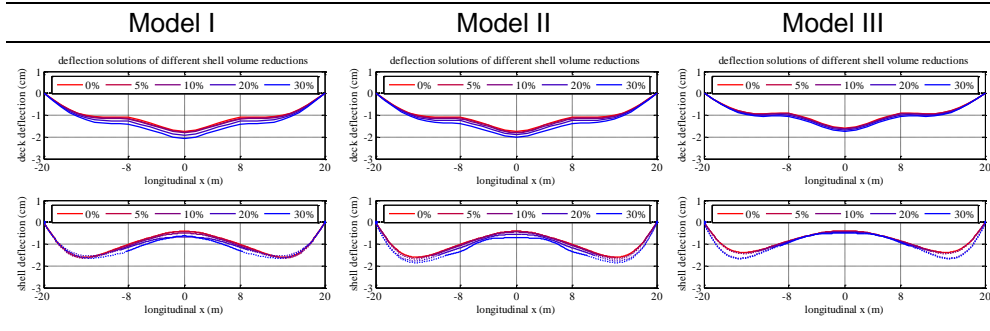


Table 19

Area of finite elements of the updated models with holes with tensile stress higher than 1.5Mpa of model  $T_{0.20}$

Finally, Table 20 shows, for all models, the maximum deflections of both deck and shell centerline for different values of the volume reduction  $VR$ . The diagrams of all models show that deflections of the shell footbridge were slightly sensitive to the variation of volume reduction.



**Table 20**  
Maximum deflections of updated models with holes of model  $T_{.0.20}$

**Identification of the best design solution**

According to the results obtained from topological optimization, for varying  $VR$ , the trend of  $RI(A,i)$  and  $RI(d,i)$  for all the three models is shown in Fig. 15. It can be noted that the trend for curves  $RI(A,i)$  decrease from 5% to 20%, meaning that inserting holes through topology optimization was an effective approach in reducing the area of shell regions where tensile stresses occurred. Besides, Fig. 15a shows that the curve  $RI(A,i)$  obtained from Model III was always significantly lower than the two curves  $RI(A,i)$  from Model I and Model II. This confirms the effectiveness of stiffening the shell edges. Fig. 15b reports the  $RI(d,i)$  trends for different models considered, which were just slightly affected by  $VR$ , confirming that the insertion of holes does not play a relevant role with reference to concrete shell deformability.

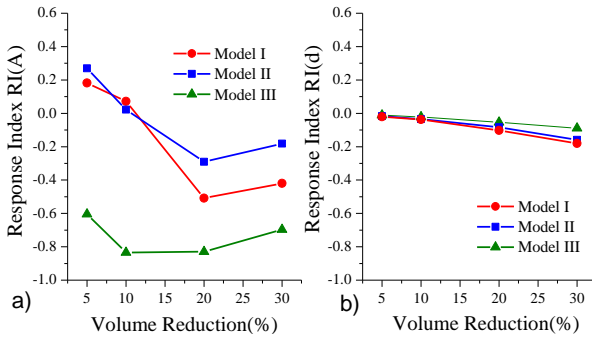


Fig. 15 Response index vs. VR diagrams of model T\_0.20: a)  $RI(A,i)$ ; b)  $RI(d,i)$ 

Table 21 reports the multi-families scaling factors  $\alpha$  on the basis of above reported results. Model I and II have same value, both concerning stress and deformation level. The corresponding value of parameter  $\alpha$  is 0.687 for stress level and 0.916 for deformation level. Conversely Model III has the highest scaling factor values and attains the maximum value equal to 1 both for stress and deformation levels.

Model	Stress Level	Deformation Level
I	0.687	0.916
II	0.687	0.916
III	1.000	1.000

Table 21

Scaling factor of model T\_0.20

The weight  $w$  of global optimization index ( $GOI^*$ ) is calculated first according to the effect size of stress and deformation level and lists in Table 23. Due to the low influence of the insertion of holes on their rigidity but significant influence on the shell stress, the weight of stress level is always higher.

Model	Stress Level	Deformation Level
I	0.777	0.223
II	0.720	0.280
III	0.944	0.056

Table 22

Weight of stress and deformation levels of model T\_0.20

The global optimization index ( $GOI^*$ ) as a function of VR assuming  $\beta=1$  is illustrated in Fig. 16. The left chart refers to the original formulation of the optimization index, namely the scaling factor  $\alpha$  is not considered. In the right chart results refer to the current formulation for  $GOI^*$ , with the effect of the  $\alpha$  scaling factor properly considered.  $GOI^*$  values represent the score assigned to each design solution. Using the updated version of the optimization index that considers the  $\alpha$  parameter, Model III is highlighted as the best for almost all the VR considered in the analysis.

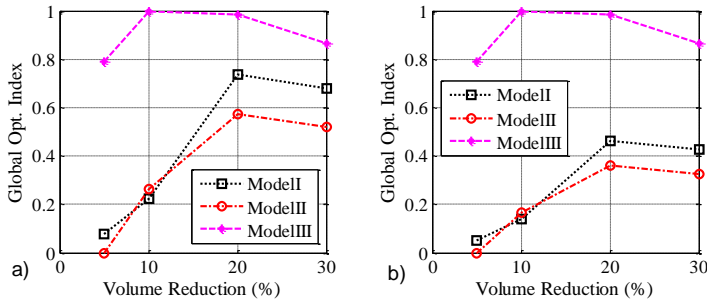


Fig. 16 Global optimization index vs. VR of model  $T_{0.20}$ : a) without  $\alpha$  b) with  $\alpha$

In Fig. 17, results are reported for several values of  $\beta$  ranging between 3 and 0. The former favors solution with lower VR, while the latter favors solution with higher VR. As  $\beta$  equal to 1, the global optimization index of Model III is always much higher than that of the other two models for varying volume reduction. For values of  $\beta$  higher than 1 Model III with 10% VR is identified as the best. Further reducing the  $\beta$  parameter until 0, Model III with 20% VR gets highlighted. For  $VR=30\%$ , the shell of all models was separated into two symmetric parts for more than one half of the total shell length. A further increase in volume reduction would not have led to remarkable improvements in structural response, but the structural scheme would have evolved from a shell to an arched layout.

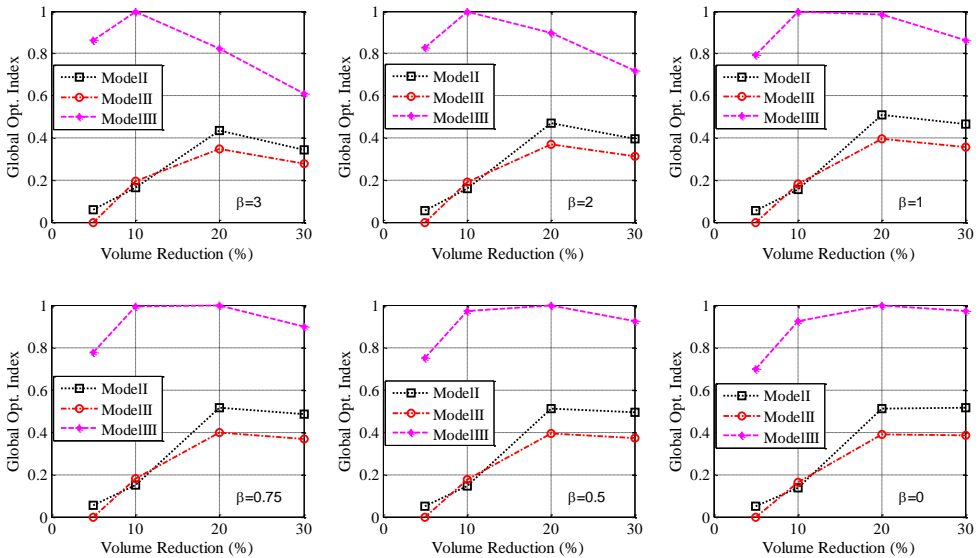


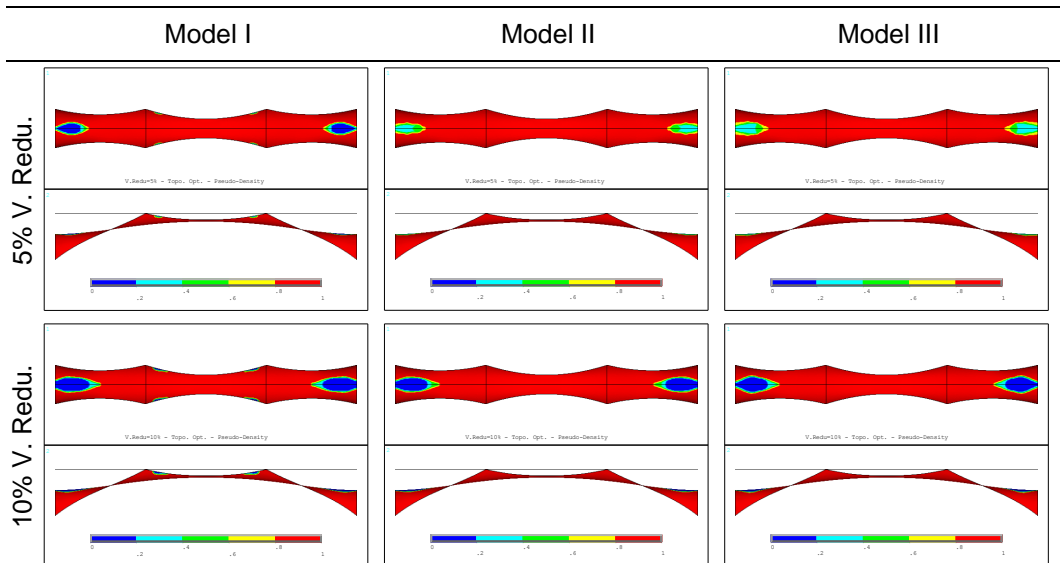
Fig. 17 Global Optimization Index vs. VR (vs  $\beta$ )

Taking into account the above results, the design solution with a volume reduction 20% of Model III appeared then to be the most suitable compromise between structural and architectural issue and even material savings.

#### 4.2.4 Results of Shell Bridge T\_0.32

Adopting the shell thickness of 32 cm, as suggested in the *Choice of Shell Thickness* Section by thickness optimization, topological optimization of the shell was performed for different values of volume reduction  $VR$ . Also, topological optimization was applied to all the load cases and  $VR$  values of 5, 10, 20 and 30% were consequently applied so that for each value of  $VR$ , three pseudo-density contours were plotted in Table 23.

All the pseudo-density contours turned out to be symmetric with respect to the symmetry axes of the bridge. For all Models, increasing the values of  $VR$  resulted in an increase in the area of shell surface with low pseudo-density (blue). This low-density region gradually extended by each part along the bridge from sections near the deck-supports to the abutments.



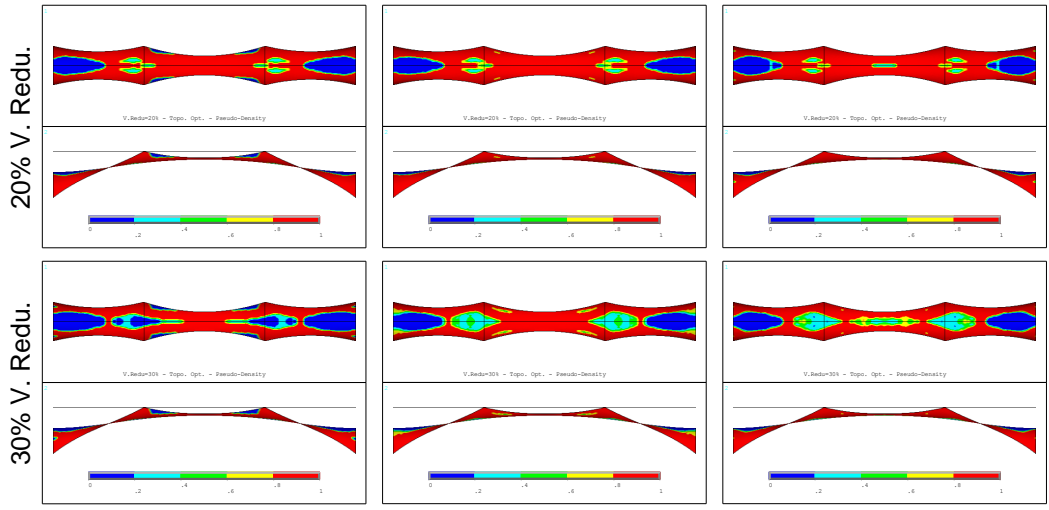


Table 23  
Pseudo-density contours from topological optimization with the SIMP method of model T\_0.32

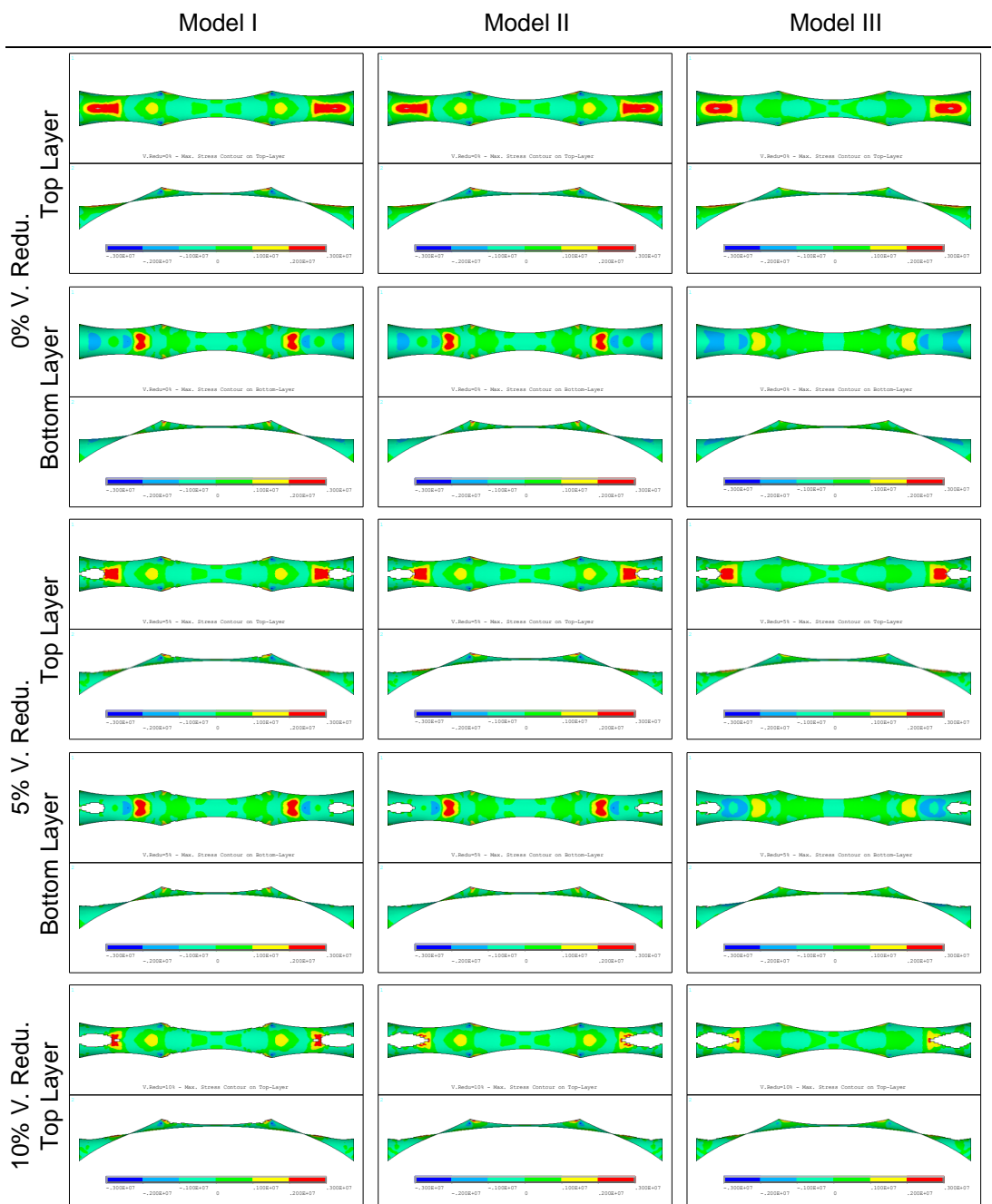
**Stresses and deformations of the updated models with holes**

On the basis of the results of topological optimization, the three models were updated by removing the elements with pseudo-density lower than a specified value, as listed in Table 24.

Volume Reduction	Model I		Model II		Model III	
	Pseudo-densities	Real Vol. Red.	Pseudo-densities	Real Vol. Red.	Pseudo-densities	Real Vol. Red.
5%	0.32	5.03%	0.69	4.86%	0.54	4.94%
10%	0.28	10.04%	0.91	9.84%	0.73	10.00%
20%	0.39	20.01%	0.98	18.70%	0.97	18.88%
30%	0.27	29.94%	0.56	29.88%	0.63	30.04%

Table 24  
Critical values of pseudo-density and real volume reductions of model T\_0.32

In Table 25, the stress contours obtained after removing these elements for each given value of volume reduction are displayed. The stress contours show that the stress distribution in Model III was more uniform than in Model I, with lower peaks of tensile stresses. This clearly showed the need to increase the stiffness of the free edges of the shell in order to limit undesirable peaks of tensile stresses arising not only along the free edges but even in the inner shell regions.



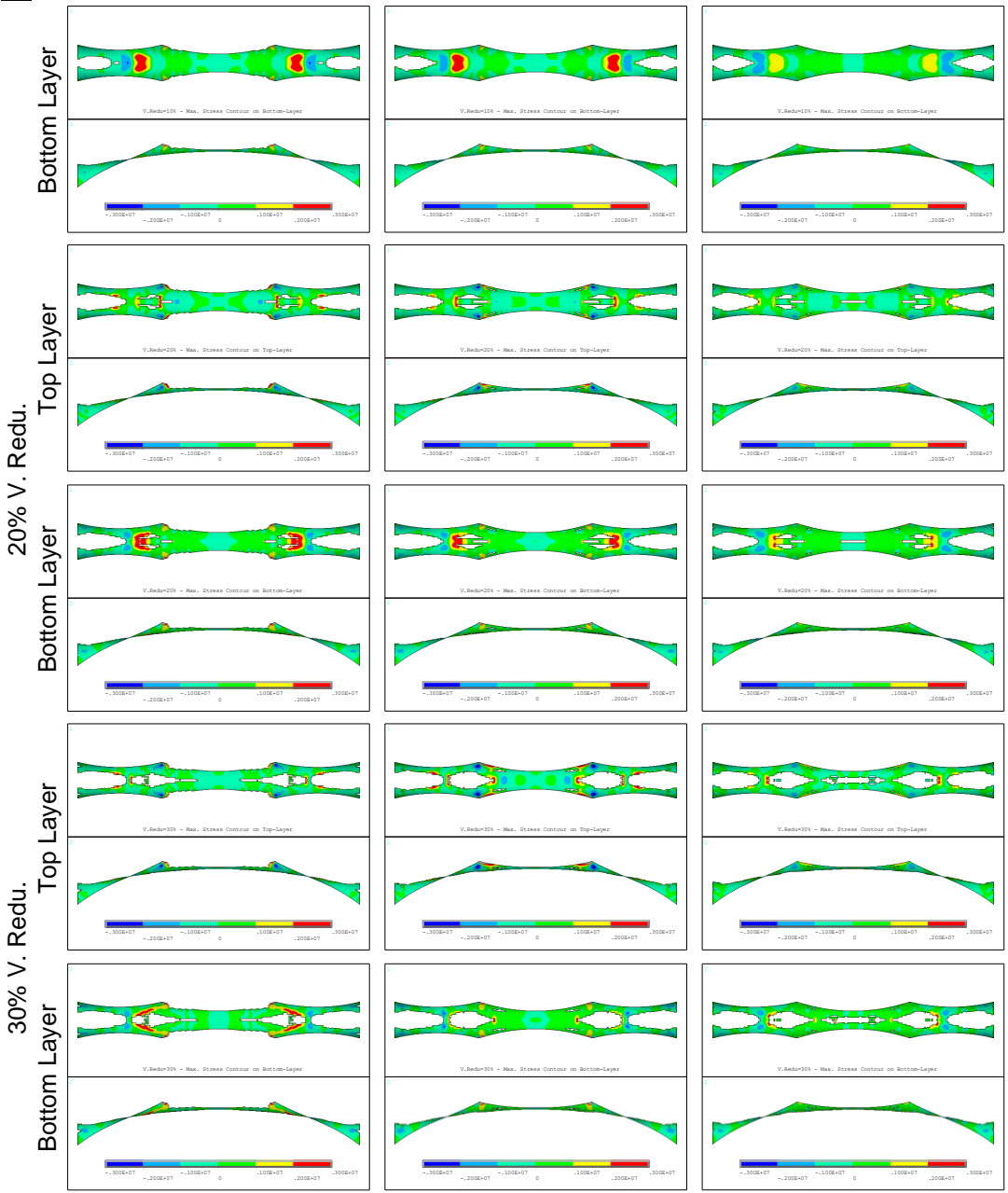


Table 25  
Maximum stress contours of updated models with holes of model  $T_{0.32}$

Considering an allowable tensile stress of concrete of 1.5MPa, the ratio between the area of the elements with tensile stress higher than 1.5MPa and the initial shell area (namely for  $VR = 0$ ) of all models for varying  $VR$  is shown in Table 26.



The effectiveness of the design method under consideration in reducing tensile stresses throughout the shell is evident, because in all models the shell surface where tensile stresses occurred was minimized by increasing values of volume reduction. Moreover, the diagrams also show the favourable effect of stiffening the free edges because, notwithstanding the removal of elements along the free edges of Model I, the total area of shell elements with tensile stresses higher than 1.5 MPa was always higher in Model I than in Model III.

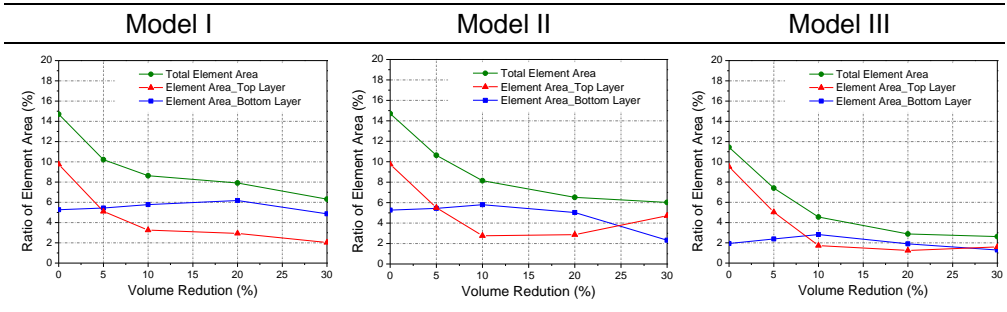


Table 26

Area of finite elements of the updated models with holes with tensile stress higher than 1.5Mpa of model T\_0.32

Finally, Table 27 shows for all models, the maximum deflections of both deck and shell centerline for different values of the volume reduction VR. The diagrams of all models show that deflections of the shell footbridge were slightly sensitive to the variation of volume reduction.

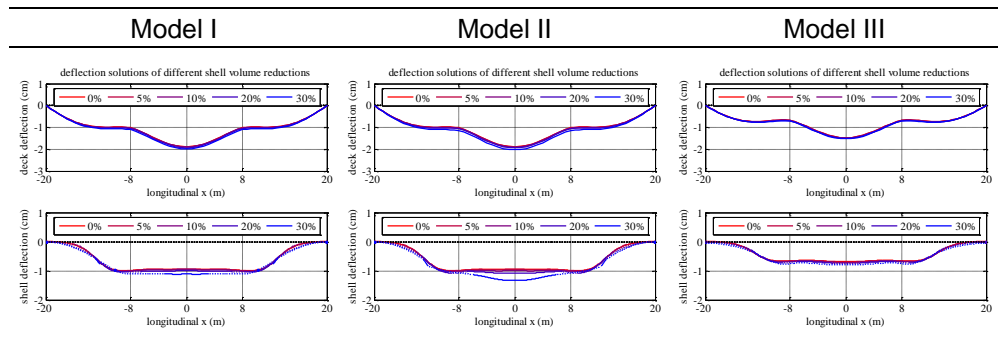


Table 27

Maximum deflections of updated models with holes of model T\_0.32

**Identification of the best design solution**

Fig. 18 illustrates the trend of identified response indexes for all the three models according to the results obtained from topological optimization for varying VR. Fig. 18a shows that the RI(A,i) decrease for increasing values of VR, meaning that inserting holes through topology optimization was an effective approach in reducing the area of shell regions where tensile stresses occurred. Fig. 18b reports the RI(d,i) trends for different models considered which were just slightly affected by VR, confirming that shell footbridges are very stiff structures.

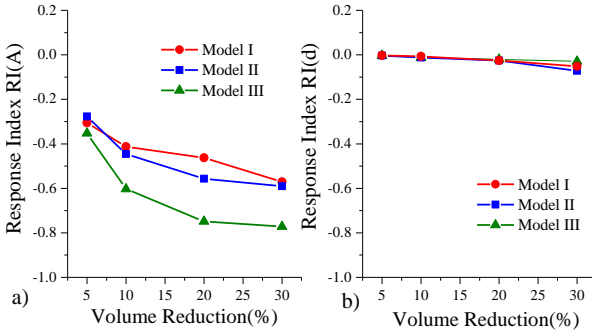


Fig. 18 Response index vs. VR diagrams of model T\_0.32: a) RI(A,i); b) RI(d,i)

Table 28 reports the multi-families scaling factors  $\alpha$  on the basis of above reported results. Model I and II have same value, both concerning stress and deformation level. The corresponding value of parameter  $\alpha$  is 0.778 for stress level and 0.782 for deformation level. Conversely Model III has the highest scaling factor values and attains the maximum value equal to 1 both for stress and deformation levels.

Model	Stress Level	Deformation Level
I	0.778	0.782
II	0.778	0.782
III	1.000	1.000

Table 28

Scaling factor of model T\_0.32

The weight  $w$  of global optimization index (GOI\*) is calculated first according to the effect size of stress and deformation level and lists in Table 29. Due to the low influence of the insertion of holes on their rigidity but significant influence on the shell stress, the weight of stress level is always higher.

Model	Stress Level	Deformation Level
I	0.953	0.047
II	0.943	0.057
III	0.974	0.026

Table 29

Weight of stress and deformation levels of model  $T_{0.32}$

The  $GOI^*$  as a function of  $VR$  assuming  $\beta=1$  is illustrated in Fig. 19. The left chart refers to the original formulation of the optimization index  $OI$  while the right chart results refer to the current formulation for  $OI^*$ , with the effect of the  $\alpha$  scaling factor properly considered.  $GOI^*$  values represent the score assigned to each design solution. However, comparing solutions coming from different starting models without introducing the scaling factor  $\alpha$ , make identification of the best overall solution not so clear and easy. On the contrary, using the updated version of the optimization index that considers the  $\alpha$  parameter, Model III is highlighted as the best for almost all the  $VR$  considered in the analysis.

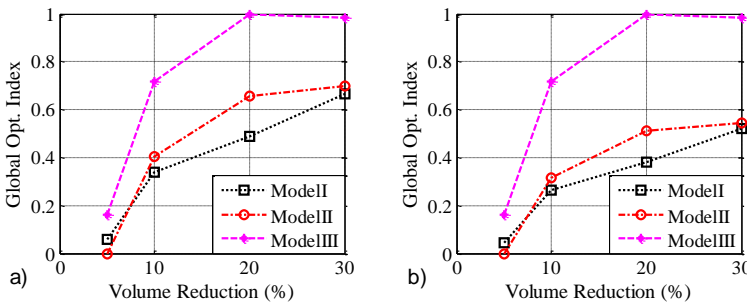


Fig. 19 Global optimization index vs.  $VR$  of model  $T_{0.32}$ : a) without  $\alpha$  b) with  $\alpha$

Evaluating the effect played by  $\beta$  parameter further helps to identify the best overall solution and chose among available ones. In Fig. 20, results are reported for several values of  $\beta$  ranging between 3 and 0. The first limit favors solution with lower  $VR$ , while the second limit favors solution with higher  $VR$ .

As  $\beta$  equal to 1, the global optimization index of Model III was always much higher than that of the other two models for varying volume reduction. For values of  $\beta$  higher than 2 Model III with 10%  $VR$  is identified as the best. Further reducing the  $\beta$  parameter until 0, Model III with 20%  $VR$  gets highlighted. A further increase in volume reduction would not have led to remarkable improvements in structural response, but the structural scheme would have evolved from a shell to an arched

layout. Taking into account the above results, the design solution with a volume reduction 20% of Model III appeared then to be the most suitable compromise between structural and architectural issue and even material savings.

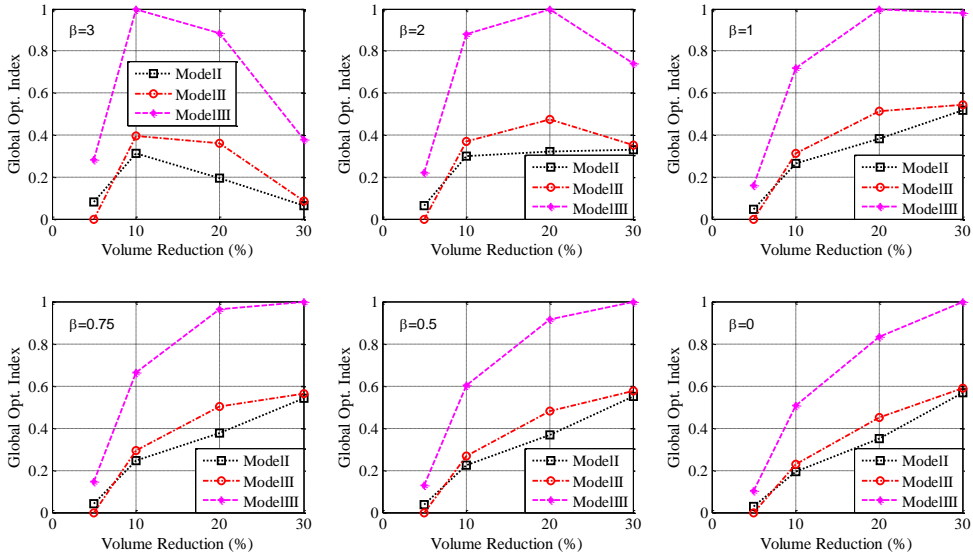


Fig. 20 Global optimization index vs. VR of model T\_0.32 (vs  $\beta$ )

#### 4.3. Comparison between Tentative Models

For each reference shell bridge, three different starting models are defined, each characterized by the same boundary conditions but different edge stiffening. Depending on different input VR ratio, for each starting model, 4 candidate solutions with voids are defined. Hence, there are 36 candidate solutions in total that is  $3 \times 3 \times 4$  (reference model  $\times$  starting model  $\times$  input VR). According to the results of entire candidate solutions, the multi-families scaling factors  $\alpha$  is calculated again and lists in Table 30. To take into account the influence of shell thickness of each reference model, T\_0.20 and T\_0.32 were calculated with shell thickness of 0.15m. The ratio of area which stress higher than 1.5 Mpa were then used to determine scaling factors.

Model	Ratio of area which stress higher than 1.5Mpa (%)			Stress Level		
	I	II	III	I	II	III
T_0.15	14.82	14.82	9.28	0.802	0.802	1.000
T_0.20	19.53	19.53	15.97	0.633	0.633	0.760

T_0.32	27.87	27.87	26.35	0.333	0.333	0.388
--------	-------	-------	-------	-------	-------	-------

Table 30

Scaling factor of all the solutions

According to the results of entire candidate solutions, the comparison of  $GOI^*$  values of all the solutions are shown in Fig. 21. The left chart refers to the original formulation of the optimization index, namely the scaling factor  $\alpha$  is not considered. In the right chart results refer to the current formulation for  $OI^*$ , with the effect of the  $\alpha$  scaling factor properly considered.

By using the updated version of the optimization index that consider the  $\alpha$  parameter, starting models of T\_0.15 are highlighted as the best for almost all the VR considered in the analysis. The results show that the structural response of starting model T\_0.15 was better than that of the other two starting models, for the positive effect that the boundary shape had on the overall rigidity of the shell footbridge. With this shape, the optimum thickness of the shell can be minimum under same load cases compared with two other shell shapes, therefore a high scaling factor was obtained.

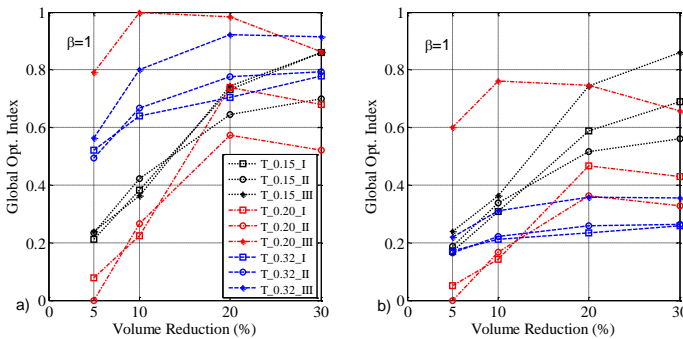


Fig. 21 Global optimization index of all solutions vs. VR: a) without  $\alpha$  b) with  $\alpha$

According to the results of entire candidate solutions and considering several values of  $\beta$  ranging between 3 and 0, the comparison of  $GOI^*$  values of all the solutions are listed in Fig. 22. The former favors solution with lower VR, while the latter favors solution with higher VR. In general, because of the better boundary shape, the global optimization index of starting model T\_0.15 are higher than that of the other two starting models, while the starting model T\_0.32 have the lowest value.

Take the  $\beta$  equal to 1 as an example, for varying VR, the global optimization index of Model III of starting model T\_0.15 is always higher than that of others except that of

Model III of starting model T\_0.20. Due to the deepest decreasing of unwished tensile stress, the latter has higher value when the *VR* is less than 20%. However, as the *VR* increasing, the positive effect of the boundary shape on the rigidity of shell footbridge revealed and led the Model III of starting model T\_0.15 with *VR* = 30% to a highest *GOI\** among total solutions.

The same results as each starting model, the variation of *GOI\** with respect to *VR* was lower for  $20\% \leq VR \leq 30\%$  than for  $10\% \leq VR \leq 20\%$ , meaning that the structural response of the shell footbridge in terms of both unwished tensile stress arising and deformation was highly affected by the insertion of holes for  $10\% \leq VR \leq 20\%$ , and less affected for  $20\% \leq VR \leq 30\%$ . Hence, although the best global response of the shell footbridge with stiffened edges occurred for *VR*= 30% , a good global response was already attained for *VR*= 20%.

For values of  $\beta$  higher than 2 Model III of starting model T\_0.20 with 10% *VR* is identified as the best. Further reducing the  $\beta$  parameter until 0, Model III of starting model T\_0.15 with 30% *VR* gets highlighted. A further increase of *VR* would have led to an unremarkable improvement of structural response, but the structural scheme would have evolved from a shell to an arched layout, losing its architectural value.

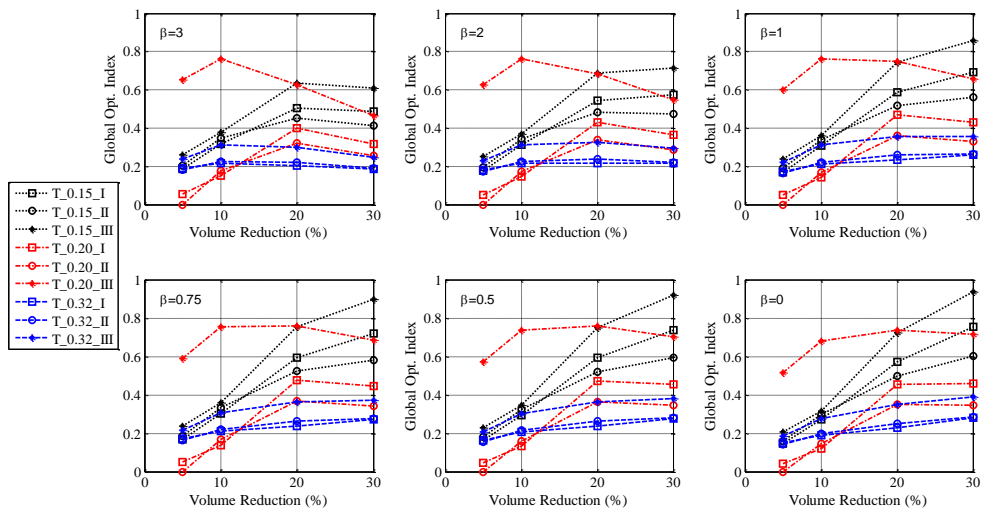


Fig. 22 Global optimization index of all solutions vs. *VR* (vs  $\beta$ )

Besides the comparison of all candidate solutions of each starting model, the comparison between solutions with same *VR* of different starting models is also

interesting. Considering several values of  $\beta$  ranging between 3 and 0, the comparison of  $GOI^*$  values of Model I between 3 reference models are listed in Fig. 23. All the solutions were obtained by topology optimization performed throughout the whole shell surface.

The results show that the overall structural performance of starting model T\_0.15 is better than that of the other two models because of the positive effect that reasonable boundary shape was used. Consider  $\beta$  equal to 1, the global optimization index of starting model T\_0.15 is always much higher than that of other two starting models for varying  $VR$ . For values of  $\beta$  higher than 2 starting model T\_0.15 with 20%  $VR$  is identified as the best. Further reducing the  $\beta$  parameter until 0, starting model T\_0.15 with 30%  $VR$  gets highlighted. A further increase of  $VR$  would have led to an unremarkable improvement of structural response, but the structural scheme would have evolved from a shell to an arched layout, losing its architectural value.

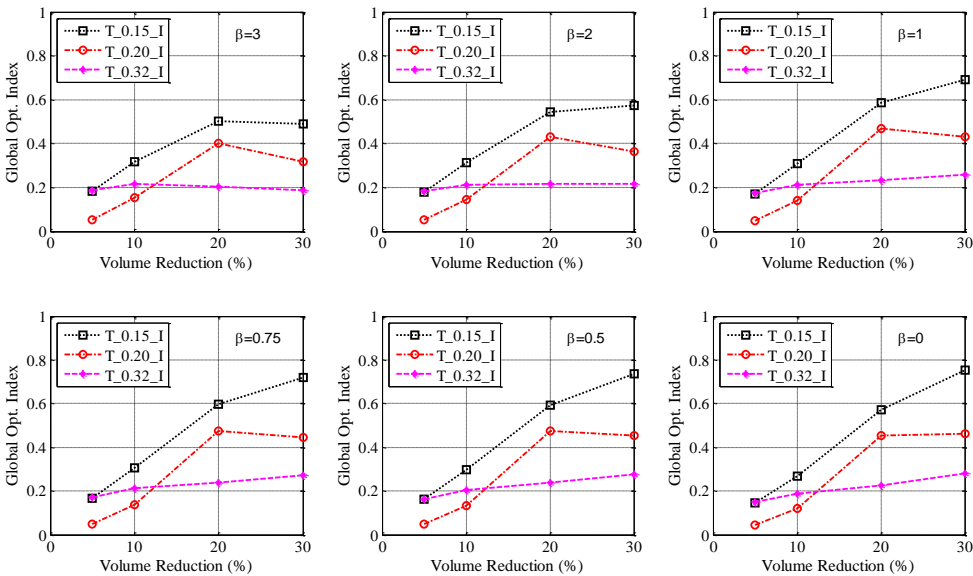


Fig. 23 Global optimization index of Model I vs. VR (vs  $\beta$ )

Considering several values of  $\beta$  ranging between 3 and 0, the comparison of  $GOI^*$  values of Model II between 3 reference models are listed in Fig. 24. All the solutions were obtained by topology optimization performed throughout the whole shell surface, but the shell regions close to the edge (for a distance of 0.20m from the edge) were excluded from topology optimization. The results are similar as Model I.

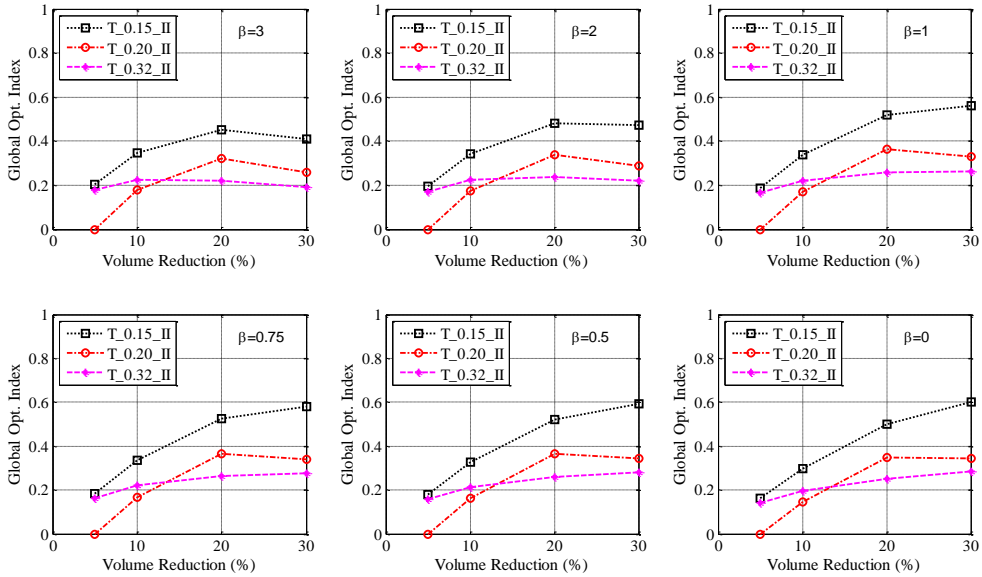


Fig. 24 Global optimization index of Model II vs VR (vs  $\beta$ )

Considering several values of  $\beta$  ranging between 3 and 0, the comparison of  $GOI^*$  values of Model III between 3 reference models are listed in Fig. 25. All the solutions were obtained by topology optimization performed throughout the whole shell surface on the basis of stiffening beam elements (width 0.20m, same depth as the shell) were added along the free edges of the shell.

The results show that the overall structural performance of starting model T\_0.32 is always worse than that of the other two models, while each of the other two has its own merits for varying VR. Starting model T\_0.15 is higher than that of model T\_0.20 for  $20\% \leq VR \leq 30\%$  but lower than the latter for  $5\% \leq VR \leq 20\%$ , that's because of the deepest decreasing of unwished tensile stress of starting model T\_0.20.

Take  $\beta$  equal to 1 as an example, the global optimization index of starting model T\_0.32 is always lowest for varying VR. Starting model T\_0.15 is higher than that of T\_0.20 for  $VR = 30\%$  but lower than the latter for  $5\% \leq VR \leq 20\%$ . Hence, for values of  $\beta$  higher than 1 starting model T\_0.20 with 10% VR is identified as the best. Further reducing the  $\beta$  parameter until 0, starting model T\_0.15 with 30% VR gets highlighted. A further increase of VR would have led to an unremarkable improvement of structural response, but the structural scheme would have evolved from a shell to an arched layout, losing its architectural value.



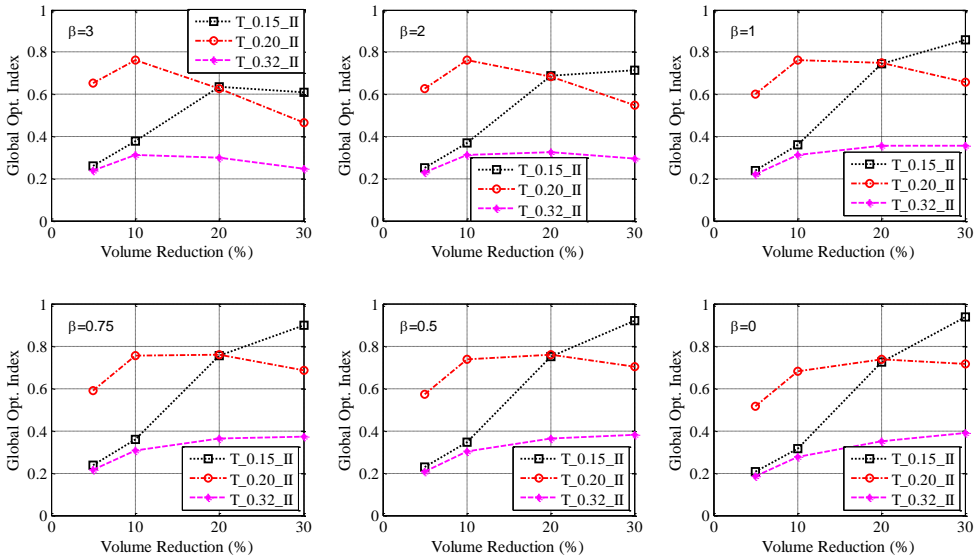


Fig. 25 Global optimization index of Model III vs. VR (vs  $\beta$ )

Until now, with the proposed optimization index, the identification of the best overall layout among multi-families multi-solutions is carried out. Besides the comparison of all the solutions together, solutions with same VR of different starting models are also compared. The results show the overall structural performance of starting model T\_0.15 is better than that of the other two models due to the positive effect of reasonable boundary shape, and the overall structural performance of Model III is better than that of the other two models due to the positive effect that edge stiffening had on the overall rigidity of the shell footbridge.

For all the starting models, the layout with holes obtained for a volume reduction of 20% was shown to have good structural response, while the solution with 30% VR gets highlighted after the introduction of penalty exponent  $\beta$ . Contrary to the latter, although the structural response of the former is slightly reduced, the former maintained the shell integrity avoiding the merging of close holes dividing a great part of the shell into two parts.

It states that even if for high values of volume reduction, the structural response could be slightly improved, the aesthetic value of these design solutions would become inappropriate. In fact, the shell tended to split into two symmetric parts with respect to its centreline. Therefore, this design solution of Model III of starting model

T\_0.15 for VR = 20% appeared to be the most appropriate, with good structural response coupled with good aesthetic value.

Fig. 26 and Fig. 27 show that the layout of Model III of starting model T\_0.15 for VR = 20% appeared to be the most suitable compromise between structural and aesthetical issues. This model still emphasizes the natural flow of forces from their point of application to the foundations respecting the integrity of the shell form but minimizing the occurrence of unwished tensile stresses.

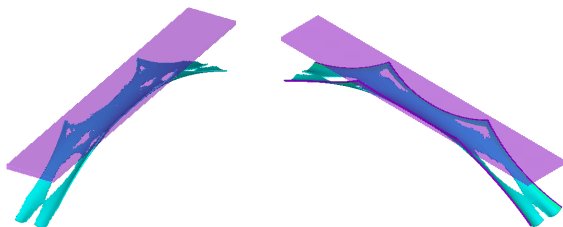


*Fig. 26 View of the FE model of the proposed design solution with VR = 20 % of starting model T\_0.15 (a) Model I ( b) Model III*



*Fig. 27 Virtual image of the bridge after the insertion of cavities required by the topology optimization procedure*

## CHAPTER 5

## 5. CALATRAVA BRIDGE OF VENICE

The Grand Canal of Venice is a large reverse-S shape canal through the central districts of Venice and divides the city into two parts. It forms one of the major water-traffic corridor which with 3,800 m long, 30–90 m wide, average depth of 5 meters. At one end, the canal leads into the lagoon near the Santa Lucia railway station and the other end leads into the sea. The Grand Canal connects at various points with a maze of smaller canals. There are over 400 bridges over these canals but only three bridges cross the Grand Canal until 2008, namely Rialto Bridge, Accademia Bridge and Scalzi Bridge in accordance with the built time from early to late, as shown in Fig. 28.

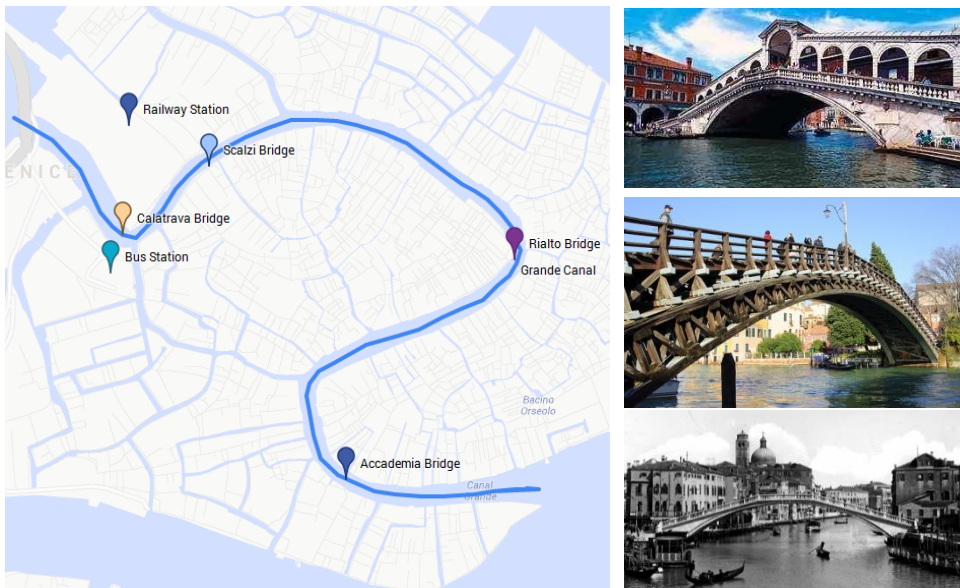


Fig. 28 Bridge over Grand Canal of Venice (From top to bottom: Rialto – Accademia – Scalzi)

The Rialto Bridge is the oldest and most famous bridge spanning the Grand Canal in the heart of Venice. It was built in 1591 and as the only way to cross the Grand Canal by foot for nearly 300 years until the construction of Accademia Bridge. Beginning in 1524, architects began submitting proposals for the new bridge but no plan was chosen until 1588, when municipal architect Antonio da Ponte was awarded the commission. The present stone bridge, a single span 28.8m and rise

6.4m, with two inclined ramps lead up to a central portico. On either side of the portico, the covered ramps carry rows of shops. The bridge has become one of the architectural icons of Venice.

The Accademia Bridge is so named because it crosses the Grand Canal at the Galleria dell'Accademia, one of the top museums in Venice. The wooden arch bridge was designed by Italian famous architect Eugenio Miozzi and built in 1933 as a temporary replacement for an iron bridge, which was demolished due to in a dangerous condition. The present wooden bridge has high arch curved with a single span 48m, remains a beloved landmark.

The Scalzi Bridge is the third bridge spanning the Grand Canal and is well-known as another masterpiece of Eugenio Miozzi. It located in front of the Santa Lucia railway station, designed and built in 1934. It is named as a church on the left side of the bridge, literally "church of the barefoot". It is a stone arch span of 40m, rising 6.75m. The bridge is only 0.8m thick at its crown, which is remarkable slender for the type and age of the bridge. Stone was chosen instead of reinforced concrete to avoid future corrosion problems (Zordan, et al., 2010).

Since there are only three bridges connecting two sides of Grand Canal, it is not good for the development of Venice's international tourism, so the construction of a fourth bridge which will connect the railway station and bus station has been proposed early. There are different opinions on the design of new bridge, conservatives feel that the new bridge should be compatible with Venice's decorative medieval architecture and the historical city like its former bridges, so the style of the new bridge would not change. Whereas others think new elements need to be added in the city, a modern architecture should embrace change and be brought into the present times.

In June 1999, the Municipality of Venice drafted a preliminary plan for a fourth bridge over the Grand Canal. After a public selection process, Spanish architect Santiago Calatrava was asked to design the new bridge in November 1999 (Scibilia and Vento, 2004). Calatrava selected to add new elements and designed a steel arch bridge with a radius of 180 m, as shown in Fig. 29.



*Fig. 29 Calatrava Bridge - Santiago Calatrava, 2008, Venice (Italy)*

Calatrava Bridge, the fourth bridge spanning the Grand Canal of Venice, later has its official name “Ponte della Costituzione”, opened to the public on September 11, 2008. The construction of the fourth bridge has assumed great importance not only in the Venice city but at national and international level too, and it has also taken on a historical significance (Scibilia and Vento, 2004). Immediately following the completion of the newest bridge, there are a lot of comments including criticism and praise. However, lack of wheelchair access, lack of necessity, bridge modern appearance and an approximately cost of 10 million euros, made heated criticism rain down on this project.

From the structural point of view, the utilization of the open star-shape cross section and the open truss arch ribs with straight-like web members and with no diagonals and 1/16 rise-to-span ratio makes the structure less rational. Huge horizontal thrust occurred due to the 1/16 rise-to-span ratio,  $\pi$ -shaped steel plates not only withstand shear force of the main arch, but also bear local bending moment, the stress of some parts reached to the critical state, the stiffness of main arch rib is small, large bending deformation occurred under asymmetric loads. Moreover, the third order vibration mode of the main arch of the bridge is close to the pedestrian step frequency, which is extremely liable to cause the pedestrian and bridge resonance (Chen, et al., 2011).

Some structural defectiveness mentioned above particularly the occurrence of huge horizontal thrust could be reduced if the bridge with better design such as more reasonable thickness distribution or considering bridge’s abutment deformability. To this aim, on basis of original design of the Calatrava Bridge, three different starting models were identified, then optimization of these three models were carried out and the results are used to validate the effectiveness of the proposed optimization index analytical formulation.

## 5.1. Calatrava Bridge

### 5.1.1 General Situation

The fourth Bridge over the Grand canal is a steel arch footbridge with a main span of 80.8m. It is 94m in total while count from two end steps. 4.67m rise gives the bridge a 1/16 rise-to-span ratio. The width varies from a minimum of 5.58m at the foot to a maximum of 9.38m in the middle of the bridge. The height is 3.2m at the foot at the steps, reaching 9.28m at the highest point in the centre (Scibilia and Vento, 2004). The general arrangement is shown in Fig. 30.

It was designed an arched truss bridge with a radius of 180m, with a central arch, two side arches and two lower arches. The axes of central arch and two lower arches are two dimension curves in vertical plane, two lower arches are symmetrically placed and 1.85m away from the central arch in transverse direction. The axes of side arches are 3 dimension curves, placed symmetrically and a 2.56m minimum at the foot to a 4.46m maximum in the middle away from the central arch.

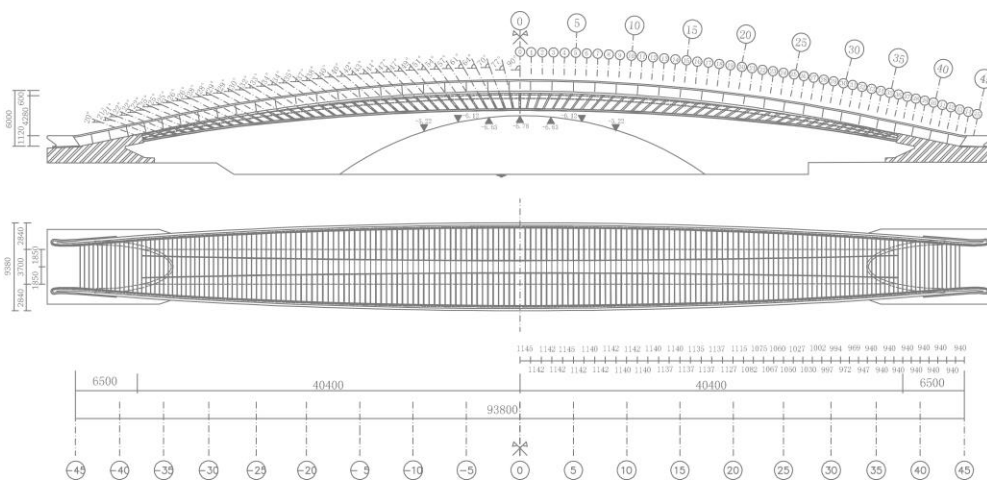


Fig. 30 General arrangement of Calatrava Bridge

Five arches are connected by girders, the latter placed perpendicular to the arches join them together. Horizontal girders connect side arches and central arch together, while vertical girders connect lower arches and central arch together. The girders consist of steel tubes and plates, which form closed section boxes. The typical cross section as shown in Fig. 31 is truss shaped without diagonal, namely open star-like or  $\pi$ -shaped cross section (Briseghella, et al., 2007). The maximum width is 9 m at

the center and with approximately 2.1 m height. There are 38 cross section for each half span and 75 cross sections in total.

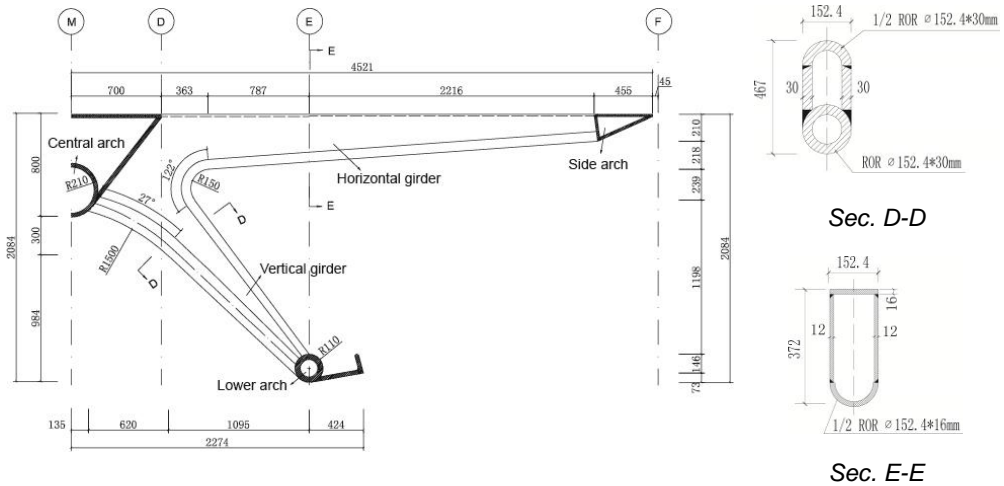


Fig. 31 Typical cross section (right half)

### 5.1.2 Finite Element Model

To perform structural optimization, the bridge is modelled with the finite element analysis software ANSYS (Fig. 32). Shell element SHELL93 is chosen for all the steel structure except two lower arches and steel tubes of girders, which are simulated with BEAM188 element. There are 110869 nodes and 44783 elements in total. All the DOFs (degree of freedom) of central arch and two lower arches at both side are fixed.

Steel grade is Fe510DD according to the Italian code, its strength is equivalent to S355 in Eurocode 3. Therefore, its yield stress is 355 MPa and tensile strength is 510 MPa. The value of the modulus of elasticity was assumed to be 210 GPa. Poisson's ratio and material density were set, respectively, to 0.3 and 7850 kg/m<sup>3</sup>.

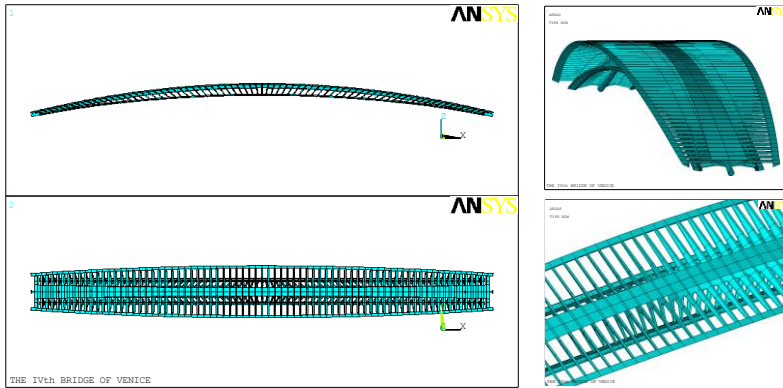


Fig. 32 FE model in ANSYS

A uniformly distributed load of pedestrians of  $6\text{kN/m}^2$  was supposed, with 7 different load cases, as presented in Table 31. These load cases are not only used to calculate the static behavior of the bridge with original parameter, but also used over and over again during optimization looping.

Load case	Loading condition(s)	Loading area(s)
1	Full length full width	
2	Full length half width	
3		
4	Half length full width	
5		
6	Two diagonal areas of half width	
7		

Table 31

The uniformly distributed load of pedestrians is  $6\text{ kN/m}^2$

### 5.1.3 Mechanical Behaviour



Table 32 gives the results of reaction force and deflection of the bridge under all load cases including self-weight and secondary dead load.  $F_x$  is horizontal reaction force with x- and x+ direction while  $F_y$  is vertical reaction force. The direction can be seen from Fig. 32.

Huge horizontal thrust occurred due to the utilization of 1/16 rise-to-span ratio. Maximum 7624.5 kN when loads add on full bridge full width. Horizontal force is 7010.3 kN under self-weight and is 3.5 times of vertical reaction.

Load Cases	x- Direction		x+ Direction		$D_{max}$ (m)
	$F_x$ (kN)	$F_y$ (kN)	$F_x$ (kN)	$F_y$ (kN)	
Self-weight	7010.3	2005.9	-7010.3	2005.9	0.042
Secondary dead load	5367.8	1494.7	-5367.8	1494.7	0.034
Full length full width	7624.5	2082.4	-7624.5	2082.4	0.049
Full length half width	3812.3	1661.6	-3812.3	420.8	0.046
Half length full width	3799.5	1039.0	-3799.5	1039.0	0.030
Two diagonal areas of half width	3789.7	1037.5	-3789.7	1037.5	0.028

Table 32

Results of reaction force and deflection under load cases

The open truss arch ribs with straight-like web members and with no diagonals makes the stiffness of main arch rib small, large bending deformation occurred under symmetric and asymmetric loads. Maximum 0.049m when loads add on full bridge full width, and the deformation shape is illustrated in Fig. 33.

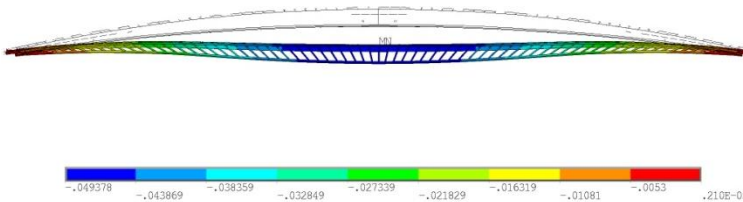


Fig. 33 Deformation shape under full bridge full width load case

Due to the utilization of open star-shape cross section,  $\pi$ -shaped steel plates not only withstand shear force of the main arch, but also bear local bending moment, the stress of some parts reached to the critical state. Maximum von Mises stress always occurred on the steel tubes of vertical girds for each load case. Under full bridge full width load case, the highest value 349 MPa reached to the critical state (Fig. 34).

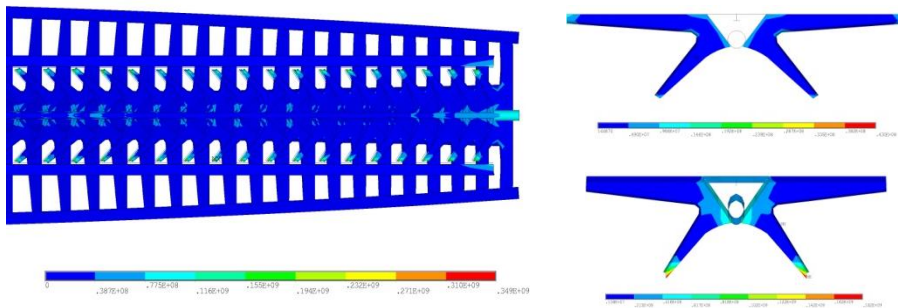


Fig. 34 Von Mises stress of  $\pi$ -shaped cross section

Moreover, the result of modal analysis shows that the third order vibration mode of the main arch of the bridge is close to the pedestrian step frequency, which is extremely liable to cause the pedestrian and bridge resonance. First four mode shapes and frequencies are shown in Fig. 35.

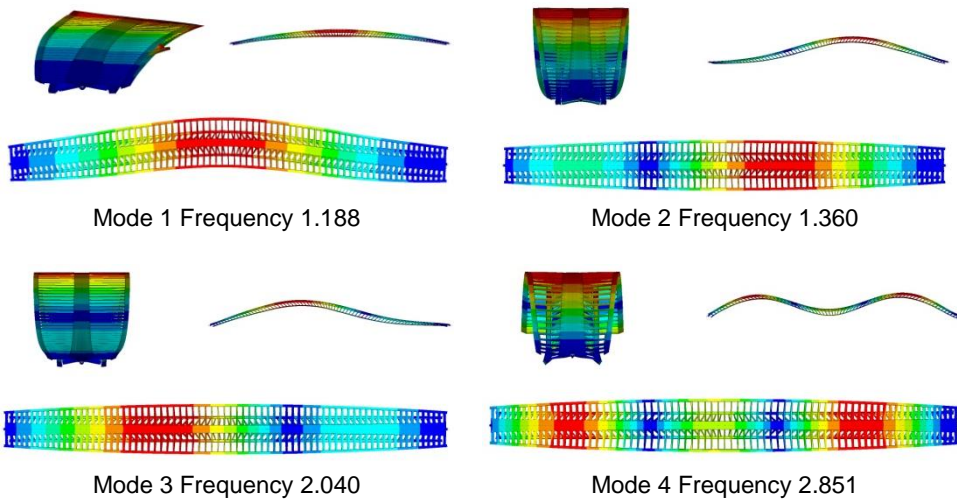


Fig. 35 First four mode shapes and frequencies

## 5.2. Structural Optimization

### 5.2.1 Different Models Considered

As the paper deals with optimization of the bridge structure, in order to identify the best form of the bridge on the basis of original design, three different starting models were hence considered:

- (1) Model I, namely original design of Calatrava bridge, with fixed ends' restraints.
- (2) Model II, same as Model I, but the horizontal constraint ( $D_x$ ) at one end of the bridge is modified from fixed to 1-D spring-damper element COMBIN14 with spring constant  $K$ .
- (3) Model III, same as Model I, but introducing stiffening elements through prestressing cables along two bottom arches of the bridge. Cable cross sectional areas are  $6.4e-3 \text{ m}^2$  (correspond to cables with diameter 90mm), and an initial strain  $\epsilon$  is added to the cables.

The steel plates and tubes thicknesses of identified models were then optimized by using the design optimization tool natively implemented in ANSYS. It provides a zero-order method, where the dependent variables are first approximated by means of least squares fitting, and the constrained minimization problem is then converted to an unconstrained one by means of penalty functions, in order to be solved using Powell's modified method.

Thickness of all steel plates and tubes were assumed as design variables with values ranging between 0.01m and 0.05m. There are 24 design variables (DVs) in total as shown in Fig. 36, named as T1 to T12 at central part and T21 to T32 at two end parts. The optimum design is found by minimizing the total weight of the bridge by imposing that stress level and deflection remaining lower than an allowable value. The state variables (SVs) considered are then stress level and deformation level of the bridge, while the objective function (OBJ) to be minimized is the total volume of steel members. Since the optimum solution is found to be depending on the initial values, different initial values are tried in order to avoid local minimum solutions.

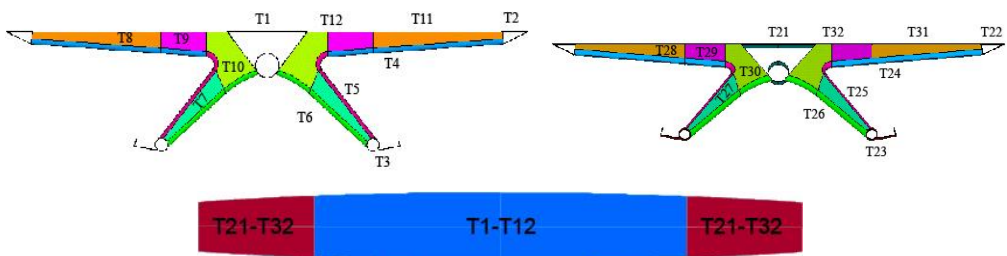


Fig. 36 Design variables of thickness optimization

5.2.2 Optimization Results of Minimizing Total Volume

**Results of Model I**

Fig. 37 illustrates the optimization iterative process of Model I, where the consistent reduction of the objective function is well appreciable. Table 43 (listed at the end of chapter) shows the values of DV, SV and OBJ at different design steps. First one is the initial values to carry out the optimization, bold one is the best design solution. It can be seen that the stress value of best design solution is close to steel yield stress, while the volume reduced by 34%.

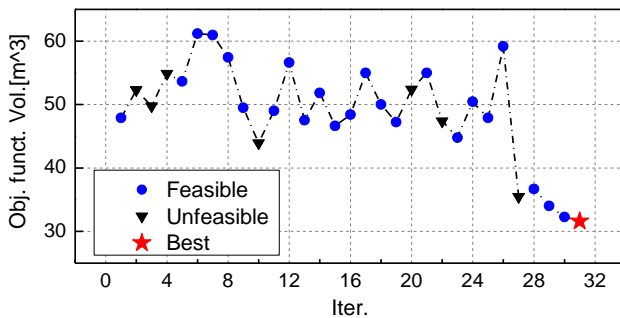


Fig. 37 Convergence iteration of optimization process of Model I

Compared with the original design, the static behavior of the optimum design under same load cases was calculated. The results of reaction force and deflection under all load cases including self-weight and secondary dead load was listed in Table 33.

Because of the thicknesses of some steel plates and tubes are decreased after optimization procedure, horizontal force due to self-weight is 4123.0 kN, corresponding to 58% of the original model. As stiffness was also decreased by the reduction of thickness of steel plates and tubes, the maximum deformation under all load cases are increased. Maximum 0.094m occurred when loads add on full length full width, and is 1.9 times of original model.

Load Cases	x- Direction		x+ Direction		D <sub>max</sub> (m)
	F <sub>x</sub> (kN)	F <sub>y</sub> (kN)	F <sub>x</sub> (kN)	F <sub>y</sub> (kN)	
Self-weight	4123.0	1327.0	-4123.0	1327.0	0.045
Secondary dead load	5159.1	1494.7	-5159.1	1494.7	0.067

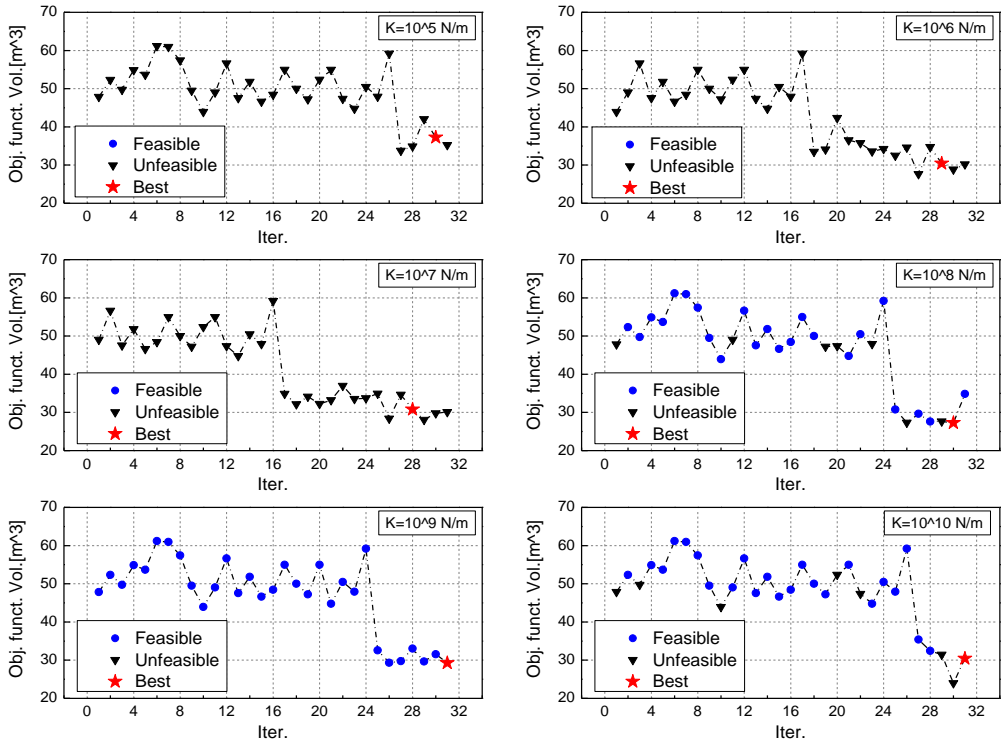
Full length full width	7332.2	2082.4	-7332.2	2082.4	0.094
Full length half width	3666.1	1675.9	-3666.1	406.5	0.086
Half length full width	3653.2	1039.0	-3653.2	1039.0	0.056
Two diagonal areas of half width	3653.1	1039.0	-3653.1	1039.0	0.053

Table 33

Results of reaction force and deflection under load cases

**Results of Model II**

Fig. 38 illustrates the optimization iterative processes of Model II with spring constant  $K$  varying from 5th to 15th power of ten with unit N/m. The consistent reduction of the objective function is well appreciable for each optimization process. There is no feasible design solution when spring constant  $K$  lower than or equal to 7th power of ten on the condition of stress and deflection level, either the limit of stress level exceeded, or the deflection is higher than the specified limit. As the spring constant  $K$  increasing, the boundary condition is getting closer to Model I, and more feasible design solutions are obtained. When the  $K$  is 15th power of ten, the iterative curve and best design solution is same as Model I.



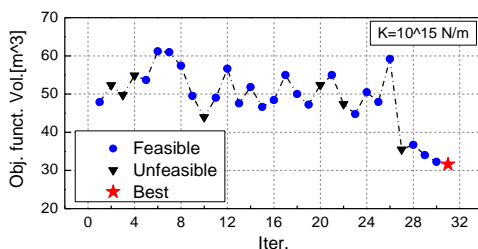


Fig. 38 Convergence iteration of optimization process of Model II

The best design solutions of all optimization iterative processes of Model II with different spring constant value are list in Table 45 (at the end of chapter), some special nodes due to the not so fine mesh of finite element are excluded from the list. Except the best one is obtained from infeasible design solutions when k is 5th or 6th power of ten, others are satisfy the constraints of stress and deflection level. The highest volume reduction is 43% when K is  $10^8$  N/m, while the lowest is 22% as K is  $10^5$  N/m.

Immediately following the optimization procedure of Model II, several candidate solutions was characterized by a specific spring constant K. Hence, the problem of choosing the most suitable solution among candidate solutions is faced. To this purpose, on the basis of the results obtained from optimization procedure, the proposed optimization index analytical formulation is discussed in detail and its effectiveness is validated.

In this real case, two response indexes (*R*'s) which summarize the overall behavior of the whole structure were defined as: Von Mises stress, the maximum throughout the whole steel structure, was considered as representative of stress level, while maximum deflection was considered as representative of deformation level. The trends of both *R*'s are shown in Fig. 39. Both of the *R*'s are decreased for increasing values of spring constant K, and deformation level is always significantly higher than stress level.

Fig. 40 shows global optimization index (*GOI*) varying the spring constant K for some values of  $\beta$  ranging between 0 and 2. The highest *GOI* obtained when spring constant K is  $10^{10}$  N/m, which design solution with a 36% volume reduction.

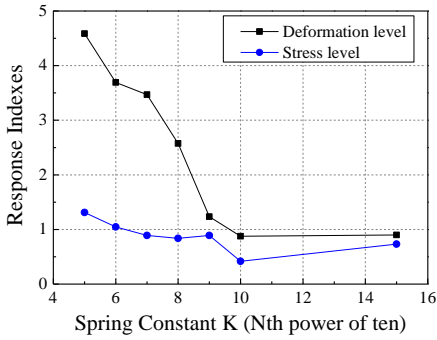


Fig. 39 Response index vs. spring constant K

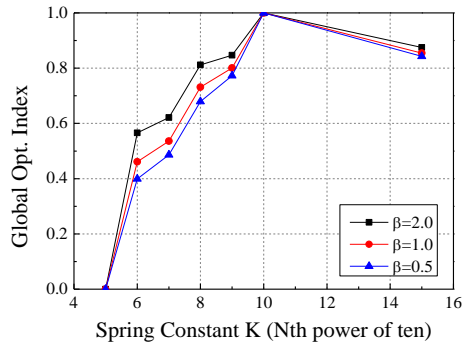


Fig. 40 Global optimization index vs. spring constant K (vs β)

Table 34 gives the results of reaction force and deflection of the bridge under all load cases including self-weight and secondary dead load when spring constant K is  $10^{10}$  N/m. Horizontal force is 4516.4 kN under self-weight and is 3.5 times of vertical reaction. The maximum deformations under all load cases are increased due to the decrease of structure stiffness. The deformation under load case of full length half width with value 0.093m exceeded load case of full length full width and become the maximum deflection under all load cases.

Load Cases	x- Direction		x+ Direction		$D_{max}$ (m)
	$F_x$ (kN)	$F_y$ (kN)	$F_x$ (kN)	$F_y$ (kN)	
Self-weight	4516.4	1278.6	-4516.4	1278.6	0.048
Secondary dead load	5505.8	1494.7	-5505.8	1494.7	0.065
Full length full width	7820.3	2082.4	-7820.3	2082.4	0.091
Full length half width	3910.2	1630.8	-3910.2	451.7	0.093
Half length full width	3897.3	1039.0	-3897.3	1039.0	0.055
Two diagonal areas of half width	3897.3	1039.0	-3897.3	1039.0	0.052

Table 34

Results of reaction force and deflection under load cases

### Results of Model III

Fig. 41 illustrates the optimization iterative processes of Model III with initial strain of stiffening cables varying from 5 to 15 times  $10^{-4}$ . The consistent reduction of the objective function is well appreciable for each optimization process, but is lower than Model II due to the increased deformation with the utilization of stiffening cables. The lower is the initial strain, the more feasible are design solutions.

The best design solutions of all optimization iterative processes of Model III with different initial strain value are list in Table 47 (at the end of chapter). All the best design solutions are satisfy the stress and deflection level constraints. The highest volume reduction is 36% when initial strain is  $8 \times 10^{-4}$ , while the lowest is 2% as initial strain is  $15 \times 10^{-4}$ .

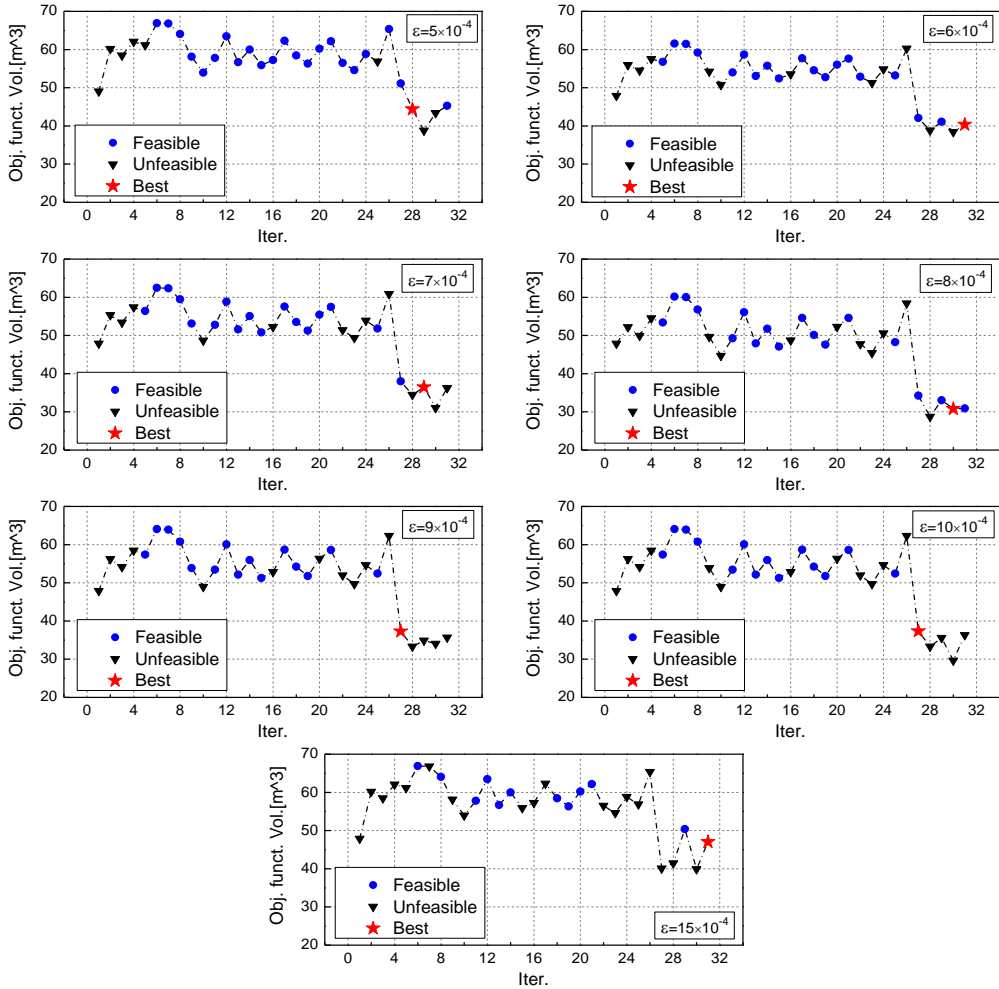


Fig. 41 Convergence iteration of optimization process of Model III

As the same case of Model II, several candidate solutions were characterized by a specific initial strain following the optimization procedure of Model III. Hence, the problem of choosing the most suitable solution is faced. In this case, two response indexes (*R*'s) also defined as the maximum Von Mises stress and the maximum deflection throughout the whole steel structure, respectively.



The trends of both *RIs* are shown in Fig. 42. The *RI* curve of deformation level is decreased for increasing values of initial strain lower than  $8 \times 10^{-4}$ , while curve increased for initial strain higher than  $8 \times 10^{-4}$ . Generally, deformation level is increased except a wave trough around point of initial strain is  $8 \times 10^{-4}$ .

Fig. 43 shows global optimization index (*GOI*) varying the initial strain for some values of  $\beta$  ranging between 0 and 2. The *GOI* decreased as the increased of Initial Strain without  $\beta$ . As mentioned before, the application of penalty exponent  $\beta$  will favour design solution with higher or lower volume reduction. In the case of  $\beta$  is 2, the highest *GOI* obtained when initial strain is  $8 \times 10^{-4}$ , which design solution with the highest volume reduction 36%.

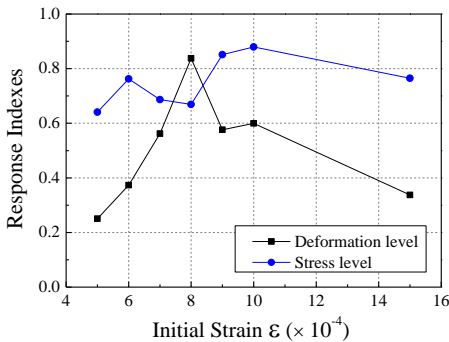


Fig. 42 Response indexes vs. initial strain

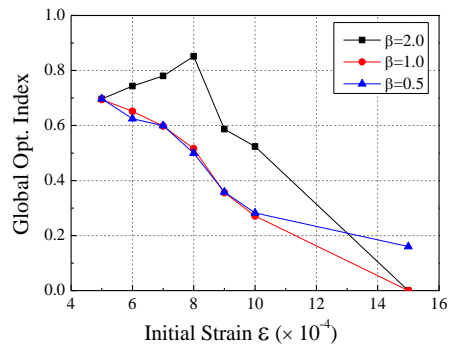


Fig. 43 Global optimization index vs. initial strain  $\epsilon$  (vs  $\beta$ )

Table 35 gives the results of reaction force and deflection of the bridge under all load cases including self-weight and secondary dead load when initial strain is  $8 \times 10^{-4}$ . Horizontal force is decreased due to the utilization of stiffening cables under all load cases. Horizontal force is 4459.9 kN under self-weight and is 3.5 times of vertical reaction. The maximum deformations under all load cases are increased due to the decrease of structure stiffness. The deformation under load case of full length half width with value 0.097m exceeded load case of full length full width and become the maximum deflection under all load cases.

Load Cases	x- Direction		x+ Direction		$D_{max}$ (m)
	$F_x$ (kN)	$F_y$ (kN)	$F_x$ (kN)	$F_y$ (kN)	
Self-weight	4459.9	1292.3	-4459.9	1292.3	0.060
Secondary dead load	5188.6	1494.7	-5188.6	1494.7	0.068
Full length full width	7662.8	2082.4	-7662.8	2082.4	0.091
Full length half width	3480.2	1583.6	-3480.2	498.8	0.097

Half length full width	3467.2	1039.0	-3467.2	1039.0	0.061
Two diagonal areas of half width	3467.1	1037.5	-3467.1	1037.5	0.058

Table 35

Results of reaction force and deflection under load cases

### 5.2.3 Optimization Results of Minimizing Horizontal Force

The same as optimization of minimize total volume, thickness of all steel plates and tubes were assumed as design variables with values ranging between 0.01m and 0.05m. The optimum design was found by minimizing the horizontal force of the bridge on condition that stress level and deflection were lower than an allowable value. The sum of horizontal force under load case of dead load and full length full width is assigned as OBJ.

#### Results of Model I

Fig. 44 illustrates the optimization iterative process of Model I, where the consistent reduction of the objective function is well appreciable. Table 44 (listed at the end of chapter) shows the values of DV, SV and OBJ at different design steps. First one is the initial values to carry out the optimization, bold one is the best design solution. It can be seen that the stress value of best design solution is close to steel yield stress, while the sum horizontal force under dead load and full length full width reduced by 22.7%, which decreased from 14635 kN to 11309 kN. The total volume of steel is decreased from 47.9 m<sup>3</sup> to 39.1 m<sup>3</sup>.

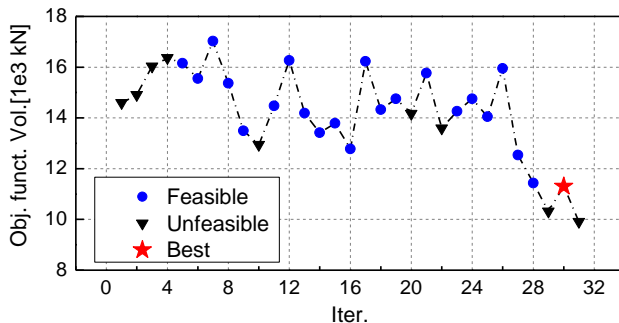


Fig. 44 Convergence iteration of optimization process of Model I

Compared with the original design, the static behavior of the optimum design under same load cases was calculated. The results of reaction force and deflection under all load cases including self-weight and secondary dead load was listed in Table 36.

Because of the thicknesses of some steel plates and tubes are decreased after optimization procedure, horizontal force is 4727.2 kN under self-weight and is 0.68 times compared with original model. As stiffness was also decreased by the reduction of thickness of steel plates and tubes, the maximum deformation occurred under all load cases are increased. Maximum 0.095m when loads add on full bridge full width, and is 1.9 times of original model.

Load Cases	x- Direction		x+ Direction		D <sub>max</sub> (m)
	F <sub>x</sub> (kN)	F <sub>y</sub> (kN)	F <sub>x</sub> (kN)	F <sub>y</sub> (kN)	
Self-weight	4727.2	1626.2	-4727.2	1626.2	0.063
Secondary dead load	4643.3	1494.7	-4643.3	1494.7	0.069
Full length full width	6581.7	2082.4	-6581.7	2082.4	0.095
Full length half width	3290.9	1726.3	-3290.9	356.2	0.078
Half length full width	3278.2	1039.0	-3278.2	1039.0	0.058
Two diagonal areas of half width	3278.0	1039.0	-3278.0	1039.0	0.053

*Table 36*

*Results of reaction force and deflection under load cases*

### **Results of Model II**

Fig. 45 illustrates the optimization iterative processes of Model II with spring constant K varying from 15th to 7th power of ten with unit N/m. The consistent reduction of the objective function is well appreciable for each optimization process.

When the K is 15th power of ten, the iterative curve and best design solution is same as Model I. However, as the spring constant K decreasing, the horizontal constraint is releasing as well as the horizontal force is reducing, but less feasible design solutions are obtained. There is no feasible design solution when spring constant K lower than 7th power of ten on the condition of stress and deflection level, either the limit of stress level exceeded, or the deflection is higher than the specified limit.

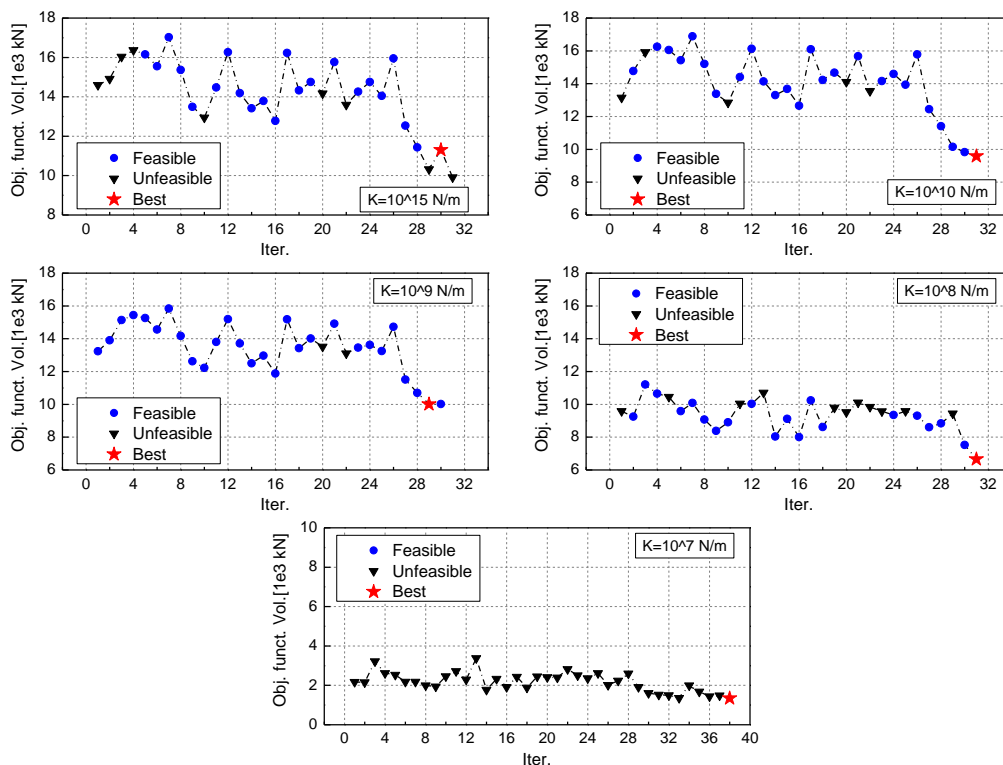


Fig. 45 Convergence iteration of optimization process of Model II

The best design solutions of all optimization iterative processes of Model II with different spring constant value are listed in Table 46 (listed at the end of chapter). Summarized information without DVs is listed in Table 37. Except the best one is obtained from infeasible design solutions when K is 7th power of ten, others are satisfy the stress and deflection level constraints. Among all the design solutions for K from 8th power of ten to 15th power of ten, the lowest horizontal force is 8101 kN when K is 8th power of ten, while the total volume is increased from 47.8 to m<sup>3</sup> to 49.2 m<sup>3</sup>. The highest volume reduction is 25.4% when K is 10th power of ten, and has 9585 kN horizontal force in the meantime, namely 34% force reduction.

K	SMAX (SV)(Pa)	DMAX (SV)(m)	FXALL (OBJ)(MN)	Force Reduction(%)	Volume (m <sup>3</sup> )	VR (%)
Design	1.9E+08	-4.5E-02	14.6	-	47.8	-
7	3.4E+08	-2.1E-01	1.3	91	48.2	-0.8
8	2.2E+08	-9.7E-02	8.1	44	49.2	-2.9
9	3.2E+08	-7.1E-02	10.0	32	41.0	14.4
10	3.5E+08	-1.0E-01	9.6	34	35.7	25.4

15	3.5E+08	-8.5E-02	11.3	23	39.1	18.2
----	---------	----------	------	----	------	------

Table 37  
Optimization results of Model II

Same as optimization of minimize total volume, several candidate solutions was characterized by a specific spring constant  $K$ . Hence, the problem of choosing the most suitable solution is faced. Two response indexes ( $RIs$ ) were defined as the maximum Von Mises stress and maximum deflection throughout the whole steel structure, respectively. The trends of both  $RIs$  are shown in Fig. 46. The  $RIs$  curves decrease for increasing values of spring constant  $K$  from 7th to 9th power of ten until the lowest value occurred when  $K$  is 8th power of ten, while deformation level is always significantly higher than stress level.

Fig. 47 shows global optimization index ( $GOI$ ) varying the spring constant  $K$  for some values of  $\beta$  ranging between 0 and 2. Without favor the solution with high VR, the highest  $GOI$  obtained when spring constant  $K$  is  $10^8$  N/m, which design solution with the highest horizontal force reduction.

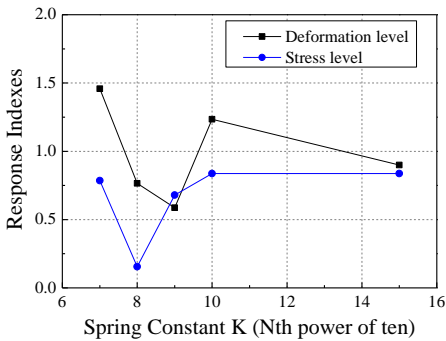


Fig. 46 Response indexes vs. spring constant  $K$

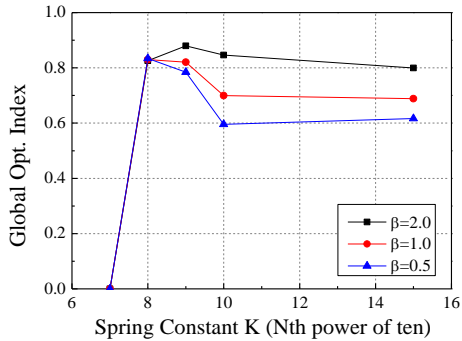


Fig. 47 Global optimization index vs. spring constant  $K$  (vs  $\beta$ )

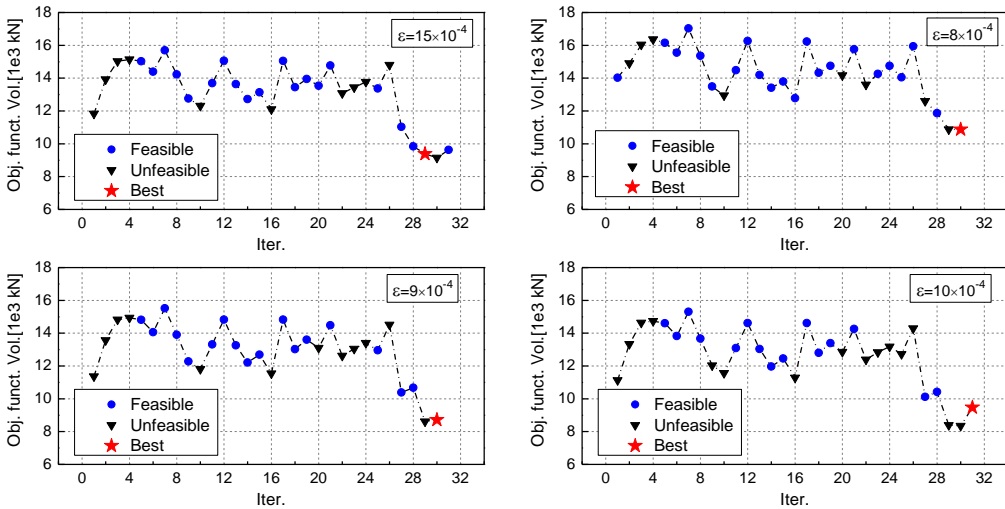
Table 38 gives the results of reaction force and deflection of the bridge under all load cases including self-weight and secondary dead load when spring constant  $K$  is  $10^8$  N/m. Horizontal force is 3974.2 kN under self-weight and is 0.68 times compared with original model. However, due to the consideration of abutment deformability, the deformation under self-weight is increased to 0.091m. The maximum deformations under all load cases are also increased due to the decrease of structure stiffness. The deformation under load case of full length full width has the highest value 0.097m.

Load Cases	x- Direction		x+ Direction		D <sub>max</sub> (m)
	F <sub>x</sub> (kN)	F <sub>y</sub> (kN)	F <sub>x</sub> (kN)	F <sub>y</sub> (kN)	
Self-weight	3974.2	2069.2	-3974.2	2069.2	0.091
Secondary dead load	2909.1	1494.7	-2909.1	1494.7	0.070
Full length full width	4127.0	2082.4	-4127.0	2082.4	0.097
Full length half width	2062.6	1687.7	-2062.6	394.7	0.064
Half length full width	2056.3	1039.0	-2056.3	1039.0	0.053
Two diagonal areas of half width	2056.3	1039.0	-2056.3	1039.0	0.050

Table 38  
Results of reaction force and deflection under load cases

**Results of Model III**

Fig. 41 illustrates the optimization iterative processes of Model III with initial strain of stiffening cables varying from 7 to 15 times  $10^{-4}$ . The consistent reduction of the objective function is well appreciable for each optimization process. Due to the utilization of stiffening cables, all the starting models have found the best design solutions which satisfy the stress and deflection level constraints. The highest horizontal force reduction is 36.3% when initial strain is  $7 \times 10^{-4}$ , while the lowest is 21.9% when initial strain is  $15 \times 10^{-4}$ .



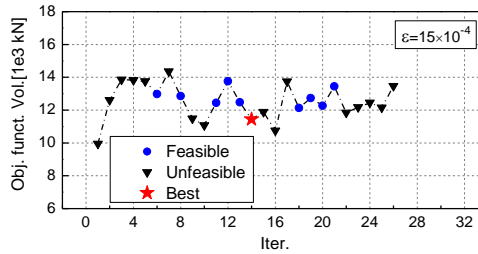


Fig. 48 Convergence iteration of optimization process of Model III

The best design solutions of all optimization iterative processes of Model III with different initial strain value are listed in Table 48 (at the end of chapter). Summarized information without DVs is listed in Table 39. Among all the design solutions for initial strain from 7 to 15 times  $10^{-4}$ , the lowest horizontal force is 9381 kN when initial strain is  $7 \times 10^{-4}$ , and the total volume is decreased from 47.8 to  $\text{m}^3$  to 41.7  $\text{m}^3$ . The highest volume reduction is 16.6% when initial strain is  $8 \times 10^{-4}$ , and has 10872 kN horizontal force in the meantime, namely 25.3% force reduction.

$\epsilon$	SMAX (SV)(Pa)	DMAX (SV)(m)	FXALL (OBJ)(MN)	Force Reduction(%)	Volume ( $\text{m}^3$ )	VR (%)
Design	1.9E+08	-4.5E-02	14.6	-	47.8	-
7	3.6E+08	-6.7E-02	9.3	36.3	41.7	12.8
8	2.9E+08	-6.0E-02	10.9	25.3	39.9	16.6
9	3.2E+08	-7.6E-02	10.2	30.1	40.8	14.6
10	3.2E+08	-6.4E-02	9.5	34.9	44.0	7.9
15	3.4E+08	-5.1E-02	11.4	21.9	60.0	-25.5

Table 39

Optimization results of Model III

As the same case of Model II, several candidate solutions were characterized by a specific initial strain following the optimization procedure of Model III. Hence, the problem of choosing the most suitable solution is faced. In this case, two response indexes (*RIs*) also defined as the maximum Von Mises stress and maximum deflection throughout the whole steel structure.

The trends of both *RIs* are shown in Fig. 49. The *RI* curve of deformation level decreased for increasing values of initial strain higher than  $8 \times 10^{-4}$ . On the contrary, the *RI* curve of stress level increased for initial strain higher than  $8 \times 10^{-4}$ . Generally, stress level is always higher than deformation level.

Fig. 50 shows global optimization index (*GOI*) varying the initial strain for some values of  $\beta$  ranging between 0 and 2. As mentioned before, the application of penalty exponent  $\beta$  will favour design solution with higher or lower volume reduction. The *GOI* decreased for increasing values of initial strain higher than  $9 \times 10^{-4}$ . The highest *GOI* obtained when initial strain is  $9 \times 10^{-4}$ , which design solution with a high horizontal force reduction 30.1% and high volume reduction 14.6%.

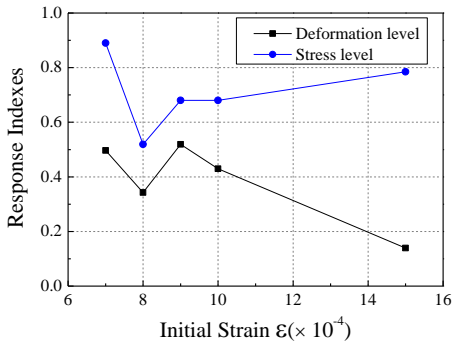


Fig. 49 Response index vs. initial strain

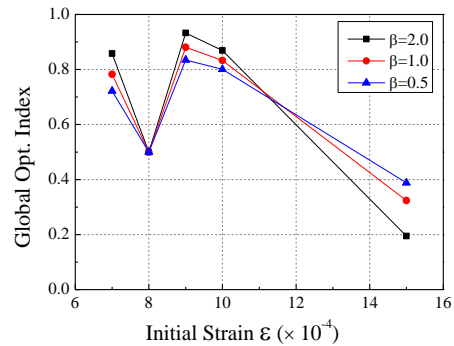


Fig. 50 Global optimization index vs. initial strain (vs  $\beta$ )

Table 40 gives the results of reaction force and deflection of the bridge under all load cases including self-weight and secondary dead load initial strain is  $9 \times 10^{-4}$ . Horizontal force is decreased due to the utilization of prestressing cables under all load cases. Horizontal force is 4381.0 kN under self-weight and is 2.55 times of vertical reaction. The maximum deformations under all load cases are increased due to the decrease of structure stiffness. The deformation under load case of full bridge full width has the highest value 0.076m.

Load Cases	x- Direction		x+ Direction		$D_{max}$ (m)
	$F_x$ (kN)	$F_y$ (kN)	$F_x$ (kN)	$F_y$ (kN)	
Self-weight	4381.0	1716.5	-4381.0	1716.5	0.059
Secondary dead load	3805.9	1494.7	-3805.9	1494.7	0.056
Full length full width	5863.6	2082.4	-5863.6	2082.4	0.076
Full length half width	2385.8	1686.2	-2385.8	396.3	0.064
Half length full width	2373.6	1039.0	-2373.6	1039.0	0.050
Two diagonal areas of half width	2373.6	1039.0	-2373.6	1039.0	0.047

Table 40

Results of reaction force and deflection under load cases



### 5.3. Identification of the Best Design Solution

The optimization results of minimizing total volume are listed in Table 41. The best design solution of model I has a 34% volume reduction compared to the original design. For Model II, the best solution corresponds to a spring constant K equal to  $10^{10}$  N/m, with a 36% volume reduction. The best design solution of Model III corresponds to an initial strain equal to  $8 \times 10^{-4}$ , and lead also in this case to a 36% volume reduction.

Model	Max Stress (Pa)	Max Deflection (m)	Volume (m <sup>3</sup> )	VR (%)
Model I	3.3E+08	-9.4E-02	31.60	34
Model II	2.7E+08	-9.3E-02	30.43	36
Model III	3.2E+08	-9.7E-02	30.83	36

*Table 41*

*Optimization results of three models minimizing total volume*

The optimization results of minimizing horizontal force are listed in Table 42. The best design solution of model I has a 18.2% volume reduction and a 22.7% horizontal force reduction compared to the original design. For Model II, the best solution corresponds to a spring constant K equal to  $10^8$  N/m, with a 44.5% horizontal force reduction but a 2.9% volume rise. The best design solution of Model III corresponds to an initial strain equal to  $9 \times 10^{-4}$ , lead in this case to a 14.6% volume reduction and 30.1% horizontal force reduction.

Model	Max Stress(Pa)	Max Deflection(m)	Horizontal Force (1e6 N)	Force Reduction(%)	Volume (m <sup>3</sup> )	VR (%)
Model I	3.5E+08	-9.5E-02	11.3	22.7	39.1	18.2
Model II	2.2E+08	-9.7E-02	8.1	44.5	49.2	-2.9
Model III	3.2E+08	-7.6E-02	10.2	30.1	40.8	14.6

*Table 42*

*Optimization results of three models minimizing horizontal force*

At the end, the best design solutions between all candidate solutions of three models with the goal of minimizing total volume and horizontal force were trying to obtain with the proposed optimization index. Model I is original design of Calatrava bridge with fixed ends' restraints, Model II modified the horizontal constraint ( $D_x$ ) at one end

of the bridge from fixed to 1-D spring-damper element COMBIN14 with spring constant  $K$  on the basis of Model I, Model III is introducing prestressing cables with initial strain  $\epsilon$  along two bottom arches of the bridge. Hence, as the spring constant  $K$  is higher enough or initial strain  $\epsilon$  is lower enough, Model II or Model III is the same as Model I therefore with same structural behaviour. It can be verified by the optimization results of Model I and Model II with spring constant  $K$  equal to  $10^{15}$  N/m. Therefore, only the results of Model II and Model III are evaluated.

The trends of  $GOI$  varying the spring constant or initial strain for some values of  $\beta$  ranging between 0 and 3 were plotted in Fig. 51 and Fig. 52. As expected, the application of  $\beta$  can favour design solutions of higher or lower volume reduction.

In the case of minimizing total volume, Model II with the spring constant  $K$  is  $10^{15}$  N/m has similar value as Model III with initial strain  $\epsilon$  is  $5 \times 10^{-4}$ . Due to the less influence of bridge stiffness by introducing stiffening cables along two bottom arches than considering bridge's abutment deformability, all the design solutions of Model III have a  $GOI$  value around 0.6 and move from 0.4 to 0.9, while the  $GOI$  value of design solutions of Model II have significant variations and is varying from 0 to 1. However, the optimization process of Model III considered the effect that the deformation and stress of bridge increased as the initial strain increasing, the optimization process of Model II considered the effect that the deformation and stress of bridge decreased as the spring constant  $K$  increasing. Eventually, the highest  $GOI$  value is obtained in Model II when spring constant  $K$  is  $10^{10}$  N/m.

In the case of minimizing horizontal force, Model II with the spring constant  $K$  is  $10^{15}$  N/m has similar value as Model III with initial strain  $\epsilon$  is  $7 \times 10^{-4}$ . The same effect in reducing horizontal force were obtained by modifying the horizontal constraint ( $D_x$ ) at one end of the bridge from fixed to 1-D spring-damper element and by introducing stiffening cables along two bottom arches. The former has lower effect size as the spring constant increasing, while the latter has larger effect size as the initial strain increasing. Considering the effect size and structural response limit in terms of stress and deformation level, both of Model II and Model III have highest  $GOI$  value when the spring constant or initial strain is intermediate value. In that case of each spring constant or initial strain, almost all the design solutions of two Models have same  $GOI$  value, while the design solution of Model III with initial strain  $9 \times 10^{-4}$  is slightly higher.

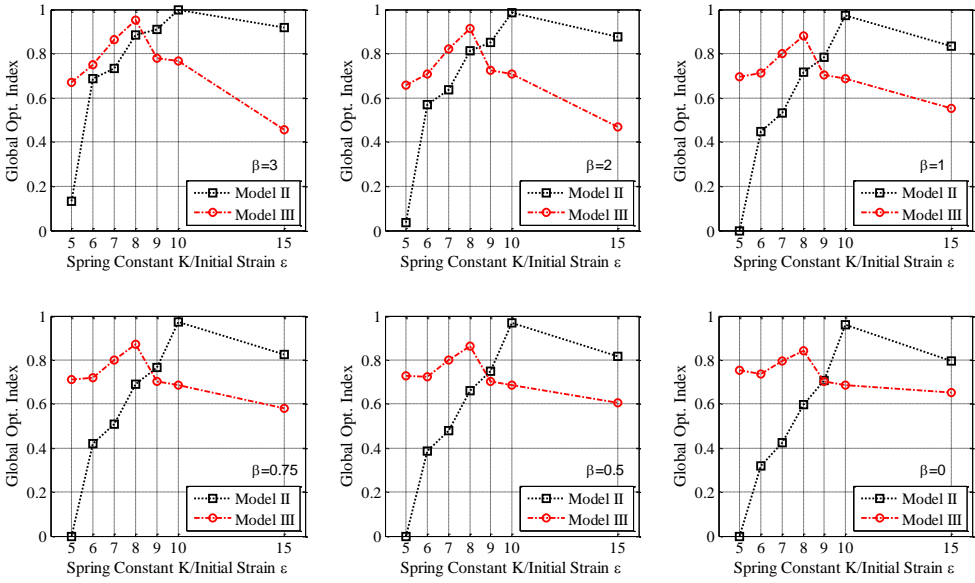


Fig. 51 Global optimization index vs. spring constant or initial strain of minimizing total volume (vs  $\beta$ )

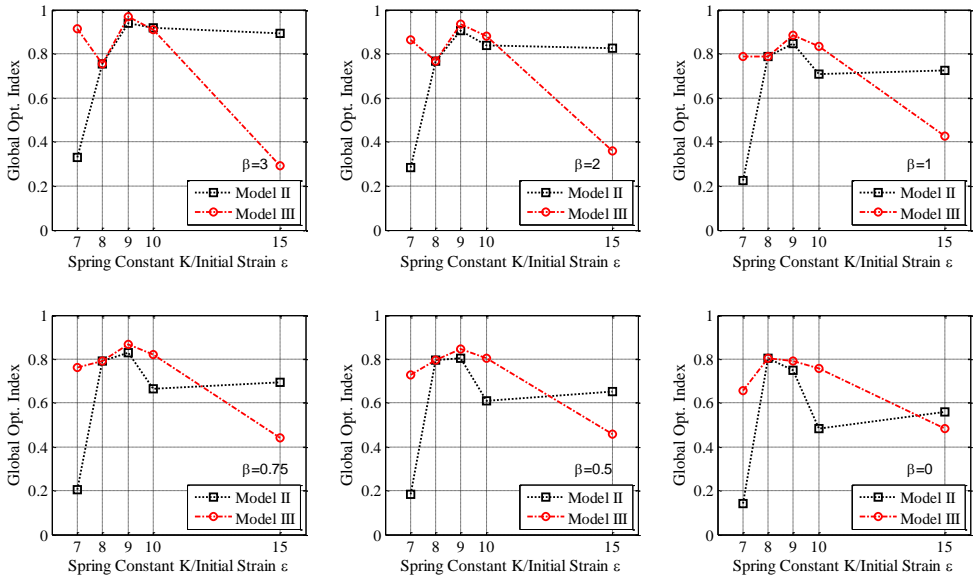


Fig. 52 Global optimization index vs. spring constant or initial strain of minimizing horizontal force (vs  $\beta$ )

No.	SMAX (SV)(Pa)	DMAX (SV)(m)	T1 (DV)	T2 (DV)	T3 (DV)	T4 (DV)	T5 (DV)	T6 (DV)	T7 (DV)	T8 (DV)	T9 (DV)	T10 (DV)	T11 (DV)	T12 (DV)
1	1.9E+08	-4.5E-02	2.5E-02	2.0E-02	4.0E-02	1.6E-02	3.0E-02	3.0E-02	3.0E-02	1.2E-02	2.0E-02	2.5E-02	1.6E-02	2.0E-02
<b>31</b>	<b>3.3E+08</b>	<b>-8.5E-02</b>	<b>1.0E-02</b>	<b>1.0E-02</b>	<b>1.2E-02</b>	<b>1.2E-02</b>	<b>2.2E-02</b>	<b>1.0E-02</b>	<b>2.9E-02</b>	<b>1.0E-02</b>	<b>2.0E-02</b>	<b>1.0E-02</b>	<b>3.5E-02</b>	<b>1.2E-02</b>

Table 43

Results of thickness optimization of Model I with goal of minimizing total volume

No.	T21 (DV)	T22 (DV)	T23 (DV)	T24 (DV)	T25 (DV)	T26 (DV)	T27 (DV)	T28 (DV)	T29 (DV)	T30 (DV)	T31 (DV)	T32 (DV)	VALL(m <sup>3</sup> ) (OBJ)
1	3.0E-02	2.0E-02	7.0E-02	2.0E-02	4.0E-02	4.0E-02	4.0E-02	2.0E-02	3.0E-02	4.0E-02	2.0E-02	3.0E-02	47.8
<b>31</b>	<b>4.1E-02</b>	<b>2.9E-02</b>	<b>2.1E-02</b>	<b>3.1E-02</b>	<b>2.0E-02</b>	<b>1.0E-02</b>	<b>4.2E-02</b>	<b>1.6E-02</b>	<b>1.0E-02</b>	<b>1.1E-02</b>	<b>2.1E-02</b>	<b>2.5E-02</b>	<b>31.6</b>

Table 43 (continued)

No.	SMAX (SV)(Pa)	DMAX (SV)(m)	T1 (DV)	T2 (DV)	T3 (DV)	T4 (DV)	T5 (DV)	T6 (DV)	T7 (DV)	T8 (DV)	T9 (DV)	T10 (DV)	T11 (DV)	T12 (DV)
1	1.9E+08	-4.5E-02	2.5E-02	2.0E-02	4.0E-02	1.6E-02	3.0E-02	3.0E-02	3.0E-02	1.2E-02	2.0E-02	2.5E-02	1.6E-02	2.0E-02
<b>30</b>	<b>3.5E+08</b>	<b>-8.5E-02</b>	<b>1.0E-02</b>	<b>2.1E-02</b>	<b>1.0E-02</b>	<b>1.2E-02</b>	<b>2.1E-02</b>	<b>1.0E-02</b>	<b>2.1E-02</b>	<b>4.4E-02</b>	<b>4.0E-02</b>	<b>1.1E-02</b>	<b>1.9E-02</b>	<b>1.2E-02</b>

Table 44

Results of thickness optimization of Model I with goal of minimizing horizontal force

No.	T21 (DV)	T22 (DV)	T23 (DV)	T24 (DV)	T25 (DV)	T26 (DV)	T27 (DV)	T28 (DV)	T29 (DV)	T30 (DV)	T31 (DV)	T32 (DV)	FXALL (MN)(OBJ)
1	3.0E-02	2.0E-02	7.0E-02	2.0E-02	4.0E-02	4.0E-02	4.0E-02	2.0E-02	3.0E-02	4.0E-02	2.0E-02	3.0E-02	14.6
<b>30</b>	<b>1.3E-02</b>	<b>1.0E-02</b>	<b>4.1E-02</b>	<b>4.5E-02</b>	<b>4.9E-02</b>	<b>4.9E-02</b>	<b>4.8E-02</b>	<b>2.8E-02</b>	<b>1.4E-02</b>	<b>4.7E-02</b>	<b>4.2E-02</b>	<b>4.2E-02</b>	<b>11.3</b>

Table 44 (continued)

K	SMAX (SV)(Pa)	DMAX (SV)(m)	T1 (DV)	T2 (DV)	T3 (DV)	T4 (DV)	T5 (DV)	T6 (DV)	T7 (DV)	T8 (DV)	T9 (DV)	T10 (DV)	T11 (DV)	T12 (DV)
5	4.4E+08	-2.5E-01	1.2E-02	1.6E-02	2.5E-02	2.9E-02	1.1E-02	3.7E-02	3.0E-02	1.2E-02	2.3E-02	1.0E-02	4.7E-02	1.3E-02
6	3.9E+08	-2.1E-01	1.1E-02	1.1E-02	1.5E-02	1.9E-02	1.7E-02	1.1E-02	4.2E-02	1.0E-02	1.1E-02	1.0E-02	1.1E-02	1.0E-02
7	3.6E+08	-2.0E-01	1.4E-02	1.0E-02	1.4E-02	2.8E-02	1.0E-02	1.1E-02	3.4E-02	1.1E-02	1.6E-02	1.0E-02	2.5E-02	2.0E-02
8	3.5E+08	-1.6E-01	1.1E-02	1.1E-02	1.0E-02	1.0E-02	1.1E-02	1.1E-02	1.1E-02	1.0E-02	1.3E-02	1.0E-02	1.9E-02	1.1E-02
9	3.6E+08	-1.0E-01	1.1E-02	1.2E-02	1.0E-02	1.0E-02	1.1E-02	1.1E-02	1.6E-02	1.0E-02	2.6E-02	1.0E-02	3.2E-02	2.3E-02
10	2.7E+08	-8.4E-02	1.1E-02	1.2E-02	1.6E-02	1.6E-02	2.4E-02	1.2E-02	2.9E-02	1.1E-02	2.0E-02	1.0E-02	3.5E-02	1.1E-02
15	3.3E+08	-8.5E-02	1.0E-02	1.0E-02	1.2E-02	1.2E-02	2.2E-02	1.0E-02	2.9E-02	1.0E-02	2.0E-02	1.0E-02	3.5E-02	1.2E-02

Table 45

Results of thickness optimization of Model II with goal of minimizing total volume

K	T21 (DV)	T22 (DV)	T23 (DV)	T24 (DV)	T25 (DV)	T26 (DV)	T27 (DV)	T28 (DV)	T29 (DV)	T30 (DV)	T31 (DV)	T32 (DV)	VALL(m <sup>3</sup> ) (OBJ)	VR (%)
5	4.7E-02	2.5E-02	2.1E-02	2.8E-02	1.1E-02	1.1E-02	4.3E-02	1.1E-02	1.1E-02	1.1E-02	1.3E-02	2.4E-02	37.235	<b>22</b>
6	4.3E-02	1.7E-02	1.8E-02	1.3E-02	2.8E-02	1.1E-02	4.8E-02	1.0E-02	1.3E-02	1.0E-02	2.1E-02	1.4E-02	30.450	<b>36</b>
7	3.4E-02	1.1E-02	2.3E-02	3.0E-02	4.3E-02	1.0E-02	4.3E-02	1.2E-02	1.0E-02	1.0E-02	2.2E-02	1.2E-02	30.806	<b>36</b>
8	3.8E-02	2.3E-02	1.3E-02	1.1E-02	1.6E-02	1.2E-02	1.2E-02	4.5E-02	1.0E-02	1.1E-02	1.8E-02	1.1E-02	27.304	<b>43</b>
9	3.7E-02	2.2E-02	1.4E-02	1.1E-02	1.1E-02	1.2E-02	1.2E-02	2.3E-02	1.0E-02	2.6E-02	3.3E-02	1.4E-02	29.277	<b>39</b>
10	3.0E-02	3.0E-02	2.1E-02	2.8E-02	1.3E-02	1.0E-02	3.0E-02	1.6E-02	1.0E-02	1.1E-02	2.1E-02	2.5E-02	30.433	<b>36</b>
15	4.1E-02	2.9E-02	2.1E-02	3.1E-02	2.0E-02	1.0E-02	4.2E-02	1.6E-02	1.0E-02	1.1E-02	2.1E-02	2.5E-02	31.591	<b>34</b>

Table 45 (continued)

K	SMAX (SV)(Pa)	DMAX (SV)(m)	T1 (DV)	T2 (DV)	T3 (DV)	T4 (DV)	T5 (DV)	T6 (DV)	T7 (DV)	T8 (DV)	T9 (DV)	T10 (DV)	T11 (DV)	T12 (DV)
7	3.4E+08	-2.1E-01	1.3E-02	1.2E-02	4.4E-02	3.6E-02	5.0E-02	2.1E-02	4.4E-02	1.2E-02	1.1E-02	2.4E-02	4.5E-02	1.7E-02
8	2.2E+08	-9.7E-02	1.1E-02	1.9E-02	4.3E-02	3.8E-02	4.1E-02	4.6E-02	4.3E-02	1.5E-02	2.0E-02	2.5E-02	4.8E-02	2.6E-02
9	3.2E+08	-7.1E-02	1.0E-02	3.8E-02	1.0E-02	1.0E-02	4.1E-02	1.0E-02	4.7E-02	4.9E-02	1.8E-02	1.5E-02	1.3E-02	1.0E-02
10	3.5E+08	-1.0E-01	1.0E-02	1.1E-02	1.0E-02	1.0E-02	1.4E-02	1.0E-02	1.5E-02	4.9E-02	3.3E-02	1.1E-02	1.2E-02	1.0E-02
15	3.5E+08	-8.5E-02	1.0E-02	2.1E-02	1.0E-02	1.2E-02	2.1E-02	1.0E-02	2.1E-02	4.4E-02	4.0E-02	1.1E-02	1.9E-02	1.2E-02

Table 46

Results of thickness optimization of Model II with goal of minimizing horizontal force

K	T21 (DV)	T22 (DV)	T23 (DV)	T24 (DV)	T25 (DV)	T26 (DV)	T27 (DV)	T28 (DV)	T29 (DV)	T30 (DV)	T31 (DV)	T32 (DV)	FXALL (MN)(OBJ)	VR (%)
7	5.0E-02	1.2E-02	4.0E-02	1.4E-02	5.0E-02	2.4E-02	4.5E-02	2.1E-02	4.4E-02	4.8E-02	1.6E-02	4.9E-02	1.3	<b>-8.3</b>
8	4.8E-02	1.0E-02	4.2E-02	2.2E-02	5.0E-02	2.1E-02	4.9E-02	1.7E-02	1.1E-02	4.9E-02	1.2E-02	5.0E-02	8.1	<b>-2.9</b>
9	2.0E-02	1.0E-02	3.2E-02	1.8E-02	5.0E-02	2.0E-02	4.3E-02	1.7E-02	3.4E-02	4.7E-02	3.8E-02	4.1E-02	10.0	<b>14.4</b>
10	1.3E-02	1.0E-02	4.1E-02	3.9E-02	4.9E-02	4.9E-02	5.0E-02	1.4E-02	2.0E-02	3.8E-02	4.9E-02	4.0E-02	9.6	<b>25.4</b>
15	1.3E-02	1.0E-02	4.1E-02	4.5E-02	4.9E-02	4.9E-02	4.8E-02	2.8E-02	1.4E-02	4.7E-02	4.2E-02	4.2E-02	11.3	<b>18.2</b>

Table 46 (continued)

$\epsilon$	SMAX (SV)(Pa)	DMAX (SV)(m)	T1 (DV)	T2 (DV)	T3 (DV)	T4 (DV)	T5 (DV)	T6 (DV)	T7 (DV)	T8 (DV)	T9 (DV)	T10 (DV)	T11 (DV)	T12 (DV)
5	3.1E+08	-5.6E-02	2.6E-02	4.8E-02	2.0E-02	2.0E-02	2.6E-02	4.4E-02	2.1E-02	2.7E-02	2.1E-02	2.0E-02	2.1E-02	3.2E-02
6	3.4E+08	-6.2E-02	2.0E-02	2.1E-02	3.3E-02	2.0E-02	2.1E-02	2.4E-02	4.4E-02	2.4E-02	3.0E-02	2.2E-02	2.0E-02	2.1E-02
7	3.2E+08	-7.0E-02	1.7E-02	1.7E-02	2.9E-02	1.6E-02	1.7E-02	2.1E-02	3.7E-02	2.3E-02	2.8E-02	2.0E-02	1.7E-02	1.8E-02
8	3.2E+08	-8.2E-02	1.2E-02	1.2E-02	2.3E-02	1.4E-02	1.3E-02	1.4E-02	4.5E-02	1.4E-02	2.8E-02	1.3E-02	1.2E-02	1.4E-02
9	3.5E+08	-7.1E-02	1.6E-02	1.6E-02	3.6E-02	1.5E-02	1.6E-02	2.3E-02	4.8E-02	2.4E-02	3.1E-02	1.9E-02	1.6E-02	1.7E-02
10	3.6E+08	-7.2E-02	1.6E-02	1.6E-02	3.7E-02	1.5E-02	1.6E-02	2.3E-02	4.8E-02	2.4E-02	3.1E-02	1.9E-02	1.6E-02	1.7E-02
15	3.4E+08	-6.0E-02	2.9E-02	3.3E-02	3.6E-02	2.7E-02	2.3E-02	2.9E-02	2.4E-02	2.1E-02	3.7E-02	2.3E-02	2.1E-02	2.1E-02

Table 47

Results of thickness optimization of Model III with goal of minimizing total volume

$\epsilon$	T21 (DV)	T22 (DV)	T23 (DV)	T24 (DV)	T25 (DV)	T26 (DV)	T27 (DV)	T28 (DV)	T29 (DV)	T30 (DV)	T31 (DV)	T32 (DV)	VALL(m <sup>3</sup> ) (OBJ)	VR (%)
5	2.1E-02	2.8E-02	2.0E-02	2.0E-02	4.9E-02	2.2E-02	2.7E-02	2.1E-02	2.5E-02	2.1E-02	4.4E-02	2.5E-02	44.416	<b>7</b>
6	2.4E-02	2.1E-02	2.2E-02	2.6E-02	2.3E-02	2.1E-02	2.1E-02	2.1E-02	2.2E-02	2.1E-02	2.0E-02	2.3E-02	40.378	<b>16</b>
7	2.3E-02	1.7E-02	2.3E-02	2.3E-02	2.0E-02	1.8E-02	3.9E-02	1.8E-02	2.0E-02	1.7E-02	1.7E-02	2.5E-02	36.456	<b>24</b>
8	2.9E-02	1.8E-02	2.2E-02	2.2E-02	1.7E-02	1.3E-02	1.3E-02	1.3E-02	1.3E-02	1.2E-02	1.2E-02	1.3E-02	30.829	<b>36</b>
9	2.3E-02	1.6E-02	2.4E-02	2.5E-02	2.2E-02	1.7E-02	1.7E-02	1.7E-02	2.2E-02	1.7E-02	1.6E-02	2.5E-02	37.309	<b>22</b>
10	2.3E-02	1.6E-02	2.4E-02	2.5E-02	2.2E-02	1.7E-02	1.7E-02	1.7E-02	2.2E-02	1.7E-02	1.6E-02	2.5E-02	37.335	<b>22</b>
15	2.4E-02	2.5E-02	3.0E-02	2.1E-02	3.5E-02	2.8E-02	2.5E-02	3.1E-02	2.7E-02	2.5E-02	2.5E-02	4.9E-02	47.055	<b>2</b>

Table 47 (continued)

$\epsilon$	SMAX (SV)(Pa)	DMAX (SV)(m)	T1 (DV)	T2 (DV)	T3 (DV)	T4 (DV)	T5 (DV)	T6 (DV)	T7 (DV)	T8 (DV)	T9 (DV)	T10 (DV)	T11 (DV)	T12 (DV)
7	3.6E+08	-6.7E-02	1.6E-02	1.7E-02	1.6E-02	2.3E-02	2.8E-02	1.6E-02	4.3E-02	2.5E-02	1.7E-02	1.8E-02	1.7E-02	3.9E-02
8	2.9E+08	-6.0E-02	1.1E-02	3.9E-02	1.3E-02	1.1E-02	3.6E-02	1.7E-02	4.9E-02	1.2E-02	1.7E-02	4.1E-02	1.4E-02	1.4E-02
9	3.2E+08	-7.6E-02	1.7E-02	1.8E-02	1.7E-02	4.1E-02	1.9E-02	1.5E-02	4.5E-02	1.6E-02	2.1E-02	1.7E-02	1.8E-02	2.1E-02
10	3.2E+08	-6.4E-02	1.9E-02	2.5E-02	2.0E-02	2.8E-02	1.9E-02	1.6E-02	2.8E-02	1.8E-02	2.9E-02	2.2E-02	2.6E-02	2.3E-02
15	3.4E+08	-5.1E-02	3.7E-02	2.2E-02	2.6E-02	4.5E-02	2.3E-02	2.4E-02	2.2E-02	2.9E-02	3.6E-02	4.7E-02	4.2E-02	2.5E-02

Table 48

Results of thickness optimization of Model III with goal of minimizing horizontal force

$\epsilon$	T21 (DV)	T22 (DV)	T23 (DV)	T24 (DV)	T25 (DV)	T26 (DV)	T27 (DV)	T28 (DV)	T29 (DV)	T30 (DV)	T31 (DV)	T32 (DV)	FXALL (MN)(OBJ)	VR (%)
7	2.2E-02	4.6E-02	1.9E-02	2.2E-02	4.7E-02	2.8E-02	4.8E-02	2.5E-02	3.2E-02	4.8E-02	3.5E-02	1.9E-02	9.3	<b>12.8</b>
8	3.5E-02	1.0E-02	1.0E-02	2.3E-02	5.0E-02	1.3E-02	3.9E-02	3.1E-02	1.2E-02	3.8E-02	3.5E-02	1.7E-02	10.9	<b>16.6</b>
9	2.4E-02	1.9E-02	2.5E-02	3.9E-02	4.9E-02	1.9E-02	4.8E-02	3.0E-02	1.7E-02	5.0E-02	3.2E-02	3.5E-02	10.2	<b>14.6</b>
10	2.1E-02	4.0E-02	3.8E-02	2.9E-02	4.9E-02	1.9E-02	4.5E-02	3.1E-02	2.3E-02	5.0E-02	2.2E-02	3.5E-02	9.5	<b>7.9</b>
15	4.5E-02	4.3E-02	4.4E-02	3.2E-02	4.8E-02	2.3E-02	3.3E-02	3.5E-02	2.1E-02	5.0E-02	3.6E-02	3.7E-02	11.4	<b>-25.5</b>

Table 48 (continued)



**CHAPTER 6****6. CABLE-STAYED BRIDGES**

The Stromsund Bridge in Sweden, completed in 1955 with a main span of 182 m is usually recognized as the world's first major cable-stayed bridge, followed in 1957 by the 260 m main span North Bridge in Dusseldorf, Germany. Since the completion of the Stromsund Bridge, the cable-stayed bridge has evolved into the most popular bridge type for long-span bridges and have been later constructed all over the world (Zadeh, 2012). The number is increasing rapidly, the span length has also increased significantly.

A cable stayed bridge is composed of three main components, namely Deck, Pylon or Tower and Cables. A typical cable-stayed bridge is a deck with one or two pylons erected above the piers in the middle of the span. The cables are attached diagonally to the girder to provide additional supports. The deck is the roadway surface of a cable-stayed bridge. Its weight has significant impact on the required stay cables, pylons, and foundations. Towers are the main component of cable stayed bridges to support the bridge self-weight and live load acting on the structure. Cables transfer the load of the structure to the towers. They are usually post-tensioned to minimize the vertical deflection of the deck and lateral deflection of the towers. The stiffness of the structure is highly dependent on the stiffness of the cables.

Cable-stayed bridges are statically indeterminate structures due to its composition. Their structural behavior is the result of a complex interaction between several parameters. The cable arrangement and stiffness distribution in the cables, deck and towers affected the structural behavior of cable-stayed bridge greatly (Walther, 1999). Some researchers made parametric studies including structural elements stiffness, anchorage positions, side-to-central span ratio, etc. between 1980 and 1990. However, few attempts have been made to use optimization techniques (Negrão and Simões, 1997).

In the design of cable-stayed bridges, to get more attractive appearance, sometimes the designer would like to change the total number of cables and angle of the tower. Both of them also play an important role in the mechanical behavior of bridges. In this Chapter, to discuss the interaction between mechanical behavior of

cable-stayed bridge and its parameters like total number of cables and tower angle, immediately following the introduction of cable force optimization methods, two cable-stayed bridges including one Single Tower Single Cable Plane cable-stayed bridge and one Twin Towers Double Cable Planes cable-stayed bridge are served as prototypes, cable cross sectional areas and corresponding initial force optimization and thickness optimization of steel plates of deck are carried out.

## 6.1. Design of Cables

### *6.1.1 Cable Force Optimization Methods*

In the design of cable-stayed bridge, an important step is determining the tensioning forces of stay cables to achieve a desired geometry of the bridge after construction, especially under the reaction of dead load. Cable tensioning has also been recognized as a tool to adjust the stress distribution and the geometry of cable-stayed bridges. Due to the high redundancy of the structural systems, tensioning one single cable also affects the forces in all other cables, the tower, and the bridge deck (Janjic, et al., 2003).

There are a lot of researches about approaches of determine the applied cable tensioning force, such as Zero Displacement Method, Force Equilibrium Method, Minimum Bending Energy, Minimum Bending Moment, Influence Matrix Method and etc. To determine the optimal cable tensioning force, different methods must be adopted for different type of bridges.

Among this approaches, Zero Displacement Method is based on the idea that the stay cables transform the structural system of the girder into a rigidly supported continuous beam. It determines the tensioning forces of stay cables to achieve a desired geometry of the bridge after construction (Janjic, et al., 2003). The method starts by assuming zero tension forces in the stay cables. Based on an assumption of zero deflections in the deck, the equilibrium position of the cable-stayed bridge under dead load action is obtained (Hassan, et al., 2012). The influence matrix describing nodal displacements was then established due to a unit force applied successively along each cable. Then a system of equations can be written for the solution of the post-tensioning force of each cable. By solving this system of equations, the unknown post-tensioning cable forces can be determined (Sung, et al., 2006).

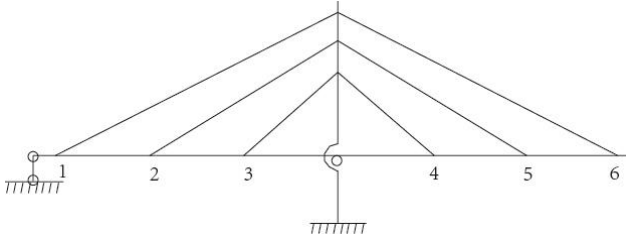


Fig. 53 Scheme of Zero Displacement Method

Take Fig. 53 as example, the first step is calculating the deformation of cable at deck end 1, 2, 3, 4, 5, 6 under self-weight but without tensioning force in cables, namely  $\Delta 1g$ ,  $\Delta 2g$ ,  $\Delta 3g$ ,  $\Delta 4g$ ,  $\Delta 5g$ ,  $\Delta 6g$ . Then the influence value  $\delta_{ki}$  ( $k$  is node number,  $i$  is cable number) are calculated when a unit force applied successively along each cable. Hence, a system of equations can be written on the condition that the deformations of all nodes are zero under self-weight and tensioning force at the same time:

$$\begin{cases} X_1\delta_{11}+X_2\delta_{12}+\cdots+X_6\delta_{16}+\Delta 1g=0 \\ X_1\delta_{21}+X_2\delta_{22}+\cdots+X_6\delta_{26}+\Delta 2g=0 \\ \cdots \\ X_1\delta_{61}+X_2\delta_{62}+\cdots+X_6\delta_{66}+\Delta 6g=0 \end{cases} \quad (18)$$

By solving this system of equations, the unknown post-tensioning cable forces can be determined.

Influence Matrix Method (Rucheng and Haifan, 1998) is a practical optimization method on the basis of general influence matrix. It can not only be applied to determine the optimum cable tensioning force of the bridges, but can also be used to construction control. As we known, for the discrete structure with  $m$  elements, the structural bending energy can be expressed as:

$$U = \sum_{i=1}^m \frac{l_i}{4E_i I_i} (M_{Li}^2 + M_{Ri}^2) \quad (19)$$

Where  $l_i$ ,  $E_i$  and  $I_i$  are length, elastic modulus and inertia moment of element  $i$  respectively,  $M_{Li}$  and  $M_{Ri}$  are left and right bending moments of element  $i$ . The formula also can be expressed as:

$$U = \{M_L\}^T [B] \{M_L\} + \{M_R\}^T [B] \{M_R\} \quad (20)$$

Where  $\{M_L\}$  and  $\{M_R\}$  are the matrix of left and right bending moments, respectively.

$$[B] = \begin{bmatrix} b_{11} & 0 & \cdots & 0 \\ 0 & b_{22} & \cdots & 0 \\ \vdots & \vdots & \vdots & \vdots \\ 0 & 0 & \cdots & b_{mm} \end{bmatrix}, b_{ii} = \frac{l_i}{4E_i I_i} \quad (i = 1, 2, \dots, m) \quad (21)$$

Set the matrix of left and right bending moments without tensioning force are  $\{M_{LO}\}$  and  $\{M_{RO}\}$  respectively, the  $l$  order vector of initial cable force is  $\{T\}$ , which is the same order as the number of cable. Hence, the matrix of left and right bending moments with tensioning force are:

$$\begin{aligned} \{M_L\} &= \{M_{LO}\} + [C_L] \{T\} \\ \{M_R\} &= \{M_{RO}\} + [C_R] \{T\} \end{aligned} \quad (22)$$

To obtain minimum bending moment of structure, then:

$$\frac{\partial U}{\partial T_i} = 0 \quad (i = 1, 2, \dots, l) \quad (23)$$

It can be expressed as:

$$\left( [C_L]^T [B] [C_L] + [C_R]^T [B] [C_R] \right) \{T\} = -[C_R]^T [B] \{M_{RO}\} - [C_L]^T [B] \{M_{LO}\} \quad (24)$$

By solving this system of equations, the unknown post-tensioning cable forces can be determined.

### 6.1.2 Optimization Problem Description

The cables to be optimized consist of two different parts, namely cable cross sectional area optimization and cable initial force optimization. For a given set of cable cross sectional area, the optimum initial cable force can be obtained through the methods mentioned above. With the purpose of minimizing the cable cross sectional area, the problem can be defined by Design Variables (DV), Constraints Function (CON) and Objective Function (OBJ).

**Design Variables (DV):** cable cross sectional areas,  $x_i = A_i$  ( $i = 1, 2, \dots, n$ ),  $n$  is the total number of cables.

**Constraints Function (CON)**

- 1) The maximum tensile stress of the cables under all load cases are no more than the allowable stress,  $\sigma_i \leq \sigma_{max}$  ( $i = 1, 2, \dots, n$ )
- 2) The deformation of cables at deck end under all load cases are no more than the allowable deformation,  $D_i \leq D_{max}$  ( $i = 1, 2, \dots, n$ )
- 3) The deformation of tower top in longitudinal direction is no more than the allowable deformation,  $u_i \leq u_{max}$ .

**Objective Function (OBJ):** total volume of cables,  $f = \sum_{i=1}^n l_i \cdot A_i$  ( $i = 1, 2, \dots, n$ ).

### 6.1.3 Programs Implemented for Optimization

There are two methods in the "Optimization toolbox" of MATLAB (MathWorks Inc., 2011), namely *fmincon* and *lsqnonlin*. The former is a trust region method in which derivative information is used to compute a good approximation of the objective function in a small trust region. The latter uses specific least squares techniques. However, both of them are all local, so there is uncertainty about the nature of the optimum and strong dependence on the initial starting values. If the starting point is too near a local minimum, it may find that point instead of the global minimum.

Therefore, the method of the Coupled Local Minimizers (CLM) is implemented as shown in Fig. 54. CLM is a recently developed global optimization technique (MathWorks Inc., 2011, Suykens, et al., 2001, Teughels, et al., 2003). In this method, the information of several local optimizers is combined to avoid local optima. The local optimizations are started from random points over the domain, and constraints are imposed to force the search points to end up in the same point. In a successful run, this point has the lowest function value, and is the global minimum. The reliability of this method is due to the evaluation of a lot of points, spread over the domain. The advantage compared to other global methods is the use of first order

information, which enforces faster convergence. To reduce calculation time, this method is used to identify the global minimum with a limited precision. When the search points have located the valley of the global minimum, the CLM-method is stopped and a local method is used until the necessary precision is reached (Cheng, 2012).

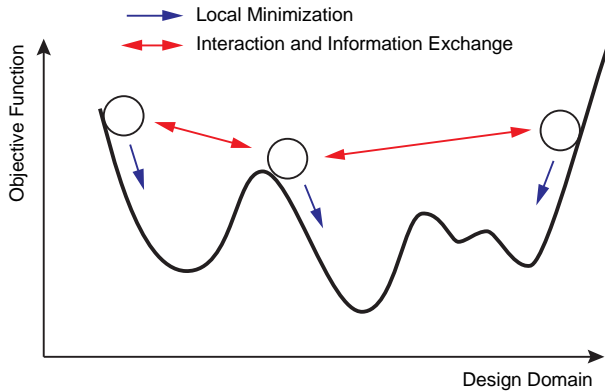


Fig. 54 Illustration of Coupled Local Minimizers

#### 6.1.4 Optimization Procedure

The optimization procedure is illustrated in Fig. 55. In the presented procedure, it is collaborated with main coding program of MATLAB and finite element modeler and solver of ANSYS. Based on the optimization description, the design variables were assigned firstly. Then their values were wrote to file and passed into ANSYS to calculate the bridge bending energy or displacement matrix and into subroutines in MATLAB to computes the constraint function and objective function. Before the verification of state variables meet the constraint function, initial tension force is calculated in MATLAB and passed into ANSYS to get the actual state variables.

Based on these loops of creating design variables (DVs) then calculating constraints (SV/CON) and objectives (OBJ), the sampling of the optimization problem was passed to the "Global Optimization" setup. Then, by setting some control parameters of global search, such as variables tolerances, maximum iteration number and search step size, coupled local minimizers would be launched, until the converged optimal solution was found, or infeasible results if tolerances or maximum iteration numbers were reached.

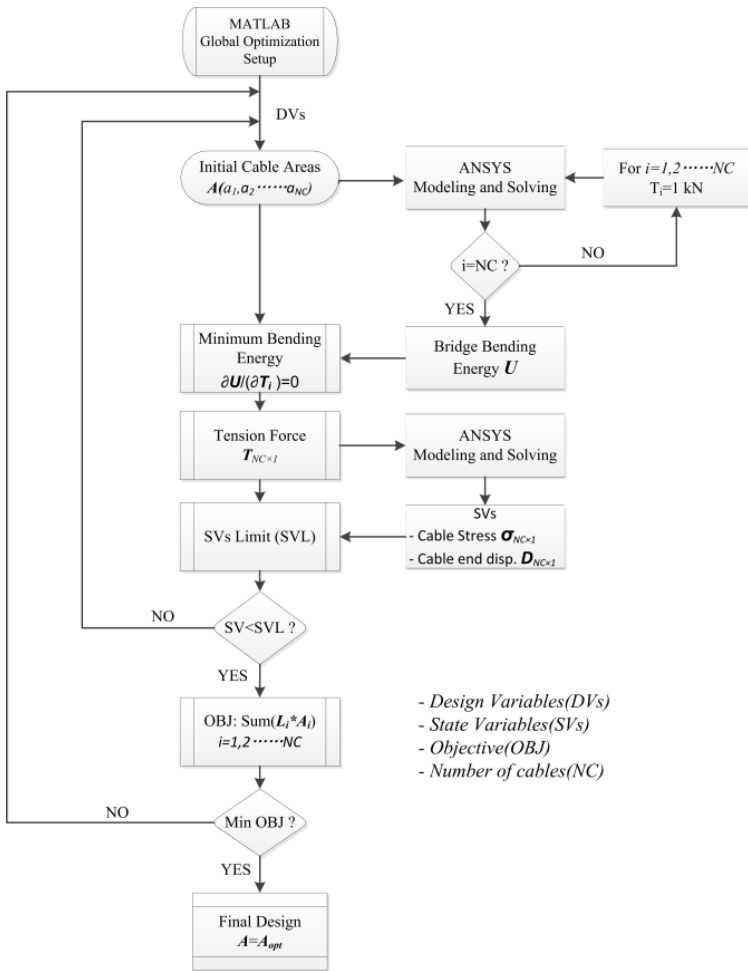


Fig. 55 Flowchart of optimization procedure

## 6.2. Single Cable Plane Cable-stayed Bridge

### 6.2.1 General Situation

The bridge is a Single Tower Single Cable Plane cable-stayed bridge as shown in Fig. 56, located in Pescara, Italy. It has a total length 118.8m from the bottom center of tower to the other end and a 86m long deck. Single inclined tower with special shape is adopted which composed of two separated part (39.5m and 52.4m high, respectively) but connected at the centre of tower.

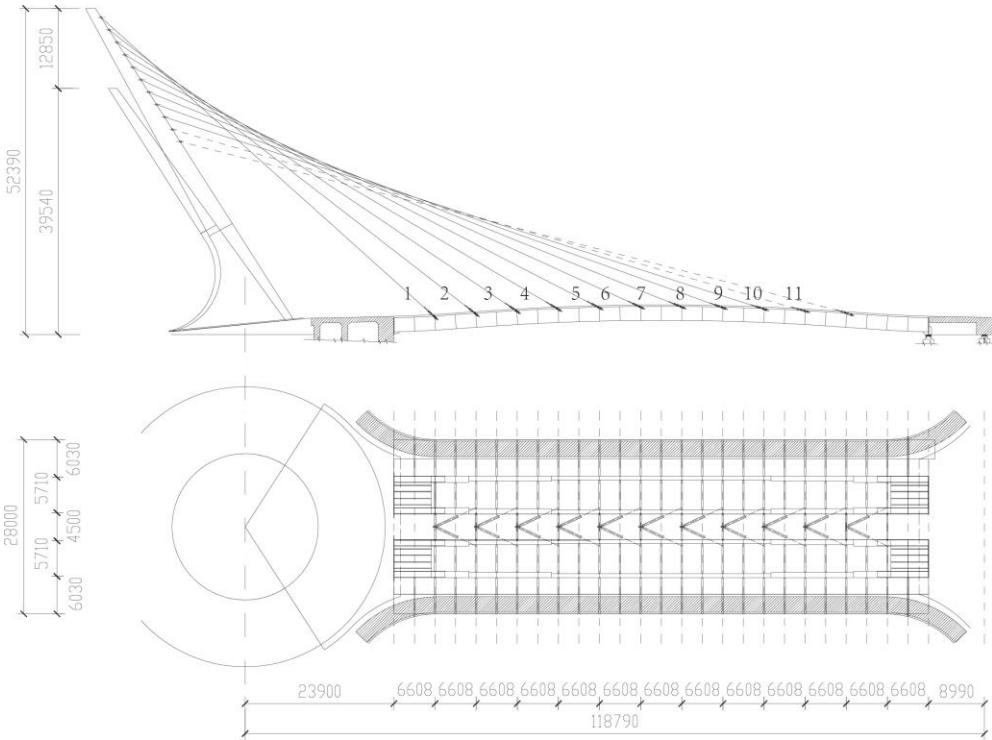


Fig. 56 Geometry of Pescara Bridge, Italy (unit: mm)

The deck section is shown in Fig. 57. The total width of deck is 28m. It has 7.9m width for lanes and 3.15m for walkway at each side. Steel plates and tubes consist of two steel boxes at each side and connect together by steel tubes, which form the typical bridge deck section. The dimensions and thicknesses of them are shown in Fig. 57.

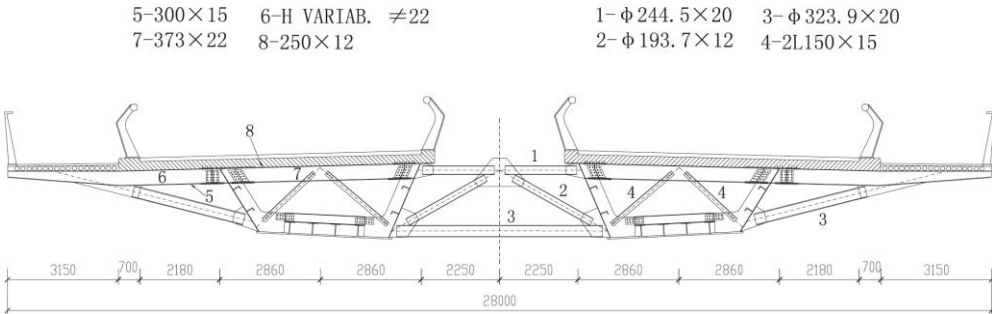


Fig. 57 Cross section of deck(unit: mm)



### 6.2.2 Finite Element Model

Using software ANSYS to build the finite element model. There are 9719 nodes and 7476 elements in total. Steel tubes and tower using Beam188 element, deck using Shell63, while cables using Link10 element. Finite element model is shown in Fig. 58. To simulate the actual boundary conditions of the bridge, the bottom of tower and two ends of the deck are fixed.

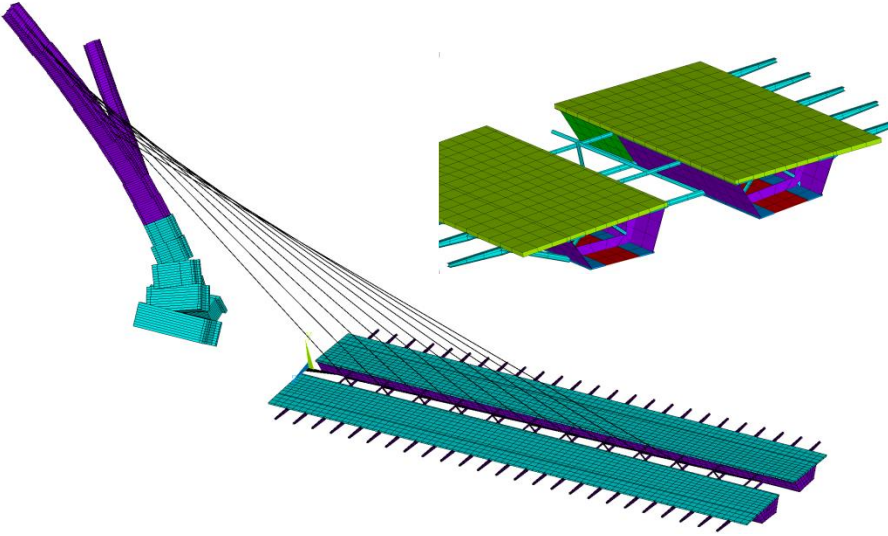


Fig. 58 Finite Element Model

Steel grade is S355 in Eurocode 3. Therefore, its yield stress is 355 MPa and tensile strength is 510 MPa. The value of the modulus of elasticity was assumed to be 210 GPa. Poisson's ratio and material density were set to 0.3 and 7850 kg/m<sup>3</sup>, respectively. According to the Eurocode 2, concrete with strength class C35/45 was chosen. Its characteristic cylinder strength was 35 MPa, the average tensile strength of concrete before cracking was 3.2 MPa ( $f_{ctm} = 0.30f_{ck}^{2/3}$ ). The value of the modulus of elasticity was assumed to be 34 GPa. Poisson's ratio and material density were set, respectively, to 0.2 and 2500 kg/m<sup>3</sup>.

5 different live loads due to pedestrian (5kN/m<sup>2</sup>) and truck loading were taken, besides permanent loads (self-weight plus dead loads due to guard-rail, asphalt and etc.). The truck loading is 9kN/m<sup>2</sup> uniformly distributed load plus 300kN × 2 concentrate loads for first lane, 2.5kN/m<sup>2</sup> uniformly distributed load for other lanes and additional plus 200kN × 2 concentrate loads for 2nd lane. In order to maximize

both bending and shear forces, 5 different positions for tandem load were considered (0,  $\frac{1}{4}$ ,  $\frac{1}{2}$ ,  $\frac{3}{4}$  and 1 of the span length).

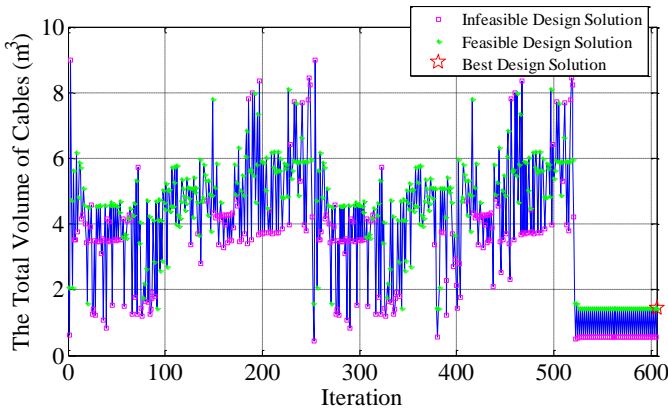
### *6.2.3 Cable Area and Initial Force Optimization Results*

To obtain the best design solution of cable-stayed bridge, different starting models were defined through the utilization of different cable number. The starting models with total number of cables 10, 9 and 11 were defined and their cable cross sectional area and corresponding initial force were optimized.

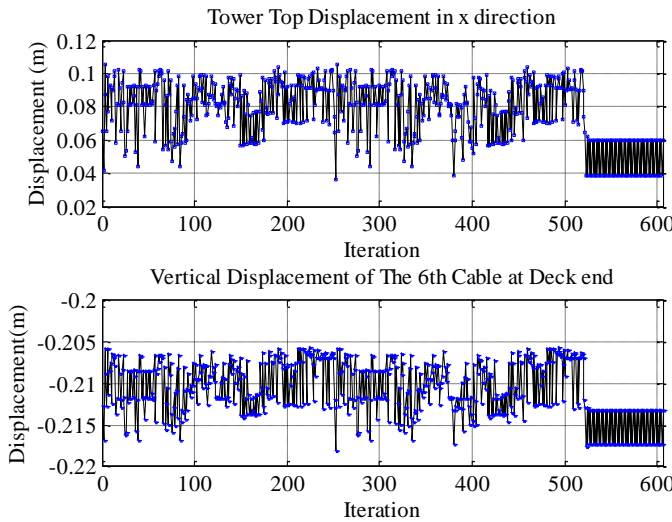
In the case of starting model with 10 cables, starting from the initial cable cross sectional areas  $2.29\text{e-}3\text{ m}^2$  (correspond to cables with diameter 54mm), which with a lower bound  $0.5\text{e-}3\text{ m}^2$  and upper limit  $10\text{ e-}3\text{ m}^2$  (correspond to cables with D25mm and D108mm, respectively), the total volume of steel cables was minimized. The optimization process converged after more than 600 iterations. Fig. 59 illustrates the optimization iterative process of total cable volume and longitudinal deformation of tower top and vertical deformation of the 6<sup>th</sup> cable at deck end.

Not all the design solutions are feasible due to the constraint function. 1000 MPa was set as the allowable maximum tensile stress of the cables under all load cases, the allowable deformations of cables at deck end and tower top were also set according to the bridge span and tower height, respectively. In the convergence iteration of total cable volume, pink square symbols show the infeasible design solutions, which not meet the requirement of stress or deformation constraints, meanwhile conversely, green star symbols show the feasible design solutions and the one among them with minimum total cable volume is the best design solution. The latter was marked with red pentagram symbol.

Concerning the objective function, the total volume of cables moves from  $1\text{ m}^3$  to  $10\text{ m}^3$ , and reached to minimum value  $1.428\text{ m}^3$  which meets the constraint function. The tower top displacement in longitudinal direction moves from 0.04m to 0.1m and with a 0.06m value when the total volume of cables is minimum. Because of two end of the deck are fixed, the initial force has little influence on the displacement of deck. The vertical displacement of the 6<sup>th</sup> cable at deck end moves from -0.22m to -0.2m and with a -0.213m value when the total volume of cables reached to minimum.



a) Convergence iteration of total cable volume



b) Convergence iteration of deformation

Fig. 59 Convergence iteration of starting model with 10 cables

The distribution of cable area and initial cable force is illustrated in Fig. 60. The optimization results lead to larger area for cables attached to both ends of the deck and cables close to the middle span. The former occurred due to they are the ones brace the tower, the latter occurred due to the deformation limit of cable deck end. The maximum cable area is  $2.72e-3 \text{ m}^2$ , correspond to cable with diameter 60mm, while the minimum is reached to the lower bound  $0.5e-3 \text{ m}^2$ . The maximum initial cable force is 1012 kN occurred in the 10<sup>th</sup> cable, and the minimum is 50 kN which is assigned due to minus value was calculated according to the cable force optimization method.

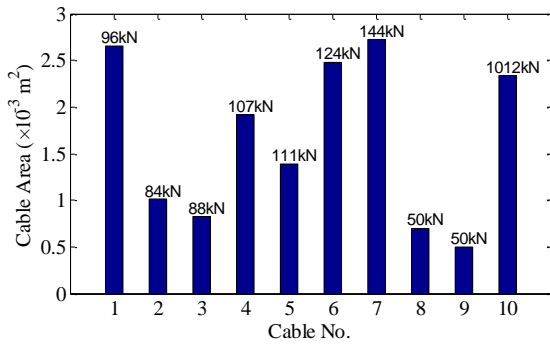
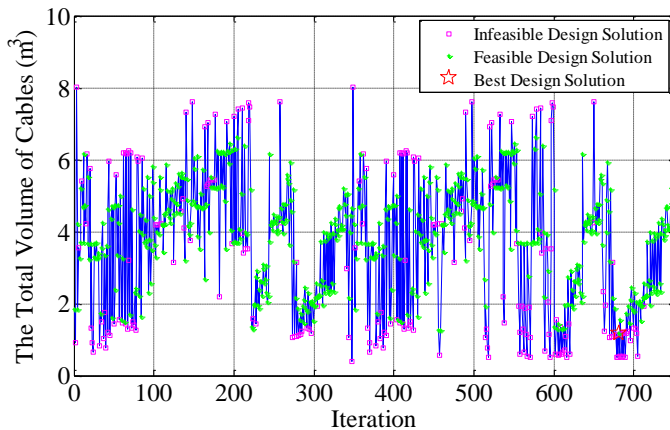


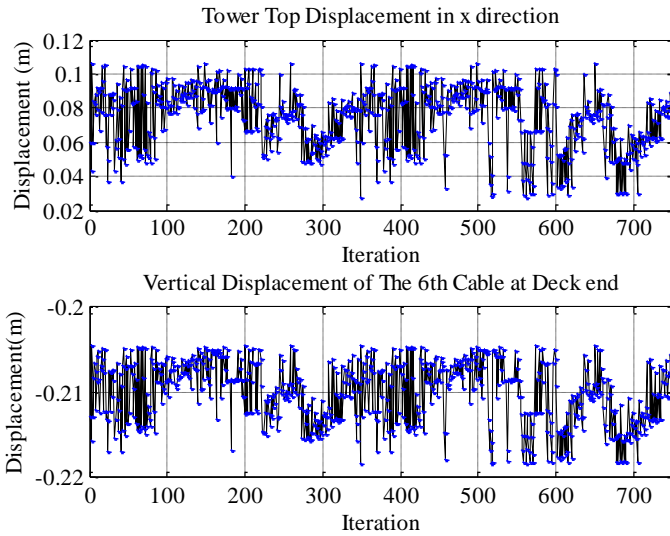
Fig. 60 Distribution of cable area and initial cable force

In the case of starting model with 9 cables, starting from the same initial cable cross sectional areas  $2.29 \times 10^{-3} \text{ m}^2$ , same lower bound  $0.5 \times 10^{-3} \text{ m}^2$  and upper limit  $10 \times 10^{-3} \text{ m}^2$ , the total volume of steel cables was minimized. The optimization process converged after more than 700 iterations. Fig. 61 illustrates the optimization iterative process of total cable volume and longitudinal deformation of tower top and vertical deformation of the 6<sup>th</sup> cable at deck end.

Concerning the objective function, the total volume of cables moves from  $1 \text{ m}^3$  to  $8 \text{ m}^3$  and reached to minimum value  $1.160 \text{ m}^3$ . The tower top displacement in longitudinal direction moves from  $0.03 \text{ m}$  to  $0.11 \text{ m}$  and with a  $0.05 \text{ m}$  value when the total volume of cables is minimum. The vertical displacement of the 6<sup>th</sup> cable at deck end moves from  $-0.22 \text{ m}$  to  $-0.2 \text{ m}$  and with a  $-0.215 \text{ m}$  value when the total volume of cables is minimum.



a) Convergence iteration of total cable volume



b) Convergence iteration of deformation

Fig. 61 Convergence iteration of cable volume with 9 cables

The distribution of cable area and initial cable force is illustrated in Fig. 62. The optimization results lead to larger area for cables attached to one end of the deck and cables close to the middle span. The maximum cable area is  $2.77\text{e-}3 \text{ m}^2$ , correspond to cable with diameter 60mm, which has the maximum initial cable force 855 kN at the same time, while the minimum is almost reached to the lower bound with a value  $0.55\text{e-}3 \text{ m}^2$ . The minimum initial cable force is 33 kN which is occurred in 7<sup>th</sup> cable.

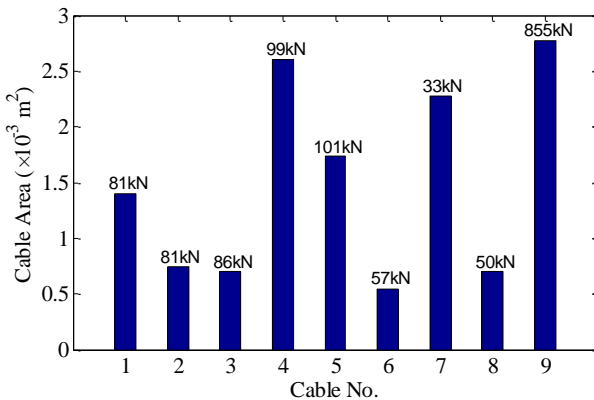
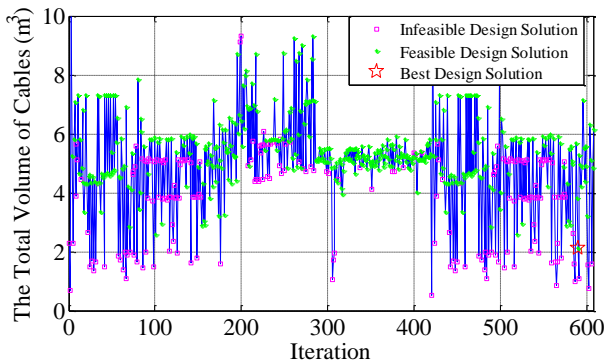


Fig. 62 Distribution of cable area and initial cable force

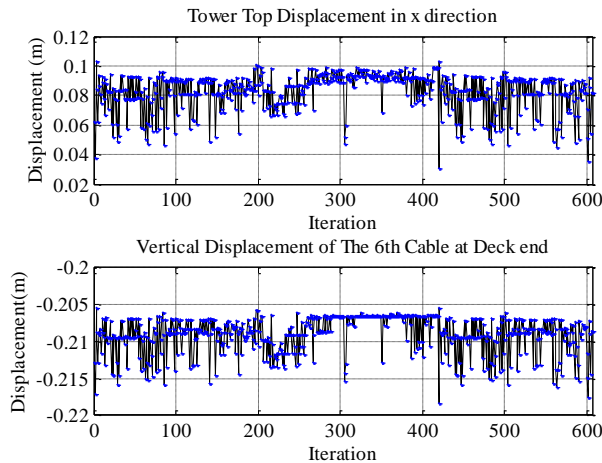
In the case of starting model with 11 cables, starting from the same initial cable cross sectional areas  $2.29\text{e-}3 \text{ m}^2$  and same lower bound  $0.5\text{e-}3 \text{ m}^2$  and upper limit

$10e-3 \text{ m}^2$ , the total volume of steel cables was minimized. The optimization process converged after more than 600 iterations. Fig. 63 illustrates the optimization iterative process of total cable volume and longitudinal deformation of tower top and vertical deformation of the 6<sup>th</sup> cable at deck end.

With regards to the objective function, the total volume of cables moves from  $1 \text{ m}^3$  to  $10 \text{ m}^3$ , and reached to minimum value  $2.103 \text{ m}^3$  which meets the constraint function. The tower top displacement in longitudinal direction moves from  $0.04 \text{ m}$  to  $0.1 \text{ m}$  and with a  $0.066 \text{ m}$  value when the total volume of cables is minimum. The vertical displacement of the 6<sup>th</sup> cable at deck end moves from  $-0.22 \text{ m}$  to  $-0.2 \text{ m}$  and with a  $-0.212 \text{ m}$  value when the total volume of cables is minimum.



a) Convergence iteration of total cable volume



b) Convergence iteration of deformation

Fig. 63 Convergence iteration of cable volume with 11 cables

The distribution of cable area and initial cable force is illustrated in Fig. 64. The optimization results lead to larger area for cables close to the middle span. It occurred due to the deformation limit of cable deck end. The maximum cable area is  $2.96 \times 10^{-3} \text{ m}^2$ , correspond to cable with diameter 62mm, while the minimum is reached to the lower bound  $0.5 \times 10^{-3} \text{ m}^2$ . The maximum initial cable force 471 kN occurred in the 10<sup>th</sup> cable, and the minimum is 50 kN which is assigned due to the minus value was calculated according to the cable force optimization method.

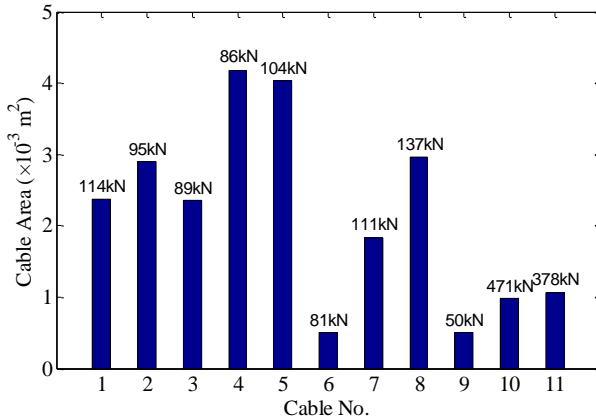


Fig. 64 Distribution of cable area and initial cable force

All the results of different starting models are listed in Table 49, including the optimized cable area and its corresponding initial cable force. The original design is obtained from design institute, which has the same area for all the cables and a roughly equal initial cable force due to the judgment of designer.

In this research, the cable area and its initial force are obtained through the optimization procedure for all the starting models. Although their values are unrealistic to apply to the actual project due to the significant variations and commercial dimensions of cables, the original values are kept to give an idea to designer about how much cross sectional area is necessary for each cable under certain stress and displacement constraints.

The structural arrangement of starting model with 10 cables is the same as original design, while the latter has a significant reduction of total cable volume which from  $2.059 \text{ m}^3$  to  $1.428 \text{ m}^3$ . The starting model with 9 cables reduced more cable volume due to one cable less after optimization process, on the contrary, the cable volume of starting model with 11 cables is slightly higher than original design due to one cable more. Optimization results of all starting models lead to larger cross sectional

area and initial tensioning force for cables attached to far end of the deck, which occurred due to it is the one brace the tower.

Cable No.	Original design		10 cables		9 cables		11 cables	
	Area (e-3 m <sup>2</sup> )	Force (kN)	Area (e-3 m <sup>2</sup> )	Force (kN)	Area (e-3 m <sup>2</sup> )	Force (kN)	Area (e-3 m <sup>2</sup> )	Force (kN)
1	2.29	133.7	2.66	95.9	1.40	81.1	2.37	114.4
2	2.29	130.2	1.01	83.8	0.74	81.1	2.90	94.9
3	2.29	153.0	0.82	88.2	0.70	85.5	2.35	89.2
4	2.29	170.1	1.92	107.0	2.61	99.2	4.18	85.6
5	2.29	179.6	1.39	111.3	1.73	101.0	4.03	103.6
6	2.29	182.3	2.48	123.8	0.55	56.8	0.50	81.1
7	2.29	189.4	2.72	144.1	2.28	33.4	1.84	111.4
8	2.29	192.0	0.70	50.0	0.70	50.0	2.96	137.1
9	2.29	195.8	0.50	50.0	2.77	855.1	0.50	50.0
10	2.29	198.0	2.33	1011.5	-	-	0.98	471.0
11	-	-	-	-	-	-	1.06	377.5
<b>Obj.(m<sup>3</sup>)</b>	<b>2.059</b>		<b>1.428</b>		<b>1.160</b>		<b>2.103</b>	

Table 49  
Initial tension force in cables

### 6.2.4 Thickness Optimization

Immediately following the cable cross sectional area and initial force optimization, for each starting model, thickness of steel plates were optimized by using the design optimization tool implemented in ANSYS. It provides a zero-order method, where the dependent variables are first approximated by means of least squares fitting, and the constrained minimization problem is then converted to an unconstrained one by means of penalty functions, in order to be solved using Powell's modified method.

Three different regions of the steel deck were identified, where thickness of web, bottom and top flanges had to be identified (Fig. 65). Thickness of steel plates were assumed as design variables with values ranging between 0.1m and 0.5m in part 2 and 3, but ranging between 0.3m to 0.8m in part 1. An optimization problem with 12 discrete variables was hence identified. The optimum thickness was found by minimizing the deck total weight on condition that stress level and deflection were lower than an allowable value.



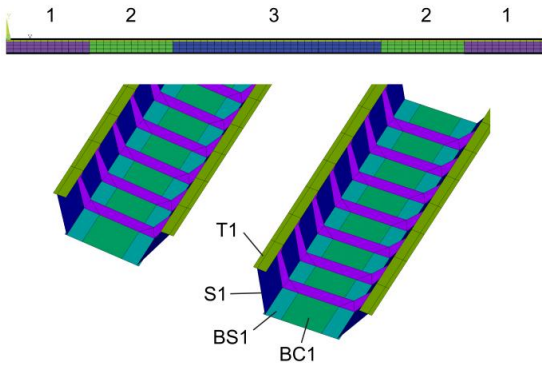


Fig. 65 Identification of different optimization “groups” for the considered deck

Since the optimum solution was found to depend on the initial values of steel plates’ thickness, different initial values were tried in order to avoid local minimum solutions. Where SV is the state variable (stress level and deformation level), OBJ is the objective function. The optimization iterative process of three different starting models and original design are shown in Fig. 66. In the convergence iteration of total volume of steel plates, black inverted triangle symbols show the infeasible design solutions, which not meet the requirement of stress or deformation constraints, meanwhile conversely, blue circle symbols show the feasible design solutions and the one among them with minimum objective is the best design solution. The latter was marked with red pentagram symbol.

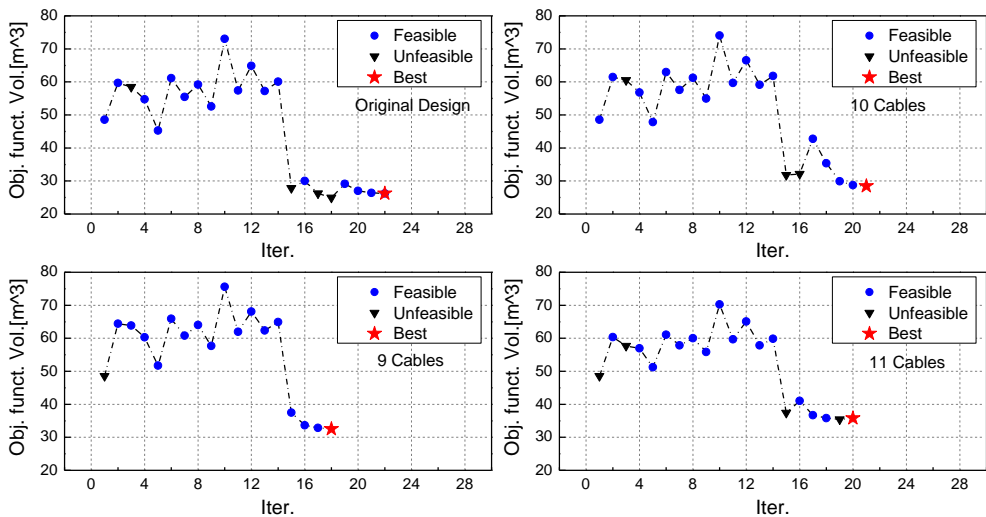


Fig. 66 Convergence iteration of optimization process

All the optimization process converged after nearly 20 iterations. The consistent decrease in the objective function (and therefore the corresponding material saving) is well appreciable. For the original design of bridge, the total volume of steel plates is decreased from 48.6 m<sup>3</sup> to 26.2 m<sup>3</sup>, namely 46.1% volume reduction. When the total cable number is 11, the volume reduction is lowest, but still has an appreciable value 26.3%.

The optimization procedure led to the optimum results are listed in Table 50. It includes state variables (maximum steel stress SV1 and maximum deformation SV2) and design variables (the thickness of steel plates). The values of state variables and design variables are listed both before and after thickness optimization process.

*c\_opt* are the results of cable cross sectional area optimization, *t\_opt* are the results of steel plates thickness optimization on the basis of cable cross sectional area and corresponding initial force optimization. For the original design model, only thickness optimization of steel plates carried out, while cable cross sectional area and corresponding initial force optimization and thickness optimization were carried out for other three starting models.

	Original design		10 cables		9 cables		11 cables	
	<i>No opt.</i>	<i>t_opt</i>	<i>c_opt</i>	<i>t_opt</i>	<i>c_opt</i>	<i>t_opt</i>	<i>c_opt</i>	<i>t_opt</i>
SV1 (MPa)	215.7	352.8	217.2	356.5	217.3	356.9	216.3	354.0
SV2 (mm)	-39.5	-39.3	-41.0	-40.9	-40.2	-40.1	-40.4	-40.0
T1 (m)	0.075	0.030	0.075	0.040	0.075	0.035	0.075	0.030
S1 (m)	0.025	0.016	0.025	0.014	0.025	0.020	0.025	0.013
BC1 (m)	0.040	0.010	0.040	0.012	0.040	0.020	0.040	0.010
BS1 (m)	0.080	0.053	0.080	0.053	0.080	0.036	0.080	0.057
T2 (m)	0.020	0.022	0.020	0.012	0.020	0.020	0.020	0.010
S2 (m)	0.020	0.010	0.020	0.012	0.020	0.015	0.020	0.020
BC2 (m)	0.018	0.010	0.018	0.012	0.018	0.015	0.018	0.020
BS2 (m)	0.025	0.010	0.025	0.012	0.025	0.015	0.025	0.020
T3 (m)	0.012	0.010	0.012	0.012	0.012	0.015	0.012	0.020
S3 (m)	0.015	0.010	0.015	0.012	0.015	0.015	0.015	0.020
BC3 (m)	0.020	0.010	0.020	0.012	0.020	0.015	0.020	0.020
BS3 (m)	0.025	0.010	0.025	0.012	0.025	0.015	0.025	0.022
<b>OBJ (m<sup>3</sup>)</b>	48.6	26.2	48.6	28.5	48.6	32.5	48.6	35.8

Table 50

Thickness optimization of single cable plane cable-stayed bridge

### 6.2.5 Comparison between Different Models

Starting from different models which defined by different number of total cables, the cable cross sectional areas and corresponding initial tensioning force are optimized, on the basis of the optimization results, the optimum cable areas and initial tensioning force are assigned to starting models to carry out thickness optimization of steel plates of bridge deck. The results show the consistent decrease in steel cable volume and steel plates volume are well appreciable.

However, as the material saving, the deformation and stress under all load cases are increased. Table 51 shows the maximum average stress of steel plates and maximum deformation of tower top under all load cases before and after thickness optimization. The volume reduction (VR) of steel cables and steel plates of deck are shown together.

	Original design		10 cables		9 cables		11 cables	
	<i>No opt.</i>	<i>t<sub>opt</sub></i>	<i>c<sub>opt</sub></i>	<i>t<sub>opt</sub></i>	<i>c<sub>opt</sub></i>	<i>t<sub>opt</sub></i>	<i>c<sub>opt</sub></i>	<i>t<sub>opt</sub></i>
Stress (MPa)	81.58	136.70	82.57	128.16	82.77	116.56	82.28	105.65
Deform. (m)	0.070	0.105	0.060	0.084	0.051	0.071	0.066	0.088
Cable VR (%)	0	0	30.6	30.6	43.7	43.7	-2.1	-2.1
Deck VR (%)	0	46.1	0	41.3	0	33.1	0	26.3
Total VR (%)	0	46.1	30.6	71.9	43.7	76.8	-2.1	24.2

*Table 51*

*Optimization results of single cable plane cable-stayed bridge*

Several candidate solutions were characterized by the total steel cables following the cable cross sectional area and corresponding initial tensioning force and thickness optimization procedure. Hence, the issue of finding the most suitable solution is faced. To identify the most suitable design solution that best balances material saving and overall performance of the structure, on the basis of the results obtained from optimization procedure, the proposed optimization index analytical formulation is discussed in detail and its effectiveness is validated.

In this case, two response indexes (*RIs*) which summarize the overall behavior of the whole structure were defined as: Von Mises stress, the average throughout the whole optimized steel structure, was considered as representative of stress level, while maximum deflection of tower top was considered as representative of deformation level. The trends of both *RIs* are shown in Fig. 67. *RI* curves include the

results of cable cross sectional area optimization (Cable Opt.), steel plates thickness optimization (Thickness Opt.) and both together (Cable and Thickness Opt.).

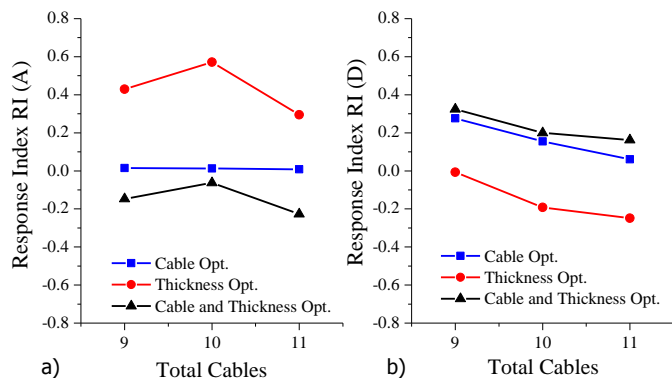


Fig. 67 Response index vs. total steel cables: a)  $RI(A,i)$ ; b)  $RI(d,i)$

Consider Cable Opt., Thickness Opt. or both of them together, thanks to the increased deformation after optimization, the  $RI$  curves of deformation level decreased for increasing values of total steel cables. However, due to the highest average stress 136.70MPa after Thickness Opt. for original design, the trend of stress level is inconsistent. Consider Thickness Opt. or Cable and Thickness Opt., the highest  $RI$  of stress level were obtained when the total cable is 10, while  $RI$  are almost the same value taking into account Cable Opt..

Fig. 51 shows the trend of  $GOI$  varying the total steel cables for some values of  $\beta$  ranging between 0 to 3. As expected, the application of  $\beta$  can favour design solutions of higher or lower volume reduction.

Consider the results of cable cross sectional area optimization, for values of  $\beta$  higher than or equal to 1, the highest  $GOI$  value was obtained when the total cable is 10. Further reducing the  $\beta$  parameter until 0, the total cable is 9 get highlighted. This is due to the latter has a volume reduction 43.7%, while the former has a volume reduction 30.6%. Thanks to the volume reduction is -2.1%, the lowest  $GOI$  value always occurred when the total cable is 11.

Consider the results of thickness optimization, due to the highest volume reduction 26.3%, the highest  $GOI$  value was obtained when the total cable is 10 for values of  $\beta$  slightly lower than 1. Further increasing the  $\beta$  parameter until 3, the total cable is 11 get highlighted. This is due to the latter has the lowest volume reduction 26.3%.

Take into account cable cross sectional area and thickness optimization together, the same as thickness optimization, for values of  $\beta$  higher than or equal to 1, the highest  $GOI$  value was obtained when the total cable is 11. Further reducing the  $\beta$  parameter until 0, the total cable is 9 or 10 get highlighted. This is due to the former has the lowest volume reduction 24.2%, while the latter has higher volume reduction 71.9% and 76.8%, respectively.

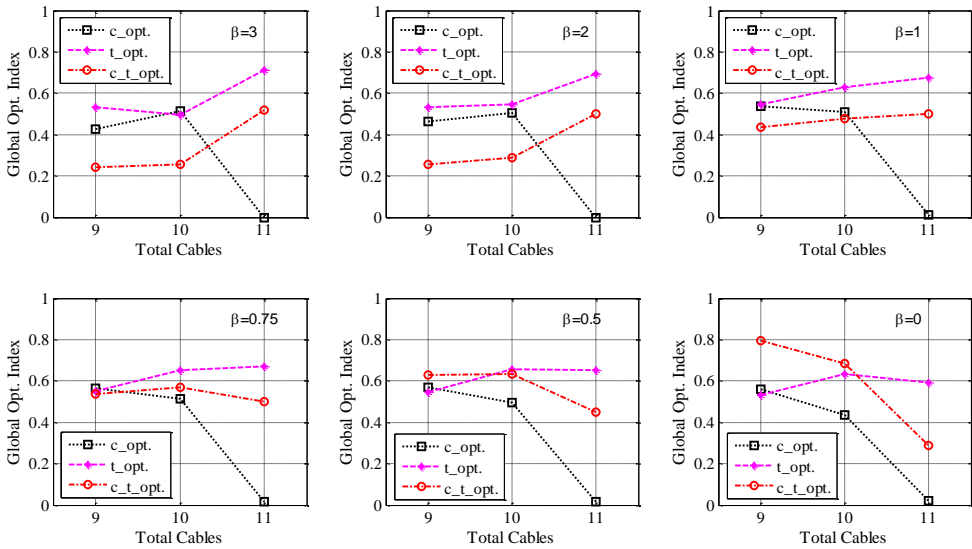


Fig. 68: Global optimization index vs. total cables (vs  $\beta$ )

### 6.3. Double Cable Planes Cable-stayed Bridge

#### 6.3.1 General Situation

The bridge is a Twin Towers Double Cable Planes cable-stayed bridge as shown in Fig. 69, located in Ferrara, Italy. It has a total length 167m with a 94m main span and two 36.5m side spans. Bridge is symmetry about the traverse centreline and has a 2.00% traverse slope. There are double inclined concrete towers, each with 10 degree angle in vertical direction.

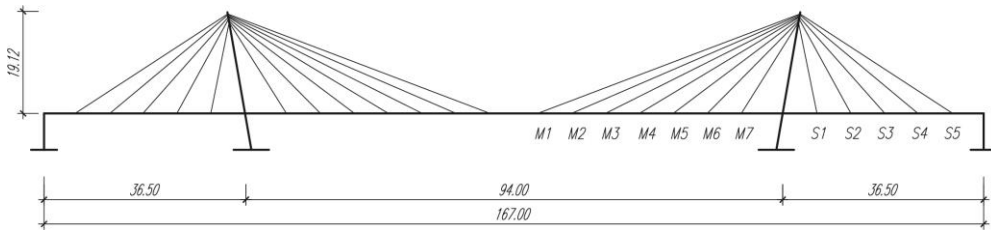


Fig. 69 Cable numbers and geometry of the bridge (unit: m)

The lateral plane and elevation plane of tower is shown in Fig. 70. Tower is consisted by three parts, namely the upper tower, middle tower and lower tower, the cross section changed from different parts. In the elevation plane, tower is 24.96m high from the ground and 19.12m high from the deck.

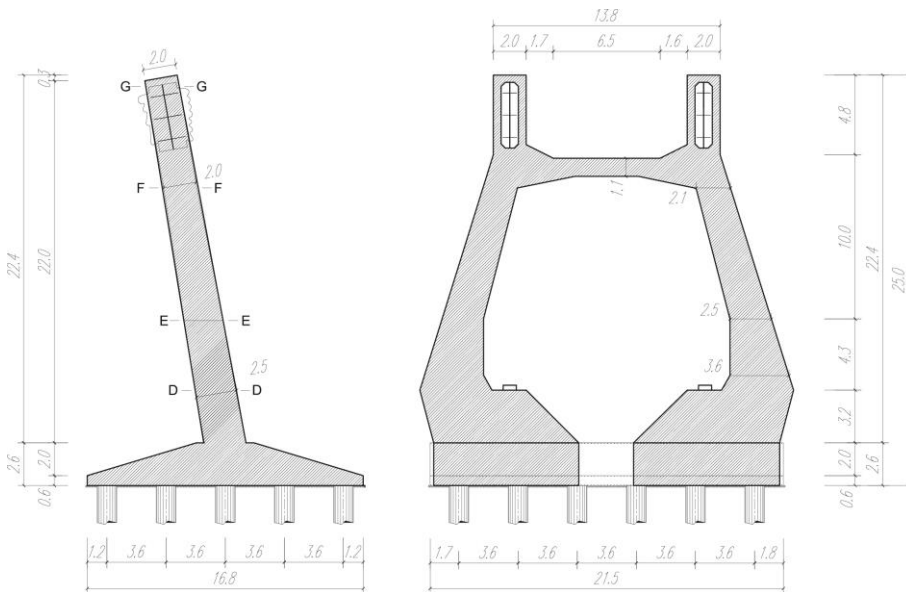


Fig. 70 Lateral plane and elevation plane of tower (unit: m)

The typical cross section of deck is shown in Fig. 71. It has a total width 14m which 10.5m width for lanes and 1.75m for walkway at each side. Main girders, secondary beams and transverse beams consist of bridge deck section. The main girder is I-shaped with 1.1m overall depth, 1m width bottom flange and 0.8m top flange. Secondary beam and cross girder also are I-shaped, the former has 0.73m overall depth, 0.6m width bottom flange and top flange, the latter has 0.45m overall depth, 0.36m width bottom flange and top flange.

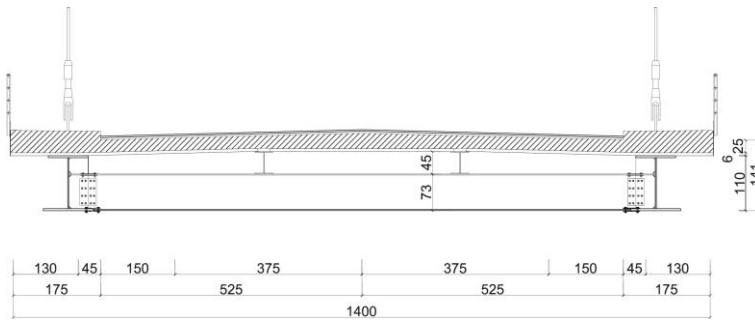


Fig. 71 Cross section of deck (unit: mm)

There are 48 cables in total, 24 cables supported by each tower. The cables are symmetry about the tower. Each side of tower has 12 cables among which 7 at the main span and 5 at side span. Horizontal distance between cables is 5m. The longest cable is 43.23m with 1232.43kg weight. Cables parameters are listed in Table 52 and the cable No. is shown as above.

Cable No.	Area (e-3 m <sup>2</sup> )	Diameter (mm)	Long (m)	Weight (kg)	Tensioning force (kN)
M1	3.632	68	43.23	1232.43	1600
M2	3.632	68	38.55	1099.01	1575
M3	2.827	60	34.01	754.86	1105
M4	2.827	60	29.68	658.76	1030
M5	1.521	44	25.68	306.52	635
M6	1.521	44	22.18	264.74	660
M7	0.804	32	19.44	122.73	230
S1	0.804	32	17.65	111.43	265
S2	0.804	32	18.94	119.57	345
S3	2.124	52	21.45	357.60	425
S4	2.827	60	24.81	550.67	520
S5	5.542	84	28.71	1248.97	3330

Table 52  
Cable parameters

### 6.3.2 Finite Element Model

Using software ANSYS to build the finite element model. There are 5911 nodes, 4 element types and 4824 elements in total. Main girder, secondary beam, transverse

beam and tower using Beam188 element, deck using Shell63, and cables using Link10 element. Finite element model is shown in Fig. 72. The cross section is shown in Table 53.

Steel grade is S355 in Eurocode 3. Therefore, its yield stress is 355 MPa and tensile strength is 510 MPa. The value of the modulus of elasticity was assumed to be 210 GPa. Poisson's ratio and material density were set to 0.3 and 7850 kg/m<sup>3</sup>, respectively. According to the Eurocode 2, concrete with strength class C20/25 was chosen. Its characteristic cylinder strength was 25 MPa, the average tensile strength of concrete before cracking was 2.6 MPa ( $f_{ctm} = 0.30f_{ck}^{2/3}$ ). The value of the modulus of elasticity was assumed to be 30 GPa. Poisson's ratio and material density were set, respectively, to 0.2 and 2500 kg/m<sup>3</sup>.

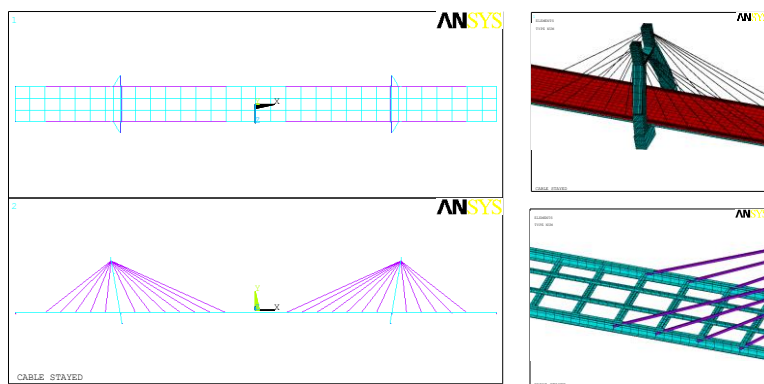


Fig. 72 Finite Element Model

Cross section	Area(m <sup>2</sup> )	I <sub>yy</sub> (m <sup>4</sup> )	I <sub>yz</sub> (m <sup>4</sup> )	I <sub>zz</sub> (m <sup>4</sup> )
Main girder	0.0924	0.0218	9.65E-18	5.04E-03
Secondary beam	0.0115	0.0004	-1.10E-20	7.78E-05
Cross girder	0.0378	0.0036	-6.78E-21	7.20E-04
Upper tower	4.0000	1.3333	9.17E-17	1.3333
Middle tower	5.9220	3.1339	-9.08E-17	2.7254
Lower tower	16.1750	56.4250	2.67E-16	8.4245

Table 53  
Cross section

For the boundary condition, all the degrees of freedom are fixed at the bottom of tower and two side piers. The constraints of bearings between deck and tower or



piers are shown in Fig. 73. There are three categories constraints, namely Fixed, Unidirectional and Bidirectional. Position 1 and 8 with Bidirectional constraint are the bearings between deck and piers, means that the degrees of freedom in longitudinal and transverse directions are released. Positions 3 and 4 with fixed constraint type are the bearings between deck and piers, other positions are unidirectional constraint. Deck is fixed on one tower, but release longitudinal direction constraint on the other tower.

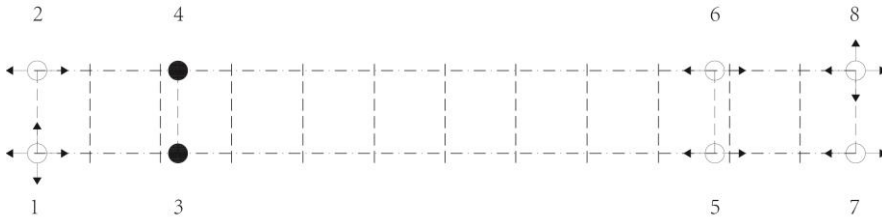


Fig. 73 Constraints of bearings

To calculate the bridge behaviour, besides permanent load, five different lanes loads are adopted and shown in Table 54. The truck loading is  $9\text{kN/m}^2$  uniformly distributed load plus  $300\text{kN} \times 2$  concentrate loads for central lane,  $2.5\text{kN/m}^2$  uniformly distributed load for other lanes and additional plus  $200\text{kN} \times 2$  or  $200\text{kN}$  concentrate loads, respectively. These load cases are not only used to calculate the static behavior of the bridge with original parameter, but also used over and over again during optimization looping.

Load case	Loading condition(s)	Loading area(s)
1	Full bridge	
2	Main span	
3	Two side span	
4	Half bridge	

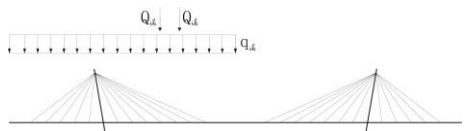


Table 54

*Different lanes load cases*

### 6.3.3 Cable Area and Cable Force Optimization Results

As we known, in the design of cable-stayed bridges, the total number of cables is an important design consideration. It plays an important role not only in the mechanical behavior of bridges, but also in aesthetic point of view. However, to get more attractive appearance, sometimes the designer would like to change the angle of the tower. In this section, different starting models were determined through changing the angle of towers in vertical direction from 0 to 20 degree and the total number of cables from 48 to 40, the optimization procedure of cable cross sectional areas and corresponding initial force were carried out.

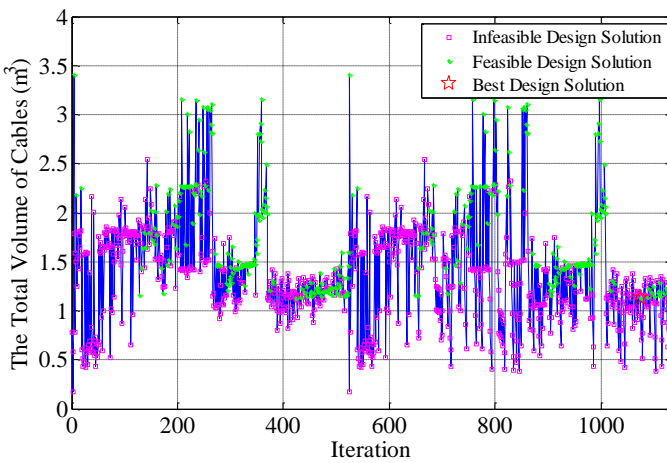
Same as single cable plane cable-stayed bridge, starting from the initial cable cross sectional areas  $2.29e-3 \text{ m}^2$  (correspond to cables with diameter 54mm), which with a lower bound  $0.5e-3 \text{ m}^2$  and upper limit  $10e-3 \text{ m}^2$  (correspond to cables with D25mm and D108mm, respectively), the total volume of steel cables was minimized. The optimum results were then assigned to the cable-stayed bridge to carry out the thickness optimization of steel plates of deck. Eventually, according to the proposed optimization index, results are discussed in detail and the optimum solution was determined.

#### **Results of bridge with 0 angle tower**

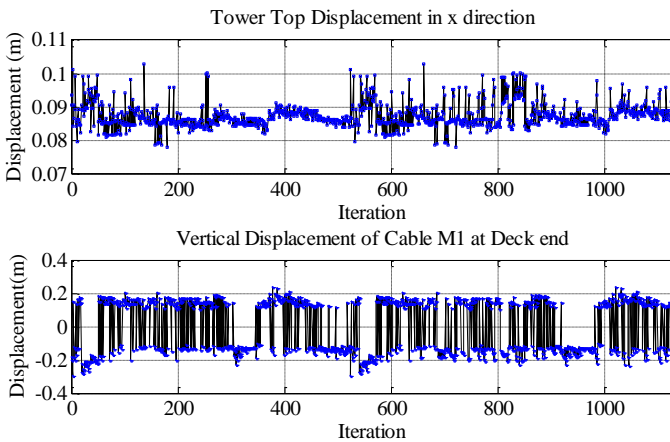
In the case of starting model with 0 degree angle tower in vertical direction, to obtain the best design solution, different starting models were defined through the utilization of different total number of cables. The starting models with total cable number 48, 44 and 40 were defined and their cable cross sectional areas and initial force were optimized.

When there is 48 cables in total, namely 12 cables in the 1/4 part, the optimization process converged after more than 1000 iterations. Fig. 74 illustrates the optimization iterative process of total cable volume and longitudinal deformation of tower top and vertical deformation of M1 cable at deck end.

Not all the design solutions are feasible due to the constraint function. 1000 MPa is set as the allowable maximum tensile stress of the cables under all load cases, the allowable deformations of cables at deck end and tower top are also set according to the bridge span and tower height, respectively. In the convergence iteration of total cable volume, pink square symbols show the infeasible design solutions, which not meet the requirement of stress or deformation, meanwhile conversely, green star symbols show the feasible design solutions and the one with minimum total cable volume is the best design solution. The latter was marked with red pentagram symbol.



a) Convergence iteration of total cable volume



b) Convergence iteration of deformation

Fig. 74 Convergence iteration of cable volume with 48 cables and 0 angle tower

Concerning the objective function, the total volume of cables moves from  $0.5 \text{ m}^3$  to  $3.5 \text{ m}^3$ , and reached to minimum value  $1.134 \text{ m}^3$  which meets the constraint function. The tower top displacement in longitudinal direction moves from  $0.07\text{m}$  to  $0.1\text{m}$  and with a  $0.0872\text{m}$  value when the total volume of cables reached to minimum. The vertical displacement of M1 cable at deck end moves from  $-0.2\text{m}$  to  $0.2\text{m}$ .

The distribution of cable area and initial cable force is illustrated in Fig. 75. The optimization results led to larger area for cables attached to both ends of the deck and cables close to the middle span. The former occurred due to they are the ones brace the tower, the latter occurred due to the deformation limit of cable deck end. The maximum cable area is  $5.45\text{e-}3 \text{ m}^2$ , corresponds to cable with diameter  $84\text{mm}$ , while the minimum is  $1.65\text{e-}3 \text{ m}^2$ , corresponds to cable with diameter  $46\text{mm}$ . The maximum initial cable force  $4493 \text{ kN}$  occurred in the M1 cable, while the minimum is  $50 \text{ kN}$  which is assigned due to the minus value calculated according to the cable force optimization method.

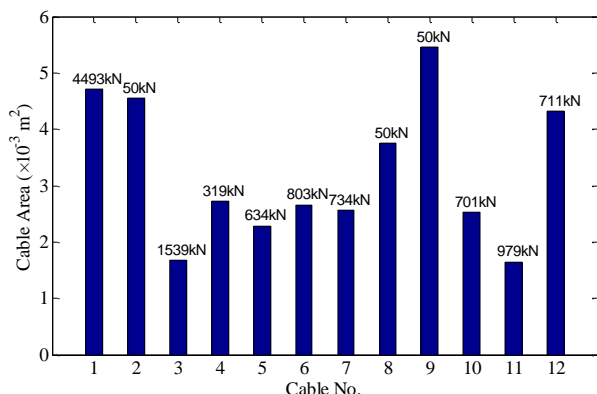
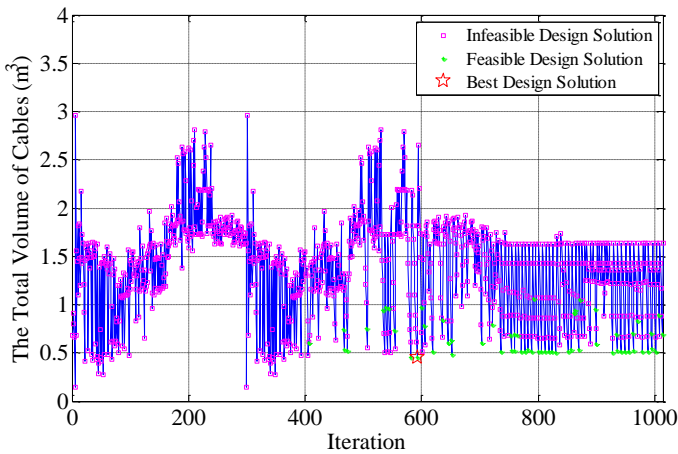


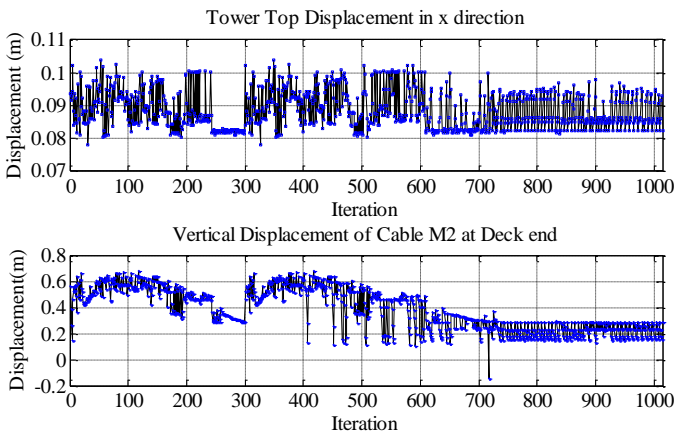
Fig. 75 Distribution of cable area and initial cable force

When there is 44 cables in total, namely 11 cables in the 1/4 part, starting from the same initial cable cross sectional areas and with same lower bound and upper limit, the total volume of steel cables was minimized. However, due to the constraint of vertical deformation of M2 cable at deck end, the initial cable force of M2 cable always has a high value that exceeds the limit of allowable maximum tensile stress under all load cases. Therefore, few feasible design solutions were obtained. To get more feasible design solutions, based on same deformation constraints, the stress limit of cables was extended to the ultimate stress  $1600 \text{ MPa}$ .

The optimization process converged after more than 1000 iterations. Fig. 76 illustrates the optimization iterative process of total cable volume and longitudinal deformation of tower top and vertical deformation of M2 cable at deck end. Concerning the objective function, the total volume of cables moves from  $0.5 \text{ m}^3$  to  $3 \text{ m}^3$ , and reached to minimum value  $0.455 \text{ m}^3$  which meets the constraint function. The tower top displacement in longitudinal direction moves from  $0.08\text{m}$  to  $0.11\text{m}$  and with a  $0.0955\text{m}$  value when the total volume of cables reached to minimum. The vertical displacement of M2 cable at deck end moves from  $-0.2\text{m}$  to  $0.8\text{m}$ .



a) Convergence iteration of total cable volume



b) Convergence iteration of deformation

Fig. 76 Convergence iteration of cable volume with 44 cables and 0 angle tower

The distribution of cable area and initial cable force is illustrated in Fig. 77. The optimization results lead to larger area for cables attached to one end. The maximum cable area is  $6.55e-3 \text{ m}^2$ , corresponds to cable with diameter 90mm, while the minimum is  $0.5e-3 \text{ m}^2$ , corresponds to cable with diameter 25mm. The maximum initial cable force 7725 kN occurred in the M2 cable, and the minimum is 50 kN which is assigned due to the minus value calculated according to the cable force optimization method.

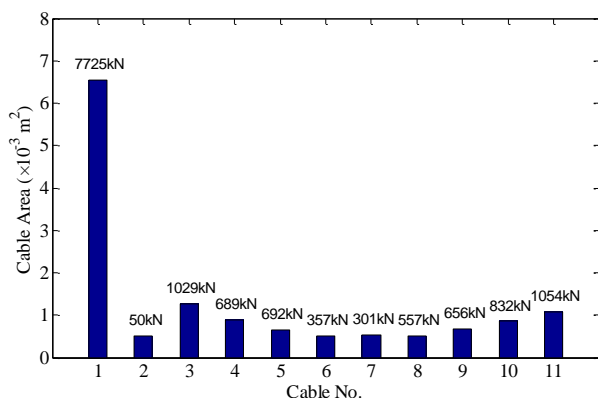
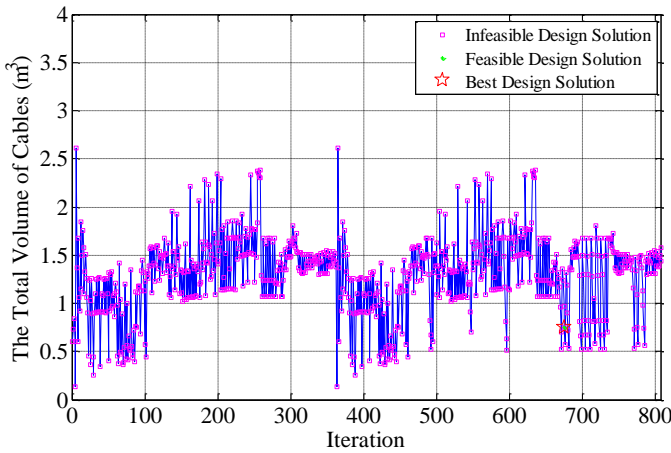


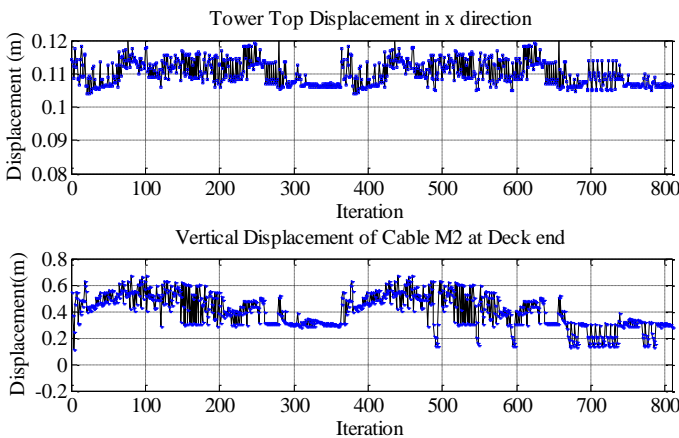
Fig. 77 Distribution of cable area and initial cable force

When there is 40 cables in total, namely 10 cables in the 1/4 part, same as starting model with 44 cables, due to the constraint of vertical deformation of M2 cable at deck end, the initial cable force of M2 cable always has a high value and exceed the limit of allowable maximum tensile stress under all load cases, therefore, few feasible design solutions were obtained. Moreover, the horizontal displacement of tower top always exceed the limit of allowable maximum displacement due to the not utilization of cable S5. Therefore, as no feasible solution found, the best design solution was chosen from the infeasible design solutions.

The optimization process terminated after more than 800 iterations but no feasible design solution found. Fig. 78 illustrates the optimization iterative process of total cable volume and longitudinal deformation of tower top and vertical deformation of M2 cable at deck end. Concerning the objective function, the total volume of cables moves from  $0.5 \text{ m}^3$  to  $3 \text{ m}^3$ , and reached to minimum value  $0.752 \text{ m}^3$  which meets the constraint function. The tower top displacement in longitudinal direction moves from 0.10m to 0.12m and with a 0.106m value when the total volume of cables reached to minimum. The vertical displacement of M2 cable at deck end moves from -0.2m to 0.8m.



a) Convergence iteration of total cable volume



b) Convergence iteration of deformation

*Fig. 78 Convergence iteration of cable volume with 40 cables and 0 angle tower*

The distribution of cable area and initial cable force is illustrated in Fig. 78. The optimization results lead to larger area for cables attached to the end located in main span. The maximum cable area is  $9.81e-3 \text{ m}^2$ , corresponds to cable with diameter 112mm, while the minimum is  $0.5e-3 \text{ m}^2$ , corresponds to cable with diameter 25mm. The maximum initial cable force 8126 kN occurred in the M2 cable, and the minimum is 50 kN which is assigned due to the value is minus which calculated according to the cable force optimization method.

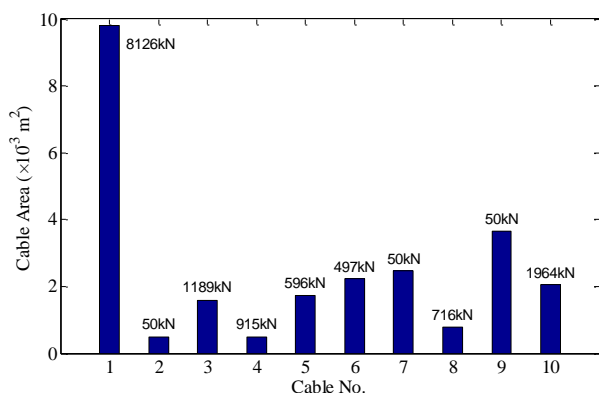


Fig. 79 Distribution of cable area and initial cable force

All the results of different starting models are listed in Table 55, including the optimized cable cross sectional area and corresponding initial cable force. Although the optimization results are unrealistic to apply to the actual project, the original values are kept to give an idea to designer about how much cross sectional area is necessary for each cable under certain stress and displacement constraints. The starting model with 48 cables has the highest total cable volume 1.134 m<sup>3</sup>. The starting model with 44 cables and 40 cables reduced objective significantly due to less cables, with total cable volume 0.455 m<sup>3</sup> and 0.752 m<sup>3</sup>, respectively. Optimization results of all starting models led to larger cross sectional area and initial tensioning force for cables attached to the end located in the main span.

Cable No.	Length (m)	48 cables		44 cables		40 cables	
		Area (e-3 m <sup>2</sup> )	Force (kN)	Area (e-3 m <sup>2</sup> )	Force (kN)	Area (e-3 m <sup>2</sup> )	Force (kN)
M1	44.38	4.71	4493.2	-	-	-	-
M2	39.00	4.55	50.0	6.55	7724.6	9.81	8125.6
M3	33.82	1.67	1539.0	0.50	50.0	0.50	50.0
M4	28.91	2.73	319.1	1.26	1029.2	1.59	1189.0
M5	24.46	2.29	633.6	0.88	688.9	0.50	915.3
M6	20.76	2.66	802.6	0.65	691.6	1.75	595.6
M7	18.28	2.56	733.7	0.50	356.7	2.23	497.2
S1	18.76	3.75	50.0	0.54	301.4	2.46	50.0
S2	21.58	5.45	50.0	0.51	556.9	0.77	715.6
S3	25.50	2.53	701.0	0.68	656.4	3.65	50.0
S4	30.08	1.65	979.2	0.85	831.9	2.05	1963.6
S5	35.07	4.32	710.7	1.07	1054.4	-	-



Obj.(m <sup>3</sup> )	1.134	0.455	0.752
-----------------------	-------	-------	-------

Table 55

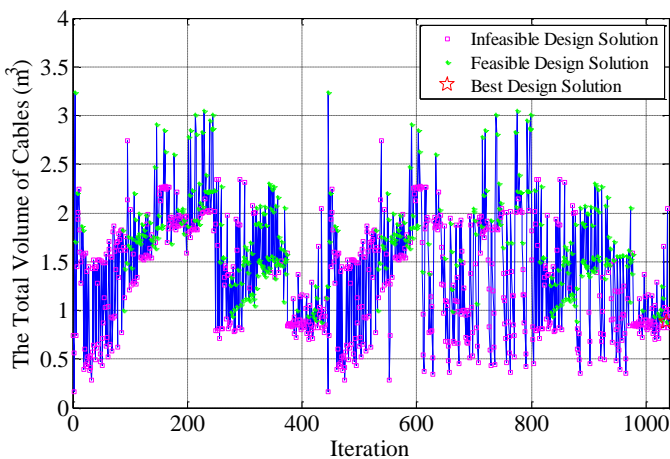
Initial tension force in cables with 0 angle tower

### Results of bridge with 10 angle tower

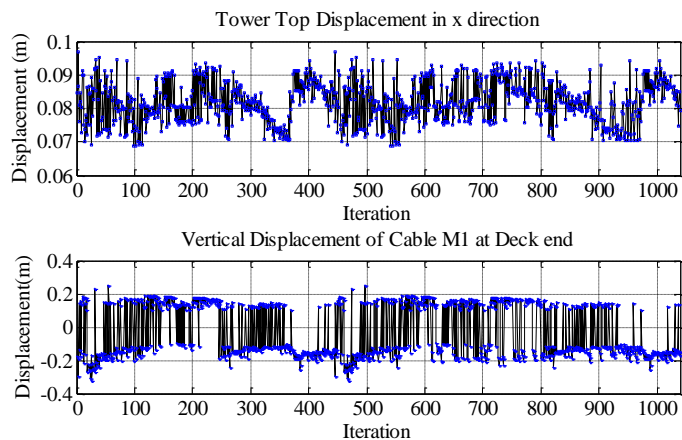
In the case of starting model with tower angle in vertical direction is 10 degree, the same as starting model with 0 degree tower angle, different starting models were defined through the utilization of different total number of cables, namely starting models with total cable number 48, 44 and 40. Starting from the same initial cable cross sectional areas  $2.29\text{e-}3\text{ m}^2$  (correspond to cables with diameter 54mm), which with a lower bound  $0.5\text{e-}3\text{ m}^2$  and upper limit  $10\text{e-}3\text{ m}^2$  (correspond to cables with D25mm and D108mm, respectively), the cable cross sectional area and corresponding initial tensioning force were optimized with the objective of minimizing the total volume of steel cables.

When there is 48 cables in total, namely 12 cables in the 1/4 part, the optimization process converged after more than 1000 iterations. Fig. 80 illustrates the optimization iterative process of total cable volume and longitudinal deformation of tower top and vertical deformation of M1 cable at deck end.

Concerning the objective function, the total volume of cables moves from  $0.5\text{ m}^3$  to  $3.5\text{ m}^3$ , and reached to minimum value  $0.883\text{ m}^3$  which meets the constraint function. The tower top displacement in longitudinal direction moves from 0.07m to 0.1m and with a 0.0851m value when the total volume of cables reached to minimum. The vertical displacement of M1 cable at deck end moves from -0.2m to 0.2m.



a) Convergence iteration of total cable volume



b) Convergence iteration of deformation

Fig. 80 Convergence iteration of cable volume with 48 cables and 10 angle tower

The distribution of cable area and initial cable force is illustrated in Fig. 81. The optimization results led to larger area for cables attached to both ends of the deck and cables close to the middle span. The maximum cable area is  $4.91 \times 10^{-3} \text{ m}^2$ , corresponds to cable with diameter 80mm, while the minimum is  $1.10 \times 10^{-3} \text{ m}^2$ , corresponds to cable with diameter 38mm. The maximum initial cable force 3705 kN occurred in the M1 cable, and the minimum is 50 kN which is assigned due to the minus value calculated according to the cable force optimization method.

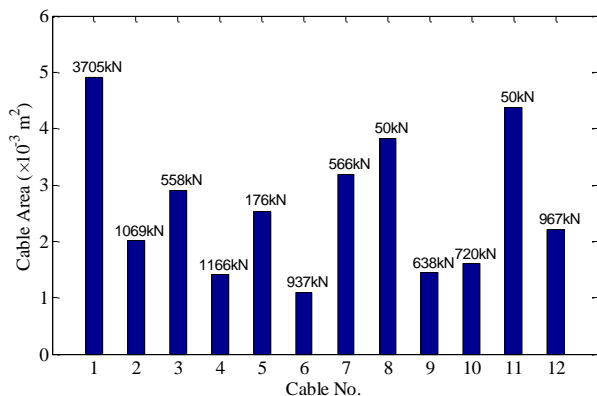
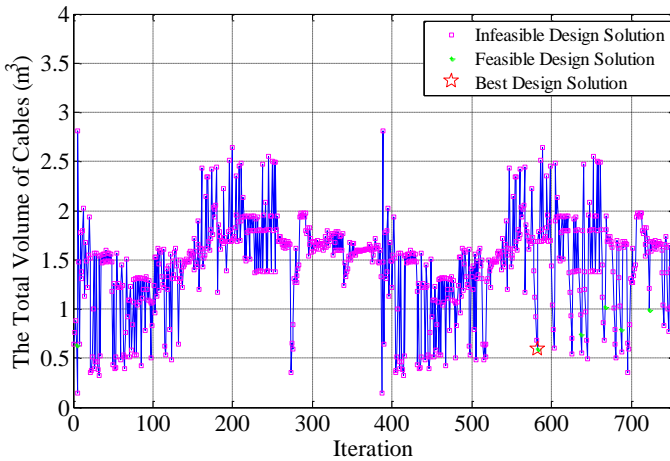


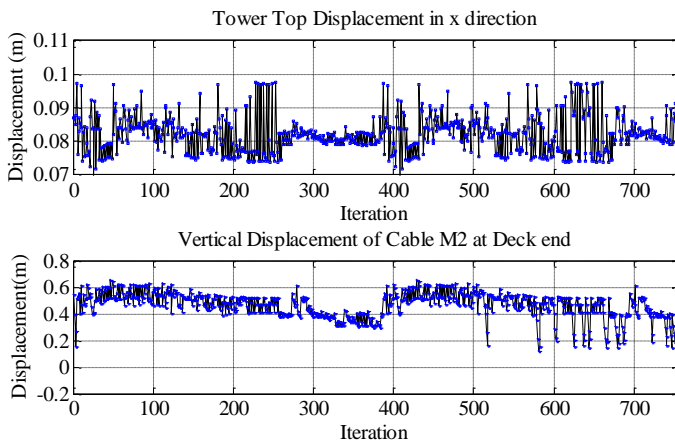
Fig. 81 Distribution of cable area and initial cable force

When there is 44 cables in total, namely 11 cables in the 1/4 part, the total volume of steel cables was minimized starting from the same initial cable cross sectional areas  $2.29 \times 10^{-3} \text{ m}^2$  and with same lower bound  $0.5 \times 10^{-3} \text{ m}^2$  and upper limit  $10 \times 10^{-3} \text{ m}^2$ . However,

due to the constraint of vertical deformation of M2 cable at deck end, the initial cable force of M2 cable always has a high value and exceed the limit of allowable maximum tensile stress under all load cases, therefore, few feasible design solutions were obtained. To get more feasible design solutions, based on same deformation constraints, the stress limit of cables was extended to the ultimate stress 1600 MPa.



a) Convergence iteration of total cable volume



b) Convergence iteration of deformation

Fig. 82 Convergence iteration of cable volume with 44 cables and 10 angle tower

The optimization process converged after more than 700 iterations. Fig. 82 illustrates the optimization iterative process of total cable volume and longitudinal deformation of tower top and vertical deformation of M2 cable at deck end. Concerning the objective function, the total volume of cables moves from  $0.5 \text{ m}^3$  to 3

$m^3$ , and reached to minimum value  $0.588 m^3$  which meets the constraint function. The tower top displacement in longitudinal direction moves from 0.07m to 0.10m and with a 0.0884m value when the total volume of cables reached to minimum. The vertical displacement of M2 cable at deck end moves from 0.2m to 0.8m.

The distribution of cable area and initial cable force is illustrated in Fig. 83. The optimization results lead to larger area for cables attached to both ends. The maximum cable area is  $9.27e-3 m^2$ , correspond to cable with diameter 108mm, while the minimum is  $0.5e-3 m^2$ , correspond to cable with diameter 25mm. The maximum initial cable force 7235 kN occurred in the M2 cable, and the minimum is 50 kN which is assigned due to the value is minus which calculated according to the cable force optimization method.

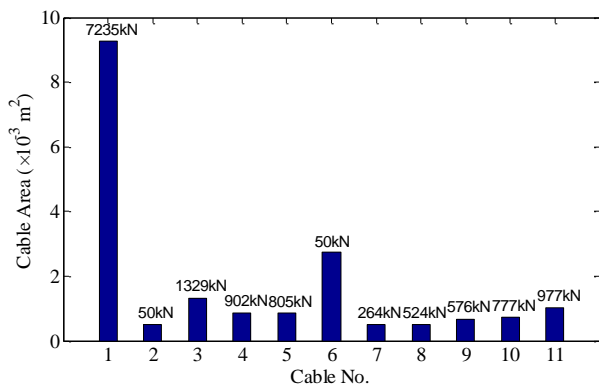
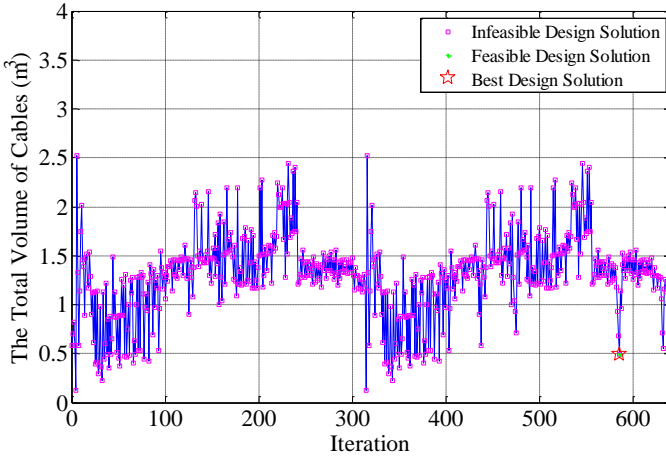


Fig. 83 Distribution of cable area and initial cable force

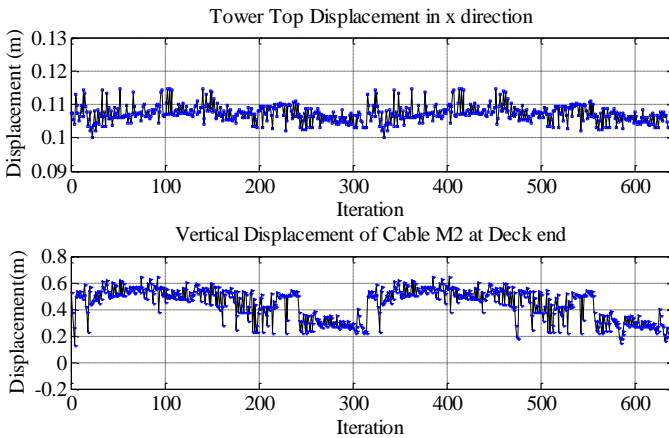
When there is 40 cables in total, namely 10 cables in the 1/4 part, due to the constraint of vertical deformation of M2 cable at deck end, the initial cable force of M2 cable always has a high value and exceed the limit of allowable maximum tensile stress under all load cases, therefore, few feasible design solutions were obtained. Moreover, the horizontal displacement of tower top always exceed the limit of allowable maximum displacement due to the not utilization of cable S5. Therefore, as no feasible solution found, the best design solution was chosen from the infeasible design solutions.

The optimization process terminated after more than 600 iterations but no feasible design solution found. Fig. 84 illustrates the optimization iterative process of total cable volume and longitudinal deformation of tower top and vertical deformation of M2 cable at deck end. Concerning the objective function, the total volume of cables moves from  $0.5 m^3$  to  $2.5 m^3$ , and reached to minimum value  $0.494 m^3$  which meets

the constraint function. The tower top displacement in longitudinal direction moves from 0.10m to 0.12m and with a 0.1062m value when the total volume of cables reached to minimum. The vertical displacement of M2 cable at deck end moves from -0.2m to 0.6m.



a) Convergence iteration of total cable volume



b) Convergence iteration of deformation

Fig. 84 Convergence iteration of cable volume with 40 cables and 10 angle tower

The distribution of cable area and initial cable force is illustrated in Fig. 85. The optimization results lead to larger area for cables attached to the end located in main span. The maximum cable area is  $7.84e-3 \text{ m}^2$ , correspond to cable with diameter 100mm, while the minimum is  $0.5e-3 \text{ m}^2$ , correspond to cable with diameter 25mm. The maximum initial cable force 7679 kN occurred in the M2 cable, and the minimum is 50 kN which is assigned due to the value is minus which calculated according to the cable force optimization method.

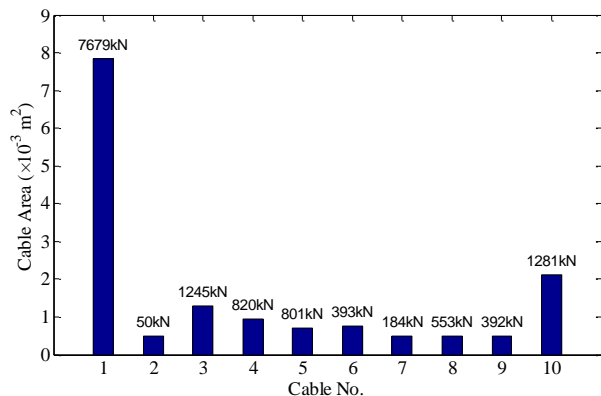


Fig. 85 Distribution of cable area and initial cable force

All the results of different starting models are listed in Table 56, including the optimized cable cross sectional area and corresponding initial tensioning force. Through the optimization procedure, for the entire starting model, the total cable volumes are optimized. The starting model with 48 cables has the highest total cable volume 0.883 m<sup>3</sup>. The starting model with 44 cables and 40 cables reduced objective significantly due to less cables, with total cable volume 0.588 m<sup>3</sup> and 0.494 m<sup>3</sup>, respectively. Optimization results of all starting models led to larger cross sectional area and initial tensioning force for cables attached to the end located in the main span.

Cable No.	Length (m)	48 cables		44 cables		40 cables	
		Area (e-3 m <sup>2</sup> )	Force (kN)	Area (e-3 m <sup>2</sup> )	Force (kN)	Area (e-3 m <sup>2</sup> )	Force (kN)
M1	43.23	4.91	3705.1	-	-	-	-
M2	38.55	2.02	1069.5	9.27	7234.6	7.84	7678.8
M3	34.01	2.91	557.8	0.50	50.0	0.50	50.0
M4	29.68	1.41	1165.9	1.32	1329.1	1.29	1245.2
M5	25.68	2.53	176.1	0.87	901.7	0.94	819.6
M6	22.18	1.10	937.5	0.85	805.4	0.70	801.3
M7	19.44	3.18	565.9	2.75	50.0	0.76	392.7
S1	17.65	3.82	50.0	0.50	264.1	0.50	184.3
S2	18.94	1.45	638.4	0.50	523.6	0.50	552.9
S3	21.45	1.60	720.5	0.67	576.5	0.50	392.0
S4	24.81	4.37	50.0	0.73	777.0	2.12	1280.7
S5	28.71	2.22	967.3	1.01	976.9	-	-
<b>Obj.(m<sup>3</sup>)</b>		<b>0.883</b>		<b>0.588</b>		<b>0.494</b>	

Table 56

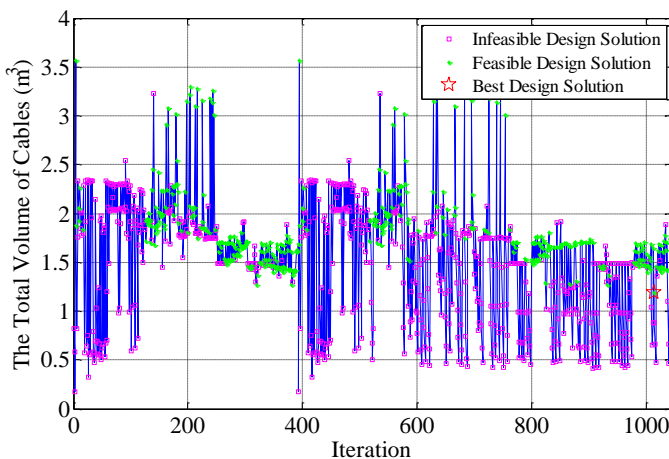
Initial tension force in cables with 10 angle tower

### Results of bridge with 20 angle tower

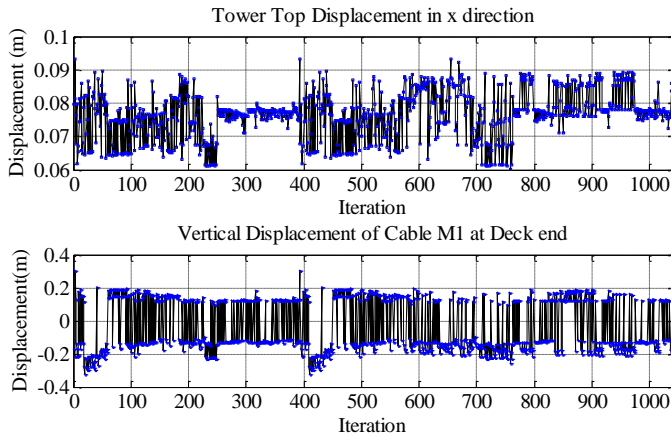
In the case of starting model with tower angle in vertical direction is 20 degree, the same as starting model with 0 degree tower angle, different starting models were defined through the utilization of different total number of cables. The starting models with total cable number 48, 44 and 40 were defined and the total steel cable volume were minimized starting from the initial cable cross sectional areas  $2.29e-3 \text{ m}^2$  (correspond to cables with diameter 54mm), which with a lower bound  $0.5e-3 \text{ m}^2$  and upper limit  $10e-3 \text{ m}^2$  (correspond to cables with D25mm and D108mm, respectively).

When there is 48 cables in total, namely 12 cables in the 1/4 part, the optimization process converged after more than 1000 iterations. Fig. 86 illustrates the optimization iterative process of total cable volume and longitudinal deformation of tower top and vertical deformation of M1 cable at deck end.

Concerning the objective function, the total volume of cables moves from  $0.5 \text{ m}^3$  to  $3.5 \text{ m}^3$ , and reached to minimum value  $2.103 \text{ m}^3$  which meets the constraint function. The tower top displacement in longitudinal direction moves from 0.06m to 0.9m and with a 0.0761m value when the total volume of cables reached to minimum. The vertical displacement of M1 cable at deck end moves from -0.2m to 0.2m.



a) Convergence iteration of total cable volume



b) Convergence iteration of deformation

Fig. 86 Convergence iteration of cable volume with 48 cables and 20 angle tower

The distribution of cable area and initial cable force is illustrated in Fig. 87. The optimization results led to larger area for cables attached to both ends of the deck and cables close to the middle span. The maximum cable area is  $5.49 \times 10^{-3} \text{ m}^2$ , corresponds to cable with diameter 84mm, while the minimum is  $1.25 \times 10^{-3} \text{ m}^2$ , corresponds to cable with diameter 40mm. The maximum initial cable force 3407 kN occurred in the M1 cable, and the minimum is 50 kN which is assigned due to the value is minus which calculated according to the cable force optimization method.

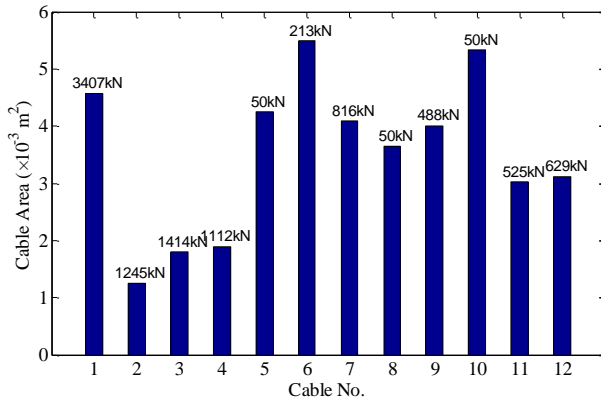
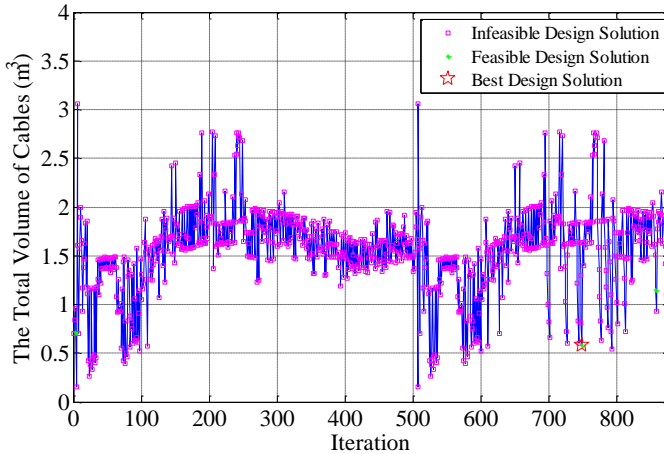


Fig. 87 Distribution of cable area and initial cable force

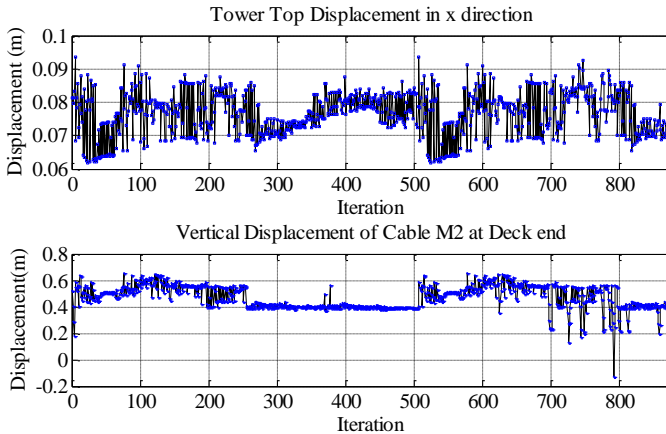
When there is 44 cables in total, namely 11 cables in the 1/4 part, starting from the same initial cable cross sectional areas  $2.29 \times 10^{-3} \text{ m}^2$  and with same lower bound  $0.5 \times 10^{-3} \text{ m}^2$  and upper limit  $10 \times 10^{-3} \text{ m}^2$ , the total volume of steel cables was minimized. However, due to the constraint of vertical deformation of M2 cable at deck end, the



initial cable force of M2 cable always has a high value and exceed the limit of allowable maximum tensile stress under all load cases, therefore, few feasible design solutions were obtained. To get more feasible design solutions, based on same deformation constraints, the stress limit of cables was extended to the ultimate stress 1600 MPa.



a) Convergence iteration of total cable volume



b) Convergence iteration of deformation

Fig. 88 Convergence iteration of cable volume with 44 cables and 20 angle tower

The optimization process converged after more than 800 iterations. Fig. 88 illustrates the optimization iterative process of total cable volume and longitudinal deformation of tower top and vertical deformation of M2 cable at deck end. With regards to the objective function, the total volume of cables moves from 0.5 m<sup>3</sup> to 3 m<sup>3</sup>, and reached to minimum value 0.580 m<sup>3</sup> which meets the constraint function.

The tower top displacement in longitudinal direction moves from 0.06m to 0.11m and with a 0.0847m value when the total volume of cables reached to minimum. The vertical displacement of M2 cable at deck end moves from -0.2m to 0.8m.

The distribution of cable area and initial cable force is illustrated in Fig. 89. The optimization results lead to larger area for cables attached to both ends. The maximum cable area is  $8.52e-3 \text{ m}^2$ , corresponds to cable with diameter 104mm, while the minimum is  $0.5e-3 \text{ m}^2$ , corresponds to cable with diameter 25mm. The maximum initial cable force 7203 kN occurred in the M2 cable, and the minimum is 50 kN which is assigned due to the value is minus which calculated according to the cable force optimization method.

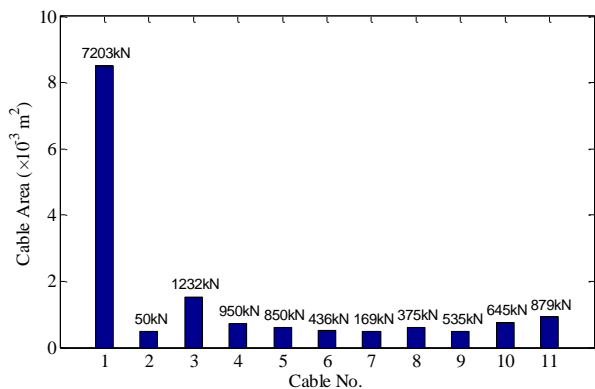
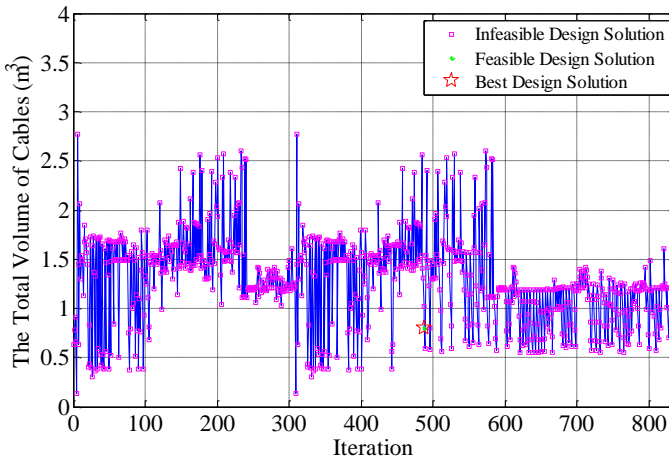


Fig. 89 Distribution of cable area and initial cable force

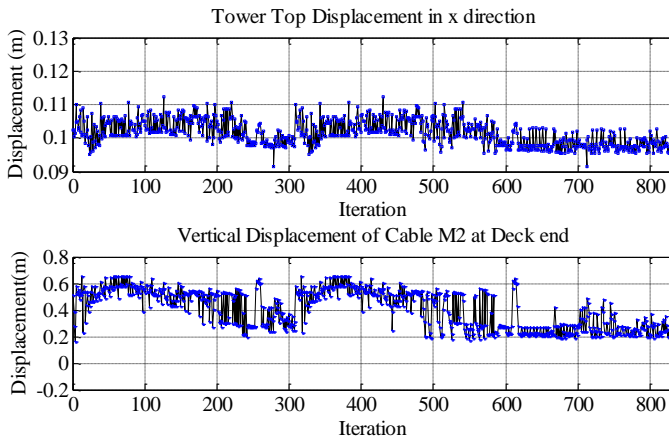
When there is 40 cables in total, namely 10 cables in the 1/4 part, due to the constraint of vertical deformation of M2 cable at deck end, the initial cable force of M2 cable always has a high value and exceed the limit of allowable maximum tensile stress under all load cases, therefore, few feasible design solutions were obtained. Moreover, the horizontal displacement of tower top always exceed the limit of allowable maximum displacement due to the not utilization of cable S5. Hence, as no feasible solution found, the best design solution was chosen from the infeasible design solutions.

The optimization process terminated after more than 800 iterations but no feasible design solution found. Fig. 90 illustrates the optimization iterative process of total cable volume and longitudinal deformation of tower top and vertical deformation of M2 cable at deck end. Concerning the objective function, the total volume of cables

moves from  $0.5 \text{ m}^3$  to  $3 \text{ m}^3$ , and reached to minimum value  $0.805 \text{ m}^3$  which meets the constraint function. The tower top displacement in longitudinal direction moves from  $0.09\text{m}$  to  $0.12\text{m}$  and with a  $0.0963\text{m}$  value when the total volume of cables reached to minimum. The vertical displacement of M2 cable at deck end moves from  $-0.2\text{m}$  to  $0.8\text{m}$ .



a) Convergence iteration of total cable volume



b) Convergence iteration of deformation

Fig. 90 Convergence iteration of cable volume with 40 cables and 20 angle tower

The distribution of cable area and initial cable force is illustrated in Fig. 91. The optimization results lead to larger area for cables attached to the end located in main span. The maximum cable area is  $10.00\text{e-}3 \text{ m}^2$ , correspond to cable with diameter

96mm, while the minimum is  $0.5e-3 \text{ m}^2$ , correspond to cable with diameter 108mm. The maximum initial cable force 8240.5 kN occurred in the M2 cable, and the minimum is 50 kN which is assigned due to the value is minus which calculated according to the cable force optimization method.

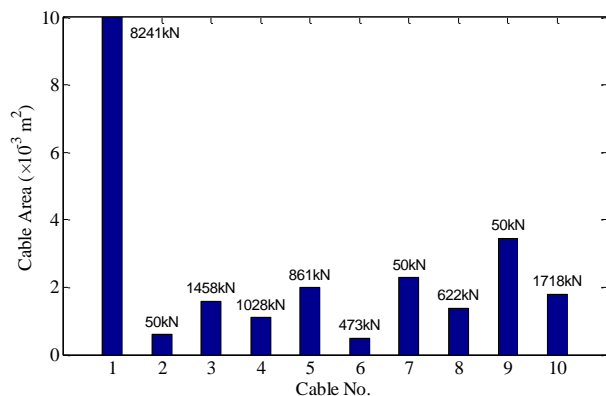


Fig. 91 Distribution of cable area and initial cable force

All the results of different starting models are listed in Table 57, including the optimized cable area and its corresponding initial cable force. Through the optimization procedure, for all starting models, the cable area and its initial force are optimized. The starting model with 48 cables has the highest total cable volume  $1.191 \text{ m}^3$ . The starting model with 44 cables and 40 cables reduced objective significantly due to less cables, with total cable volume  $0.580 \text{ m}^3$  and  $0.805 \text{ m}^3$ , respectively. Optimization results of all starting models led to larger cross sectional area and initial tensioning force for cables attached to the end located in the main span.

Cable No.	Length (m)	48 cables		44 cables		40 cables	
		Area (e-3 m <sup>2</sup> )	Force (kN)	Area (e-3 m <sup>2</sup> )	Force (kN)	Area (e-3 m <sup>2</sup> )	Force (kN)
M1	50.50	4.57	3406.6	-	-	-	-
M2	44.98	1.25	1244.8	8.52	7203.3	10.00	8240.5
M3	39.59	1.79	1414.3	0.50	50.0	0.60	50.0
M4	34.38	1.90	1112.4	1.53	1231.8	1.59	1457.9
M5	29.43	4.25	50.0	0.73	949.8	1.10	1028.3
M6	24.92	5.49	212.6	0.61	850.3	1.99	861.2
M7	21.12	4.09	816.4	0.51	436.4	0.50	472.8
S1	17.53	3.65	50.0	0.50	168.6	2.28	50.0

S2	18.53	4.01	488.2	0.61	374.6	1.38	621.9
S3	21.20	5.33	50.0	0.50	535.4	3.45	50.0
S4	25.03	3.02	524.8	0.76	644.6	1.79	1717.8
S5	29.55	3.12	628.8	0.92	878.6	-	-
<b>Obj.(m<sup>3</sup>)</b>	<b>1.191</b>			<b>0.580</b>		<b>0.805</b>	

Table 57

Initial tension force in cables with 20 angle tower

#### 6.3.4 Thickness Optimization

Immediately following the cable cross sectional area and cable force optimization, for each starting model, thickness of steel plates was optimized by using the design optimization tool implemented in ANSYS. It provides a zero-order method, where the dependent variables are first approximated by means of least squares fitting, and the constrained minimization problem is then converted to an unconstrained one by means of penalty functions, in order to be solved using Powell's modified method.

Three different regions of the steel deck, namely main girder, secondary beam and transverse beam were identified, where width of the top and bottom flanges, overall depth, flange thicknesses and web thicknesses had to be identified (Fig. 92). Width of the top and bottom flanges of main girder (W1M and W2M) were assumed as design variables with values ranging between 0.5m and 1m, overall depth (W3M) ranging between 0.9m to 1.2m, flange thickness and web thickness (T1M and T3M) ranging between 0.01m to 0.05m.

Width of the top and bottom flanges of secondary beam (W1) was assumed as design variable with values ranging between 0.5m and 1m, overall depth (W3) is calculated from overall depth of main girder (W3M) and overall depth of transverse beam (W3B), flange thickness and web thickness (T1 and T3) ranging between 0.01m to 0.05m. Width of the top and bottom flanges of transverse beam (W1B) was assumed as design variables with values ranging between 0.5m and 1m, overall depth (W3B) ranging between 0.4m to 0.7m, flange thickness and web thickness (T1B and T3B) ranging between 0.01m to 0.05m.

An optimization problem with 12 discrete variables was hence identified. The optimum thickness was found by minimizing the deck total weight on condition that stress level and deflection were lower than an allowable value. Bending stress 200

MPa on the element -Z side of the beam was set as the stress level limit, while maximum 0.2m and minimum -0.2m deflection under all load cases were set as the deflection level limit.

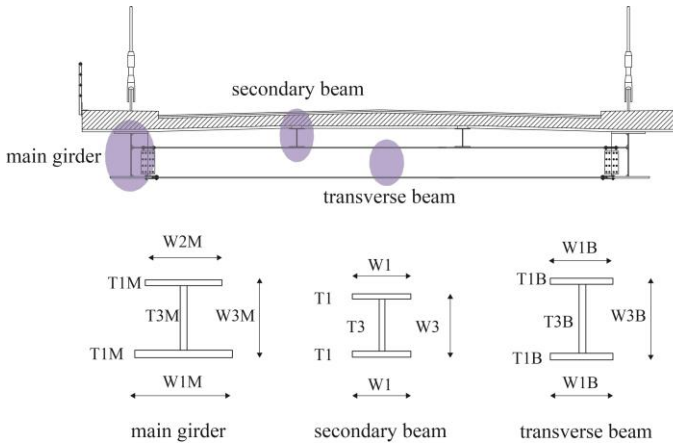


Fig. 92 Identification of different optimization “groups” for the considered deck

Since the optimum solution was found to depend on the initial values of design variables, different initial values were tried in order to avoid local minimum solutions. The optimization iterative processes of three different starting models and original design with 0 angle of tower in vertical direction are shown in Fig. 93. In the convergence iteration of total volume of steel plates, black inverted triangle symbols show the infeasible design solutions, which not meet the requirement of stress or deformation constraints, meanwhile conversely, blue circle symbols show the feasible design solutions and the one among them with minimum objective is the best design solution.

All of them started from same design variables and converged after nearly 20 times iteration. The consistent decrease in the objective function (and therefore the corresponding material saving) is well appreciable. For the original design of bridge, the total volume of steel plates is decreased from 49.6 m<sup>3</sup> to 27.1 m<sup>3</sup>, namely 45.4% volume reduction. When the total cable number is 44, the volume reduction has lowest value -6.5%.

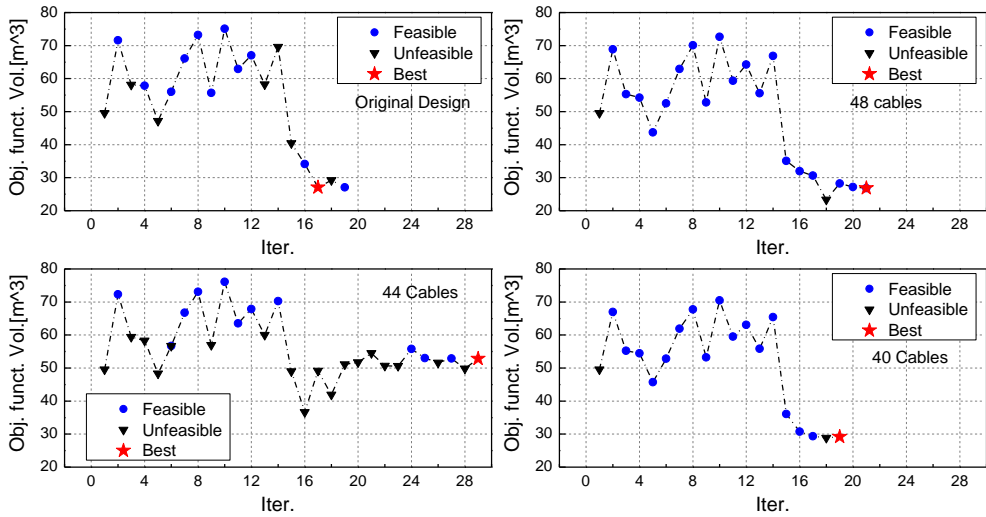


Fig. 93 Convergence iteration of optimization process with 0 angle tower

The optimization procedure led to the optimum results are listed in Table 58. It includes state variables (maximum steel stress, maximum and minimum deformation) and design variables. The values of state variables and design variables are listed both before and after thickness optimization process. For the original design model, only thickness optimization of steel beams carried out, while cable cross sectional area and thickness optimization were carried out for other three starting models.

	Design		0_48		0_44		0_40	
	No opt.	t_opt	c_opt	t_opt	c_opt	t_opt	c_opt	t_opt
<i>Smax (MPa)</i>	126.2	183.1	101.5	160.8	119.0	109.1	111.3	193.8
<i>Dmin (m)</i>	-0.158	-0.201	-0.135	-0.135	-0.061	-0.071	-0.077	-0.103
<i>Dmax (m)</i>	0.059	0.089	0.120	0.194	0.201	0.201	0.136	0.168
<i>W1M (m)</i>	1.000	0.608	1.000	0.940	1.000	0.867	1.000	0.682
<i>W2M (m)</i>	0.800	0.994	0.800	0.533	0.800	0.717	0.800	0.620
<i>W3M (m)</i>	1.100	1.093	1.100	1.023	1.100	1.132	1.100	1.119
<i>T1M (m)</i>	0.040	0.020	0.040	0.021	0.040	0.045	0.040	0.019
<i>T3M (m)</i>	0.020	0.013	0.020	0.010	0.020	0.013	0.020	0.017
<i>W1 (m)</i>	0.360	0.238	0.360	0.202	0.360	0.399	0.360	0.231
<i>T1 (m)</i>	0.010	0.014	0.010	0.017	0.010	0.032	0.010	0.036
<i>T3 (m)</i>	0.010	0.013	0.010	0.049	0.010	0.018	0.010	0.014
<i>W1B (m)</i>	0.600	0.553	0.600	0.501	0.600	0.655	0.600	0.534
<i>W3B (m)</i>	0.730	0.682	0.730	0.679	0.730	0.675	0.730	0.651
<i>T1B (m)</i>	0.020	0.015	0.020	0.010	0.020	0.025	0.020	0.013

<i>T3B (m)</i>	0.020	0.011	0.020	0.011	0.020	0.031	0.020	0.013
<b>OBJ (m<sup>3</sup>)</b>	<b>49.6</b>	<b>27.1</b>	<b>49.6</b>	<b>26.8</b>	<b>49.6</b>	<b>52.8</b>	<b>49.6</b>	<b>29.2</b>

Table 58

Thickness optimization of cable-stayed bridge with 0 angle tower

When the angle of tower in vertical direction is 10, the optimization iterative processes of three different starting models are shown in Fig. 94. All of them started from same design variables and converged after nearly 20 times iteration. The consistent decrease in the objective function is well appreciable. For the starting model with 48 cables, the total volume of steel plates is decreased from 49.6 m<sup>3</sup> to 17.1 m<sup>3</sup>, namely 65.5% volume reduction. When the total cable number is 40, the volume reduction is lowest, but still has an appreciable value 11.3%.

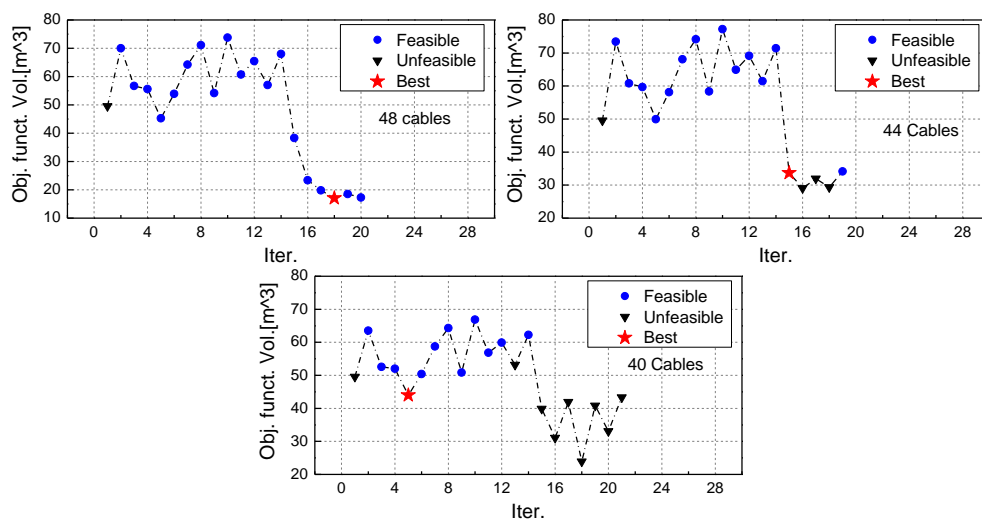


Fig. 94 Convergence iteration of optimization process with 10 angle tower

The optimization procedure led to the optimum results are listed in Table 59. It includes state variables (maximum steel stress, maximum and maximum deformation) and design variables. The values of state variables and design variables are listed after cable cross sectional area optimization and after thickness optimization process for all the three starting models.

	10_48		10_44		10_40	
	c_opt	t_opt	c_opt	t_opt	c_opt	t_opt
<i>Smax (MPa)</i>	98.8	159.4	104.4	191.0	106.9	138.3
<i>Dmin (m)</i>	-0.170	-0.185	-0.066	-0.083	-0.069	-0.102
<i>Dmax (m)</i>	0.076	0.177	0.154	0.185	0.175	0.202



<i>W1M (m)</i>	1.000	0.606	1.000	0.968	1.000	0.856
<i>W2M(m)</i>	0.800	0.516	0.800	0.624	0.800	0.827
<i>W3M (m)</i>	1.100	0.932	1.100	1.145	1.100	0.951
<i>T1M (m)</i>	0.040	0.011	0.040	0.020	0.040	0.032
<i>T3M (m)</i>	0.020	0.011	0.020	0.018	0.020	0.025
<i>W1 (m)</i>	0.360	0.211	0.360	0.359	0.360	0.243
<i>T1 (m)</i>	0.010	0.016	0.010	0.014	0.010	0.014
<i>T3 (m)</i>	0.010	0.011	0.010	0.018	0.010	0.028
<i>W1B (m)</i>	0.600	0.516	0.600	0.619	0.600	0.760
<i>W3B (m)</i>	0.730	0.669	0.730	0.634	0.730	0.438
<i>T1B (m)</i>	0.020	0.011	0.020	0.014	0.020	0.015
<i>T3B (m)</i>	0.020	0.011	0.020	0.020	0.020	0.033
<b>OBJ (m<sup>3</sup>)</b>	<b>49.6</b>	<b>17.1</b>	<b>49.6</b>	<b>33.7</b>	<b>49.6</b>	<b>44.0</b>

Table 59

Thickness optimization of cable-stayed bridge with 10 angle tower

When the angle of tower in vertical direction is 20, the optimization iterative processes of three different starting models are shown in Fig. 95. All of them started from same design variables and converged after nearly 20 times iteration. The consistent decrease in the objective function is well appreciable. For the starting model with 48 cables, the total volume of steel plates is decreased from 49.6 m<sup>3</sup> to 30.8 m<sup>3</sup>, namely 37.9% volume reduction. When the total cable number is 40, the volume reduction has lowest value 1.6%.

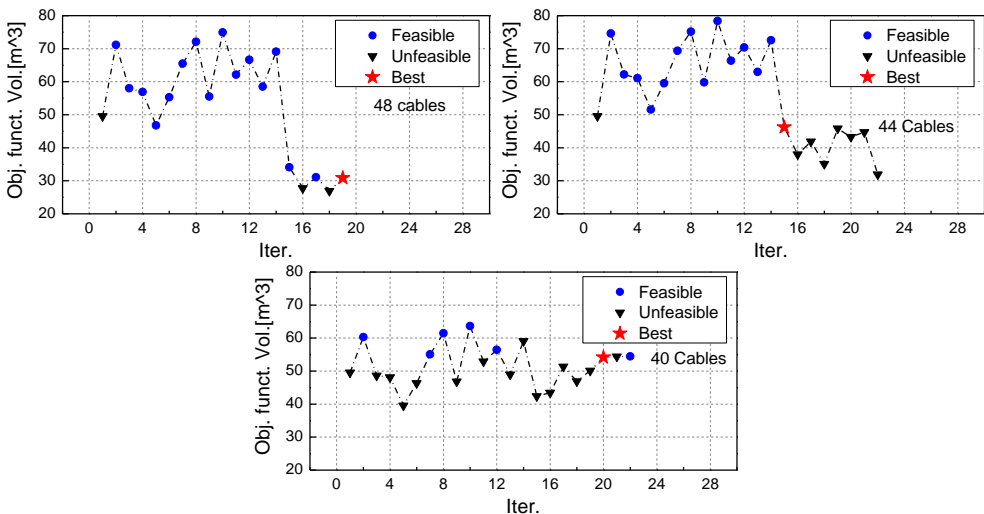


Fig. 95 Convergence iteration of optimization process with 20 angle tower

The optimization procedure led to the optimum results are listed in Table 60. It includes state variables (maximum steel stress, maximum and maximum deformation) and design variables. The values of state variables and design variables are listed after cable cross sectional area optimization and after thickness optimization process for all the three starting models.

	20_48		20_44		20_40	
	c_opt	t_opt	c_opt	t_opt	c_opt	t_opt
<i>S</i> max (MPa)	99.0	145.5	104.5	120.3	116.8	128.3
<i>D</i> min (m)	-0.151	-0.137	-0.059	-0.069	-0.055	-0.076
<i>D</i> max (m)	0.121	0.197	0.187	0.201	0.200	0.202
<i>W</i> 1M(m)	1.000	0.983	1.000	0.966	1.000	0.819
<i>W</i> 2M(m)	0.800	0.683	0.800	0.858	0.800	0.734
<i>W</i> 3M(m)	1.100	1.024	1.100	1.147	1.100	1.075
<i>T</i> 1M (m)	0.040	0.016	0.040	0.032	0.040	0.042
<i>T</i> 3M (m)	0.020	0.013	0.020	0.025	0.020	0.011
<i>W</i> 1 (m)	0.360	0.433	0.360	0.344	0.360	0.377
<i>T</i> 1 (m)	0.010	0.016	0.010	0.015	0.010	0.034
<i>T</i> 3 (m)	0.010	0.023	0.010	0.019	0.010	0.029
<i>W</i> 1B (m)	0.600	0.653	0.600	0.683	0.600	0.871
<i>W</i> 3B (m)	0.730	0.498	0.730	0.607	0.730	0.402
<i>T</i> 1B (m)	0.020	0.013	0.020	0.015	0.020	0.022
<i>T</i> 3B (m)	0.020	0.024	0.020	0.020	0.020	0.015
<b>OBJ (m<sup>3</sup>)</b>	<b>49.6</b>	<b>30.8</b>	<b>49.6</b>	<b>46.2</b>	<b>49.6</b>	<b>54.2</b>

Table 60  
Thickness optimization of cable-stayed bridge with 20 angle tower

### 6.3.5 Comparison between Different Models

Starting from different models which defined by different number of total cables, the cable cross sectional areas and corresponding initial cable force are optimized, on the basis of the optimization results, the optimum cable areas and initial cable force are assigned to starting models to carry out thickness optimization of steel plates of bridge deck. The consistent decrease in steel cable volume and steel plates volume are well appreciable.

However, as the material saving, the deformation and stress of several bridges under all load cases are increased. The maximum average stress of steel beams

and maximum deformation of tower top of all the starting models under all load cases before and after thickness optimization are shown in Table 61 to Table 63. The volume reduction (VR) of steel cables and steel beams are shown together.

Therefore, several candidate solutions were characterized by the total steel cables following the cable cross sectional area and thickness optimization procedure. Hence, the problem of choosing the most suitable solution is faced. To identify the most suitable design solution, on the basis of the results obtained from optimization procedure, the proposed optimization index analytical formulation is discussed in detail and its effectiveness is validated.

	Original design		0_48		0_44		0_40	
	No opt.	t_opt	c_opt	t_opt	c_opt	t_opt	c_opt	t_opt
Stress (MPa)	42.41	49.88	45.35	59.92	46.92	43.86	47.17	56.27
Deform. (m)	-0.042	-0.051	-0.084	-0.092	-0.094	-0.096	-0.103	-0.109
Deck VR (%)	-	45.4	-	46.0	-	-6.5	-	41.1
Cable VR (%)	-	-	-30.3	-30.3	47.7	47.7	13.6	13.6
Total VR (%)	0	45.4	-30.3	15.7	47.7	33.4	13.6	54.7

*Table 61*

*Optimization results of cable-stayed bridge with 0 angle tower*

	10_48		10_44		10_40	
	No opt	opt.	No opt	opt.	No opt	opt.
Stress (MPa)	43.66	63.81	45.20	49.92	46.41	41.58
Deformation (m)	-0.082	-0.094	-0.087	-0.089	-0.104	-0.110
Deck VR (%)	-	65.5	-	32.1	-	11.3
Cable VR (%)	-1.5	-1.5	32.4	32.4	43.2	43.2
Total VR (%)	-1.5	64.0	32.4	64.5	43.2	54.5

*Table 62*

*Optimization results of cable-stayed bridge with 10 angle tower*

	20_48		20_44		20_40	
	No opt	opt.	No opt	opt.	No opt	opt.
Stress (MPa)	45.20	47.78	45.13	50.23	48.83	35.46
Deformation (m)	-0.073	-0.082	-0.083	-0.087	-0.093	-0.099
Deck VR (%)	0	37.9	0	6.9	0	-9.3
Cable VR (%)	-141.7	-141.7	33.3	33.3	7.4	7.4
Total VR (%)	-141.7	-103.8	33.3	40.2	7.4	-1.9

*Table 63*

*Optimization results of cable-stayed bridge with 20 angle tower*

In this case, two response indexes (*RIs*) which summarize the overall behavior of the whole structure were defined as: Von Mises stress, the average bending stress on the element -Z side of the beam throughout the whole optimized steel structure, was considered as representative of stress level, while maximum deflection of tower top was considered as representative of deformation level. The trends of both *RIs* are shown in Fig. 96 to Fig. 98. *RI* curves include the results of cable cross sectional area optimization (Cable Opt.), steel plates thickness optimization (Thickness Opt.) and both together (Cable and Thickness Opt.).

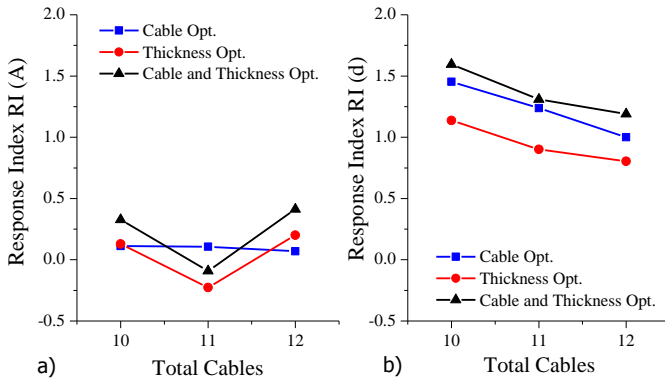


Fig. 96 Response indexes with 0 angle tower vs. total steel cables: a)  $RI(A,i)$ ; b)  $RI(d,i)$

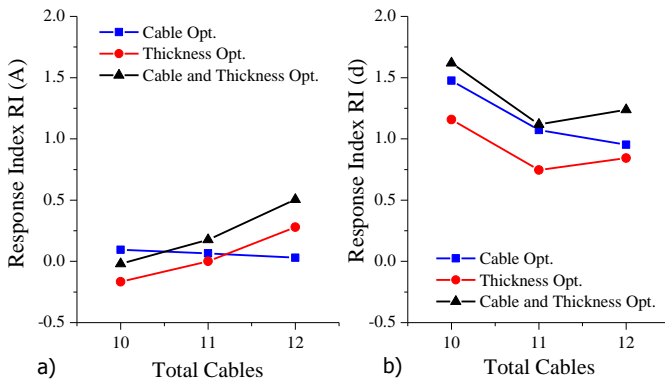


Fig. 97 Response indexes with 10 angle tower vs. total steel cables: a)  $RI(A,i)$ ; b)  $RI(d,i)$

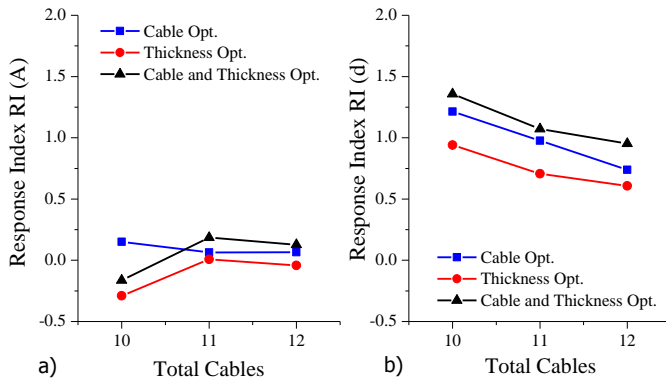


Fig. 98 Response indexes with 20 angle tower vs. total steel cables: a)  $RI(A,i)$ ; b)  $RI(d,i)$

Fig. 99 shows the trend of  $GOI$  varying the total steel cables for some values of  $\beta$  ranging between 0 and 3 when the cable-stayed bridge with 0 angle tower. As expected, the application of  $\beta$  can favour design solutions of higher or lower volume reduction.

In the case of cable cross sectional area optimization, for values of  $\beta$  between 0 and 3, due to the highest volume reduction 47.7%, the highest  $GOI$  value was obtained when the total cable is 11. Take into account cable cross sectional area and thickness optimization together, thanks to the appreciable volume reduction 33.4%, the highest  $GOI$  value was obtained when the total cable is 11. Consider thickness optimization only, due to the lowest volume reduction -6.5%, the lowest  $GOI$  value was obtained when the total cable is 11 for values of  $\beta$  between 0 and 3.

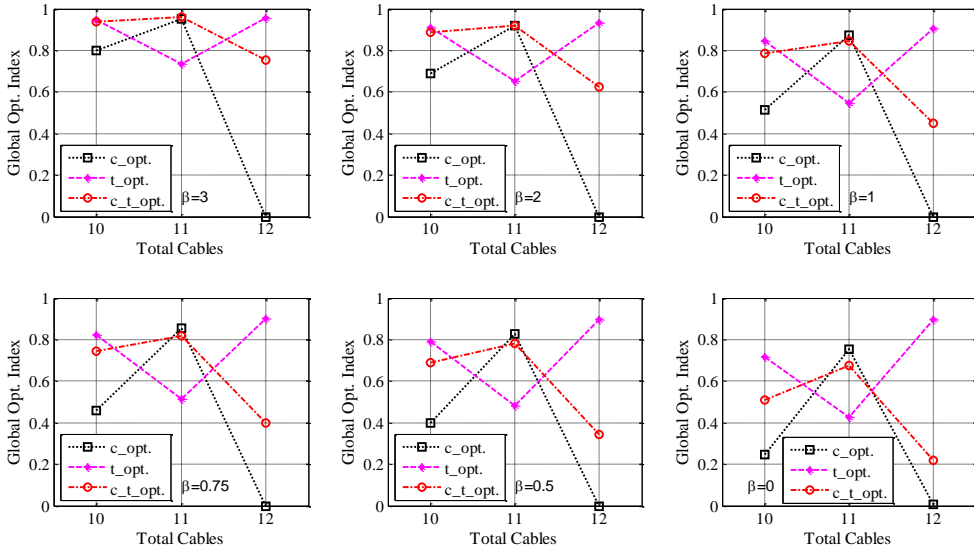


Fig. 99 Global optimization index with 0 angle tower vs. total cables (vs  $\beta$ )

Fig. 100 shows the trend of  $GOI$  varying the total steel cables for some values of  $\beta$  ranging between 0 and 3 when the cable-stayed bridge with 10 angle tower. Consider cable cross sectional area optimization or thickness optimization or both of them together, the same trend of  $GOI$  was obtained. For values of  $\beta$  higher than 1, the highest  $GOI$  value was obtained when the total cable is 10. Further reducing the  $\beta$  parameter until 0, the total cable is 11 get highlighted. This is due to the latter has a cable volume reduction 32.4% and total volume reduction 64.5%, while the former has a cable volume reduction 43.2% and total volume reduction 54.5%.

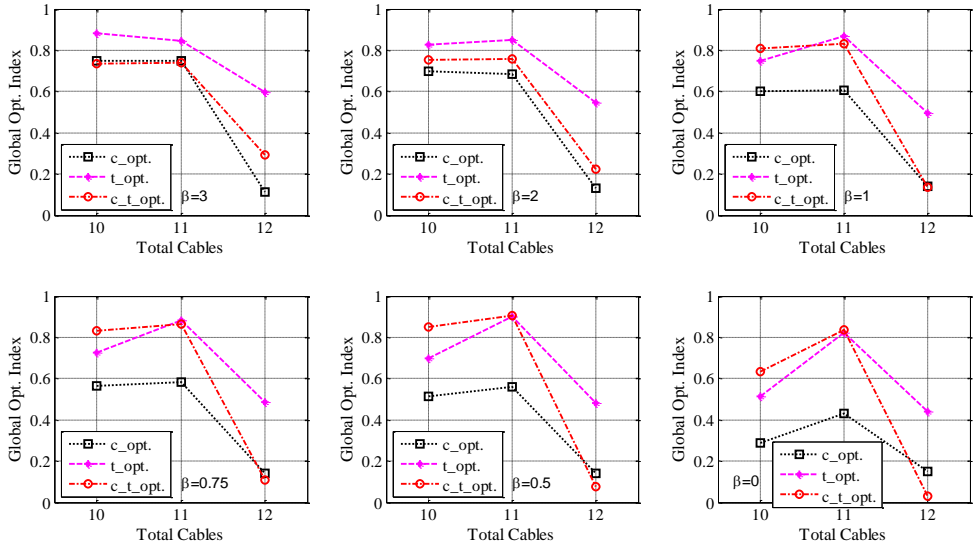


Fig. 100 Global optimization index with 10 angle tower vs. total cables (vs  $\beta$ )

Fig. 101 shows the trend of  $GOI$  varying the total steel cables for some values of  $\beta$  ranging between 0 to 3 when the cable-stayed bridge with 20 angle tower. For values of  $\beta$  between 0 to 3, consider cable cross sectional area optimization, the highest  $GOI$  value was obtained when the total cable is 11 due to the highest cable volume reduction 33.3%. Consider cable cross sectional area optimization and thickness optimization together, the highest  $GOI$  value was obtained when the total cable is 11 due to the highest cable volume reduction 40.2%. In the case of thickness optimization, due to the highest deck volume reduction 37.9%, the highest  $GOI$  value was obtained when the total cable is 12 for values of  $\beta$  ranging between 0 to 3.

AN OPTIMIZATION INDEX TO IDENTIFY THE OPTIMAL DESIGN SOLUTION OF BRIDGES

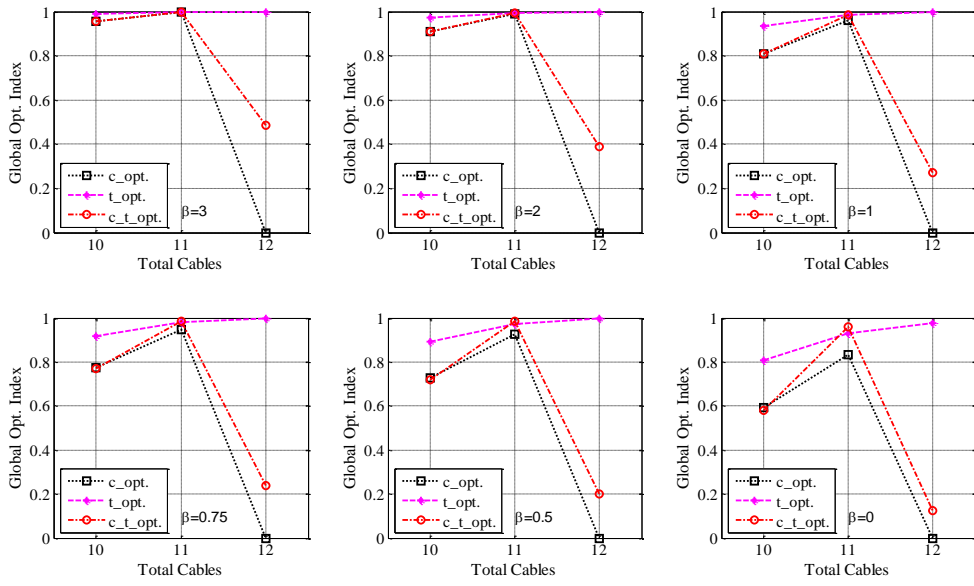


Fig. 101: Global optimization index with 20 angle tower vs. total cables (vs  $\beta$ )



## CONCLUSIONS

This research proposed an optimization index on basis of the work have done by Bruno Briseghella et al. to provide a formal mathematical procedure able to highlight the best choice among several candidate solutions obtained by optimization procedure. It provides the designer an assistant tool to identify the best design solution that representing the best compromise between material saving and structural response. The original optimization index was applied to the structural optimization of a steel-concrete arch bridge built in the province of Venice successfully. In the generalized version, through the introduction of a scaling factor vector  $\alpha$  to the two optimization indexes (*O/s*), proposed optimization index allows not only to identify best candidate solution originated by a unique reference model, but even comparing structural performances between candidates solution derived by several starting trial solutions. Moreover, through the introduction of weight vector  $w$  rather than giving the same weight to deformation and stress level, the optimization index considered the effect size of two *O/s*\*. Following the proposed optimization index, three case studies were carried out. Structural optimization procedures were performed on several different types of bridge and the results showed the effectiveness of proposed optimization index.

### Conclusions

When the topology optimization procedures were carried out and the optimization index was applied in the shell supported footbridges:

- Topology optimization is very efficient and robust in greatly reducing the area of the shell regions subjected to unwished bending moments (therefore tensile stresses) in any case arise because of second-order displacements and the bending stiffness of the RC shell.
- For a given value of volume reduction, the SIMP method identified shell regions with low pseudo-density whose finite elements were to be removed. As the values of given volume reduction increasing, inefficient material was progressively removed and shell layouts with holes with the same volume reduction were obtained.

- For low values of volume reduction, the structural responses of shell bridges were significantly improved and the shells integrity were maintained. On the contrary, for high values of volume reduction, the structural response of shell bridges were slightly improved but the aesthetic value of these design solutions become inappropriate that the shells tended to split into two symmetric parts with respect to its centreline.
- 36 candidate solutions in total were obtained on the basis of 3 reference models with different boundary shape, 3 different starting models characterized by different edge stiffening for each reference models and 4 different input *VR*s ratio. *GOI* scores for these candidate solutions were assigned through the proposed optimization index.
- Between reference models with different boundary shape, namely model T\_0.15, T\_0.20 and T\_0.32, the score of global optimization index of model T\_0.15 is always much higher than that of other two starting models for varying *VR* due to the positive effect of reasonable shell boundary shape.
- Between starting models characterized by different edge stiffening, namely Mode I, Model II and Model III, the score of global optimization index of Model III is always much higher than that of other two models for varying *VR* due to the positive effect that the edge stiffening beam had on the overall rigidity of the shell footbridge.
- Between different input *VR* ratio, the structural response of the shell footbridges in terms of both unwished tensile stress arising and deformation was highly affected by the insertion of holes for  $10\% \leq VR \leq 20\%$ , and less affected for  $20\% \leq VR \leq 30\%$ . The layout with holes obtained for a *VR* of 20% was shown to have good structural response, only slightly lower than that obtained for *VR* of 30%, but contrary to the latter, the former maintained the shell integrity avoiding the merging of close holes dividing a great part of the shell into two parts.
- Through the introduction of scaling factor vector  $\alpha$ , the design solutions of starting model T\_0.15 and Model III were highlighted. Through the introduction of weight vector  $w$ , the higher effect size of stress level was considered.

- The layout of Model III of T\_0.15 shell model for VR = 20% appeared to be the most suitable compromise between structural and aesthetical issues.

When the thickness optimization procedure was carried out and the optimization index was applied in the Calatrave Bridge:

- Three tentative starting models were defined by considering bridge's abutment deformability through spring-damper elements (Model II) and introducing stiffening cables along two bottom arches of the bridge (Model III) on the basis of original design model (Model I). Thickness optimization procedures of minimizing total volume and horizontal force were carried out.
- The optimization results of Model I and Model II with spring constant  $K$  equal to  $10^{15}$  N/m verified that as the spring constant  $K$  is high enough or initial strain  $\epsilon$  is low enough, Model II or Model III is the same as Model I therefore with same structural behavior and optimization results.
- For starting model I, an optimum design that meets requirements of stress and deformation levels yet demands a minimum total volume was determined. For Model II and Model III, different optimum designs were determined for different spring constant  $K$  of spring-damper element and different initial strain of stiffening cables, respectively.
- In the case of minimizing total volume, the optimization results show, best design solution of model I has a volume reduced 34%. For Model II, the highest  $GOI$  value obtained when spring constant  $K$  is  $10^{10}$  N/m, which with a 36% volume reduction, while the best design solution of Model III obtained when initial strain is  $8 \times 10^{-4}$ , which design solution with 36% volume reduction.
- In the case of minimizing total volume, Model II with the spring constant  $K$  is  $10^{15}$  N/m has similar value as Model III with initial strain  $\epsilon$  is  $5 \times 10^{-4}$ . All the design solutions of Model III have a  $GOI$  value around 0.6 and move from 0.4 to 0.9, while the  $GOI$  value of design solutions of Model II have significant variations and was varying from 0 to 1. The design solution when spring constant  $K$  is  $10^{10}$  N/m of Model II with a 36% volume reduction got the highest  $GOI$  value.

- In the case of minimizing sum horizontal force under load cases of dead load and full length full width, the optimization results show, best design solution of model I with horizontal force reduced 22.7%. For Model II, the highest *GOI* value obtained when spring constant  $K$  is  $10^8$  N/m, which with a 44% horizontal force reduction, while the best design solution of Model III obtained when initial strain is  $9 \times 10^{-4}$ , which design solution with 30.1% horizontal force reduction.
- In the case of minimizing horizontal force, Model II with the spring constant  $K$  is  $10^{15}$  N/m has similar value as Model III with initial strain  $\epsilon$  is  $7 \times 10^{-4}$ . Both of Model II and Model III have highest *GOI* value when the spring constant or initial strain is intermediate value, with which almost all the design solutions of two models have same *GOI* value. The design solution of Model III when initial strain  $9 \times 10^{-4}$  with 30.1% horizontal force reduction is slightly higher.

When the structural optimization procedures were carried out and the optimization index was applied in two cable-stayed bridges:

- The cable cross sectional areas and corresponding initial tensioning force were optimized. The optimization results lead to larger area for cables attached to both ends of the deck and cables close to the middle span. The former occurred due to they are the ones brace the tower, the latter occurred due to the deformation limit of cable deck end.
- The cable optimization results shown that a small modification in the cable areas can affect the requirement of constraints far away from the location where the changes are produced. In addition to the consistent decrease in steel cable volume, the optimization procedure gave an idea to designer about how much cross sectional area is necessary for each cable under certain stress and displacement constraints.
- The optimum cable areas and initial tensioning force obtained from optimization procedures are assigned to starting models to carry out thickness optimization of steel plates of bridge deck. The results shown the consistent decrease in steel plates volume are well appreciable.
- No matter consider the results of cable cross sectional area optimization, or consider the results of thickness optimization, or take into account them

together, suitable score for each design solution of specific starting layout was assigned. A straightforward selection of optimum design solution was provided.

- For the Single Tower Single Cable Plane cable-stayed bridge, the starting model with 10 cables has a significant reduction of total cable volume which from  $2.059 \text{ m}^3$  to  $1.428 \text{ m}^3$  compared with original design. The starting model with 9 cables reduced more cable volume due to one cable less after optimization process, on the contrary, the cable volume of starting model with 11 cables is slightly higher than original design due to one cable more. The total volume of steel plates of the original bridge design is decreased from  $48.6 \text{ m}^3$  to  $26.2 \text{ m}^3$ , namely 46.1% volume reduction. When the total cable number is 11, the volume reduction of steel plates is lowest, but still has an appreciable value 26.3%.
- For the Twin Towers Double Cable Planes cable-stayed bridge with 0 angel tower, the starting model with 48 cables has the highest total cable volume  $1.134 \text{ m}^3$ . The starting model with 44 cables and 40 cables reduced objective significantly due to less cables, with total cable volume  $0.455 \text{ m}^3$  and  $0.752 \text{ m}^3$ , respectively. For the original design of bridge, the total volume of steel plates was decreased from  $49.6 \text{ m}^3$  to  $27.1 \text{ m}^3$ , namely 45.4% reduction. When the total cable number is 44, the volume reduction of steel plates has lowest value -6.5%.
- For the Twin Towers Double Cable Planes cable-stayed bridge with 10 angel tower, the starting model with 48 cables has the highest total cable volume  $0.883 \text{ m}^3$ , while the total volume of steel plates is decreased from  $49.6 \text{ m}^3$  to  $17.1 \text{ m}^3$ , namely 65.5% reduction. The starting model with 44 cables and 40 cables reduced objective significantly due to less cables, with total cable volume  $0.588 \text{ m}^3$  and  $0.494 \text{ m}^3$ , respectively. When the total cable number is 40, the volume reduction is lowest, but still has an appreciable value 11.3%.
- For the Twin Towers Double Cable Planes cable-stayed bridge with 20 angel tower, the starting model with 48 cables has the highest total cable volume  $1.191 \text{ m}^3$ , while the total volume of steel plates is decreased from  $49.6 \text{ m}^3$  to  $30.8 \text{ m}^3$ , namely 37.9% reduction. The starting model with 44 cables and 40 cables reduced objective significantly due to less cables, with total cable volume  $0.580 \text{ m}^3$  and  $0.805 \text{ m}^3$ , respectively. When the total cable number is 40, the volume reduction has lowest value 1.6%.

### **Recommendation for Future Investigations**

Although the research provided a formal mathematical procedure able to highlight the best choice among several candidate solutions obtained by optimization procedure, some parameters need to be take out from finite element software and optimization index need to be calculate by hand. A FE code implemented in the finite element software which will calculate the global optimization index automatically is recommendation for future investigations.

## BIBLIOGRAPHY

Abolbashari, M. H., and Keshavarzmanesh, S. (2006). "On various aspects of application of the evolutionary structural optimization method for 2D and 3D continuum structures." *Finite Elements in Analysis and Design*, 42(6), 478-491.

Achtziger, W., and Kocvara, M. (2007). "Structural topology optimization with eigenvalues." *SIAM Journal on Optimization*, 18(4), 1129-1164.

Akin, J., and Arjona-Baez, J. (2001). "Enhancing structural topology optimization." *Engineering Computations*, 18(3/4), 663-675.

Allaire, G., Aubry, S., and Jouve, F. (2001). "Eigenfrequency optimization in optimal design." *Computer Methods in Applied Mechanics and Engineering*, 190(28), 3565-3579.

Allaire, G., Jouve, F., and Toader, A.-M. (2002). "A level-set method for shape optimization." *Comptes Rendus Mathematique*, 334(12), 1125-1130.

Andreassen, E., Clausen, A., Schevenels, M., Lazarov, B. S., and Sigmund, O. (2010). "Efficient topology optimization in MATLAB using 88 lines of code." *Structural and Multidisciplinary Optimization*, 43(1), 1-16.

Ansys, R. (2007). "11.0." *Documentation for Ansys*.

Arora, J. (2004). *Introduction to optimum design*, Academic Press.

Banichuk, N. V., and Neittaanmäki, P. (2010). *Structural optimization with uncertainties*, Springer.

Belegundu, A. D., and Chandrupatla, T. R. (2011). *Optimization concepts and applications in engineering*, Cambridge University Press.

Bendsøe, M. P., and Kikuchi, N. (1988). "Generating optimal topologies in structural design using a homogenization method." *Computer Methods in Applied Mechanics and Engineering*, 71(2), 197-224.

Bendsøe, M. P. (1989). "Optimal shape design as a material distribution problem." *Structural optimization*, 1(4), 193-202.

Bendsøe, M. P., and Sigmund, O. (1999). "Material interpolation schemes in topology optimization." *Archive of Applied Mechanics*, 69(9-10), 635-654.

Bendsoe, M. P., and Sigmund, O. (2003). *Topology optimization: theory, methods and applications*, Springer Verlag.

Bradie, B. (2006). *A Friendly Introduction to Numerical Analysis: With C and MATLAB Materials on Website*, Person Prentice Hall.

Brandt, A., and Wasiutynski, Z. (1963). "Survey of the literature on various existing methods and approaches to the solution of problems of optimum design."

Briseghella, B., Siviero, E., and Zordan, T. "The IV Bridge over the Grand Canal of Venice: from conceptual design to construction." *Proc., Proceedings of IASS Symposium: Structural Architecture - Towards the future looking to the past*.

Briseghella, B., Fenu, L., Lan, C., Mazzarolo, E., and Zordan, T. (2012). "An Application of Topological Optimization to Bridge Design." *Journal of Bridge Engineering*, 1, 297.

Briseghella, B., Fenu, L., Feng, Y., Mazzarolo, E., and Zordan, T. (2013). "Topology Optimization of Bridges Supported by a Concrete Shell." *Structural Engineering International*, 23(3), 285-294.

Bruns, T. E. (2005). "A reevaluation of the SIMP method with filtering and an alternative formulation for solid-void topology optimization." *Structural and Multidisciplinary Optimization*, 30(6), 428-436.

Burns, S. A. "Recent advances in optimal structural design." American Society of Civil Engineers.

Chen, B.-c., Feng, Y., and Briseghella, B. (2011). "The Fourth Bridge over the Grand Canal in Venice." *World Bridges*, 1, 002.

Cheng, L. (2012). "ON THE PERFORMANCE OF SUPER-LONG INTEGRAL ABUTMENT BRIDGES." PhD, Trento.

Choi, K., and Kim, N.-H. (2005). *Structural Sensitivity Analysis and Optimization 2: Nonlinear Systems and Applications (Mechanical Engineering Series)*, Berlin: Springer.

Choi, K. K., and Kim, N. H. (2005). *Structural sensitivity analysis and optimization 1: linear systems*, Springer Science+ Business Media.

Christensen, P. W., and Klarbring, A. (2009). *An introduction to structural optimization*, Springer.

Chu, D. N., Xie, Y., Hira, A., and Steven, G. (1996). "Evolutionary structural optimization for problems with stiffness constraints." *Finite Elements in Analysis and Design*, 21(4), 239-251.

Cohn, M., and Dinovitzer, A. (1994). "Application of structural optimization." *Journal of Structural Engineering*, 120(2), 617-650.



Dantzig, G. B. (1998). *Linear programming and extensions*, Princeton university press.

Diaz, A., and Sigmund, O. (1995). "Checkerboard patterns in layout optimization." *Structural optimization*, 10(1), 40-45.

Diehl, M. G., F.; Jarlebring, E.; Michiels, W. (2010). *Recent advances in optimization and its applications in Engineering*, Springer Verlag.

Ding, Y. (1986). "Shape optimization of structures: a literature survey." *Computers & Structures*, 24(6), 985-1004.

Edwards, C. S., Kim, H. A., and Budd, C. J. (2007). "An evaluative study on ESO and SIMP for optimising a cantilever tie—beam." *Structural and Multidisciplinary Optimization*, 34(5), 403-414.

Elishakoff, I., and Ohsaki, M. (2010). *Optimization and anti-optimization of structures under uncertainty*, World Scientific.

Eschenauer, H. A., and Olhoff, N. (2001). "Topology optimization of continuum structures: A review." *Applied Mechanics Reviews*, 54(4), 331.

Fenu, L., Madama, G (2005). "A Method of Shaping R/C Shells With Heuristic Algorithms and With Reference To Musmeci's work." *studies and researches*, 25, 199-238.

Flügge, S. (1973). "Stresses in shells." *Berlin: Springer, 1973, 2nd ed.*, 1.

Groenwold, A. A., and Etman, L. F. P. (2009). "A simple heuristic for gray-scale suppression in optimality criterion-based topology optimization." *Structural and Multidisciplinary Optimization*, 39(2), 217-225.

Guan, H., Chen, Y.-J., Loo, Y.-C., Xie, Y.-M., and Steven, G. P. (2003). "Bridge topology optimisation with stress, displacement and frequency constraints." *Computers & Structures*, 81(3), 131-145.

Guide, M. U. s. (1998). "The mathworks." *Inc., Natick, MA*, 5.

Hassan, M., Nassef, A., and El Damatty, A. (2012). "Determination of optimum post-tensioning cable forces of cable-stayed bridges." *Engineering Structures*, 44, 248-259.

Hildebrand, F. B. (1987). *Introduction to numerical analysis*, Courier Dover Publications.

Hsu, Y.-L. (1994). "A review of structural shape optimization." *Computers in Industry*, 25(1), 3-13.

Huang, X., and Xie, Y. (2008). "A new look at ESO and BESO optimization methods." *Structural and Multidisciplinary Optimization*, 35(1), 89-92.

Huang, X., and Xie, Y. M. (2009). "Evolutionary topology optimization of continuum structures with an additional displacement constraint." *Structural and Multidisciplinary Optimization*, 40(1-6), 409-416.

Huang, X., and Xie, M. (2010). *Evolutionary topology optimization of continuum structures: methods and applications*, Wiley.

Janjic, D., Pircher, M., and Pircher, H. (2003). "Optimization of cable tensioning in cable-stayed bridges." *Journal of Bridge Engineering*, 8(3), 131-137.

Kaveh, A., Hassani, B., Shojaee, S., and Tavakkoli, S. M. (2008). "Structural topology optimization using ant colony methodology." *Engineering Structures*, 30(9), 2559-2565.

Kim, H., Querin, O., and Steven, G. (2002). "On the development of structural optimisation and its relevance in engineering design." *Design studies*, 23(1), 85-102.

Li, H.-S., and Au, S.-K. (2010). "Design optimization using Subset Simulation algorithm." *Structural Safety*, 32(6), 384-392.

Liang, Q. Q. (2004). *Performance-based Optimization of Structures: Theory and applications*, Taylor & Francis.

Luigi Fenu, G. M., Sergio Tattoni (2006). "On the conceptual design of R/C footbridges made of deck and shells of minimal surface." *studies and researches*, 26, 103-126.

Madeira, J. F. A., Pina, H. L., and Rodrigues, H. C. (2009). "GA topology optimization using random keys for tree encoding of structures." *Structural and Multidisciplinary Optimization*, 40(1-6), 227-240.

Martí, J. V., and González-Vidosa, F. (2010). "Design of prestressed concrete precast pedestrian bridges by heuristic optimization." *Advances in Engineering Software*, 41(7-8), 916-922.

MathWorks Inc. (2011). "MATLAB - Product Documentation." Natick, Massachusetts, USA.

Min, S., Nishiwaki, S., and Kikuchi, N. (2000). "Unified topology design of static and vibrating structures using multiobjective optimization." *Computers & Structures*, 75(1), 93-116.

Musmeci, S. (1977). "Ponte sul Basento a Potenza." *Industria Italiana del Cemento*, 2, 77-98.

Negrão, J., and Simões, L. (1997). "Optimization of cable-stayed bridges with three-dimensional modelling." *Computers & Structures*, 64(1), 741-758.

Nocedal, J., and Wright, S. (2006). "Numerical optimization, series in operations research and financial engineering." *Springer, New York*.

Osher, S., and Sethian, J. A. (1988). "Fronts propagating with curvature-dependent speed: algorithms based on Hamilton-Jacobi formulations." *Journal of computational physics*, 79(1), 12-49.

Osher, S., and Fedkiw, R. P. (2001). "Level set methods: an overview and some recent results." *Journal of computational physics*, 169(2), 463-502.

Otto, F., Trostel, R., and Schleyer, F. K. (1973). *Tensile structures; design, structure, and calculation of buildings of cables, nets, and membranes*, The MIT Press.

Pedersen, N. L. (2000). "Maximization of eigenvalues using topology optimization." *Structural and Multidisciplinary Optimization*, 20(1), 2-11.

Perea, C., Alcalá, J., Yepes, V., Gonzalez-Vidosa, F., and Hospitaler, A. (2008). "Design of reinforced concrete bridge frames by heuristic optimization." *Advances in Engineering Software*, 39(8), 676-688.

Prager, W., and Taylor, J. (1967). "Problems of Optimal Structural Design1."

Rahmatalla, S., and Swan, C. C. (2003). "Form finding of sparse structures with continuum topology optimization." *Journal of Structural Engineering*, 129(12), 1707-1716.

Rao, S. S., and Rao, S. (2009). *Engineering optimization: theory and practice*, John Wiley & Sons.

Ravindran, A., Reklaitis, G. V., and Ragsdell, K. M. (2006). *Engineering optimization: Methods and applications*, Wiley. com.

Release, A. (2007). "11.0." *ANSYS Academic Research, ANSYS Inc., Canonsburg, Pennsylvania*.

Roy, R., Hinduja, S., and Teti, R. (2008). "Recent advances in engineering design optimisation: Challenges and future trends." *CIRP Annals - Manufacturing Technology*, 57(2), 697-715.

Rozvany, G. (2001). "Aims, scope, methods, history and unified terminology of computer-aided topology optimization in structural mechanics." *Structural and Multidisciplinary Optimization*, 21(2), 90-108.

- Rozvany, G. I. N. (2008). "A critical review of established methods of structural topology optimization." *Structural and Multidisciplinary Optimization*, 37(3), 217-237.
- Rucheng, X., and Haifan, X. (1998). "Optimization method of cable prestresses of cable stayed bridges and its engineering applications [J]." *Chinese Journal of Computational Mechanics*, 1.
- Schmit, L. "Structural design by systematic synthesis." *Proc., Proc. of the Second ASCE Conference on Electronic Computation*, 105-122.
- Schoofs, A. (1993). "Structural Optimization History and State-of-the-Art." *Topics in Applied Mechanics*, Springer, 339-345.
- Scibilia, R., and Vento, S. "Fourth bridge over the grand canal between Piazzale Roma and Venice railway." *Proc., Steelbridge 2004*, 103-105.
- Sethian, J. A., and Wiegmann, A. (2000). "Structural boundary design via level set and immersed interface methods." *Journal of computational physics*, 163(2), 489-528.
- Sigmund, O., and Petersson, J. (1998). "Numerical instabilities in topology optimization: a survey on procedures dealing with checkerboards, mesh-dependencies and local minima." *Structural optimization*, 16(1), 68-75.
- Sigmund, O. (2001). "A 99 line topology optimization code written in Matlab." *Structural and Multidisciplinary Optimization*, 21(2), 120-127.
- Sigmund, O. (2007). "Morphology-based black and white filters for topology optimization." *Structural and Multidisciplinary Optimization*, 33(4-5), 401-424.
- Sigmund, O., and Maute, K. (2013). "Topology optimization approaches A comparative review." *Structural and Multidisciplinary Optimization*, 48(6), 1031-1055.
- Spillers, W. R., and MacBain, K. M. (2009). *Structural optimization*, Springer.
- Sung, Y.-C., Chang, D.-W., and Teo, E.-H. (2006). "Optimum post-tensioning cable forces of Mau-Lo Hsi cable-stayed bridge." *Engineering Structures*, 28(10), 1407-1417.
- Suykens, J. A. K., Vandewalle, J., and De Moor, B. (2001). "Intelligence and Cooperative Search by Coupled Local Minimizers." *International Journal of Bifurcation and Chaos*, 11(8), 2133-2144.
- Suzuki, K., and Kikuchi, N. (1991). "A homogenization method for shape and topology optimization." *Computer Methods in Applied Mechanics and Engineering*, 93(3), 291-318.

Tanskanen, P. (2002). "The evolutionary structural optimization method: theoretical aspects." *Computer Methods in Applied Mechanics and Engineering*, 191(47), 5485-5498.

Teughels, A., De Roeck, G., and Suykens, J. A. K. (2003). "Global Optimization by Coupled Local Minimizers and its Application to FE Model Updating." *Computers & structures*, 81(24-25), 2337-2351.

Vanderplaats, G. (1982). "Structural optimization-past, present, and future." *AIAA Journal*, 20(7), 992-1000.

Venkayya, V. (1989). "Optimality criteria: a basis for multidisciplinary design optimization." *Computational Mechanics*, 5(1), 1-21.

Venkayya, V. B. (1978). "Structural optimization: a review and some recommendations." *International Journal for Numerical Methods in Engineering*, 13(2), 203-228.

Walther, R. (1999). *Cable stayed bridges*, Thomas Telford.

Wang, M. Y., Wang, X., and Guo, D. (2003). "A level set method for structural topology optimization." *Computer Methods in Applied Mechanics and Engineering*, 192(1), 227-246.

Xia, Q., Shi, T., Liu, S., and Wang, M. Y. (2012). "A level set solution to the stress-based structural shape and topology optimization." *Computers & Structures*, 90, 55-64.

Xie, Y., and Steven, G. P. (1993). "A simple evolutionary procedure for structural optimization." *Computers & Structures*, 49(5), 885-896.

Young, V., Querin, O., Steven, G., and Xie, Y. (1999). "3D and multiple load case bi-directional evolutionary structural optimization (BESO)." *Structural optimization*, 18(2-3), 183-192.

Zadeh, O. S. (2012). "Comparison Between Three Types of Cable Stayed Bridges Using Structural Optimization." The University of Western Ontario.

Zhou, M., and Rozvany, G. (2001). "On the validity of ESO type methods in topology optimization." *Structural and Multidisciplinary Optimization*, 21(1), 80-83.

Zordan, T., Briseghella, B., and Siviero, E. (2010). "The Fourth Bridge over the Grand Canal in Venice: From Idea to Analysis and Construction." *Structural Engineering International*, 20(1), 6-12.